74-6986

SMITH, Roger Lair, 1938-
AERODYNAMICS OF CHANNEL AND RING WINGS.

The University of Oklahoma, Ph.D., 1973
Aerospace Studies

University Microfilms, A XEROX Company, Ann Arbor, Michigan

THE UNIVERSITY OF OKLAHOMA

GRADUATE COLLEGE

AERODYNAMICS OF CHANNEL AND RING WINGS

A DISSERTATION

SUBMITTED TO THE GRADUATE COLLEGE

in partial fulfillment of the requirements for the

degree of

DOCTOR OF PHILOSOPHY

BY

ROGER L. SMITH

Norman, Oklahoma

1973

AERODYNAMICS OF CHANNEL AND RING WINGS

APPROVED BY

Edward F. Blick

Maurice Rasmussen

William N. Huff

Raymond Kaser

DISSERTATION COMMITTEE

ACKNOWLEDGMENTS

The inspiration, encouragement, and guidance of Professor E. F. Blick during this study and throughout the graduate program are gratefully acknowledged by the author. Also, the interest, time and effort of Professor W. N. Huff, Dr. M. C. Jischke, and Professor M. L. Rasmussen have been greatly appreciated.

The financial assistance of the National Science Foundation by means of a graduate traineeship was indispensable.

The technical counsel of Professor L. A. Comp in model design and wind tunnel operation was invaluable to the author. The assistance of Mr. E. Parsons and Mr. E. Finch in wind tunnel model construction and modification was sincerely appreciated. The Custer Channel Wing Corporation deserves the author's thanks for its contribution of the mahogony for one of the wind tunnel models. The author gratefully acknowledges the lively interest in this study of his colleagues of the United States Army Air Mobility Research and Development Laboratory.

The author is indebted to the typists, Janet Haskenhoff, Dorothy Sheppard, and Ruth Ann Ference for their patience and perseverance in the preparation of the manuscript.

This work is dedicated to my wife, Nancy, in appreciation of her material and moral contributions to its advancement.

ABSTRACT

The results of a deflected streamtube theory for the lift and induced drag of isolated ring wings are briefly reviewed, and a similar theory for channel wings is presented. The ring wing theory, and methods derived from its general conclusions, are compared with other theoretical derivations and with experimental data. A wind tunnel test of two channel wings of aspect ratio 1.0 and 2.8 is described, and the data are compared with the channel wing deflected streamtube theory. It is shown that the ring wing theory yields good agreement with experiment and with other developments, but the channel wing deflected streamtube theory does not. The experimental results for channel wings and ring wings indicate that these wings achieve span efficiency factors of approximately 1.5 and 2.0, respectively.

A lifting arc theory for channel wings is derived and shown to agree with the experimental data. A digital computer program which implements this theory is provided. The computer program allows rapid calculation of lift and drag coefficients of isolated channel wings as a function of wing geometry, airfoil section characteristics, and angle of attack.

Power required, range, and endurance of aircraft with channel or ring wings are estimated, and compared with that for plane wing aircraft. The latter requires more power over a significant portion

of the low speed (high lift coefficient) flight regime than the former, at the same aspect ratio. The width of this speed range increases as aspect ratio decreases. Power effects on wing aerodynamics are not considered. The channel wing aircraft with reciprocating engine propulsion will have a significant increase in endurance as compared to a plane wing aircraft, and a lesser increase in range. The ring wing aircraft requires more power and has less range and endurance than the channel wing aircraft.

TABLE OF CONTENTS

Page

APPENDICES

LIST OF TABLES

LIST OF ILLUSTRATIONS

Figure Page

Figure		Page

LIST OF SYMBOLS

A	area
A_F	model frontal area
A_n	Fourier series coefficient for circulation distribution
A_{TS}	wind tunnel test section cross-sectional area
$\mathcal{R}$	aspect ratio, $(\text{span})^2/(\text{projected area})$
B	wind tunnel jet width
C_D	drag coefficient
C_{D_b}	drag coefficient of a circular cylinder perpendicular to flow
C_{D_c}	corrected drag coefficient of wind tunnel model
C_{D_i}	induced drag coefficient
$C_{D_{INV}}$	drag coefficient of wind tunnel model in inverted position
C_{D_N}	drag coefficient of wind tunnel model in normal upright position
C_{D_o}	profile drag coefficient
C_{D_o}'	profile drag coefficient increased to account for non-planar wing
$C_{D_{TJ}}$	drag coefficient of wind tunnel model tail jack arm
C_f	skin friction coefficient
C_{D_u}	uncorrected drag coefficient
C_L	lift coefficient
$C_{L_{INV}}$	lift coefficient of wind tunnel model in inverted position

C_{L_N}	lift coefficient of wind tunnel model in normal upright position
$C_{L_{TJ}}$	lift coefficient of wind tunnel model tail jack arm
C_{L_U}	uncorrected lift coefficient
C_M	pitching moment coefficient
C_N	normal force coefficient
C_0, C_1, C_2	series coefficients for vortex density distribution of ring wing
D	drag
D_g	grit diameter
D_i	induced drag
D_M	drag of wind tunnel model
D_{M_I}	drag of wind tunnel model in inverted position
D_{M_N}	drag of wind tunnel model in normal upright position
D_o	profile drag
D_1	indicated drag of wind tunnel model in normal upright position
D_2	indicated drag of wind tunnel model in upright position, with image support system
D_3	indicated drag of wind tunnel model in inverted position
D_4	indicated drag of wind tunnel model in inverted position with image support system
E_{max}	maximum endurance
F_n'	magnitude of aerodynamic force, per unit arc length, normal to both V and local wing section
F_p'	magnitude of aerodynamic force, per unit arc length, parallel to V
I_D	induced drag integral in equation (6.51)
I_L	$I_{LB/M} + I_{LW/M} + I_{M/LB}$

$I_{LB/M}$	aerodynamic interference force on wind tunnel model due to the lower bayonet
$I_{LW/M}$	aerodynamic interference force on wind tunnel model due to the lower windscreen
$I_{M/LB}$	aerodynamic interference force on lower bayonet due to the wind tunnel model
$I_{M/UB}$	aerodynamic interference force on upper bayonet due to the wind tunnel model
I_U	$I_{UB/M} + I_{UW/M} + I_{M/UB}$
$I_{UB/M}$	aerodynamic interference force on wind tunnel model due to the upper bayonet
$I_{UW/M}$	aerodynamic interference force on wind tunnel model due to the upper windscreen
J_n , K_n	recurrence relations, see equation (6.36)
L	lift
L_M	lift of wind tunnel model
L_{M_I}	lift of wind tunnel model in inverted position
L_{M_N}	lift of wind tunnel model in normal position
L_1	indicated lift of wind tunnel model in normal position
L_2	indicated lift of wind tunnel model in upright position, with image support system
L_3	indicated lift of wind tunnel model in inverted position
L_4	indicated lift of wind tunnel model in inverted position, with image support system
L/D	lift to drag ratio
$(L/D)_{max}$	maximum lift to drag ratio
M	pitching moment
M_∞	free-stream Mach number
N	aerodynamic force normal to local section of wing

P	pressure
P	power
$P_{(L/D)_{max}}$	power required at $V_{(L/D)_{max}}$
R	radius of channel or ring wing
R_{max}	maximum range
Re	Reynolds number, $\rho V l/\mu$
S	projected area of plane, channel, or ring wing
S_{rc}	projected area of a right circular cylinder
S_T	total wing area (not projected area)
T	thrust
T_{LB}	aerodynamic tare force on lower bayonet
$T_{(L/D)_{max}}$	thrust required at $V_{(L/D)_{max}}$
T_{UB}	aerodynamic tare force on upper bayonet
TF	wind tunnel turbulence factor
V	model volume
V	free-stream velocity; corrected wind tunnel test section velocity
$V_{(L/D)_{max}}$	velocity for $(L/D)_{max}$ (minimum thrust required)
V_r	radial component of free-stream velocity
$V_{(T)_{min}}$	velocity for minimum thrust required (minimum drag)
V_u	uncorrected wind tunnel test section velocity
V_x	component of free-stream velocity along x axis
W	gross weight of aircraft with planar wings
W'	aircraft gross weight increased to account for non-planar wing
W_f	fuel weight

W_o	initial weight
W_1	final weight
a	slope of lift curve, $dC_L/d\alpha$
a_o	airfoil section lift curve slope
b	wing span
c	wing chord
c_d	section drag coefficient
c_l	section lift coefficient
c_o	chord in constant-chord section of wing
d	diameter of a circular cylinder
d	differentiation operator
$d\gamma$	strength of a vortex filament
e	span efficiency factor
k	integer constant in wing tip chord distribution
l	linear dimension in streamwise direction
l	length of a cylinder
n	index of Fourier coefficient
q	dynamic pressure, $\rho/2\ V^2$
q	induced velocity
q_n	surface-normal component of local induced velocity
q_s	induced velocity component, due to bound vortex, acting parallel to V
q_u	uncorrected wind tunnel test section dynamic pressure
r	distance from point $P'(\xi, \eta)$ to point P (y, z) of lifting arc

s	curvilinear coordinate along lifting arc, positive starboard
$\hat{s}$	unit tangent vector along lifting arc, positive starboard
s_t	lifting arc curvilinear semispan
sfc	specific fuel consumption in pounds per brake horsepower-hour
$(sfc)'$	specific fuel consumption in pounds per hour per pound of thrust
t	model thickness
t_m	maximum model thickness
w	induced downwash
w_r	radially induced velocity
x	chordwise coordinate, measured from wing leading edge or from lifting line, positive aft
x_{cp}	chordwise location of wing center of pressure
y, ζ	spanwise coordinate, measured from wing centerline, positive starboard
z, η	vertical coordinate, positive upward
Γ	circulation
Γ_0	circulation at wing centerline
ΔC_{D_i}	model induced drag increment due to tunnel test section boundary-induced upwash
$\Delta C_{D_{WB}}$	coefficient of drag increment due to wake blockage
ΔD_B	drag increment due to model buoyancy
ΔP	pressure difference; force loading
$\Delta \alpha$	model angle of attack increment due to tunnel test section boundary-induced upwash and streamline curvature

$\Delta\alpha_i$	model angle of attack increment due to tunnel test section boundary-induced upwash
α	angle of attack
α_a	local absolute angle of attack
α_c	wing centerline angle of attack
α_i	induced angle of attack
α_L	local airfoil section geometric angle of attack
$\alpha_{L=0}$	angle of zero-lift line with chord line
α_o	local effective angle of attack
α_t	change in angle of attack at wing tip due to wing twist
α_u	uncorrected model angle of attack
β, ϕ	angle of radius vector R with horizontal, channel wing
$\gamma(x,\theta)$	vortex surface density distribution
δ	factor for wind tunnel boundary corrections, see equations (4.39) and (4.40)
ϵ	downwash angle at the wing
ϵ	ratio of model frontal area to tunnel test section area
ϵ_A	small parameter in asymptotic expansion procedure, here inversely proportional to aspect ratio
η	propulsive efficiency
θ	angle of radius vector R with horizontal, ring wing
θ	angle of vector r with horizontal, channel wing
μ	viscosity
π_R	ratio of cylinder surface area to projected area
ρ	density
σ	ρ/ρ_0

τ local dihedral angle

τ_1 factor for drag increment due to wake blockage, see equation (4.35)

τ_2 factor for angle of attack increment due to boundary-induced streamline curvature, see equation (4.41)

Ψ angle subtended by channel wing tip region curvilinear span

INTRODUCTION

Although full-scale channel wing and ring wing aircraft have been built and flown (the Custer Channel Wing aircraft and the Bell X-22A are examples, respectively), few analyses of the aerodynamics of these wings have been published. Also, the aircraft mentioned operate with each channel or ring submerged in a propeller slipstream. Simple methods of predicting the lift and drag of isolated channel wings and ring wings are needed in order to evaluate the possible advantages of these wings.

This paper undertakes to evaluate the validity of published theory for the lift and drag of ring wings, to develop a suitable analysis for channel wings, to experimentally verify the latter, and to investigate briefly the performance advantages, if any, of these nonplanar wings. Of necessity, the experimental data for isolated channel wings were obtained by the author by means of a wind tunnel test program, which is reported herein.

CHAPTER I

DEFLECTED STREAMTUBE THEORY

Ribner's Theory for the Ring Wing

Ribner [1] published a brief deflected streamtube theory for ring airfoils at angle of attack in 1947. He assumed that the streamtube threading the ring wing is deflected as a rigid circular cylinder. Combining this assumption with the notion of a vortex bound in the ring allowed the determination of the circulation distribution and the downwash angle. A detailed account of Ribner's derivation will not be given here, since a similar derivation is presented for the channel wing. Ribner's result for ring wing lift was:

$$L = \frac{4R/\pi c}{1 + 4R/\pi c} \rho V^2 \pi^2 R c \alpha_c \quad . \tag{1.1}$$

Nomenclature for the ring wing are shown in Figure 1.

The ring wing induced drag is easily obtained from Ribner's [1] equations for outward normal force and downwash angle:

$$\frac{dN}{R\,d\theta} = \frac{4R/\pi c}{1 + 4R/\pi c} \rho V^2 \pi c \alpha_c \sin\theta \tag{1.2}$$

$$\epsilon = \frac{\alpha_c}{1 + 4R/\pi c} \quad . \tag{1.3}$$

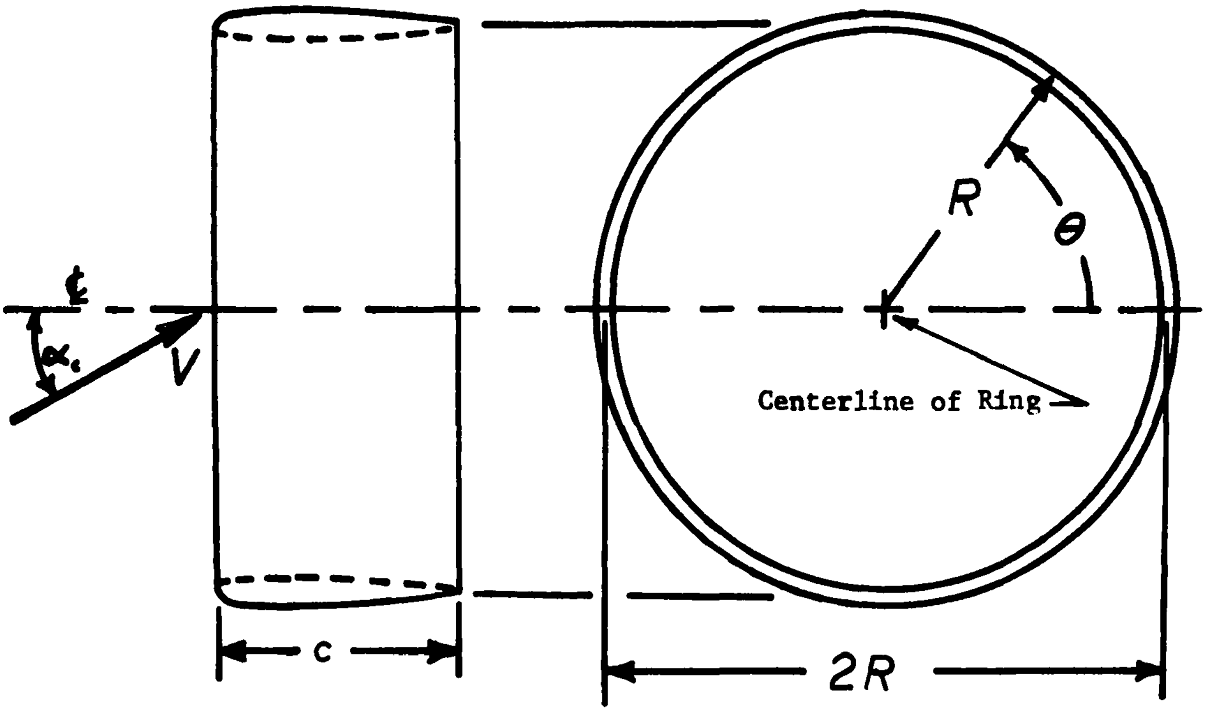

Projected Wing Area $S = 2Rc$

Total Wing Area = $2\pi Rc$

$AR = \frac{2R}{c}$

Figure 1. Ring wing nomenclature.

The local induced angle of attack, consistent with Ribner's assumptions, is:

$$\alpha_i = \dot{\epsilon} \sin\theta \quad . \tag{1.4}$$

Then the induced drag per unit arc is:

$$\frac{dD_i}{R\,d\theta} = \frac{dN}{R\,d\theta}\sin\alpha_i \approx \frac{dN}{R\,d\theta}\alpha_i$$

$$\frac{dD_i}{R\,d\theta} = \frac{dN}{R\,d\theta}\dot{\epsilon}\sin\theta \ , \tag{1.5}$$

where $dN/R\,d\theta$ is the outward normal force per unit arc. Substituting equations (1.2) and (1.3), we find that

$$\frac{dD_i}{R\,d\theta} = \frac{4R/\pi c}{(1 + 4R/\pi c)^2}\rho V^2 \pi c\,\alpha_c^2 \sin^2\theta \quad . \tag{1.6}$$

Integration of equation (1.6) gives the total induced drag of the ring wing:

$$D_i = \frac{4R/\pi c}{(1 + 4R/\pi c)^2}\rho V^2 \pi c R\,\alpha_c^2 \int_0^{2\pi} \sin^2\theta\, d\theta$$

$$D_i = \frac{4R/\pi c}{(1 + 4R/\pi c)^2}\rho V^2 \pi^2 R c\,\alpha_c^2 \quad . \tag{1.7}$$

Recalling equation (1.1), we see that the ring wing induced drag can be written as

$$D = \frac{L\,\alpha_c}{(1 + 4R/\pi c)} \quad . \tag{1.8}$$

However, equation (1.1) can also be solved for α_c, yielding

$$\alpha_c = \frac{L(4R/\pi c + 1)}{\rho V^2 \pi^2 R c\,(4R/\pi c)} = \frac{L(1 + 4R/\pi c)}{8\pi R^2 q} \quad . \tag{1.9}$$

With equation (1.9), the ring wing induced drag reduces to

$$D_i = \frac{L^2}{8\pi R^2 q} \quad . \tag{1.10}$$

The ring wing lift and induced drag coefficients are defined with the projected wing area, S = 2Rc:

$$C_L = L/qS \qquad \text{and} \qquad C_{D_i} = D_i/qS \quad .$$

Thus,

$$C_L = \frac{4R/\pi c \;\; \pi^2 \alpha_c}{(1 + 4R/\pi c)} = \frac{\pi^2}{(1 + \pi c/4R)} \alpha_c \quad , \tag{1.11}$$

and

$$C_{D_i} = \frac{C_L^2 S}{8\pi R^2} = \frac{C_L^2 c}{4\pi R} \quad . \tag{1.12}$$

By analogy to the standard definition for wing aspect ratio, the ring wing aspect ratio is defined as the square of the diameter, divided by the projected area:

$$AR = \frac{(2R)^2}{2Rc} = \frac{2R}{c} \quad . \tag{1.13}$$

Thus the lift and induced drag coefficients may be written as

$$C_L = \frac{\pi^2}{(1 + \pi/2AR)} \alpha_c \tag{1.14}$$

$$C_{D_i} = \frac{C_L^2}{2\pi AR} \quad . \tag{1.15}$$

Deflected Streamtube Theory for the Channel Wing

Adopting the approach used by Ribner [1] for the ring wing, assume that the streamtube which threads the channel wing is deflected essentially as a rigid cylinder, that at least the lower part of this cylinder is circular (with radius R), and that the channel wing may be represented by a line vortex bound in the wing. The vortex filaments streaming from the bound vortex will form a distribution of vorticity around the lower surface of the streamtube. This distribution is such as to produce the assumed deflection of the streamtube. Nomenclature used for the channel wing is shown in Figure 2.

The velocity induced at the point of intersection of the center line of the deflected streamtube and the vertical plane containing the bound vortex, due to one vortex filament, is

$$dq = \frac{d\gamma}{4\pi R}\,; \tag{1.16}$$

(Kuethe and Schetzer [2]), where $d\gamma$ is the strength of the filament. This induced velocity is perpendicular to a line connecting the vortex filament and the streamtube centerline. The vertical component of dq is $dq\cos\beta$, and the total induced downwash at the centerline due to the half-ring of trailing filaments is

$$w = \int_0^{\pi} \frac{d\gamma\cos\beta}{4\pi R}\,. \tag{1.17}$$

Now if the circulation about the bound vortex is denoted by Γ , then the strength of a vortex filament is

$$d\gamma = d\Gamma\,;$$

and, assuming that Γ is proportional to sin β , we write

$$d\gamma = d\Gamma = K\cos\beta\, d\beta\,, \tag{1.18}$$

where K is a constant. Thus,

$$w = \frac{K}{4\pi R}\int_0^{\pi}\cos^2\beta\, d\beta = \frac{K}{4\pi R}\left(\pi/2\right)$$

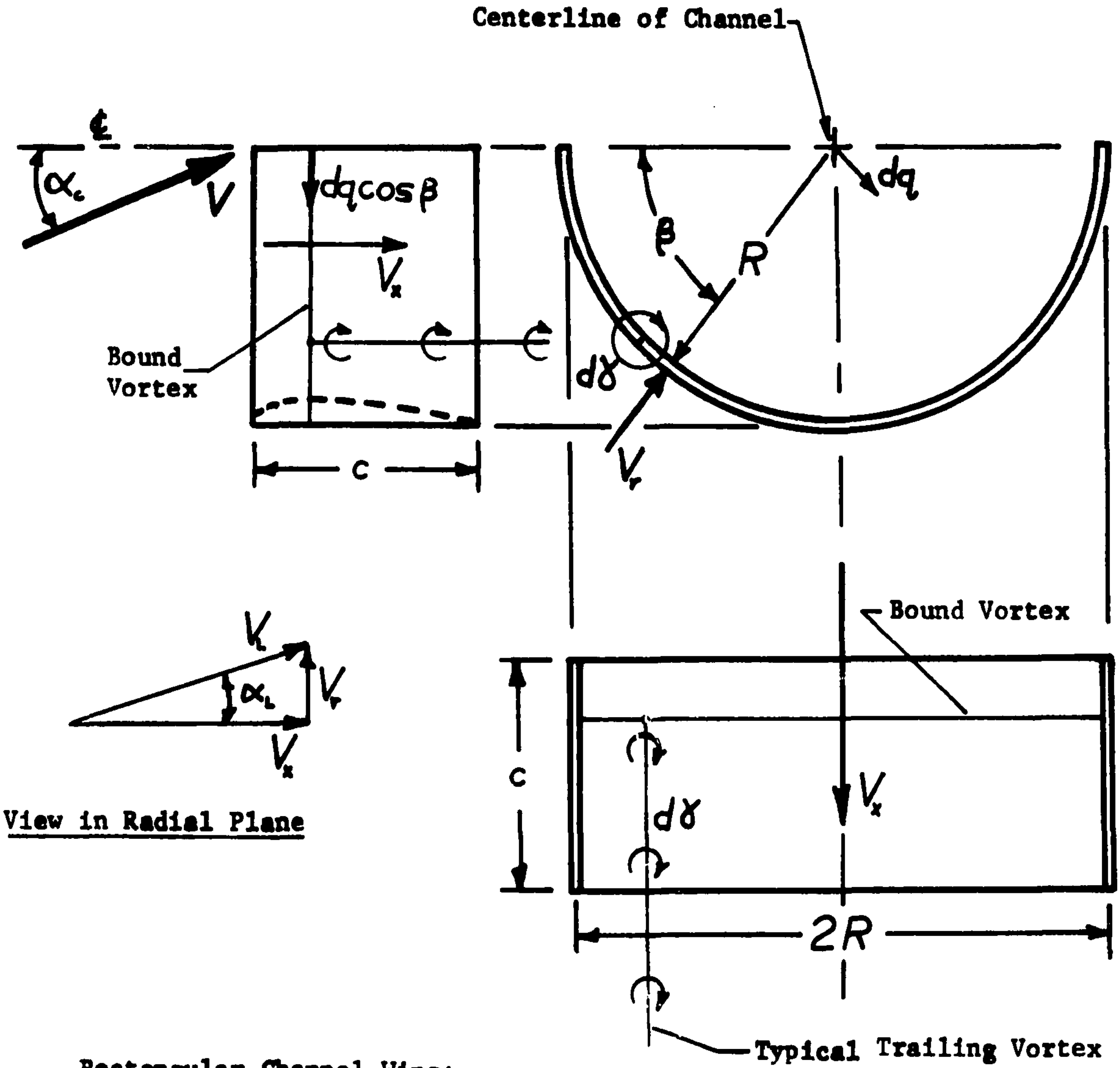

Rectangular Channel Wing:

Projected Wing Area $S = 2Rc$

Total Wing Area $S_c = \pi Rc$

$$AR = \frac{2R}{c}$$

Figure 2. Channel wing nomenclature.

$$w = \frac{K}{8R} , \qquad \text{or} \qquad K = 8Rw ,$$

so that

$$\Gamma = 8Rw \sin\beta \quad . \tag{1.19}$$

Then the circulation distribution is

$$\frac{d\Gamma}{R\,d\beta} = 8w\cos\beta \quad . \tag{1.20}$$

The downwash angle is given by

$$\tan\epsilon = w/V \quad .$$

If it is assumed that $w/V \ll 1$, then

$$w = V\epsilon ,$$

and

$$\frac{d\Gamma}{R\,d\beta} = 8V\epsilon\cos\beta \quad . \tag{1.21}$$

Consistent with the assumption of the form of Γ , the local velocity induced radially outward at the channel wing is

$$w_r = w\sin\beta ,$$

or

$$w_r = V\epsilon\sin\beta \quad . \tag{1.22}$$

Then the local induced angle of attack is

$$\alpha_i = \tan^{-1}\frac{w_r}{V} \approx \frac{w_r}{V} = \frac{V\epsilon\sin\beta}{V}$$

$$\alpha_i = \epsilon\sin\beta \quad . \tag{1.23}$$

The local airfoil section geometric angle of attack for an untwisted channel wing is derived in Chapter VI:

$$\alpha_L = \tan^{-1}(\tan\alpha_c \sin\beta) \tag{1.24}$$

where α_c is the channel centerline angle of attack. For small α_c, α_L can be approximated with small error by

$$\alpha_L = \alpha_c \sin\beta \quad , \tag{1.25}$$

and this simplification will be used in the present case. Then the local effective angle of attack is

$$\alpha_o = \alpha_L - \alpha_i$$

$$= \alpha_c \sin\beta - \epsilon \sin\beta$$

$$\alpha_o = (\alpha_c - \epsilon)\sin\beta \tag{1.26}$$

(only symmetric airfoil sections are considered here).

By the Kutta-Joukowski theorem, the normal force per unit arc is

$$\frac{dN}{R\,d\beta} = \rho V \Gamma \quad . \tag{1.27}$$

But also, by definition,

$$\frac{dN}{R\,d\beta} = q\, c_l\, c \cdot (1) = \frac{\rho}{2} V^2 c_l\, c \quad . \tag{1.28}$$

Solving for the circulation, we obtain

$$\Gamma = \frac{1}{2} V c_l\, c \quad . \tag{1.29}$$

If it is assumed, for convenience, that the section lift-curve slope is 2π, then the section lift coefficient is

$$c_l = 2\pi\alpha_o \quad ,$$

and the circulation is

$$\Gamma = \pi V c \alpha_o \quad . \tag{1.30}$$

With the substitution of equation (1.26), the circulation becomes

$$\Gamma = \pi V c \left(\alpha_c - \epsilon\right) \sin\beta \ ; \tag{1.31}$$

thus the circulation distribution is

$$\frac{d\Gamma}{R\, d\beta} = \frac{\pi V c}{R}\left(\alpha_c - \epsilon\right)\cos\beta \quad . \tag{1.32}$$

Equating equations (1.21) and (1.32) yields the downwash angle at the channel wing:

$$8 V \epsilon \cos\beta = \frac{\pi V c}{R}\left(\alpha_c - \epsilon\right)\cos\beta$$

$$8\epsilon + \frac{\pi c}{R}\epsilon = \frac{\pi c}{R}\alpha_c$$

$$\epsilon = \frac{1}{(1 + 8R/\pi c)}\alpha_c \quad . \tag{1.33}$$

The circulation can now be obtained with equations (1.31) and (1.33):

$$\Gamma = \pi V c \left[\alpha_c - \frac{1}{(1 + 8R/\pi c)}\alpha_c\right]\sin\beta$$

$$= \pi V c \left[\frac{1 + 8R/\pi c - 1}{8R/\pi c + 1}\right]\alpha_c \sin\beta$$

$$\Gamma = \left(\frac{8R/\pi c}{8R/\pi c + 1}\right)\pi V c\, \alpha_c \sin\beta \quad . \tag{1.34}$$

Again using the Kutta-Joukowski theorem, the inward normal force per unit arc is

$$\frac{dN}{R\,d\beta} = \rho V \Gamma = \left(\frac{8R/\pi c}{8R/\pi c + 1}\right) \rho V^2 \pi c \alpha_c \sin\beta \quad . \qquad (1.35)$$

Now consider the incremental lift force:

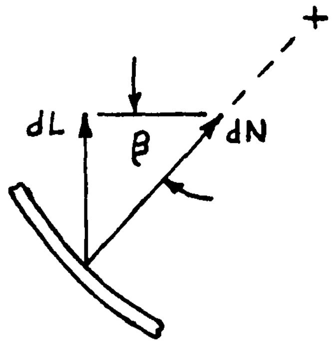

$$dL = dN \sin\beta$$

$$\frac{dL}{R\,d\beta} = \frac{dN}{R\,d\beta} \sin\beta \,.$$

Then, with equation (1.35),

$$\frac{dL}{R\,d\beta} = \left(\frac{8R/\pi c}{8R/\pi c + 1}\right) \rho V^2 \pi c \alpha_c \sin^2\beta \quad . \qquad (1.36)$$

The total lift is obtained by integrating equation (1.36) around the channel:

$$L = \left(\frac{8R/\pi c}{8R/\pi c + 1}\right) \rho V^2 \pi R c \alpha_c \int_0^{\pi} \sin^2\beta \, d\beta$$

$$= \left(\frac{8R/\pi c}{8R/\pi c + 1}\right) \rho V^2 \pi R c \alpha_c \left(\pi/2\right)$$

$$L = \left(\frac{4R/\pi c}{8R/\pi c + 1}\right) \rho V^2 \pi^2 R c \alpha_c \quad . \qquad (1.37)$$

Equation (1.37) represents the total lift produced by a semicircular channel wing (below the stall).

The channel wing induced drag per unit arc is

$$\frac{dD_i}{R\,d\beta} = \frac{dN}{R\,d\beta}\sin\alpha_i \approx \frac{dN}{R\,d\beta}\alpha_i \quad . \tag{1.38}$$

Recalling equation (1.23), we obtain

$$\frac{dD_i}{R\,d\beta} = \frac{dN}{R\,d\beta}\,\epsilon\sin\beta \quad . \tag{1.39}$$

Substitution of equations (1.33) and (1.35) yields

$$\frac{dD_i}{R\,d\beta} = \left[\left(\frac{8R/\pi c}{8R/\pi c + 1}\right)\rho V^2 \pi c\,\alpha_c \sin\beta\right]\left[\left(\frac{\sin\beta}{8R/\pi c + 1}\right)\alpha_c\right]$$

$$\frac{dD_i}{R\,d\beta} = \frac{8R/\pi c}{(8R/\pi c + 1)^2}\,\rho V^2 \pi c\,\alpha_c^2 \sin^2\beta \ , \tag{1.40}$$

and integration around the channel gives the total induced drag:

$$D_i = \frac{8R/\pi c}{(8R/\pi c + 1)^2}\,\rho V^2 \pi R c\,\alpha_c^2 \int_0^\pi \sin^2\beta\,d\beta$$

$$D_i = \frac{4R/\pi c}{(8R/\pi c + 1)^2}\,\rho V^2 \pi^2 R c\,\alpha_c^2 \quad . \tag{1.41}$$

With equation (1.37), this result can be written as

$$D_i = \frac{L\,\alpha_c}{8R/\pi c + 1} \quad . \tag{1.42}$$

But equation (1.37) can also be solved for α_c :

$$\alpha_c = \frac{L\left(8R/\pi c + 1\right)}{\left(4R/\pi c\right)\rho V^2 \pi^2 Rc} = \frac{L\left(8R/\pi c + 1\right)}{8\pi q R^2} \quad . \tag{1.43}$$

Substituting in equation (1.42), we find the channel wing induced drag to be given by

$$D_i = \frac{L^2}{8\pi q R^2} \quad . \tag{1.44}$$

As for the ring wing, it is convenient to base the channel wing induced lift and drag coefficients on the projected wing area:

$$C_L = \frac{L}{qS} \qquad \text{and} \qquad C_{D_i} = \frac{D_i}{qS} \quad ,$$

where S = 2Rc (constant wing chord is assumed). Then

$$C_L = \frac{4R/\pi c}{\left(8R/\pi c + 1\right)} \cdot \frac{\rho V^2 \pi^2 Rc\alpha_c}{\left(\tfrac{1}{2}\rho V^2\right)(2Rc)}$$

$$= \frac{\left(4R/\pi c\right)\pi^2 \alpha_c}{8R/\pi c + 1}$$

$$C_L = \left(\frac{\pi^2}{2 + \pi c/4R}\right)\alpha_c \quad , \tag{1.45}$$

and

$$C_{D_i} = \frac{C_L^2\, q^2 S^2}{8\pi q R^2 q S} = \frac{C_L^2\,(2Rc)}{8\pi R^2}$$

$$C_{D_i} = \frac{C_L^2}{4\pi R/c} \quad . \tag{1.46}$$

Again as for the ring wing, the channel wing aspect ratio is defined as

$$\mathcal{R} = \frac{2R}{c},$$

so that

$$C_L = \left(\frac{\pi^2}{2 + \pi/2\mathcal{R}} \right) \alpha_c \tag{1.47}$$

and

$$C_{D_i} = \frac{C_L^2}{2\pi \mathcal{R}} \,. \tag{1.48}$$

These are the lift and induced drag coefficients resulting from a deflected streamtube theory for the channel wing.

CHAPTER II

COMPARISON OF DEFLECTED STREAMTUBE THEORY WITH EXPERIMENT AND OTHER THEORIES

Ring Wing

NACA TN 4117

Fletcher [3] reports the results of a wind tunnel test on model ring wings of aspect ratio 3, 1.5, 1.0, 2/3 and 1/3. Figure 3 presents measured lift coefficient for three of these wings, along with calculations from the Ribner deflected streamtube theory. Correlation is good for $\mathcal{R} = 3$, but the theoretical lift-curve slope is too high for the lower aspect ratios. The theoretical value is obtained from equation (1.14):

$$a = \frac{dC_L}{d\alpha_c} = \frac{\pi^2}{1 + \pi/2\mathcal{R}} \quad . \tag{2.1}$$

It should be noted that Fletcher [3] used a Clark Y airfoil section, whereas the Ribner theory was derived only for a symmetrical section. However, that does not account for the lack of agreement at low aspect ratio shown in Figure 3, since that disagreement is in the slope of the lift curves, not in the angle for zero lift.

In Reference [1] Ribner predicts the failure of the theory at very low aspect ratios, but his physical explanation (that the wake would align itself with the ring axis) is not supported by the wake

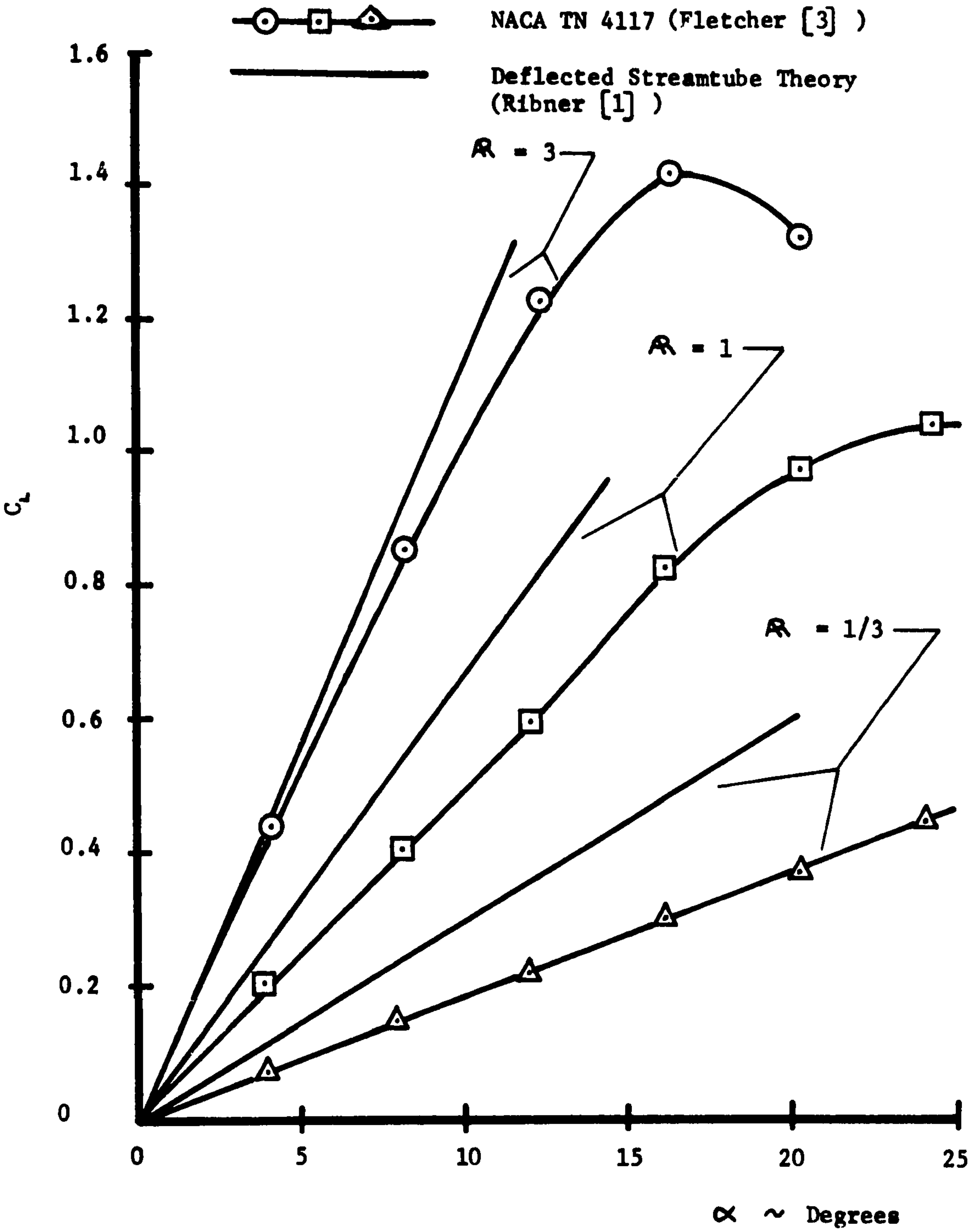

Figure 3. Comparison of deflected streamtube theory with experimental data for ring wings of low aspect ratio.

observations reported by Fletcher [3] .

Ribner [1] found as a general conclusion that the ring wing has twice the lift of a plane elliptic wing which spans the ring diameter and has one-quarter the total (not projected) area of the ring. That is, the elliptic wing has area

$$S_e = \frac{\pi(2R)c}{4} = \frac{\pi}{2} Rc \tag{2.2}$$

and aspect ratio

$$Æ_e = \frac{(2R)^2}{S_e} = \frac{4R^2}{\pi/2 \, Rc} = \frac{8R}{\pi c} \quad . \tag{2.3}$$

In terms of the aspect ratio $Æ$ of the ring wing,

$$Æ_e = \frac{4}{\pi}\left(\frac{2R}{c}\right) = \frac{4}{\pi} Æ \quad . \tag{2.4}$$

Therefore, with

$$a = a_o \frac{Æ}{Æ + 3} \ , \tag{2.5}$$

as recommended for low aspect ratio wings by Wood [4] , and a_o = 0.092/degree for the Clark Y airfoil section (Jacobs and Rhode [5]), the ring wing lift-curve slope by this method is

$$a = (2)\, a_o \frac{Æ_e}{Æ_e + 3} = 2a_o \frac{4/\pi \, Æ}{4/\pi \, Æ + 3}$$

$$a = a_o\left(\frac{8Æ}{4Æ + 3\pi}\right) \quad . \tag{2.6}$$

This result is labeled Method 1 in Figure 4, and exactly correlates the linear portion of the experimental data for $Æ = 3$. Agreement with experiment is good for $Æ = 1$, but poor for $Æ = 1/3$.

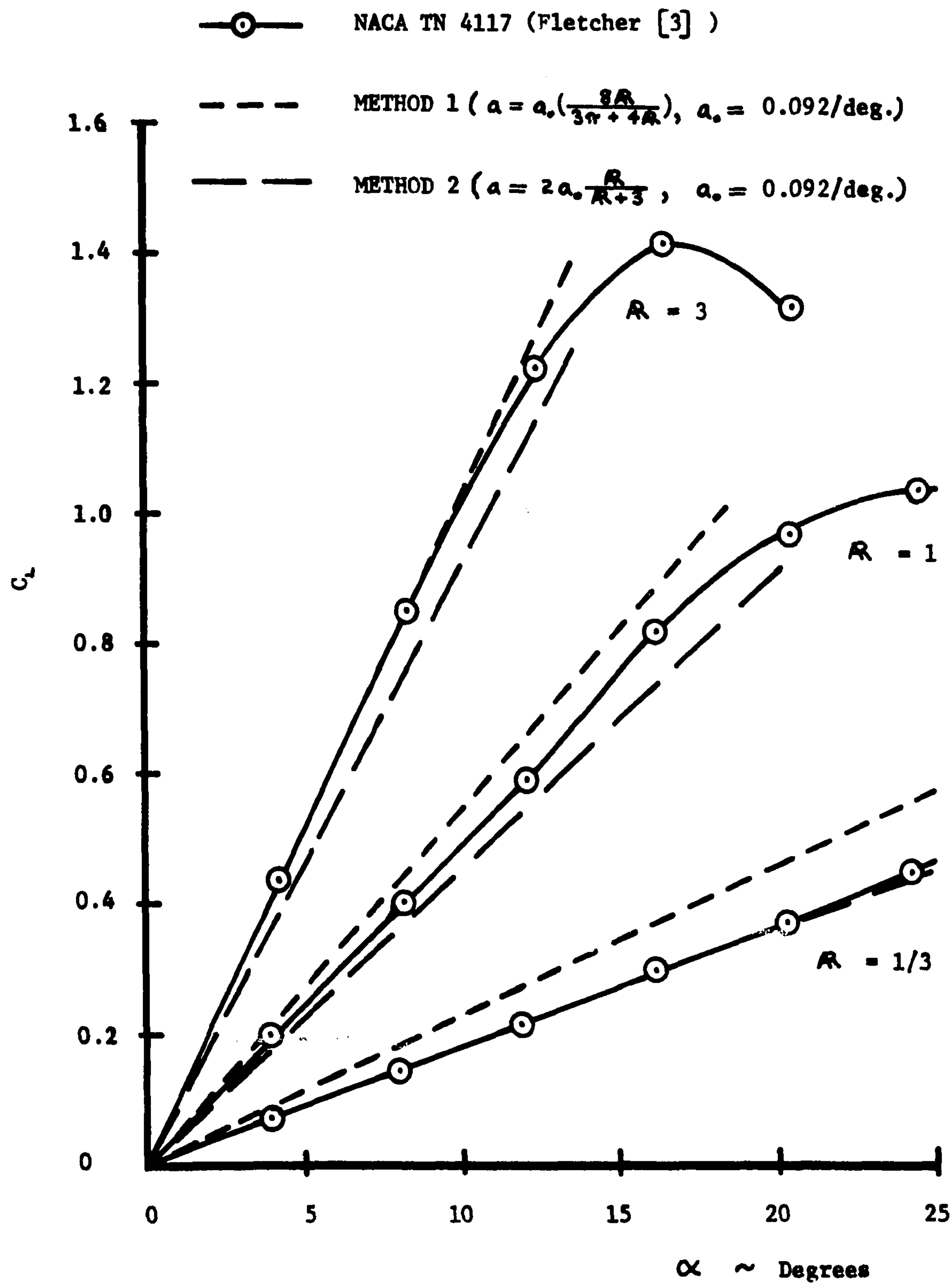

Figure 4. Lift coefficient for ring wings of low aspect ratio.

Method 2 in Figure 4 is simply twice the lift-curve slope (equation (2.5)) of a rectangular plane wing of the same aspect ratio as the ring wing, as recommended by Fletcher [3] . This method exactly correlates the experimental data for $\mathcal{R}$ = 1/3, but is a little low at $\mathcal{R}$ = 1. It is seen in Figure 4 that the average of Methods 1 and 2 would agree very well with experiment at $\mathcal{R}$ = 1.

Fletcher [3] found very good agreement with Ribner's deflected streamtube theory result for induced drag. The total wing drag was calculated using the measured C_D at $C_L = 0$ for the (constant) C_{D_0} :

$$C_D = C_{D_0} + \frac{C_L^2}{2\pi \mathcal{R}} \quad . \tag{2.7}$$

Drag polars, for $\mathcal{R}$ = 1/3 and 3, calculated in this manner are compared with the experimental data in Figure 5. Correlation of theory and experiment is good in both cases, but better for the $\mathcal{R}$ = 3 case.

<u>Experiments by Milla</u>

Milla [6] conducted wind tunnel tests in 1966 of a model airplane with ring wings and tail. A 14 inch diameter, $\mathcal{R}$ = 2.8, ring wing was attached directly to each side of the fuselage, and a smaller ring served as the empennage. Milla found that direct application of Ribner's theory would not correlate the experimental lift, but that an interference lift contribution was required.

Milla also found that an interference drag contribution to the Ribner theory was required. However, part of this lack of correlation was due to an incorrect derivation of the induced drag from

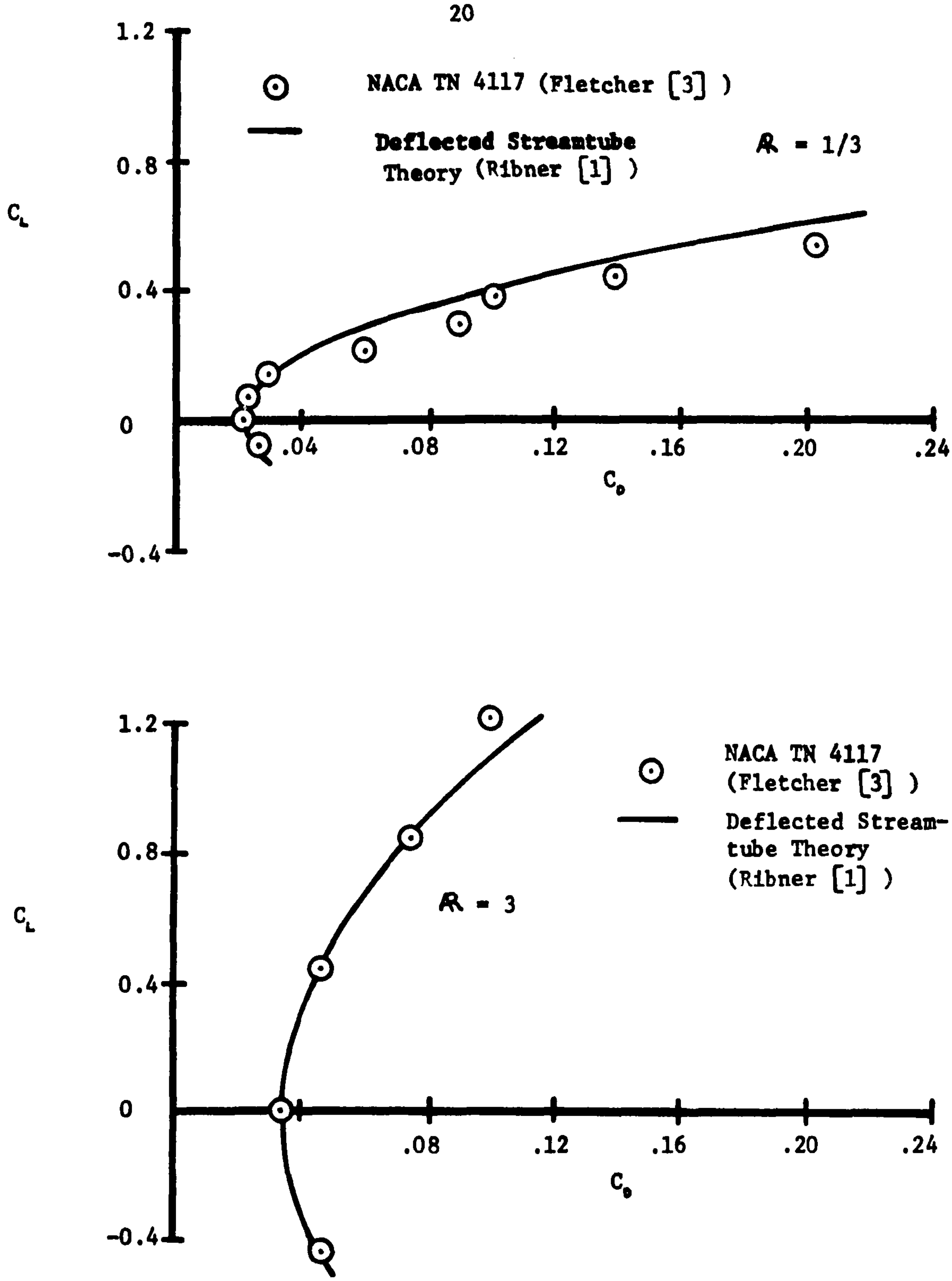

Figure 5. Drag polars for ring wings of low aspect ratio.

the results of Reference [1] :

$$C_{D_i} = \frac{C_L^2}{\pi^2 \text{AR}} \quad . \tag{2.8}$$

The correct relation is

$$C_{D_i} = \frac{C_L^2}{2\pi \text{AR}} \quad . \tag{1.15}$$

<u>NACA TR R-139</u>

Cone [7] predicted the circulation distributions required for minimum induced drag, and the corresponding maximum span efficiency factors, for many nonplanar wings. This optimization was performed on the basis of Munk's [8] theorem for minimum induced drag: the normal (to the local surface) component of the local induced velocity must be proportional to the cosine of the local "dihedral angle,"

$$q_n = K \cos \gamma \quad .$$

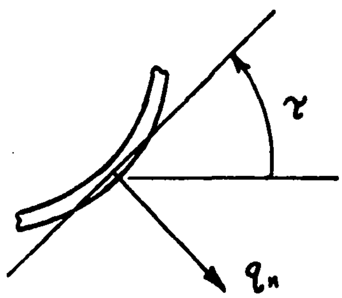

Solutions were obtained by conformal transformation, and by electrical/potential-flow analog techniques for the more complex forms. For the ring wing, Cone's result was

$$e = 2.0 \ ,$$

where the span efficiency factor e is defined by

$$C_{D_i} = \frac{C_L^2}{\pi e AR} \ , \tag{2.9}$$

and the aspect ratio AR is based on the projected wing span. Comparing equation (2.9) and equation (1.15), it is seen that Ribner's [1] theory yields exactly the same span efficiency factor, $e = 2.0$, for ring wings.

NAVWEPS RPT 8401

Reynolds [9] developed a lifting surface theory for the lift and pitching moment of a ring wing. The ring was represented by a cylindrical vortex surface at angle of attack, with Weissinger's general boundary condition imposed (radial component of induced flow is zero at vortex surface). The Kutta condition at the trailing edge is also imposed. These boundary conditions allow evaluation of a series representation for the vortex density distribution in the vortex surface, as a function of aspect ratio. Then the local force loading is given by the Kutta-Joukowski relation

$$\Delta P = \rho V \gamma (x, \theta) \ ,$$

where $\gamma(x, \theta)$ is the vortex surface density distribution.

Reynolds [9] gives the ring wing lift coefficient as

$$C_L' = \pi/2 \left(C_0 + 1/2 \, C_i \right) \alpha_c \ , \tag{2.10}$$

where C_L' is based on total surface area $2\pi Rc$. If this expression is converted to C_L based on projected area S = 2Rc, we have

$$C_L = \frac{\pi^2}{2}\left(C_0 + \tfrac{1}{2} C_1\right)\alpha_c \quad . \qquad (2.11)$$

Reynolds [9] evaluated the series coefficients for three aspect ratios:

TABLE 1

SERIES COEFFICIENTS FOR VORTEX DENSITY DISTRIBUTION OF RING WING, DUE TO REYNOLDS [9]

$A\!\!R$	c_0	c_1	c_2
∞	2.000	0	0
2.0	1.098	-0.238	-0.018
1.0	0.796	-0.415	-0.068

Infinite aspect ratio corresponds to the lifting-line case:

$$C_L = \frac{\pi^2}{2}(2)\alpha = \pi^2\alpha_c ,$$

and this agrees exactly with Ribner's [1] result, equation (1.14), when $A\!\!R = \infty$. For $A\!\!R$ = 1, however, the lifting surface theory gives

$$C_L = \frac{\pi^2}{2}(.796 - .207)\alpha_c = 2.90\,\alpha_c ,$$

while Ribner's theory (equation (1.14)) yields

$$C_L = \frac{\pi^2}{1 + \pi/2}\alpha_c = 3.84\,\alpha_c ,$$

a 32% difference. These results are compared in Figure 6, with Fletcher's [3] experimental data for $Æ = 1.0$. Reynolds' lifting-surface theory almost exactly correlates the wind tunnel data, while the Ribner theory is too optimistic. It is clear that the lifting-surface theory predicts lift coefficient more accurately at low aspect ratio than does the Ribner theory. Of course, for aspect ratios other than 1.0 or 2.0, the user would have to carry out the series evaluations required. For rapid estimates, the modifications of Ribner's theory (methods 1 and 2, Figure 4) may be preferred.

The ring wing pitching moment derived by Reynolds [9] (converted to the projected area) is

$$C_M = \frac{\pi^2}{16}\left(C_2 - C_1 \right) \alpha_e \,, \tag{2.12}$$

where the moment is measured about the quarter-chord point, and is positive nose-up. Equation (2.12) is compared in Figure 7 with Fletcher's [3] experimental data for ring wings of aspect ratio 1.0. Agreement is good, except for angles of attack around zero. Fletcher did not comment on the failure of the experimental pitching moment data to go to zero at zero angle of attack, as would be expected for a symmetrical ring wing.

Equation (2.12) yields a positive value for pitching moment (for positive angle of attack) for all aspect ratios evaluated by Reynolds [9] , except for $Æ = \infty$, where $C_M = 0$ is predicted. This trend with aspect ratio does not agree with the experimental trend found by Fletcher [3] , who measured a zero pitching moment slope

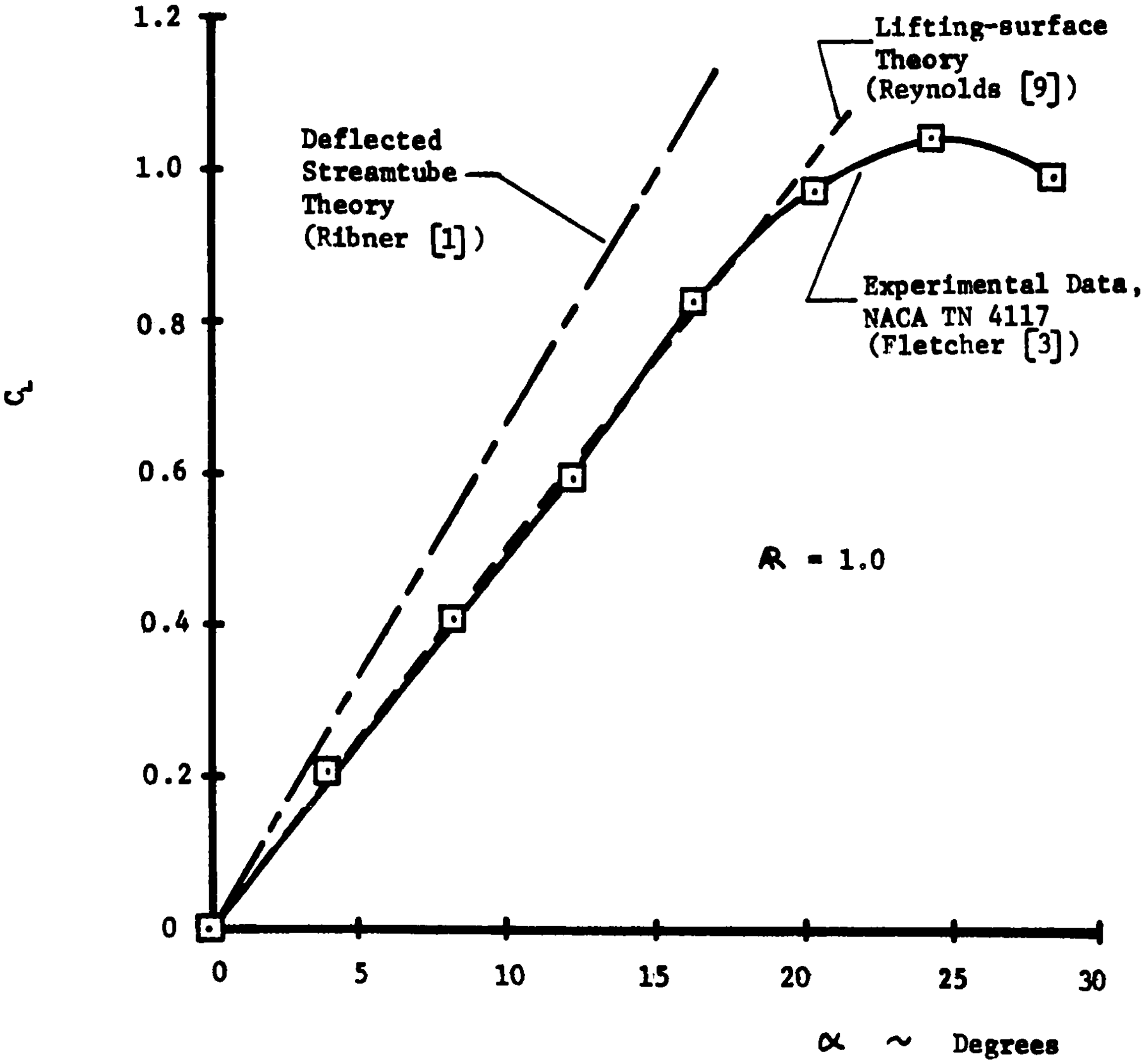

Figure 6. Comparison of lifting-surface and deflected streamtube theories for ring wing lift coefficient with experimental data.

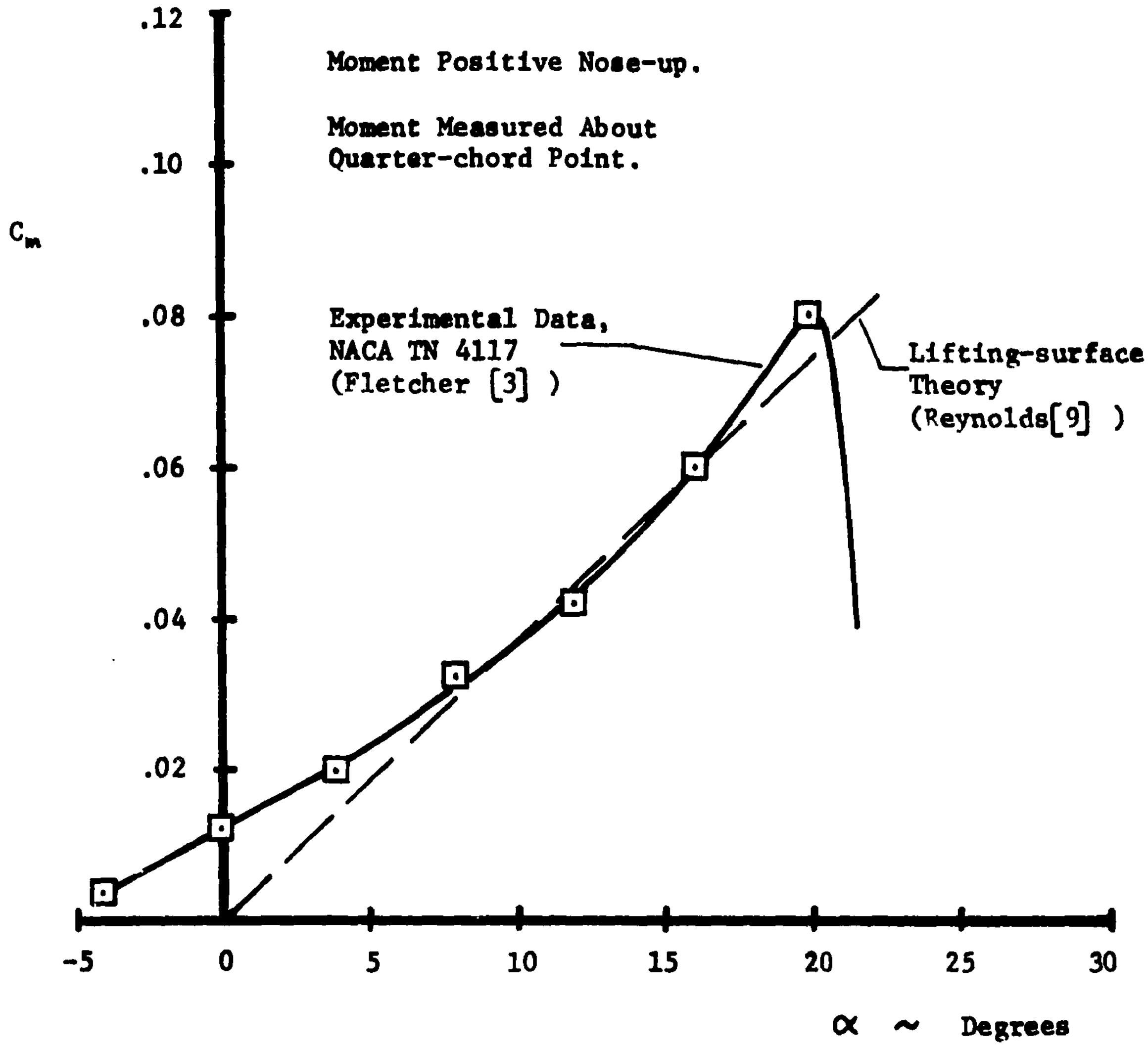

Figure 7. Pitching moment for ring wings of aspect ratio 1.0.

for $\mathcal{R}$ = 1.5, and a negative slope for $\mathcal{R}$ = 3.0.

The ring wing center of pressure location can be determined from Reynolds' [9] results for lift and pitching moment:

$$X_{cp} = \frac{c}{4} - \frac{M}{L} = \frac{c}{4} - \frac{c\,C_M}{C_L}\,, \tag{2.13}$$

where M is measured about the quarter-chord point, and X_{cp} is measured from the wing leading edge, positive rearward. Substitution of equations (2.11) and (2.12) into equation (2.13) yields

$$X_{cp} = \frac{c}{4} - \frac{c\,\frac{\pi^2}{16}(C_2 - C_1)\alpha}{\frac{\pi^2}{2}(C_0 + \frac{1}{2}C_1)\alpha} = \frac{c}{4}\left[1 - \frac{C_2 - C_1}{2(C_0 + \frac{1}{2}C_1)}\right]$$

$$X_{cp}/c = \frac{1}{4}\left(1 + \frac{C_1 - C_2}{2C_0 + C_1}\right)\,. \tag{2.14}$$

This equation gives X_{cp} = c/4 at infinite aspect ratio, which is the two-dimensional airfoil section classical theory (Glauert [10]) result for airfoils with C_M = 0 at zero lift. Results for other aspect ratios are shown in Figure 8. Correlation with Fletcher's [3] wind tunnel data is good for $\mathcal{R}$ = 1.0, but deteriorates as aspect ratio increases. The experimental center of pressure is at c/4 for aspect ratio of only 1.5, and is considerably aft of c/4 for aspect ratio of 3.0. This results in the negative slope of moment about the quarter-chord point.

<u>Conclusions for Ring Wing</u>

Ribner's [1] deflected streamtube theory gives good results for induced drag of isolated ring wings of any aspect ratio, and for lift of ring wings of aspect ratio about 3.0 and larger. Lift and

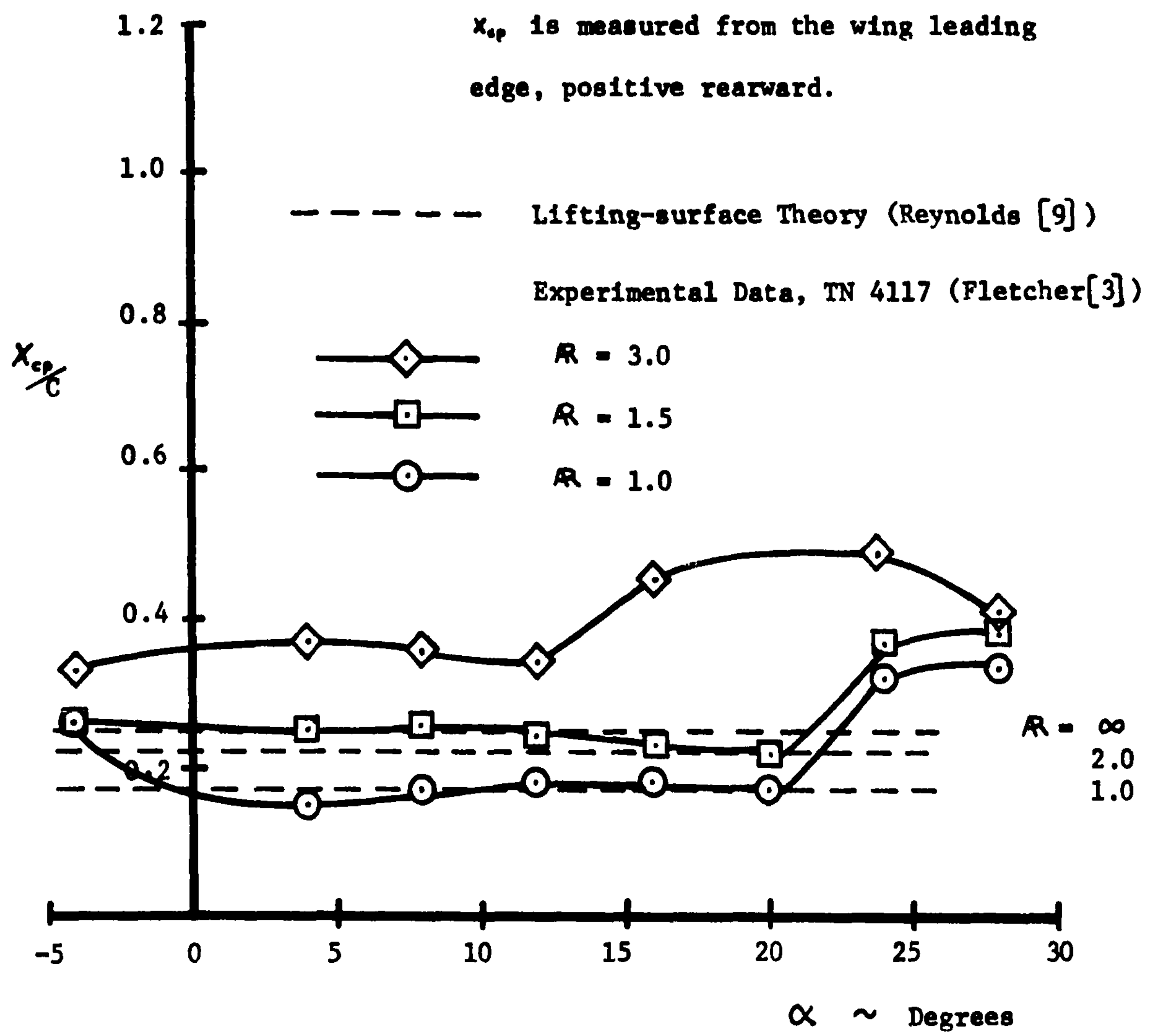

Figure 8. Ring wing center of pressure location.

induced drag coefficients are easily and rapidly calculable with this theory. Reynolds' [9] lifting surface theory accurately predicts the lift of ring wings, but is considerably more difficult to calculate than Ribner's results. Reynolds' theory also allows calculation of pitching moment, but the theoretical values do not agree with experiment for aspect ratios above 1.0.

Methods 1 and 2 (Figure 4), which are modifications of Ribner's theory [1] , are easy to use and yield good estimates for lift of low aspect ratio ring wings. The span efficiency factor of Ribner's theory is identical to the maximum value predicted by Cone [7] for ring wings, and agrees well with experimental data (Fletcher [3]). Ribner's deflected streamtube theory and Reynolds' lifting surface theory give identical results for lift at infinite aspect ratio.

Channel Wing

Despite a thorough literature search, the author was unable to find experimental data for isolated channel wings. Crook [11] and Chamberlain [12] conducted wind tunnel tests of plane rectangular wings, before and after the center section had been replaced by a semicircular channel:

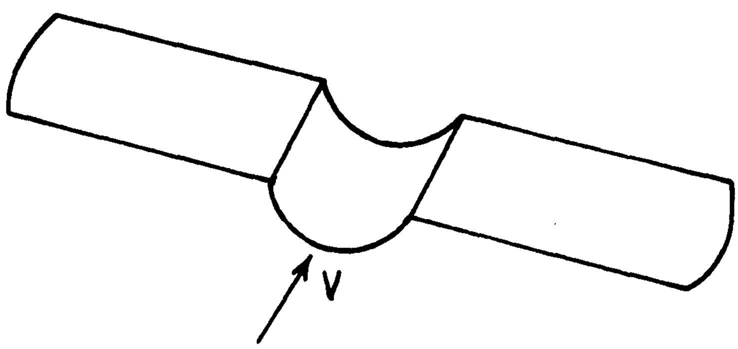

These channel sections were relatively small compared to the planar wing sections: in the first case, the channel diameter was approximately one-fourth the wing span, while in the latter case, it was one-sixth the wing span. The data reported in both cases indicate a slight advantage in lift and drag for the wing with the channel section. Unfortunately, the data in both references were not in dimensionless coefficient form (lift and drag), but were given in pounds-force, and the ambient conditions of the tests were not given. Thus references [11] and [12] are considered to have no significance for verification of theoretical predictions for isolated channel wings, and the data of these references are not presented here.

Hermes Lifting Surface Theory

Hermes [13] developed a lifting-surface theory for the channel wing, including the effect of a propeller operating in the channel as utilized by the Custer channel wing aircraft. The method is quite detailed and requires extensive machine computation. Certain calculated data for zero propeller lift and drag were extracted from Reference [13] and are compared herein with the deflected streamtube theory for the channel wing.

Figure 9 presents channel wing lift-curve slope as a function of aspect ratio, as calculated by Hermes' [13] lifting-surface theory and by the deflected streamtube theory developed in Chapter I. A rectangular planar wing is included for comparison. The latter curve was calculated using the finite wing lift-curve slope formulas

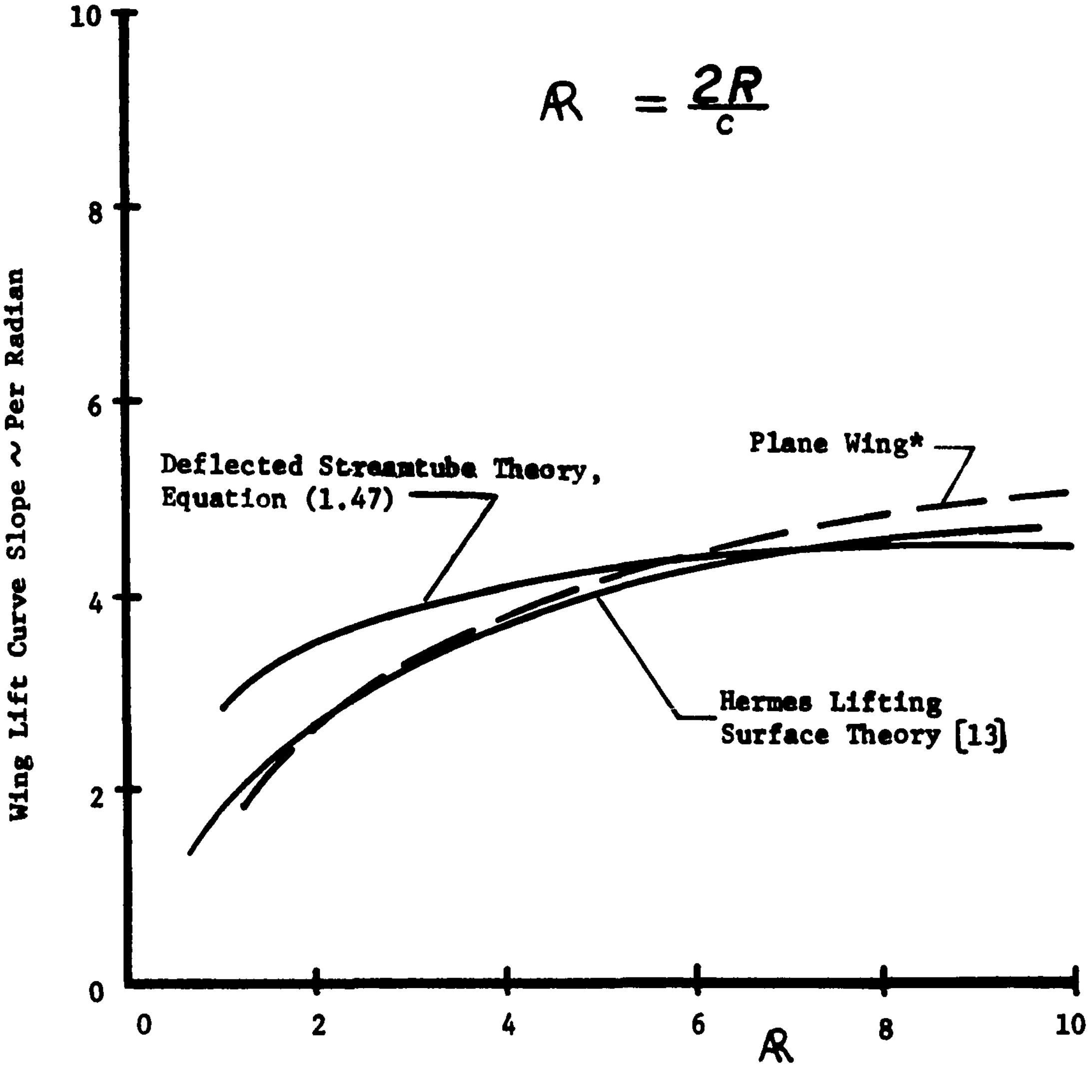

* Plane rectangular wing with $a_o = 2\pi$ assumed, and

$$a = \frac{a_o}{1 + \frac{a_o}{\pi AR}(1.17)} \qquad AR \geq 6 \qquad (2.15)$$

$$a = a_o \frac{AR}{AR + 3} \qquad AR < 6 \qquad (2.16)$$

Figure 9. Comparison of lifting-surface and deflected streamtube theories for channel wing lift-curve slope.

$$a = \frac{a_0}{1 + \frac{1.17 a_0}{\pi AR}} , \qquad AR \geq 6 , \tag{2.15}$$

$$a = a_0 \frac{AR}{AR + 3} , \qquad AR < 6 , \tag{2.16}$$

recommended by Dommasch, Sherby, and Connolly [14] and by Wood [4], respectively. Above $AR = 6$, the two channel wing theories yield approximately the same lift-curve slope, and both results are lower than for the plane wing. At low aspect ratio, the deflected streamtube theory is considerably more optimistic than either the Hermes theory or the planar wing.

Channel wing induced drag predicted by the two theories is shown in Figure 10. The calculations for a planar wing included for comparison utilized the equation

$$C_{D_i} = \frac{C_L^2}{0.95 \pi AR} , \tag{2.17}$$

recommended by Dommasch, Sherby, and Connolly [14]. The deflected streamtube theory gives a lower induced drag, for the same C_L, than does the Hermes lifting-surface theory. Both are lower than the planar wing.

NACA TR R-139

Cone's [7] theoretical result for maximum span efficiency factor for semicircular channel wings is

$$e = 1.5 ,$$

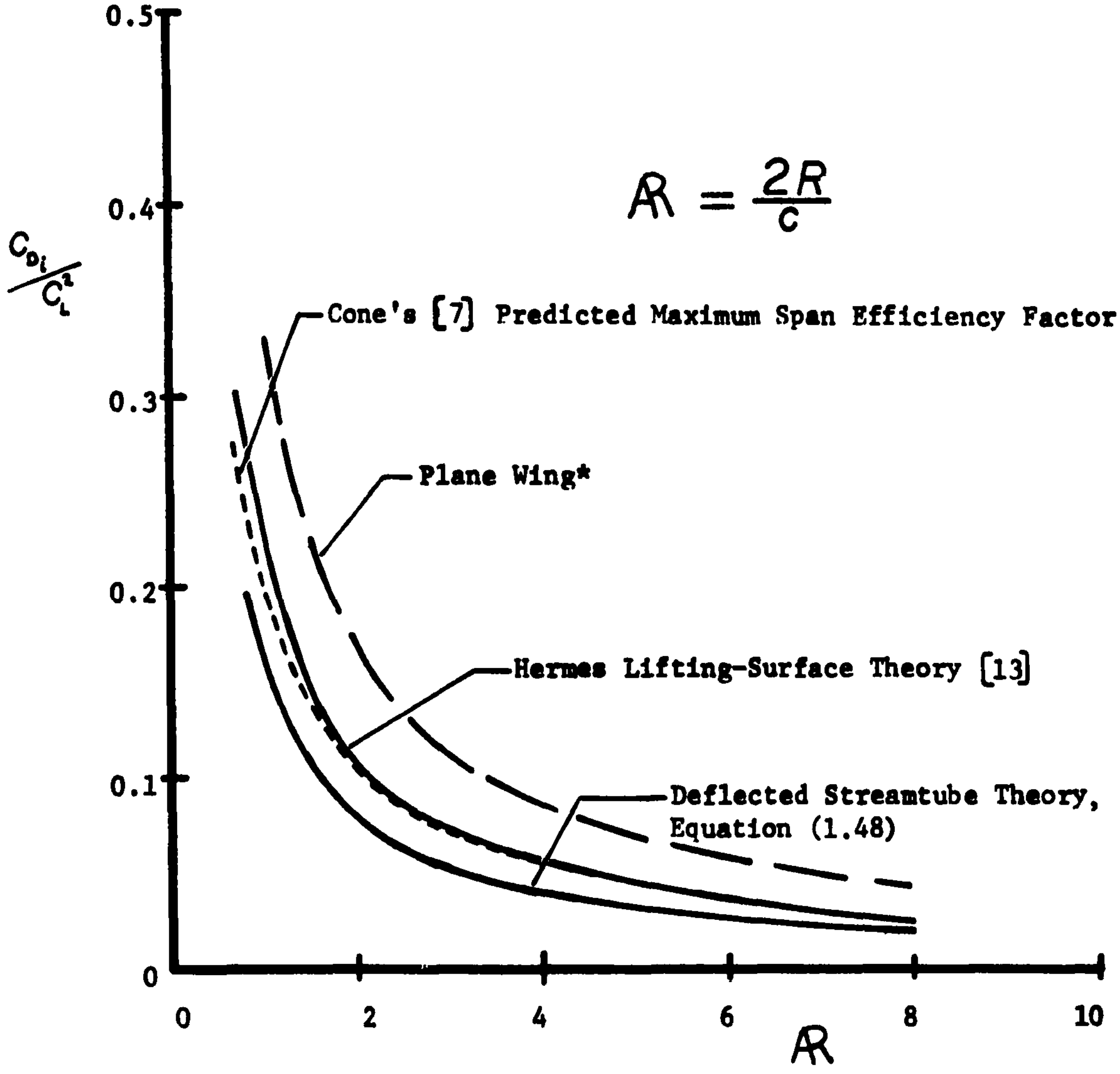

* Plane rectangular wing, $C_{D_i} = \frac{C_L^2}{(0.95)\,\pi\,AR}$ (2.17)

Figure 10. Comparison of lifting-surface and deflected streamtube theories for channel wing induced drag.

where

$$\pi e A\!\!R = C_L^2 / C_{D_i} \quad . \tag{2.18}$$

However, inspection of equation (1.48) indicates that the deflected streamtube theory predicts $e = 2.0$ for the channel wing. The value $e = 1.5$ gives approximately the same C_{D_i}/C_L^2 as Hermes' [13] lifting-surface theory, for $A\!\!R \geq 2$ (see Figure 10).

Conclusions for Channel Wing

A literature search revealed no experimental data for isolated channel wings. The deflected streamtube theory developed in Chapter I is optimistic with regard to induced drag, as compared to other theoretical developments. The channel wing wind tunnel tests described in the following chapters were planned and conducted to provide experimental data to resolve this lack of agreement.

CHAPTER III

CHANNEL WING WIND TUNNEL TEST PROGRAM

Test Program Requirements

The requirements established for the channel wing wing tunnel test program were:

1. Obtain reliable lift and drag data for isolated channel wings at low aspect ratio.
2. Minimize costs of the program.

Data for low aspect ratios were preferred because (1) the lifting line theory was expected to be less accurate at low aspect ratios, and (2) applications of channel wings to aircraft would be expected to be at low aspect ratios. The second requirement was necessitated by the lack of any formal or complete financial support for this study.

Wind Tunnel Test Facility

The subsonic wind tunnel of the University of Oklahoma was utilized for the channel wing wind tunnel test program. This test facility is used for the undergraduate aerodynamics laboratory course, for research by faculty and graduate students, and by aircraft and other companies for research and development work. The wind tunnel is described in detail, and operation instructions are given, by Comp [15] . The tunnel facility is briefly described here.

The University of Oklahoma subsonic wind tunnel is a vertical (single) return, closed throat, atmospheric pressure tunnel. The test section has a 4-foot by 6-foot cross-section, made up of a rectangle 4-foot high by 2-foot wide and capped on each end with a semicircle of 2-foot radius. In appearance the cross-section appears almost elliptical; the area is 20.6 ft^2. The test section is 11 feet long.

The tunnel fan is a three-bladed, 7-foot diameter propeller driven through an extension shaft by an Allison V1710 1200 horsepower engine. The test section velocity range is 100 mph to 200 mph, and the turbulence factor is 1.35. A pneumatic engine control device, utilizing differential pressure between the settling chamber and the test section, automatically holds the set test section dynamic pressure. A cross-section of the tunnel is shown in Figure 11.

The balance system is a six component pyramidal-type with a single, central model support. Model forces are sensed by electrical resistance strain guages mounted on the weighing beams and are read directly from SR-4 strain indicators. The balance system capacities are:

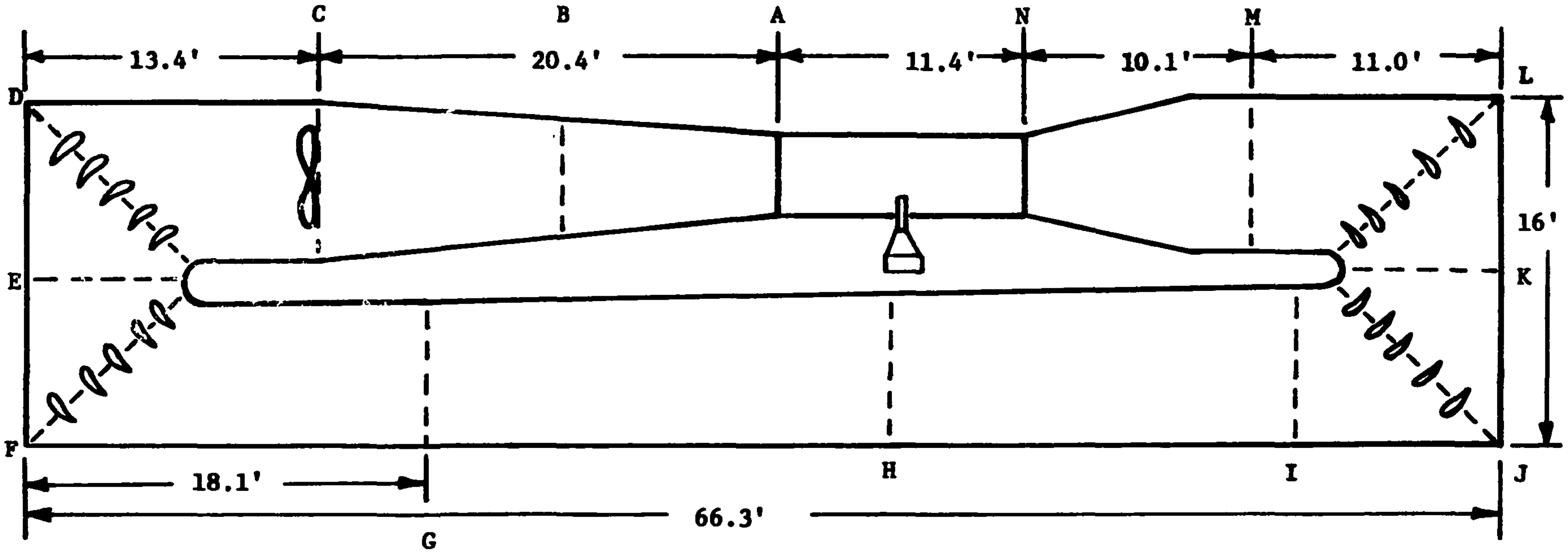

STATION	AREA ~ FT^2
A	20.6
B	31.6
C	38.5
D	47.8
E	58.9
F	57.3
G to M	70.0

Figure 11. University of Oklahoma subsonic wind tunnel.

TABLE 2

THE UNIVERSITY OF OKLAHOMA SUBSONIC WIND TUNNEL
BALANCE SYSTEM CAPACITIES

Component	Capacity	Component	Capacity
Lift	+500/-300 lbs.	Pitching Moment	± 1200 in.-lbs.
Drag	± 200 lbs.	Rolling Moment	± 500 in.-lbs.
Side Force	± 150 lbs.	Yawing Moment	± 600 in.-lbs.
Pitch Angle	+25°/-15° (nominal)	Yaw Angle	± 30°

The actual pitch angle available depends, of course, on the tail jack system geometry of the individual model. Test section dynamic pressure is indicated by an inclined water manometer.

Modifications of Model Mounting System

Since the stall characteristics of isolated channel wings were not known, it was necessaty to provide the capability for testing to relatively high angles of attack. This required modification of the tail jack system and of the standard mounting ring which is bolted to the test model and pinned to the top of the tunnel mounting system bayonet. Mr. Earl Finch, University of Oklahoma Aerospace Engineering machinist, fabricated a 6-inch extension for the lower arm of the tail jack system. With Mr. Finch's assistance, the author milled the bayonet clearance slot of a spare mounting ring to allow a greater angle of attack range. Selective filing of the attachment bolt heads was also found necessary. A full-scale layout of the modified model mounting and pitch control systems indicated the length required for the tail jack arm for each model. These modifications allowed an angle of attack range of $\pm$ 28° for the wind tunnel models. The large negative range was required because evaluation of interference lift and drag required the testing of each model in the inverted as well as the upright position.

Wind Tunnel Models

Aspect Ratio = 2.8 Model

The ring-wing model built and tested by Milla [6] was made available to the author by Professor Edward F. Blick of the University of Oklahoma. Milla constructed the wings of this model by bending an aluminum box spar into a circle, bonding on sections of balsa wood, and then shaping the balsa wood to an NACA 0015 section. One wing, Figure 12, of this model was cut in half, to obtain a channel wing with NACA 0015 (symmetrical) section, 14 inches diameter, and 5 inches chord, or an aspect ratio of 2.8, based on projected span. This model channel wing required extensive modifications to prepare it for use in the wind tunnel. These modifications were carried out by the author in the University of Oklahoma Aerospace Engineering Machine Shop. The modifications consisted principally of (1) fabricating and mounting a tail jack arm for wing tunnel pitch control, (2) machining the bayonet clearance slot in the box spar, (3) drilling mounting holes, (4) fabricating wing tips, and (5) refinishing

Figure 12. Milla's ring wing wind tunnel model.

the model. A special jig had to be built to hold the channel wing during the drilling and machining operations. The aspect ratio 2.8 channel wing model is shown on the left in Figure 13.

The small thickness of the wing model (as compared to a fuselage) and the large angle of attack range caused the model mounting ring and bayonet head to be exposed to the windstream at high angles of attack. Since the model support image system does not include these items, it was necessary to build special windscreens to shield them. These windscreens are shown in Figure 13 with both of the wind tunnel models. The complete set of items shown in front of each model in the figure accommodated the four run-configurations required for each model (upright, inverted, with and without the image system: see the discussion in Chapter IV on evaluation of interference and tare drag). The special windscreens attached directly to the model mounting plate. The aspect ratio 2.8 model is shown mounted in the wind tunnel in Figure 14.

Aspect Ratio = 1.0 Model

The aspect ratio 1.0 model used in this wind tunnel test program was one of two initially identical channel wing models built jointly by the author and another University of Oklahoma graduate student, Mr. Edward Parsons. A 12-inch diameter, 12-inch chord ring wing was built first, then cut in half to yield two channel wing models. Mr. Parsons modified his channel wing for testing with an engine and propeller.

As the first step in the construction of the aspect ratio

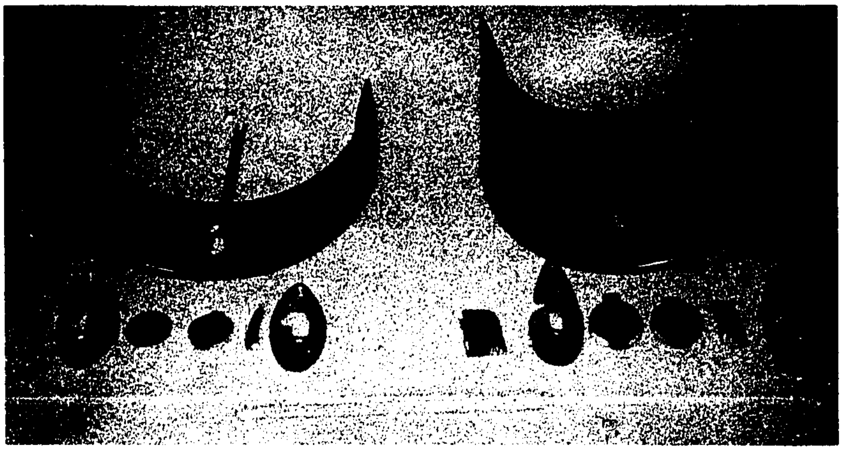

Figure 13. Channel wing wind tunnel models, with special windscreen devices.

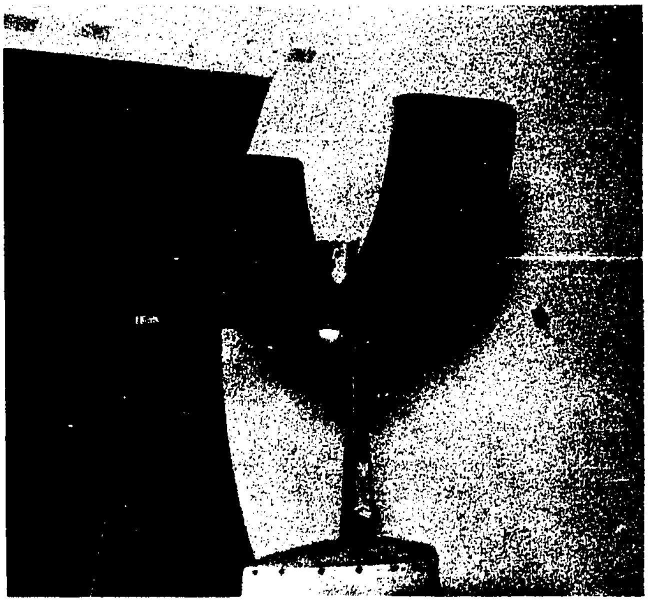

Figure 14. Aspect ratio 2.8 channel wing model mounted in wind tunnel.

1.0 ring wing model, steel plates for each planned channel wing were drilled for mounting bolts and milled for bayonet clearance. The plates were bent to fit the wing curvature by heating with a welding torch and hammering with a sledge, while clamped in a vise. The plates were then quenched in water.

Next, a "blank" for lathe turning was constructed by laminating ½ inch thick strips of Honduras mahogany with glue into the octagonal block shown in Figure 15. Note that the center was left hollow to reduce labor and the amount of wood required. The steel mounting plates were imbedded in carefully measured positions in the block during the laminating process. The use of Honduras mahogany for wind tunnel models was recommended by Pope and Harper [16] . The cost of this wood was donated by the Custer Channel Wing Corporation.

After curing, the laminated block was mounted in a wood lathe in the University of Oklahoma Wood Working Shop and turned to a ring wing with NACA 4412 airfoil section, 12-inch diameter (measured to chord line), and 12-inch chord, Figure 16. The camber of the 4412 section was turned outwards; that is, the "top" of the section was toward the inside. Finally, the completed ring wing was cut in half to obtain two channel wings of aspect ratio 1.0.

Construction of the model was completed by drilling to expose the bolt holes and bayonet clearance slot in the mounting plate, and fabricating and installing of tail jack arm. This model also required special windscreens, as discussed above for the aspect ratio 2.8 model. The aspect ratio 1.0 model is shown on the right in

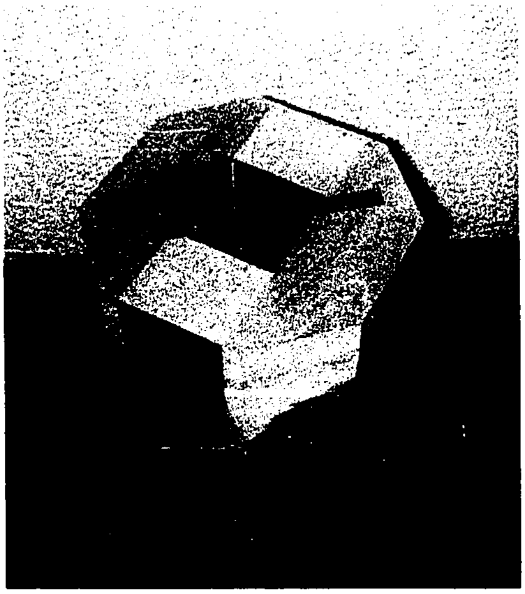

Figure 15. Mahogony "blank" for wood lathe turning of ring wing.

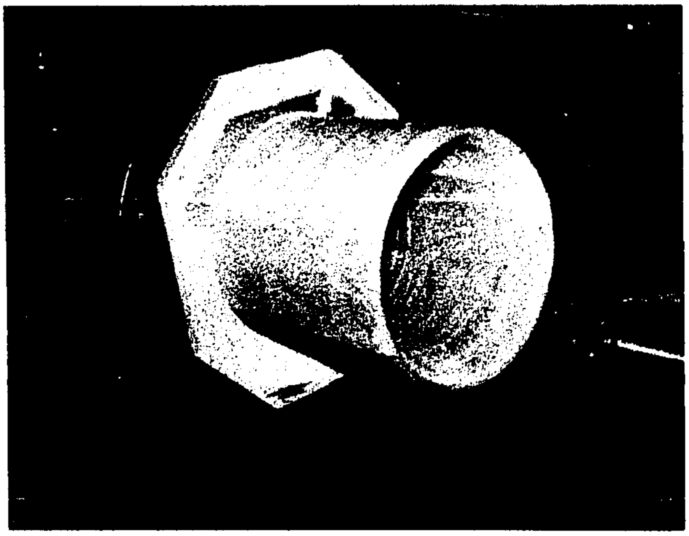

Figure 16. Aspect ratio 1.0 wing before separation into two channel wings.

Figure 13, and mounted in the wind tunnel, Figure 17.

Both models were finished with three coats of clear and two coats of colored model airplane dope, with light sanding with fine sandpaper between coats. Model airplane dope was used because the aspect ratio 2.8 model had previously been finished (as part of Milla's model) with this type of paint. Before application of the clear dope, the aspect ratio 1.0 model was sanded with rough sandpaper and sealed with model airplane sanding sealer. The color coats were sprayed on both models.

Boundary Layer Transition Strips

On the advice of Pope and Harper [16] , the author planned the wind tunnel tests to include tests with and without boundary layer transition strips. Pope and Harper caution that laminar separation effects may cause difficulty in wind tunnel testing at (relatively) low Reynolds numbers, and advise that testing be done with boundary layer transition strips installed on the model to force transition to a turbulent boundary, thus avoiding premature separation.

Pope and Harper [16] recommend a transition strip 1/8 to 1/4 inch wide, composed of carborundum grit, and located at about 5% chord and at 5% fuselage length. The formula

$$D_g = 4800/Re \quad \text{inches} \qquad (3.1)$$

is suggested for the grit diameter. Considering the smaller (chord) model, the Reynolds number was expected to be about 500,000. Thus,

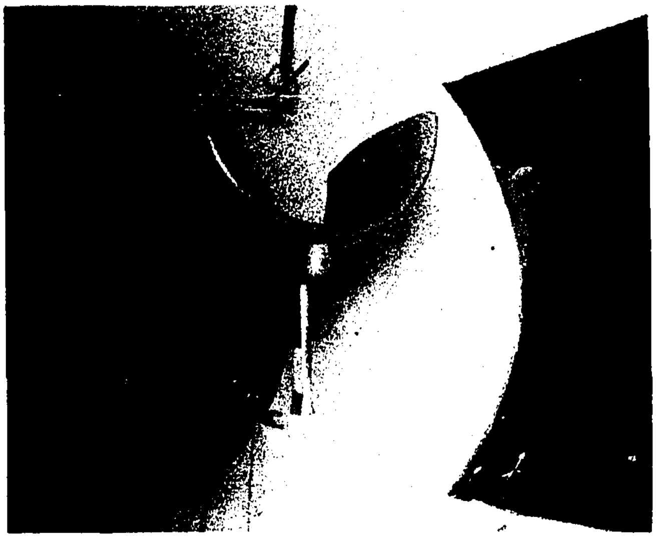

Figure 17. Aspect ratio 1.0 channel wing model mounted in wind tunnel.

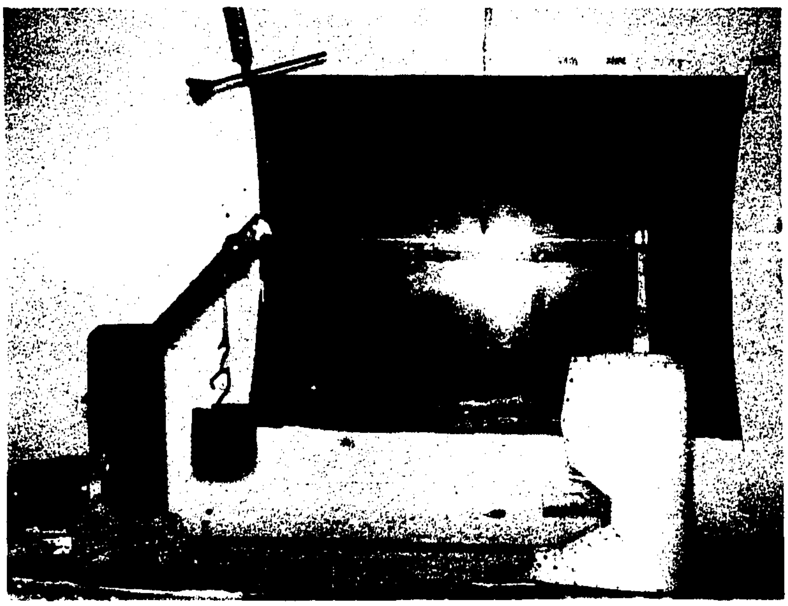

Figure 18. Calibration of drag scale, University of Oklahoma subsonic wind tunnel.

$$D_s = \frac{4800}{5.0 \times 10^5} = 0.0096 \text{ inches},$$

which corresponds to a commercial carborundum grit number of 70. The author was unable to obtain this carborundum grit; however, sand sifted to #100 mesh size, which yields grains of approximately 0.01 inch diameter, was obtained from the University of Oklahoma Department of Civil Engineering.

The sand was applied to one side of 1/8 inch wide strips of Scotch brand "Double-Sticky" tape, which were then attached to the wind tunnel models, top and bottom, at 5% chord.

Wind Tunnel Balance Calibration

During operation of the University of Oklahoma subsonic wind tunnel, model forces and moments are sensed as deflections of weighing beams by electrical resistance strain gauges, and the deflections are read directly from strain indicators. Conversion factors are required to obtain the actual forces from the measured deflections. These conversion factors are obtained by calibrating the balance system by applying known forces and moments and recording the resultant strain indicator readings. Special care must be exercised to insure that the known force is applied solely in the direction desired.

Calibration of the drag scale is shown in Figure 18. Drag weights were hung on a steel cable led over a pulley and attached to the bayonet head by means of a swivel and pin which applied the drag force as would a model. The plumb bob shown in the photograph was used to align the cable with the tunnel centerline, and a spirit level was used to insure that the cable was level. For the lift calibration, a similar method was used, except that a special scaffold with two pulleys was necessary to enable the cable to pull directly upward, as indicated by a plumb bob. Negative lift forces were simulated by stacking weights directly on the bayonet model attachment point. The alignment of the calibrating force was verified by observing that no deflection was indicated in the other channels (e.g., no deflection in lift and side force while calibrating drag).

The applied calibration forces and resulting strain guage deflection readings for lift and drag calibration are plotted in Figure 19. It may be seen in the figure that both calibration curves are linear; therefore, the slope of the curve may be used as a calibration factor. The lift and drag calibration factors as measured by the author were

$$\text{Drag:}\quad 0.118\ \frac{\text{pounds}}{\text{microinch}} \qquad\qquad \text{Lift:}\quad 0.290\ \frac{\text{pounds}}{\text{microinch}}\ .$$

Comp [15] gives

$$\text{Drag:}\quad 0.117\ \frac{\text{pounds}}{\text{microinch}} \qquad\qquad \text{Lift:}\quad 0.290\ \frac{\text{pounds}}{\text{microinch}}\ .$$

The close agreement lends confidence in the calibration factors measured in this program. The factors measured by the author were used in the data reduction because it was considered probable that they reflected the conditions under which the data were obtained

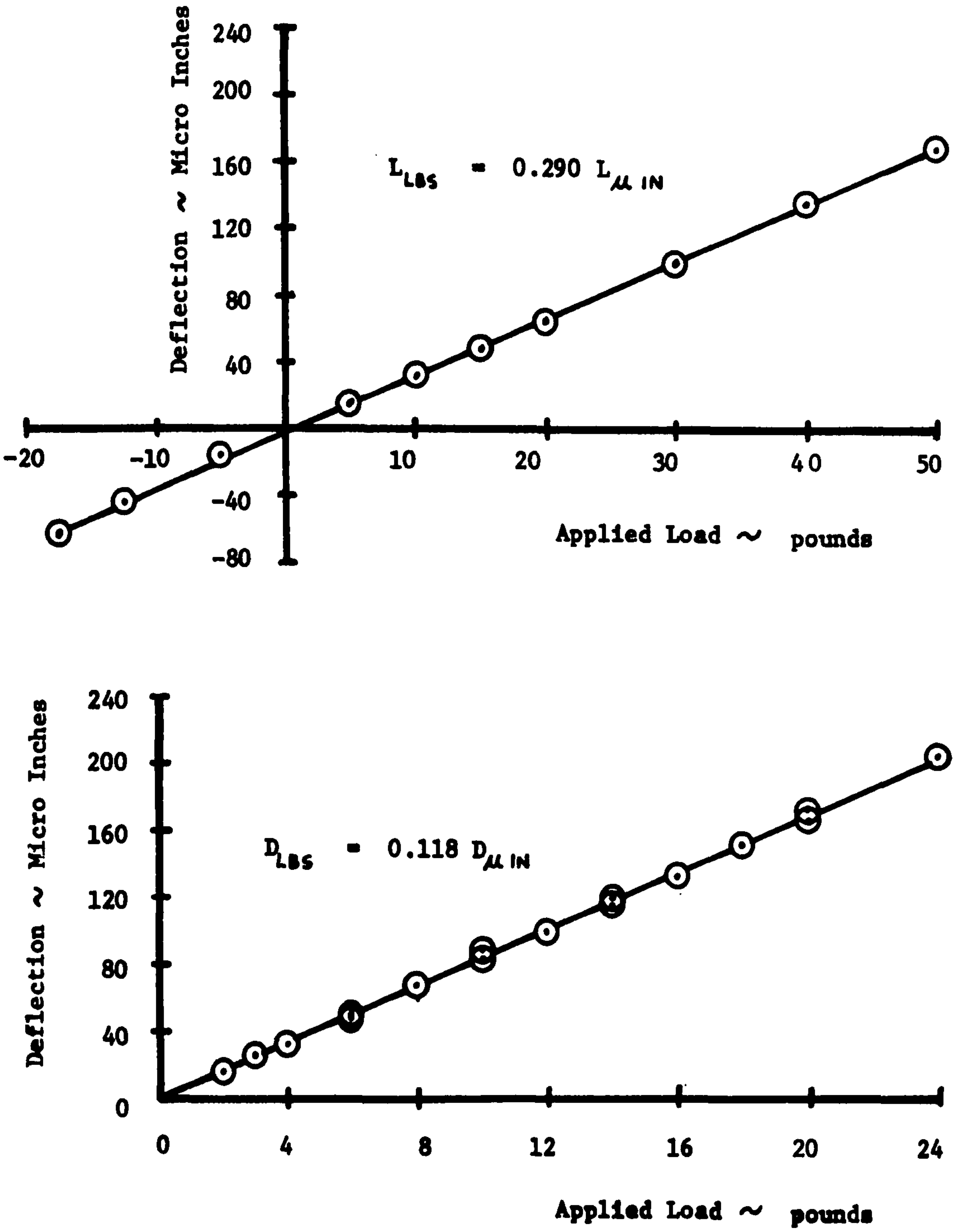

Figure 19. Wind tunnel balance calibration.

more correctly than calibration factors measured several years before.

Calibration of the model pitch angle indicator scale was necessary because the actual pitch angle of the model depends on the model and tail jack dimensions and geometry. This calibration was achieved by measuring the model pitch angle with a spirit level for several pitch indicator readings. In making these measurements, it was found that the backlash in the pitch change mechanism was so severe that repeatable settings could be achieved only by always approaching a pitch setting from the same direction. Consequently, throughout the wind tunnel test program reported herein, pitch settings were approached always from a more nose-down position. The pitch angle calibrations for both models are shown in Figure 20.

Test Plan

As described above, two channel wing tunnel models were constructed: an aspect ratio 2.8 model and an aspect ratio 1.0 model, where aspect ratio is based on projected span. It was desired to test each model both with and without a boundary layer transition strip. Also, as discussed in Chapter IV, four test runs (upright, inverted, with and without support image system) are required for each model configuration in order to evaluate tare and interference lift and drag. Thus a total of 16 tunnel runs were planned.

The order of the tunnel test runs was planned to minimize model change time and thus minimize wind tunnel down time. This objective may seen of minor importance in a university wind tunnel, but it becomes very important indeed in industrial and government

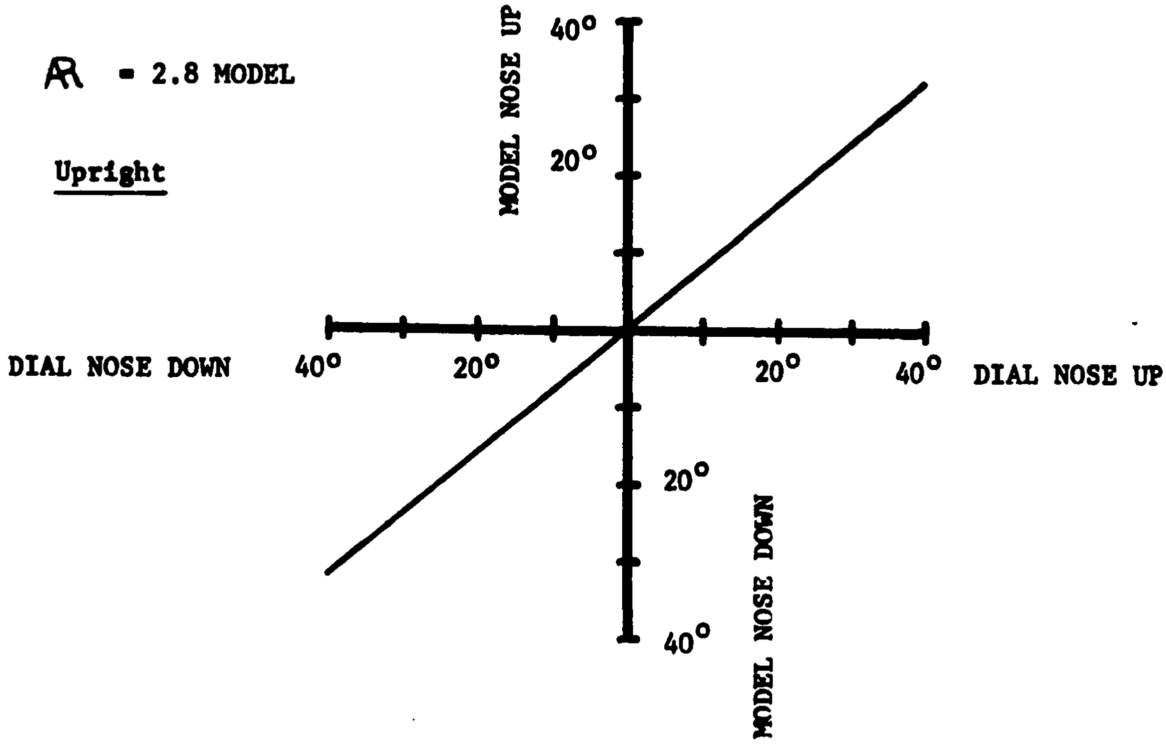

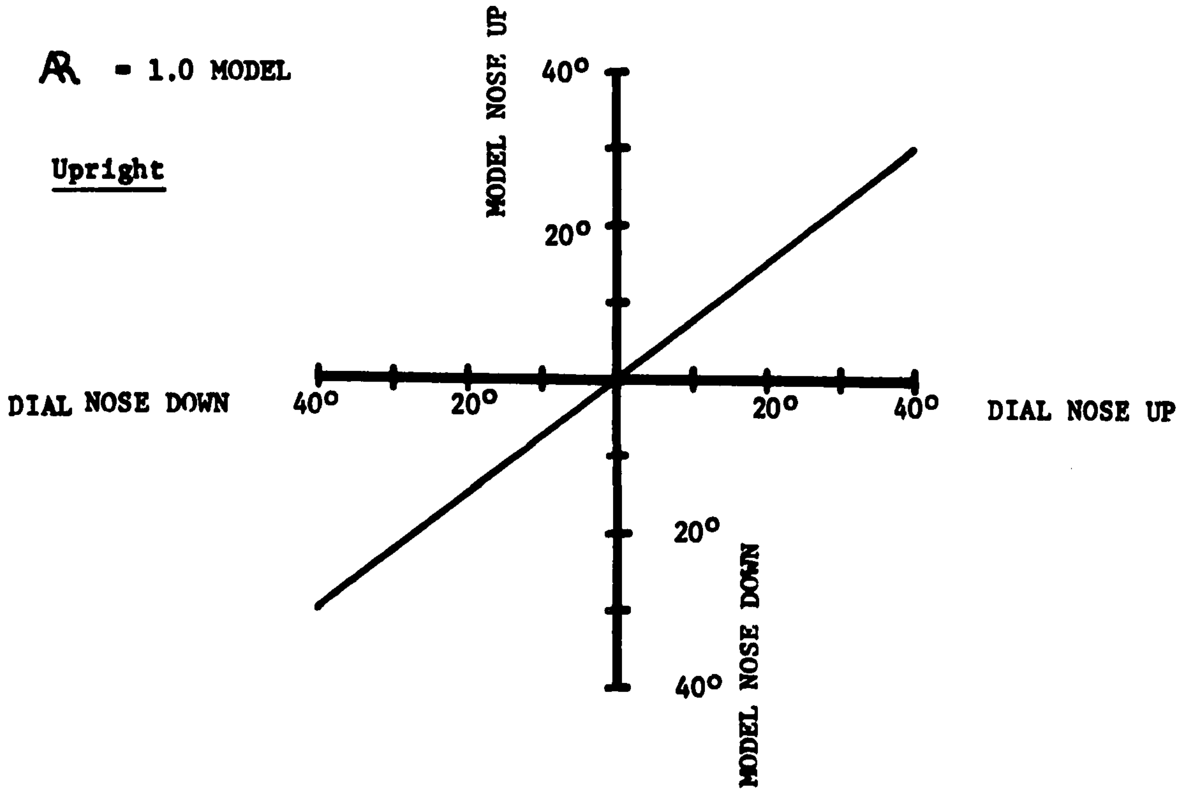

Figure 20. Wind tunnel model pitch angle calibrations.

wind tunnels, where the investigator is charged for each hour of tunnel occupancy. In any case, an orderly test plan is desirable. In order of increasing time required, the model changes expected were: (1) install or remove dummy bayonet, windscreen, and tail jack; (2) install or removed boundary layer transition strip; and (3) invert model.

With these considerations and the additional objective of avoiding time-consuming combinations of model changes, the following test plan was formed:

TABLE 3

INITIAL WIND TUNNEL TEST PLAN

Run	AR=2.8 Model	AR=1.0 Model	Transition Strip	Model Upright		Model Inverted	
					With Dummy Support		With Dummy Support
1	X			X			
2	X				X		
3	X		X		X		
4	X		X	X			
5	X		X			X	
6	X		X				X
7	X						X
8	X					X	
9		X		X			
10		X			X		
11		X	X		X		
12		X	X	X			
13		X	X			X	
14		X	X				X
15		X					X
16		X				X	

The primary data desired were lift and drag coefficients of each model as a function of model angle of attack. Model pitching moment was of much less interest, since the deflected streamtube theory for the channel wing does not predict pitching moment. It was originally intended to record pitching moment along with the lift and drag data. However, during the test program, the pitching moment strain indicator experienced large drift, became very erratic, and eventually became inoperative before the test program was completed. Therefore, no attempt was made to reduce or use the pitching moment data recorded.

The independent variable in each test run was the model angle of attack, which was varied in two-degree steps. The angle of attack range for the aspect ratio 2.8 model (which had a symmetrical airfoil section) was planned to be from -4° to several degrees past the stall, which was found to occur at $+14^\circ$. Thus data were taken through $+20^\circ$. The aspect ratio 1.0 model, which had a cambered section, was tested from -6° to $+28^\circ$, the stall occurring at $+22^\circ$.

The University of Oklahoma subsonic wind tunnel has a nominal speed range of 100 to 200 mph, or approximately 147 to 293 ft/sec. In the present case, the operating air speed was a compromise between the desire to maximize Reynolds number and the need to limit test section and engine temperature, since the tests were conducted in July and August. The target operating speed chosen for the wind tunnel tests was 220 ft/sec., or 75% of the tunnel maximum speed. Even at this air speed, test section air temperature reached

115° F and engine oil consumption was excessive on several especially hot days. At 115° F, the tape and modeling clay used to seal access hatches on the models began to soften and release.

A test run was conducted as follows: With no air movement in the tunnel, the initial strain indicator readings were recorded. After engine start and stabilization, the desired test section dynamic pressure was set with the manual mode of the engine speed control system. Then, engagement of the automatic mode of the pneumatic engine control maintained this dynamic pressure. The model was set to the most nose-down position required for that test run. The readings of the lift, drag, and pitching moment strain indicators, ΔP as indicated by the manometer, and the test section air temperature were recorded. Then the model was pitched nose-up two degrees, and data recorded again. This process was repeated until the required model angle of attack range was covered. After engine shut-down and cessation of air movement, final strain indicator readings were recorded.

The initial test plan shown in Table 3 was not followed precisely because three test runs had to be repeated. This was due to difficulties with a hatch sealing block blowing loose at high angle of attack. However, all the test runs represented in Table 3 were completed. In all, 19 test runs were made.

CHAPTER IV

WIND TUNNEL DATA REDUCTION AND CORRECTIONS

Reduction to Uncorrected Lift and Drag Coefficients

The raw lift and drag data were obtained as the difference between the strain indicator reading for each wind-on data point and the average of the initial and final wind-off indicator readings for the particular test run. The pitching moment strain indicator was erratic and eventually failed; consequently the pitching moment data were not reduced. The indicated lift and drag forces were calculated by use of the balance calibration factors:

$$L_{lbs} = 0.290\ L_{\mu\,in.} \tag{4.1}$$

$$D_{lbs} = 0.118\ D_{\mu\,in.} \quad . \tag{4.2}$$

Then the uncorrected lift and drag coefficients were obtained as

$$C_{L_u} = \frac{L_{lbs}}{q\,S} \tag{4.3}$$

$$C_{D_u} = \frac{D_{lbs}}{q\,S} \ , \tag{4.4}$$

where S = model (projected) planform area

q = test section dynamic pressure.

The test section dynamic pressure, q , is determined in the University of Oklahoma subsonic wind tunnel by means of the static pressure difference, ΔP , between the settling chamber and the test section. During tunnel operations, ΔP is read from an inclined water manometer. As the result of several measurements of ΔP and q , Comp [15] obtained the following calibrations:

$$q = 0.0920 \; \rho_{H_2O} \, \Delta P \quad , \tag{4.5}$$

where, with ρ_{H_2O} in lbm/ft^3 and ΔP in inches of water, q is given in lbf/ft^2 . The manometer water density ρ_{H_2O} is based on the balance room ambient temperature.

In conducting the test runs, it was found that the automatic engine speed control, which provided control of ΔP , was unable to hold ΔP constant to an accuracy greater than about $\pm$0.05 inches of water, as indicated by the manometer. That is, ΔP and thus q exhibited short-period excursions of $\pm$0.05 inches of water. Indeed, occasional oscillations to $\pm$0.1 inches were observed. Since all data items could not be recorded simultaneously, it is possible that the ΔP recorded for a data point did not in fact obtain at the instant when one or more model force readings were recorded. Therefore, there is a minimum uncertainty in the measured q of approximately

$$.05/8.9\ (100) = 0.56\% \ ,$$

and perhaps as much as 1.1%. Since the lift and drag coefficients are of the form

$$\frac{\text{Force}}{q\,S} \ ,$$

and S is assumed to be known with high accuracy, the uncertainty in q translates into an uncertainty of the same magnitude in the lift and drag coefficients. This uncertainty was especially important when the magnitude of possible data corrections was considered.

Test section air temperature was recorded for each data point; however, it was not considered necessary to calculate a Reynolds number for each data point. Reynolds number was calculated for each test run using air density and viscosity values based on the recorded barometric pressure and the average test section air temperature for that run. The length parameter used in Reynolds number was the model chord.

The tunnel test Reynolds number was corrected to the "free air effective Reynolds number" with the turbulence factor, as recommended by Pope and Harper [16] :

$$Re_{eff} = (TF) \cdot (Re) \ . \tag{4.6}$$

The turbulence factor for the University of Oklahoma subsonic wind tunnel is given by Comp [15] as TF = 1.35.

The raw wind tunnel data and uncorrected lift and drag coefficients for each test run are tabulated in Appendix A.

Correction for Tare, Interference and Flow Misalignment

Tare is the portion of the drag reading due to the model support system drag, while the effect of the support system on the air flow about the model is termed interference. Flow misalignment refers to the (usual) condition of the test section air stream not being perfectly aligned with the balance system, so that a component of lift appears in the drag reading, and conversely. Correction of the wind tunnel data for these effects is discussed in Pope and Harper [16] and in Comp [15] ; the derivation below is drawn from those discussions.

The indicated drag of the model mounted in the normal upright position may be represented as

$$D_I = D_{M_N} + I_{LB/M} + I_{M/LB} + I_{LW/M} + T_{LB} \ , \tag{4.7}$$

or

$$D_I = D_{M_N} + I_L + T_{LB} \ . \tag{4.8}$$

An explanation of the symbols used is given in the List of Symbols. For purposes of the evaluation considered here, the special windscreens used to shield the bayonet head and model mounting plate (see Chapter III) are considered part of the bayonet windscreen. With the model still mounted upright, the image support system is installed. This image system consists of a dummy bayonet, dummy (bayonet) windscreen, and a dummy tail jack. The dummy bayonet and tail jack are attached to the model but touch nothing else, while the dummy windscreen is attached to the tunnel roof. The image support system, installed with the (inverted) aspect ratio 1.0 model, is shown in Figure 21. Then the measured drag will be

$$D_2 = D_{M_N} + I_{LB/M} + I_{M/LB} + I_{LW/M} + T_{LB} + I_{UB/M}$$
$$+ I_{M/UB} + I_{UW/M} + T_{UB}$$

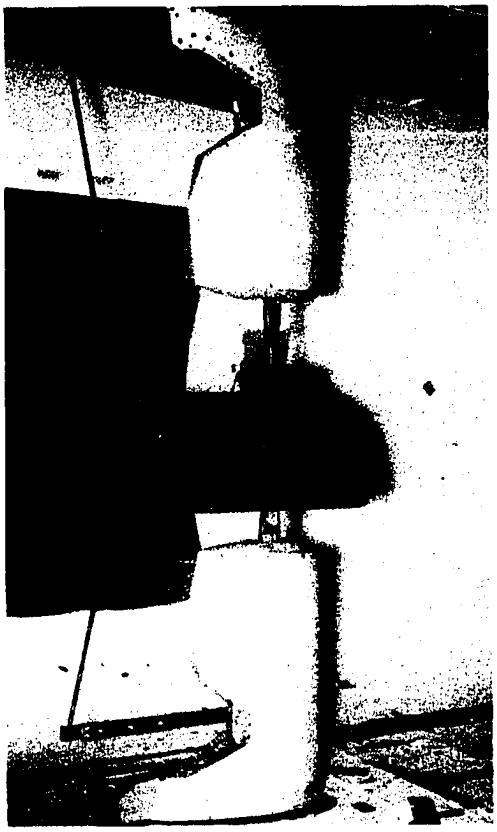

Figure 21. Image model support system installed with the (inverted) aspect ratio 1.0 channel wing model.

$$D_2 = D_{M_N} + I_L + T_{LS} + I_U + T_{US} \quad . \tag{4.9}$$

Next, the model is tested mounted inverted. The drag measured will consist of

$$D_3 = D_{M_I} + I_{US/M} + I_{M/US} + I_{UW/M} + T_{US}$$

$$D_3 = D_{M_I} + I_U + T_{US} \quad , \tag{4.10}$$

since in this position the support system appears to the model as the upper or dummy system. Finally, the inverted model is tested with the image support system installed. The drag is

$$D_4 = D_{M_I} + I_U + T_{US} + I_L + T_{LS} \quad , \tag{4.11}$$

because the image system has the same influence as the model support system.

Now, the drag of the model in the upright position is found by writing

$$D_1 + D_3 - D_4 = D_{M_N} + I_L + T_{LS} + D_{M_I} + I_U + T_{US}$$

$$- D_{M_I} - I_U - T_{US} - I_L - T_{LS} \quad ,$$

or,

$$D_{M_N} = D_1 + D_3 - D_4 \quad . \tag{4.12}$$

Similarly, the drag of the model in the inverted position is given by

$$D_1 + D_3 - D_2 = D_{M_N} + I_L + T_{LS} + D_{M_I} + I_U + T_{US}$$

$$- D_{M_N} - I_L - T_{LS} - I_U - T_{US} \quad ,$$

or,

$$D_{M_I} = D_1 + D_3 - D_2 \quad . \tag{4.13}$$

The same procedure yields comparable results for the lift; that is,

$$L_{M_N} = L_1 + L_3 - L_4 \quad , \tag{4.14}$$

and

$$L_{M_I} = L_1 + L_3 - L_2 \quad , \tag{4.15}$$

The flow misalignment is indicated by the differences in lift and drag between model upright and model inverted (Pope and Harper [16]). For example, the angle of attack setting error due to the tunnel airflow not being exactly perpendicular to the lift scale is shown for the aspect ratio 2.8 model in Figure 22. The curves indicate that the balance system was tipped forward with respect to the test section airstream. A similar plot of C_L vs C_D would show the drag error due to misalignment. The most direct procedure, however, is to simply average the data for the model normal and inverted; that is,

$$L_M = \frac{L_{M_N} + L_{M_I}}{2} \tag{4.16}$$

and

$$D_M = \frac{D_{M_N} + D_{M_I}}{2} \quad . \tag{4.17}$$

This procedure was used for the tunnel tests reported herein; tabulations of the data are presented in Appendix A.

Model Buoyancy Correction

A negative static pressure gradient will exist along the wind tunnel test section in the downstream direction due to the progressive thickening of the wall boundary layer, which constricts the

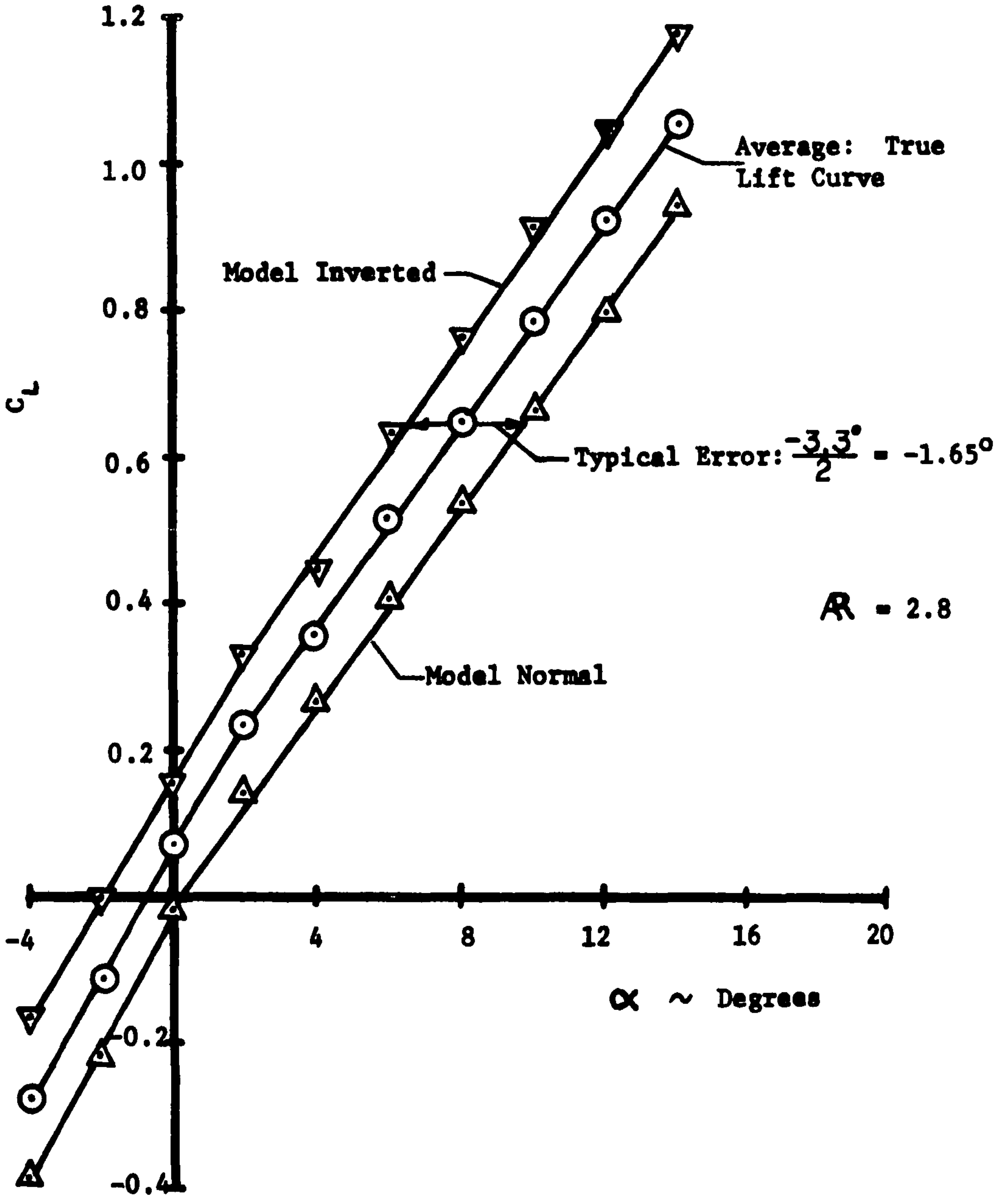

Figure 22. Angle of attack setting error due to tunnel flow misalignment.

flow area. Therefore, the model will tend to "float" downstream due to "horizontal buoyancy." Pope and Harper [16] recommend

$$\frac{dP}{d\ell} = -k\ q/B \tag{4.18}$$

for this pressure gradient, where the factor k may vary from 0.016 to 0.040, and B is the jet width. The factor k has not been determined for the University of Oklahoma subsonic wind tunnel. The maximum pressure gradient to be expected along the test section for the tests reported herein was calculated using $k = 0.040$ and $B = 4.0$ (the smaller dimension):

$$\frac{dP}{d\ell} = -(.040)\,\frac{51.5}{4.0} = -0.515 \quad \frac{\mathrm{lbf/ft^2}}{\mathrm{ft}} .$$

The drag increment due to model buoyancy is

$$\Delta D_B = -\frac{\pi}{4}\,\lambda_B\, t_m^3 \left(\frac{dP}{d\ell}\right) , \tag{4.19}$$

(Pope and Harper [16]), where the factor λ_B is plotted in Figure 6:14 of the same reference as a function of fineness ratio, and is the maximum thickness of the model. The fineness ratio of the aspect ratio 1.0 model was

$$\frac{\ell}{t_m} = 1.0/.12 = 8.34 \ ;$$

and the figure cited gives $\lambda_B = 4.4$ for this ℓ/t_m.

Then,

$$\Delta D_B = -\ \pi/4(4.4)(0.12)^3 \cdot (-0.515) = 0.00308 \text{ lbf} ,$$

or, in coefficient form,

$$\Delta C_{D_B} = \frac{0.00308}{(51.5)(1.0)} = 0.000060 \ .$$

But the minimum C_D measured for the aspect ratio 1.0 model was

.0221, so the maximum buoyancy correction would be only about 0.3% of the smallest C_D value. Since there was a basic uncertainty in C_D of approximately 1% due to an uncertainty in dynamic pressure, the buoyancy correction is seen to be negligible. The buoyancy correction for the aspect ratio 2.8 model would be even smaller.

Lift and Drag of the Model Tail Jack Arms

The tail jack system, which moves the wind tunnel model in angle of attack, contributes to the measured lift and drag. Since the lower and vertical arms are duplicated by the dummy tail jack, the effects of these members are removed by the corrections for tare and interference. However, the upper tail jack arm, which is fixed to the model, cannot be duplicated by the image system. The lift and drag contributions of the model tail jack arms will be estimated.

The tail jack arm of each model was a smooth, circular cross section, half inch diameter aluminum rod. The so-called "cross-flow principal," as applied to circular cylinders, asserts that the fluid dynamic pressure forces on an inclined cylinder correspond to the velocity component normal to the axis only (Hoerner [17]). Therefore, based on the projected area $S_{P_L} = d \cdot l$,

$$C_N \equiv \frac{N}{q\, S_{P_L}} = \frac{C_{D_b} \frac{\rho}{2} (V \sin\alpha)^2 \, S_{P_L}}{q\, S_{P_L}} = \frac{C_{D_b}\, q \sin^2\alpha}{q}$$

$$C_N = C_D \sin^2\alpha\,, \qquad (4.20)$$

where C_{D_b} , or C_D basic, is the drag coefficient of the cylinder at

$\alpha = 90°$. Then the lift experienced by the inclined cylinder is

$$C_L = C_N \cos\alpha = C_{D_b} \sin^2\alpha \cos\alpha , \qquad (4.21)$$

and the drag is

$$C_D = C_N \left|\sin\alpha\right| = C_{D_b} \left|\sin^3\alpha\right| . \qquad (4.22)$$

Hoerner [17] recommends the addition of a skin friction component to the drag coefficient:

$$C_D = C_{D_b} \left|\sin^3\alpha\right| + \pi_R C_F , \qquad (4.23)$$

where C_F is the skin friction coefficient, and π_R is the surface area ratio,

$$\pi_R = \frac{\text{cylinder surface area}}{\text{reference area } S_{F_b}} .$$

In the present case of a circular cylinder,

$$\pi_R = \frac{\pi d l}{d l} = \pi .$$

The Reynolds number based on the cylinder diameter is approximately

$$Re = \frac{\rho V d}{\mu} = \frac{(.00213)(220)(0.5/12)}{3.95 \times 10^{-7}} = 49{,}500 ,$$

a Reynolds number very much below the critical range. However, since the tail jack arm is attached to the wing in the chord plane and fairs into the wing, its boundary layer should be strongly dependent on the wing boundary layer. For the aspect ratio 2.8 model, for example, the local Reynolds number at the midpoint of the 6-inch tail jack arm would be

$$Re = \frac{(.00213)(220)(8/12)}{3.95 \times 10^{-7}} = 790{,}000 ,$$

which is into the transition range.

These rather conflicting results for Reynolds number illustrate the difficulty of arriving at a simple model for the lift and drag of the tail jack. However, the lower Re value actually represents the case of $\alpha = 90^\circ$, which was not approached in the wind tunnel tests (where $-6^\circ \le \alpha \le 28^\circ$). A conservative approach would seem to be the following: assume C_{D_b} to be that of a circular cylinder (in cross-flow) before transition, and assume C_f corresponding to forced turbulent flow at a low Reynolds number. Thus, from Hoerner [17] ,

$$C_{D_b} = 1.1 \text{ and } C_f = 0.009 .$$

These values were in fact used. Therefore, the lift and drag coefficients of the tail jack arms, based on their own projected areas, were estimated to be

$$C_{L_{TJ}} = (1.1) \cos\alpha \sin^2\alpha \tag{4.24}$$

$$C_{D_{TJ}} = (1.1) \left| \sin^3\alpha \right| + 0.009\pi \quad . \tag{4.25}$$

This estimate neglects end effects, of course. For convenience, these coefficients were converted to the same reference areas as the wind tunnel models:

$$C_{L_{TJ}} = S_{P_t}/S \; (1.1) \cos\alpha \sin^2\alpha \tag{4.26}$$

$$C_{D_{TJ}} = S_{P_t}/S \; (1.1) \left| \sin^3\alpha \right| + 0.0283 \; S_{P_t}/S \; , \tag{4.27}$$

where $S_{P_t} = d \cdot \ell$ (of tail jack arm)

$S = 2Rc$ (projected wing area).

For both wind tunnel models, the tail jack arm was mounted in the chord plane, so that the angle of attack α was the same as that of the model.

The exposed length of the tail jack arm of the aspect ratio 2.8 model was 6.5 inches, so that

$$S_{P_t}/S = \frac{(0.5)(6.5)}{(2)(7)(5)} = 0.0464 \; ,$$

and

$$C_{L_{TJ}} = 0.051 \sin^2\alpha \cos\alpha \tag{4.28}$$

$$C_{D_{TJ}} = 0.051 \left|\sin^3\alpha\right| + 0.00131 \; . \tag{4.29}$$

Using these expressions, $C_{L_{TJ}}$ and $C_{D_{TJ}}$ were evaluated for the angle of attack range used in testing the aspect ratio 2.8 model. The drag coefficient correction ranged from 1.5% to 4%, but the maximum lift coefficient correction was only 0.8%. Since there was a basic uncertainty in C_L of about 1% due to uncertainty in dynamic pressure q, the correction for lift of the tail jack arm was not used. The drag coefficient of the tail jack arm, $C_{D_{TJ}}$, is shown as one of the columns in the tabulation of data corrections, Appendix A.

For the aspect ratio 1.0 model, the length of the tail jack arm was 2 inches, thus

$$S_{P_t}/S = \frac{(0.5)(2)}{(2)(6)(12)} = 0.00695 \; ,$$

and

$$C_{L_{TJ}} = 0.00765 \cos\alpha \sin^2\alpha \tag{4.30}$$

$$C_{D_{TJ}} = 0.00765 \left|\sin^3\alpha\right| + 0.000197 \; . \tag{4.31}$$

Upon evaluating these equations over the angle of attack range tested, it was found that the maximum lift coefficient correction was about 0.1%, while the maximum drag coefficient correction was 0.9%. Referring again to the uncertainty in q of about 1%, these corrections were seen to be not significant and so were not used.

Model and Wake Blockage

The presence of the wind tunnel walls produces a lateral constraint on the flow about the model and the model wake (Pope and Harper [16]) termed model, or solid, blocking and wake blocking, respectively. The model reduces the test section flow area, thus increasing the air velocity in the model vicinity as a function of model size, thickness, and thickness distribution. However, the solid blocking velocity increase is much less than the direct flow area reduction.

The model wake has an average velocity lower than the freestream, thus the velocity outside the wake in the test section must have a higher velocity than the undisturbed test section freestream. The velocity increase results in a pressure decrease placing the model in a negative pressure gradient, which is measured as a model drag increase.

Pope and Harper [16] present combined theoretical-empirical analyses for both model and wake blockage; however, the wake blockage calculation requires a prior knowledge of the model C_D , which varies with angle of attack. Fortunately, it has been found experimentally that the total velocity increment due to model and wake blockage is well represented by

$$\epsilon = (1/4)\,\frac{\text{model frontal area}}{\text{test section area}}\ , \qquad (4.32)$$

where

$$V = V_u\,(1 + \epsilon)\ . \qquad (4.33)$$

Upon expanding and dropping higher order terms, we find that

$$q = q_u\,(1 + 2\epsilon)\ . \qquad (4.34)$$

The drag increment due to wake blockage is given by Pope and Harper as

$$\Delta C_{D_{WB}} = \frac{K_1\,\tau_1\,V}{(A_{TS})^{3/2}}\,C_{D_u}\ , \qquad (4.35)$$

where V is model volume, and K_1 and τ_1 are empirical functions of model thickness ratio and model span/tunnel width ratio, respectively, and are presented in graphical form in Pope and Harper [16] .

No correction was required for support system blockage since the image method of evaluating tare and interference removes any blocking contribution of the mounting system.

Consider the aspect ratio 1.0 model at an angle of attack. The frontal area is the projected area in the chord plane multiplied by the sine of the angle of attack:

$$A_F = (1.0)(\sin\alpha_c)\ .$$

The tunnel test section area is 20.58 ft.^{2} (Comp [15]), so that

$$\epsilon = (1/4)\,\frac{(1.0)\sin\alpha_c}{20.58} = 0.01215\,\sin\alpha_c\ . \qquad (4.36)$$

The aspect ratio 1.0 model was found to stall at 22°; therefore the maximum blocking condition was

$$\epsilon = 0.01215(0.375) = 0.00455\ ;$$

leading to

$$q = q_u\left[1 + (2)(.00455)\right] = (51.5)(1.00910) = 52.0 \text{ lbf/ft}^2.$$

Thus the maximum correction to dynamic pressue due to model and wake blockage was

$$E = \frac{52.0 - 51.5}{51.5}(100) = 0.97\% \ .$$

But, as discussed above on page 56, the uncertainty in the measurement of q was approximately 1.1%; therefore, the calculated model and wake blockage correction for dynamic pressure was neglected for both models.

The drag increment due to wake blockage for the aspect ratio 1.0 model was evaluated with equation (4.35) and the graphical functions in Pope and Harper [16] :

$$\Delta C_{D_{WB}} = \frac{(1.01)(0.88)\mathcal{V}}{(20.58)^{3/2}} C_{D_u} = 0.00953\,\mathcal{V} C_{D_u} \quad . \qquad (4.37)$$

For wing volume, Pope and Harper suggest

$$\mathcal{V} = (0.7)\,t\,c\,b \ ,$$

where b is the wing span, and in the case of the non-planar wing must be the curvilinear span. Thus,

$$\mathcal{V} = (0.7)(0.12)(1.0)(\pi)(1/2) = 0.132 \text{ ft.}^3,$$

and $$\Delta C_{D_{WB}} = 0.00126\ C_{D_u} \quad . \qquad (4.38)$$

The drag coefficient, adjusted for tare, interference, and flow misalignment, but uncorrected otherwise, of the aspect ratio 1.0 model at $\alpha_c = 22^\circ$, was 0.297. Then the drag correction for wake blockage was

$$\Delta C_{D_{WB}} = (0.00126)(0.297) = 0.000375 \ ,$$

which was outside the range of significant figures carried for the drag coefficient, or a correction of approximately 0.1%. Therefore, the drag correction for wake blockage was not used for either model.

Boundary Induced Upwash and Streamline Curvature Corrections

The tunnel test section boundaries alter the normal downwash such that the measured lift is too large and the measured drag is too small. The lift error is usually treated by a correction to the geometric angle of attack, since the increased lift is due to an upwash (increasing the angle of attack). Pope and Harper [16] develop the corrections by representing the boundaries with images of the model wing "horseshoe" vortex. The resulting equations are

$$\Delta \alpha_i = \delta \left(S/A_{TS} \right) C_L \tag{4.39}$$

$$\Delta C_{D_i} = \delta \left(S/A_{TS} \right) C_L^2 \ , \tag{4.40}$$

where δ is a function of

(1) span load distribution,

(2) ratio of model span to tunnel width,

(3) shape of tunnel test section,

(4) whether or not model is on tunnel centerline.

The equations assume that the upwash at the tunnel centerline may be taken as the average upwash. This condition will hold if the wing span is less than 80% of the tunnel width (Pope and Harper [16]).

The normal curvature of the air flow about a lifting wing is altered by the test section boundaries so that the lift, moment (about the quarter chord), and angle of attack are increased. The effect is treated as a variation of the boundary-induced upwash along the wing chord:

$$\alpha = \alpha_u + \Delta\alpha_i + \tau_2 \Delta\alpha_i = \alpha_u + (1 + \tau_2)\Delta\alpha_i$$

$$\alpha = \alpha_u + (1 + \tau_2)\,\delta\left(S/A_{TS}\right) C_L \quad . \tag{4.41}$$

Since the streamline curvature effect is more pronounced at the model tail than at the wing, Pope and Harper [16] present graphical data for τ_2 as a function of "tail length." For the wing, the tail length is taken as one-half the wing chord.

The factor δ was determined for the subject models and wind tunnel by means of graphical data presented in Pope and Harper [16] . It was assumed that the channel wings could be considered as flat wings of the same projected wing span. Pope and Harper give data for both uniform and elliptical span load distribution, but for the subject conditions there was no appreciable difference in δ . The results were

$$\delta = 0.114$$

for both the aspect ratio 1.0 model and the aspect ratio 2.8 model. The factor τ_2 was found to be

$$\tau_2 = 0.23 \text{ for the aspect ratio 1.0 model,}$$

and

$$\tau_2 = 0.10 \text{ for the aspect ratio 2.8 model.}$$

The maximum drag and angle of attack corrections due to boundary induced upwash and streamline curvature were

$$\Delta C_{D_i} = (0.114)\left(\frac{1.0}{20.58}\right)(1.097)^2 = 0.00667$$

and

$$\Delta\alpha = (1 + 0.23)(.114)\left(\frac{1.0}{20.58}\right)(1.097) = .00749 \text{ rad} = 0.43^\circ$$

for the aspect ratio 1.0 model, occurring at $\alpha_c = 22^\circ$. These represent percentage corrections of 2.3% and 1.95%, respectively. As discussed above, the basic uncertainty in C_D was considered to be about 1.1%, and the uncertainty in setting the angle of attack was estimated to be at least $\pm 0.25^\circ$. Therefore, these corrections were considered to be significant, and were retained. The percentage corrections at low C_L were much lower of course, but were retained for completeness.

Similarly, maximum values for the aspect ratio 2.8 model were

$$\Delta C_{D_i} = (.114)\left(\frac{0.486}{20.58}\right)(1.061)^2 = 0.00303$$

and

$$\Delta\alpha = (1 + 0.10)(.114)\left(\frac{0.486}{20.58}\right)(1.061) = .00314 \text{ rad} = 0.18^\circ,$$

or corrections of 2.75% and 1.28%, respectively, at $\alpha_c = 14^\circ$. The angle of attack correction here may have been within the setting uncertainty, but was retained on the data sheets since it required so little extra calculation effort after obtaining ΔC_{D_i}.

CHAPTER V

RESULTS OF CHANNEL WING WIND TUNNEL TESTS

Transition Strip

Both channel wing wind tunnel models were tested with and without boundary layer transition strips, as recommended by Pope and Harper [16] , and discussed in Chapter III above. However, the transition strip results were not satisfactory; indeed, the lift and drag data readings were more erratic for the transition strip cases than those with no transition strip. This is illustrated in Figures 23 and 24 for the $\mathcal{R}$ = 2.8 model. Similar results were obtained for the $\mathcal{R}$ = 1.0 model. Contrariwise, the data from the tests with no transition strips were much more orderly, especially the lift data. Therefore, the transition strip data will not be presented herein.

Premature Stall

The four-run method for evaluation of tare and interference described in Chapter IV led to difficulties with the aspect ratio 1.0 model. For test runs of types 2, 3, and 4, that is, those with the bayonet or dummy bayonet extending into the "channel" of the wing, (see Chapter IV, page 58) this model experienced premature stall at an angle of attack of about 4 degrees. This resulted in a

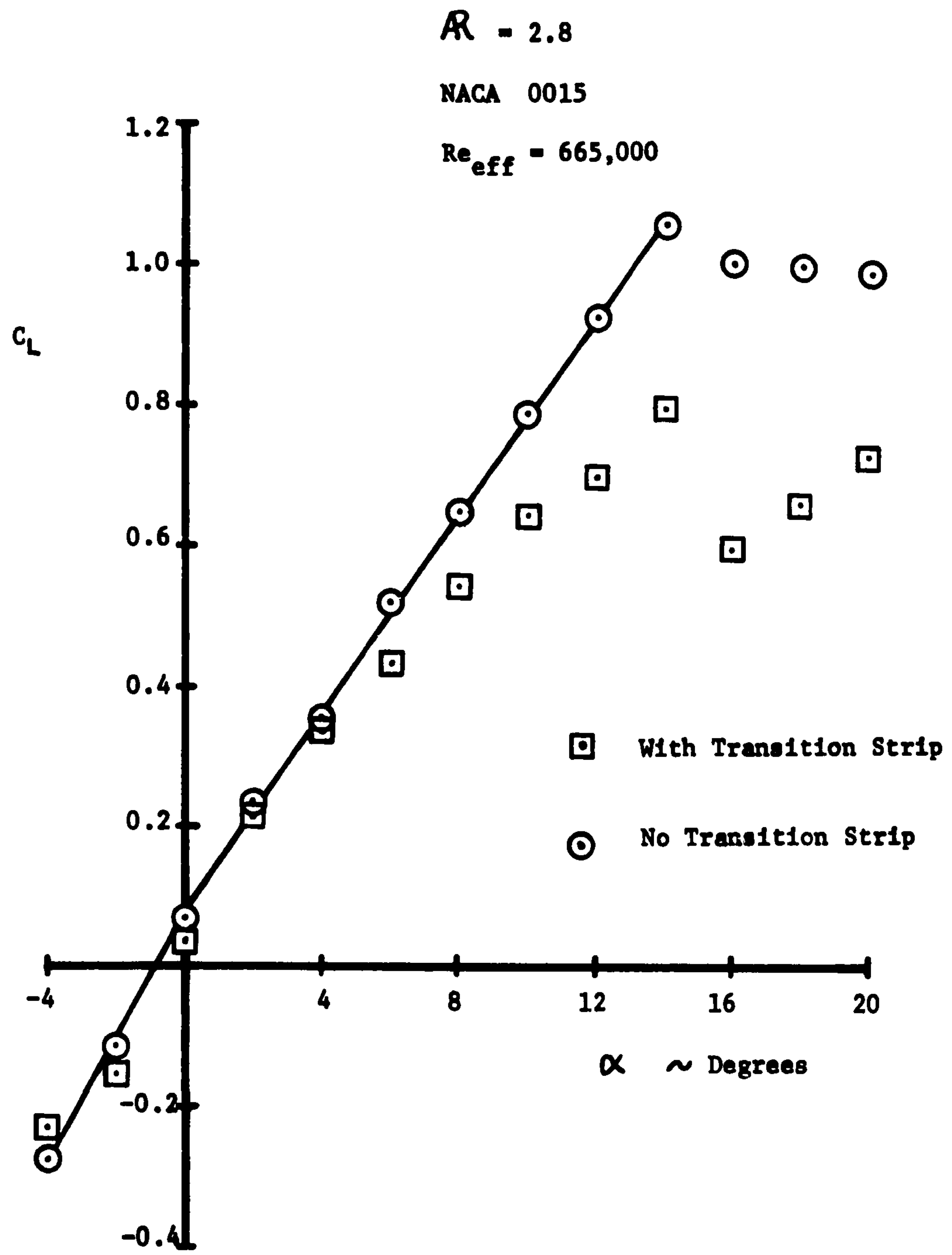

Figure 23. Comparison of lift coefficient for the AR = 2.8 model with and without transition strips.

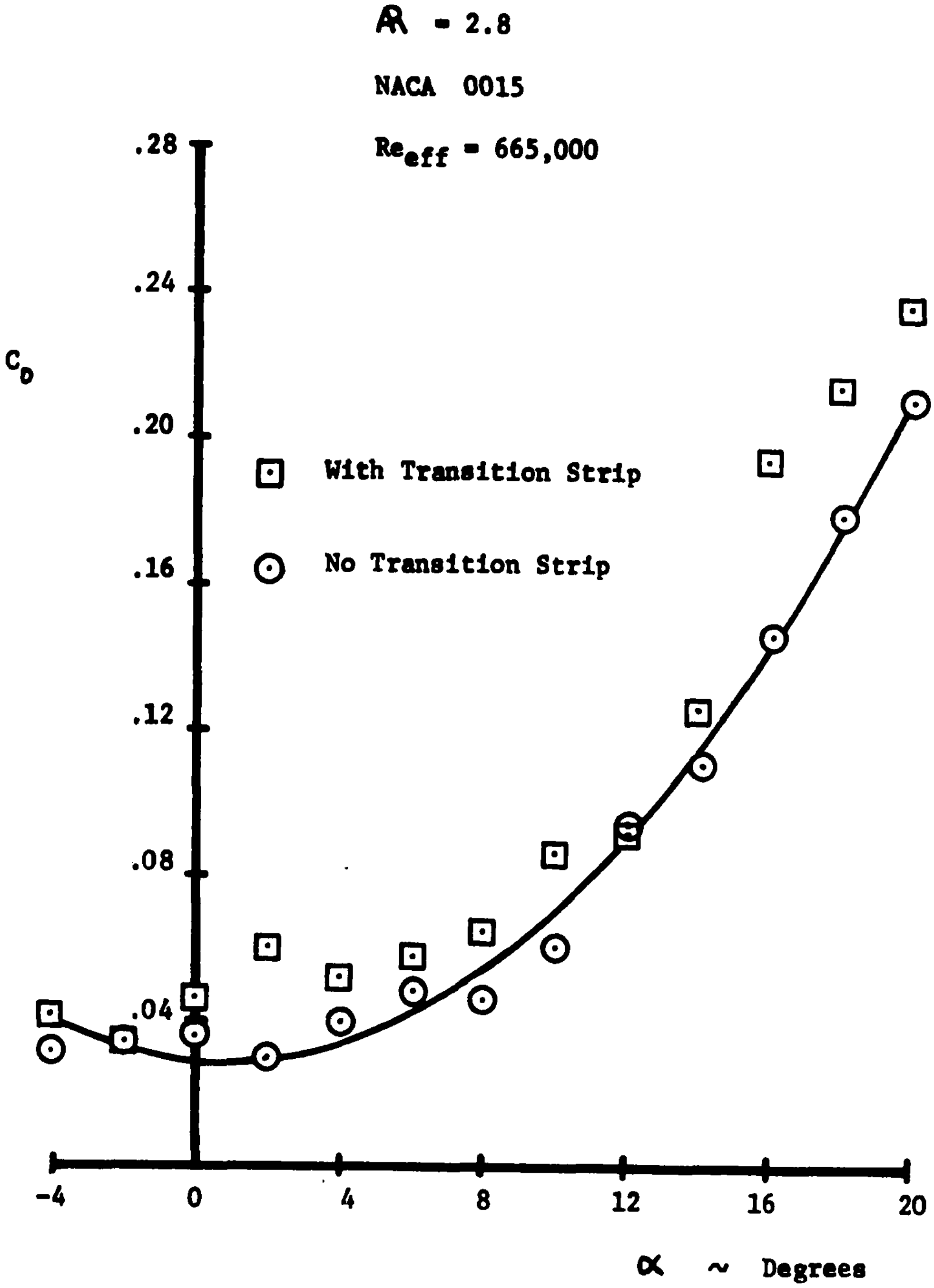

Figure 24. Comparison of drag coefficient for the AR = 2.8 model with and without transition strips.

pronounced dip in the lift curve slope after the data were combined as described in Chapter IV (see Figure 25). Evidently the pressure field and/or separated flow due to the presence of the bayonet, bayonet windscreen, and special windscreen for the bayonet head and model mounting plate produced the early stall of the wing. Due to its thinner section and larger diameter, the aspect ratio 2.8 wing had a larger channel area than did the aspect ratio 1.0 model, so the former did not suffer this effect.

Since the lift curve obtained from the run of type 1 was linear to the stall at 20 degrees, the prematurely stalled lift curves of the runs of types 2, 3, and 4 were linearly extended, at their slope prior to the premature stall, to the same final stall, as shown in Figure 26. These faired data were then used in the four-run method to eliminate the tare, interference, and flow misalignment. The validity of this approach is illustrated in Figure 27, where it is seen that the faired and unfaired data merge again when sufficiently removed from the premature stall area.

Lift and Drag Coefficients

The experimentally determined lift and drag coefficients for the aspect ratio 1.0 and 2.8 models are presented in Figures 28 through 31. The data have been reduced and corrected as described above and in Chapter IV. Tabulations of the raw data and the reduction steps are presented in Appendix A.

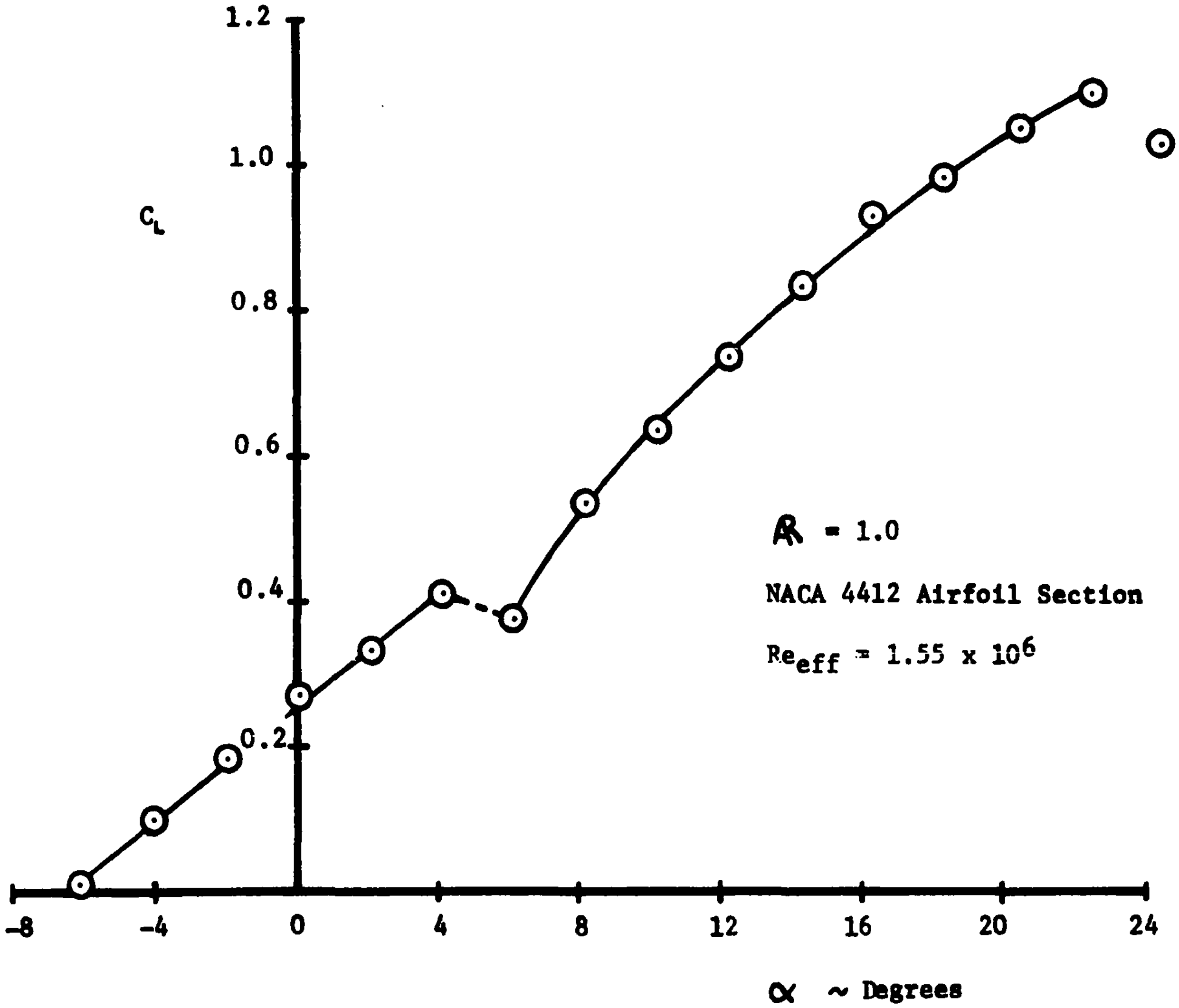

Figure 25. Lift coefficient of aspect ratio 1.0 model, showing premature stall due to presence of bayonet in channel.

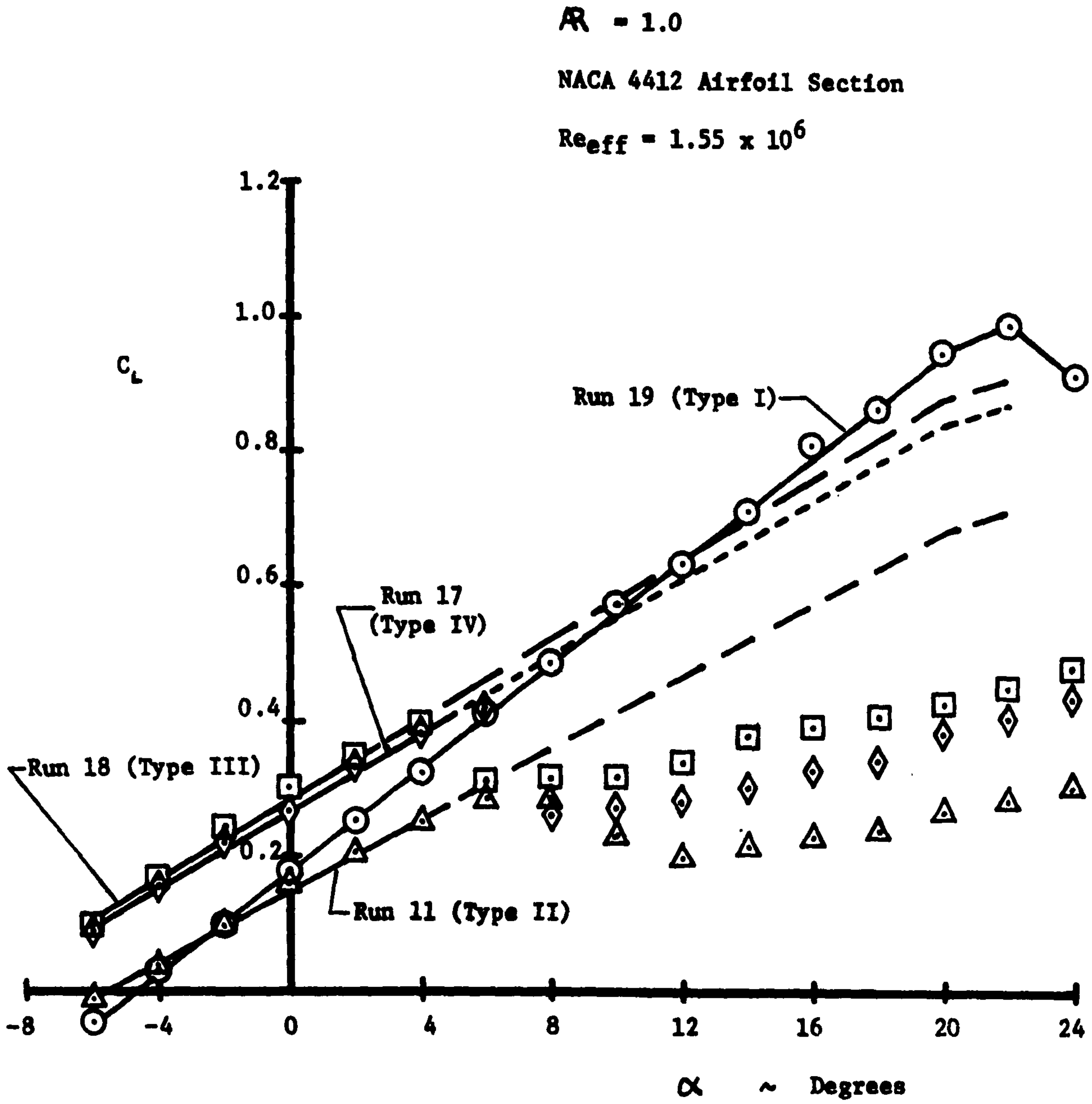

Figure 26. Fairing of lift data to eliminate premature stall due to presence of bayonet in channel.

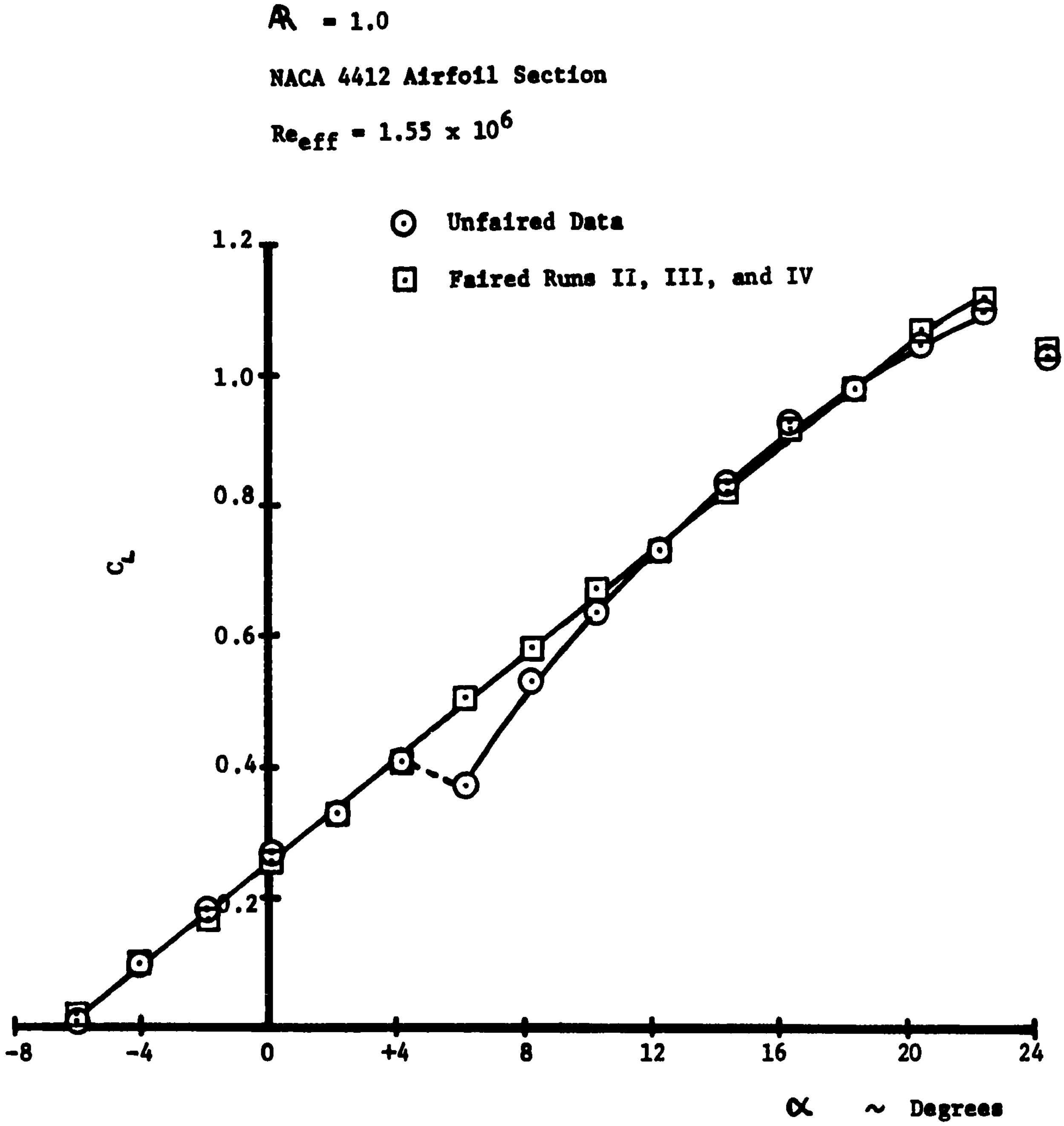

Figure 27. Comparison of faired and unfaired lift data for the aspect ratio 1.0 channel wing model.

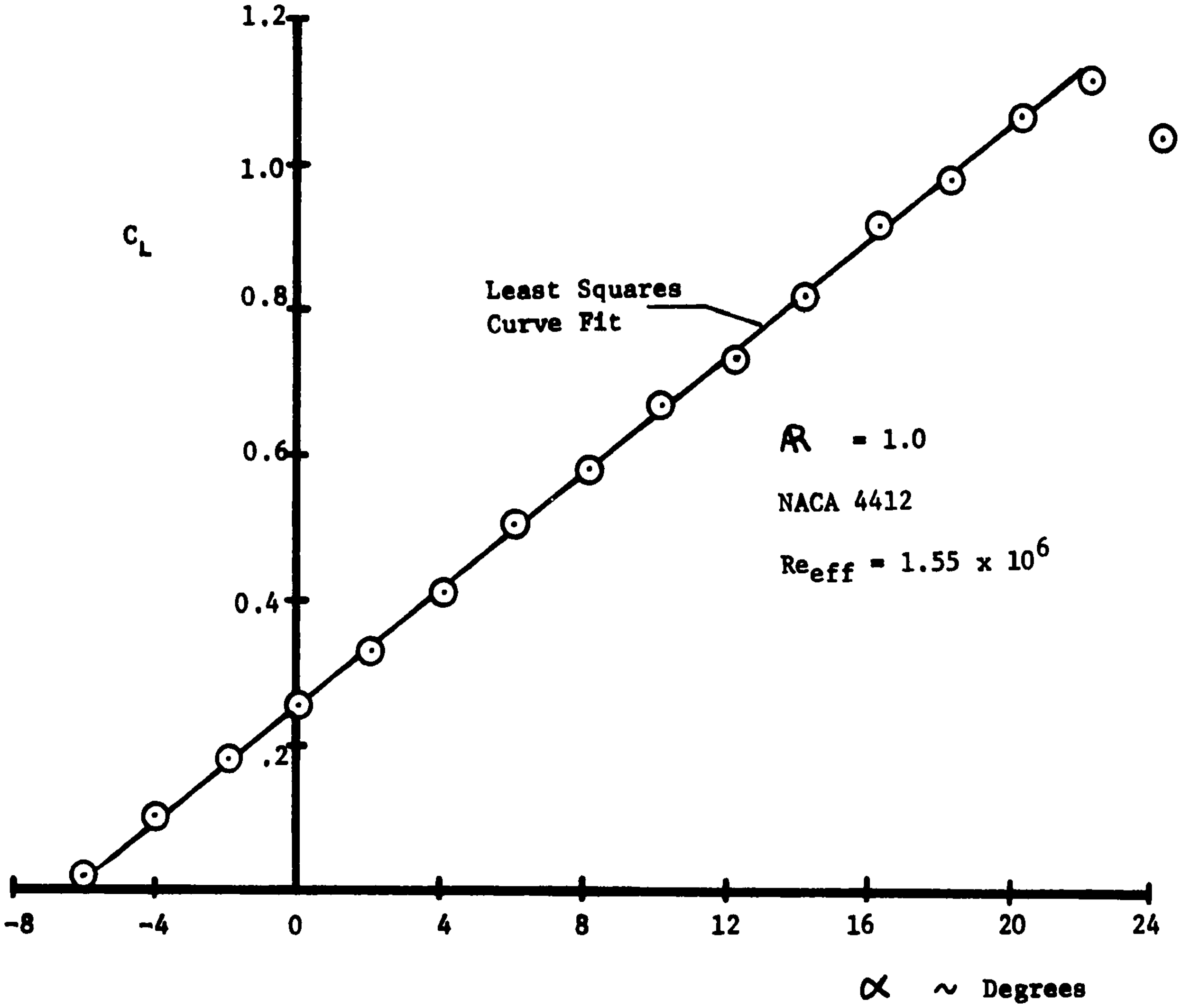

Figure 28. Lift coefficient of Æ = 1.0 channel wing model.

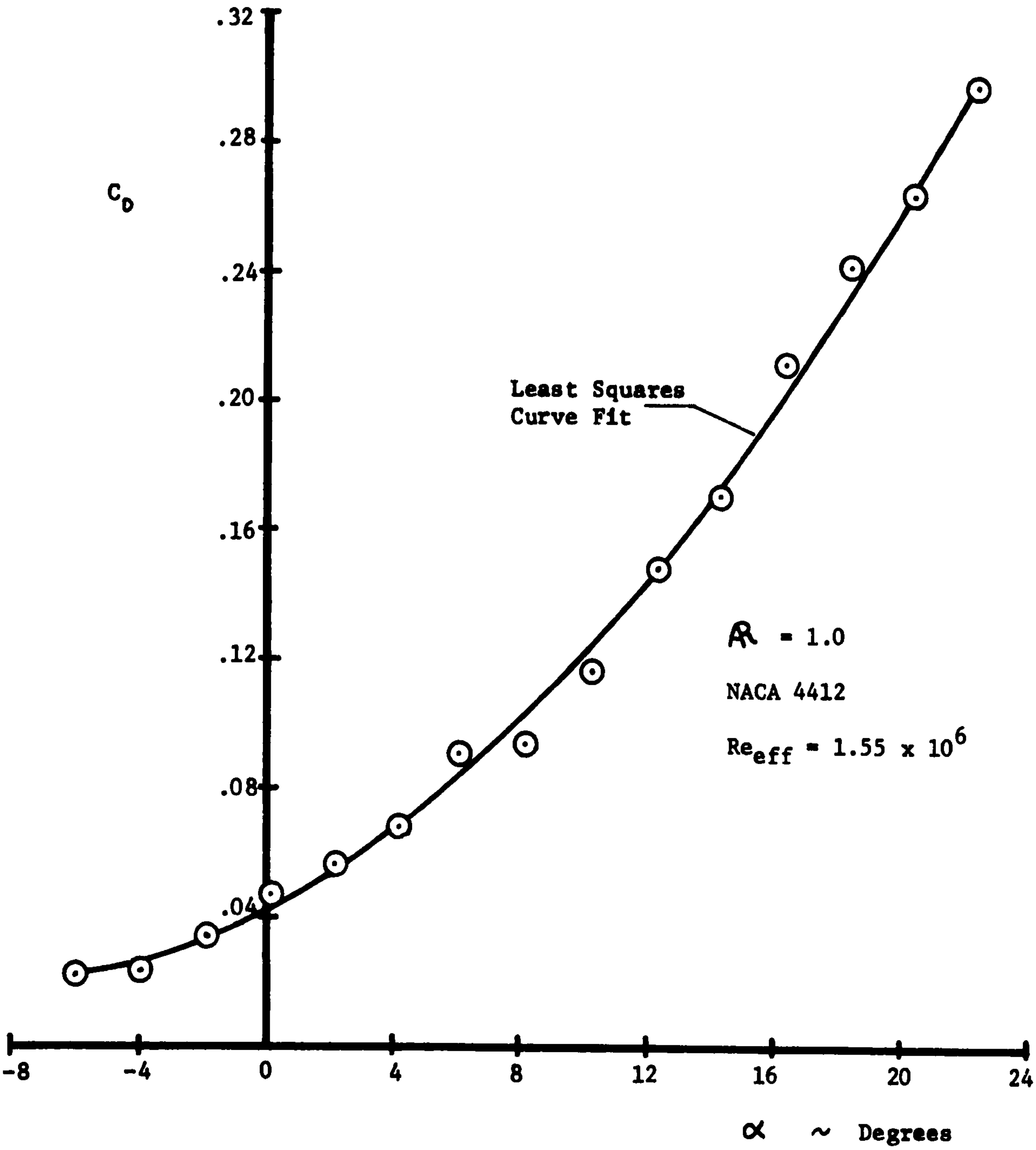

Figure 29. Drag coefficient of $\mathcal{R}$ = 1.0 channel wing model.

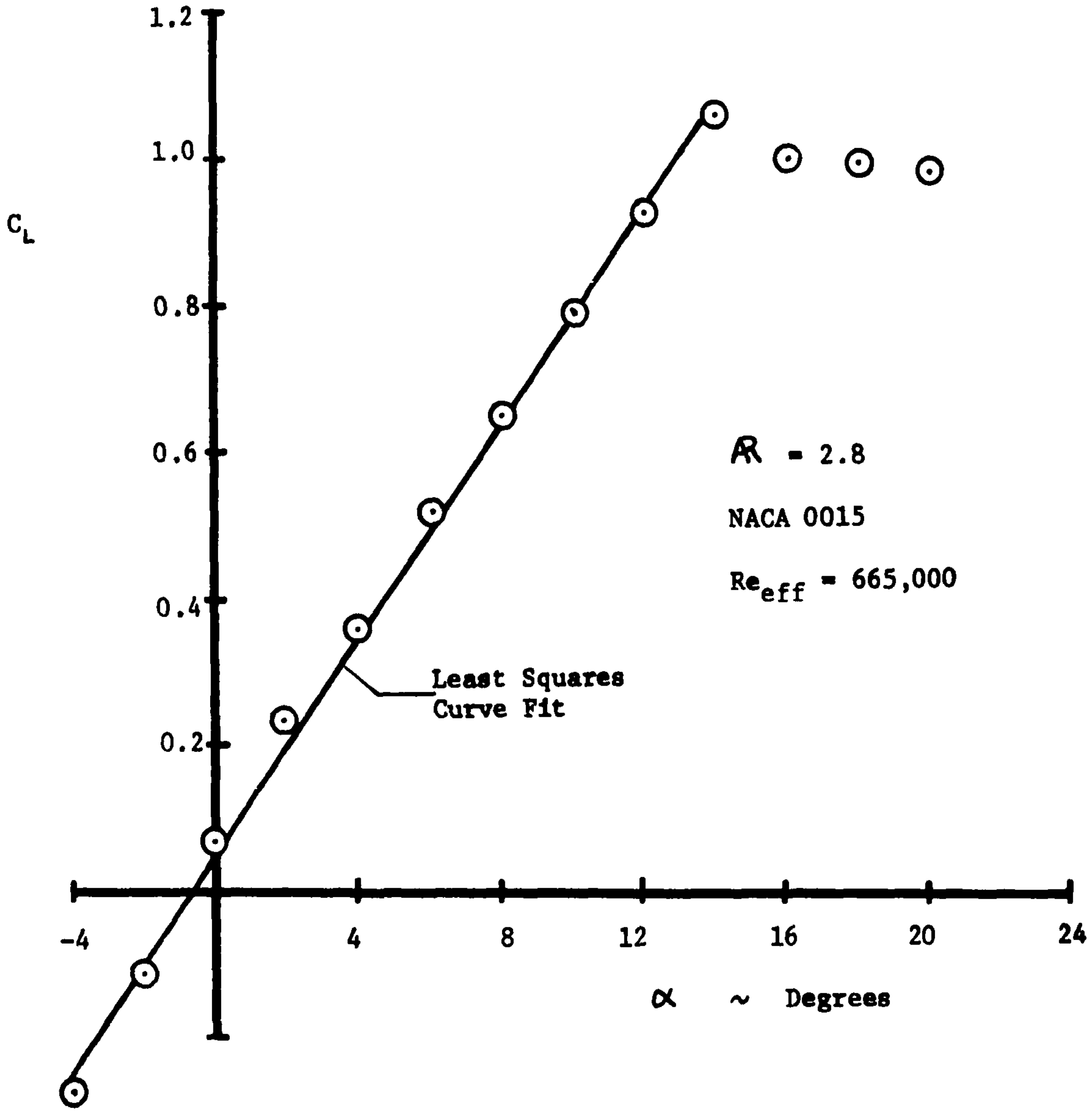

Figure 30. Lift coefficient of AR = 2.8 channel wing model.

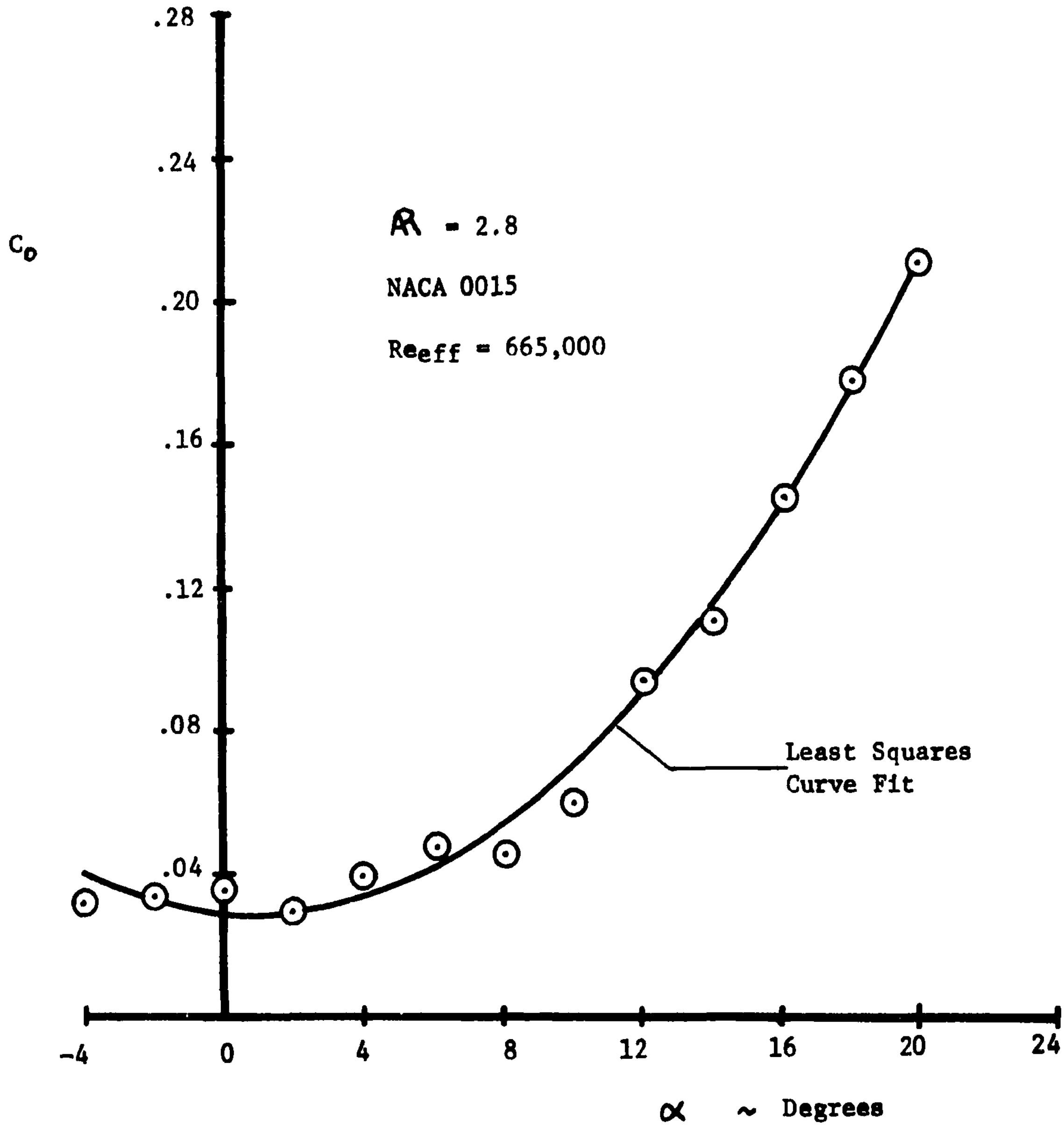

Figure 31. Drag coefficient of Æ = 2.8 channel wing model.

The lift data were correlated with a linear least-squares curve fit,[1] and the drag data with a parabolic least-squares curve fit.[2] It may be seen in Figures 28 and 30 that the linear fit of the lift data is very good. The drag data are somewhat scattered, but still well represented by the parabolic curve.

Experimental values of channel wing lift curve slope, $dC_L/d\alpha_c$, were obtained from the linear curve-fit of lift coefficient in Figures 28 and 30:

$$dC_L/d\alpha_c = 0.040 \text{ per degree} \qquad \mathcal{R} = 1.0$$

$$dC_L/d\alpha_c = 0.073 \text{ per degree} \qquad \mathcal{R} = 2.8 \ .$$

Span Efficiency Factor

An experimental determination of channel wing span efficiency was obtained from the lift and drag data. If the drag coefficient is written in the form

$$C_D \simeq C_{D_0} + \frac{C_L^2}{\pi e \mathcal{R}} \ , \tag{5.1}$$

where e is the span efficiency factor, then e can be related to the slope of a straight line through the data plotted in the form C_D vs. C_L^2. The data plotted were the parabolic fit of C_D, and the square of the linear fit of C_L, Figure 32. The former was chosen because of the scatter in C_D, while the fit of C_L was used only for

---

[1]Program IV-2 of the Statistical Package Library for the Hewlett-Packard Model 9100B programmable calculator.

[2]*Ibid.*, Program IV-8.

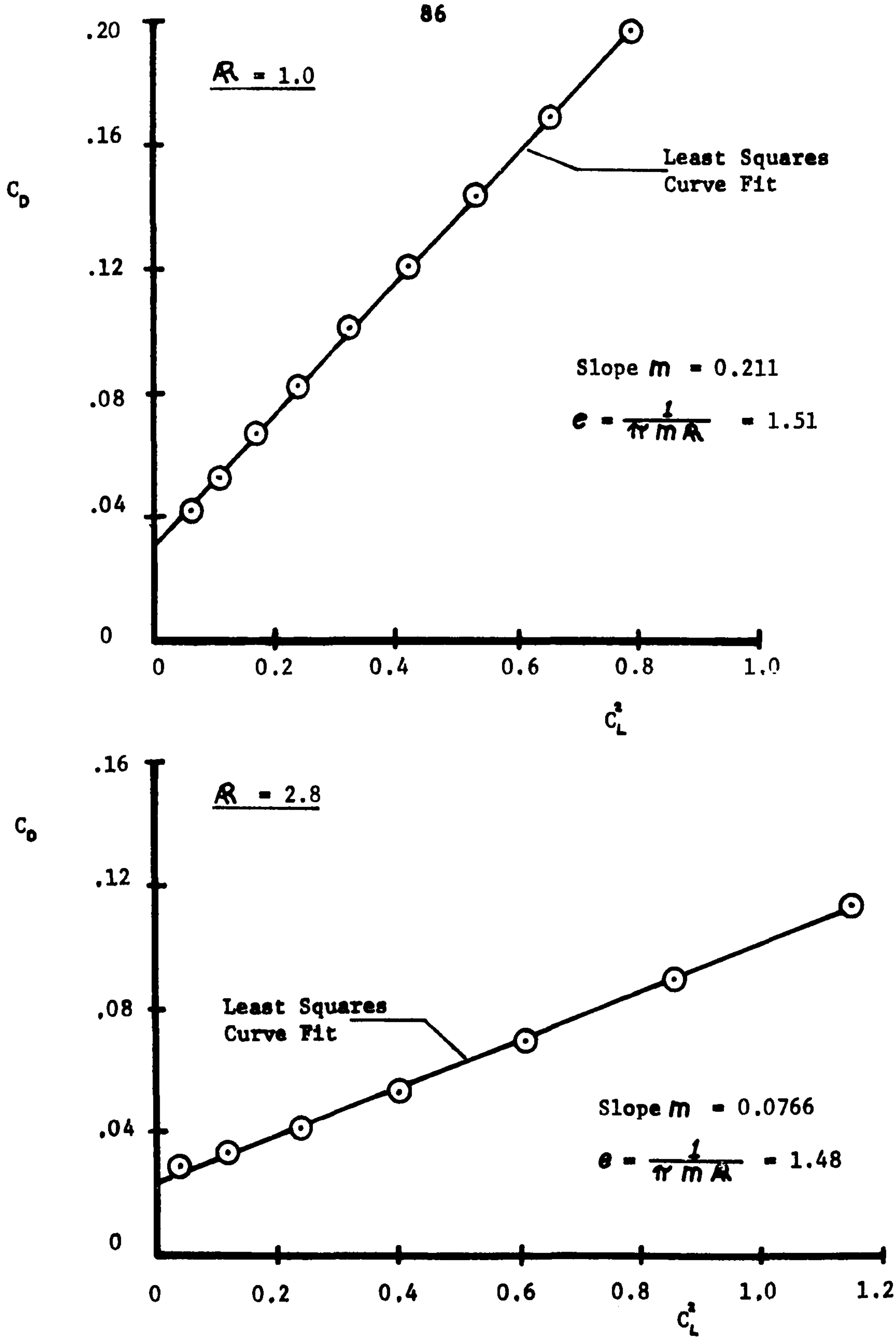

Figure 32. Experimental determination of channel wing span efficiency factor.

convenience. The results were

$$e = 1.51 \qquad\qquad Æ = 1.0$$

$$e = 1.48 \qquad\qquad Æ = 2.8 \ .$$

The 2% difference in measured e is attributed to data scatter rather than to a trend with aspect ratio.

Angle of Attack Error

Referring to Figure 30, it is seen that the experimental lift coefficient for the Æ = 2.8 model does not pass through zero for (wing angle of attack) $\alpha_c = 0^\circ$, as would be expected with a symmetrical airfoil section. The lift coefficient was not expected to be zero at $\alpha_c = 0^\circ$ for the Æ = 1.0 model, since a cambered airfoil section was used for this model. If a constant error of one degree (negative) in setting the channel wing angle of attack during the wind tunnel tests were assumed, then the lift coefficient of the Æ = 2.8 model would pass approximately through $C_L = 0$ at $\alpha_c = 0^\circ$. The author, of course, exercised care to prevent this type of occurrence, but the existence of such a systematic error cannot be ruled out. Also, a one degree positive shift in all the data of the wind tunnel tests reported here would afford better correlation with the lifting arc theory (see Chapter VIII). However, the latter observation cannot be considered to be as objective as the failure of the lift curve of a symmetrical-section wing to pass through the origin. Still, an inadvertent angle of attack shift in the lift and drag curves seems to be the best explanation for the location of the lift curve of the Æ = 2.8 wing, and the same error would probably have existed for both models. Thus the author recommends that the reader desiring to use the experimental lift and drag curves presented herein shift them to the right the amount required to make the lift curve of the AR = 2.8 model pass through the point $\alpha_c = 0^\circ$, $C_L = 0$.

Conclusion

The deflected streamtube theory developed in Chapter I for the channel wing predicted a span efficiency factor of $e = 2.0$, while Cone's [7] theoretical maximum for semicircular channel wings is $e = 1.5$. Thus the wind tunnel tests reported here have resolved this lack of agreement in favor of Cone's value, $e = 1.5$.

It is speculated that the failure of the channel wing deflected streamtube theory is due to the fact that the channel wing is not a closed shape, as is the ring wing. Apparently the concept of a streamtube "threading" the wing, and being deflected as a rigid cylinder of definite cross-sectional shape, is not valid for an open wing. The lifting arc theory presented in Chapter VI was developed in response to the apparent failure of the deflected streamtube theory to adequately predict the span efficiency factor and induced drag in channel wings. It is evident that a satisfactory theory must predict span efficiency factors of approximately 1.5 for channel wings.

CHAPTER VI

LIFTING ARC THEORY FOR CHANNEL WINGS

Linearizing Assumptions

Consider a bound-vortex arc representing a channel wing. The arc is visualized as having the same spanwise curvature as the channel wing, and is situated in a plane perpendicular to the steady free-stream flow $\vec{V}$. The bound-vortex arc has the (to be prescribed subsequently) circulation distribution $\Gamma(s)$, assumed to be symmetrical about the wing longitudinal centerline and falling to zero at the tips. Between the points s and (s + ds) on the arc, the circulation changes by the amount $(d\Gamma/ds)\cdot ds$; therefore, a trailing vortex line of this strength emanates from the arc element ds and extends downstream to infinity (Glauert [10]). The trailing vortex filaments from all elements of the bound-vortex arc together form a trailing vortex sheet as sketched in Figure 33. Using the induced velocity law of Biot and Savart, Cone [7] gives the resulting flow field as

$$\vec{q} = \vec{V} + \frac{1}{4\pi}\iint^{\Sigma} \vec{\Omega}_{\Sigma} \times \frac{\vec{r}}{r^3}\, dS + \frac{1}{4\pi}\int^{s} \Gamma(s)\,\hat{s} \times \frac{\vec{r}}{r^3}\, ds\,, \qquad (6.1)$$

where $\iint^{\Sigma}$ indicates area integration over the trailing semi-infinite vortex sheet, $\int^{s}$ indicates line integration along the bound-vortex arc, and $\vec{\Omega}_{\Sigma}$ is the vorticity intensity vector of the vortex sheet.

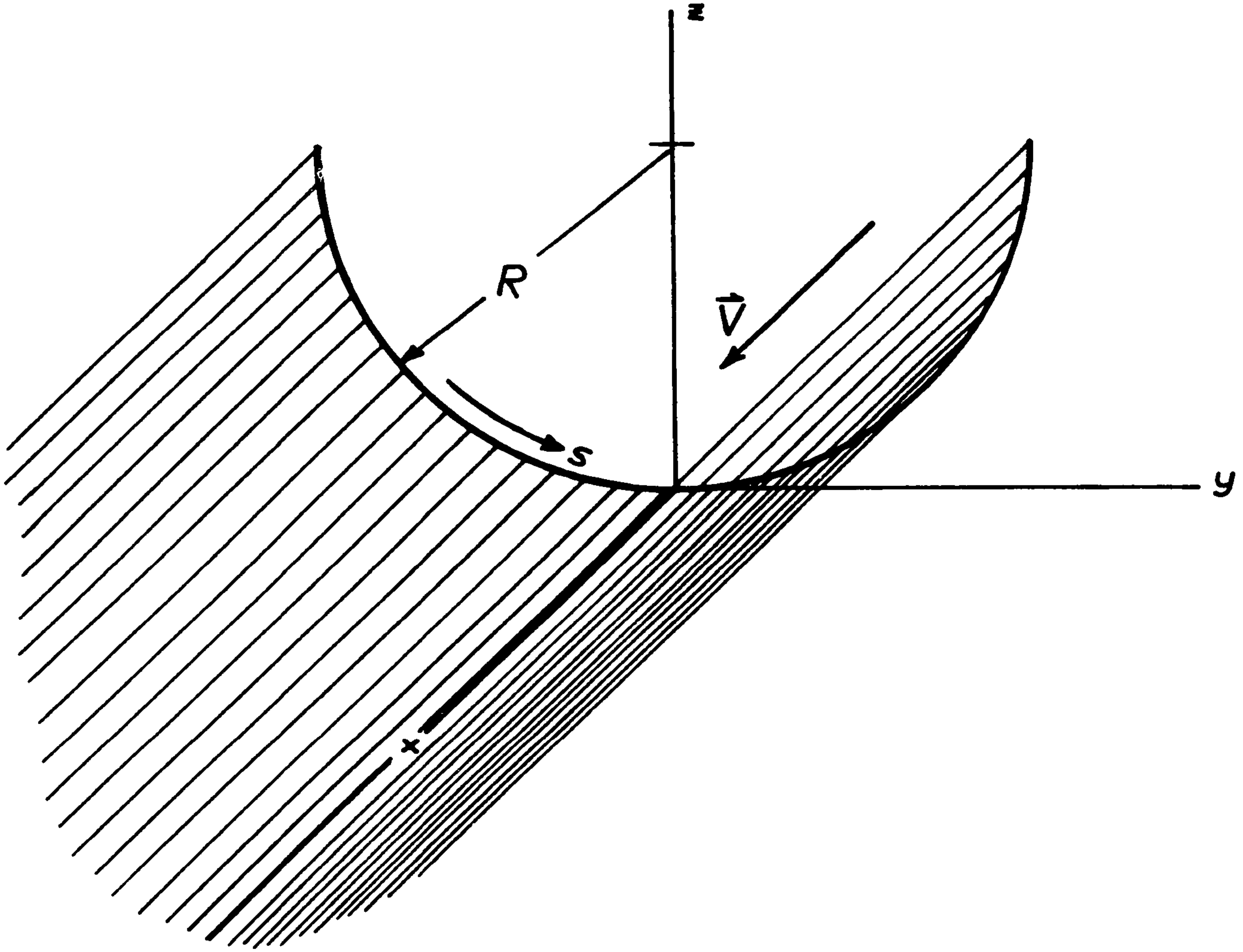

Figure 33. Bound vortex arc with trailing vortex filaments.

This equation is not limited to a bound-vortex arc representing a channel wing, of course.

Now the field $\vec{q}$ is not in general uniform, so the wake will react upon itself, producing distortion of the vortex sheet and introducing non-linear effects (Cone [7]). However, if the rate of change of circulation along the bound-vortex arc is relatively small, then the wake induced velocity (second term in equation (6.1)) will be small compared to $\vec{V}$, and the non-linear wake deformation effects may be neglected. That is, the vortex sheet is assumed to extend unaltered to infinity, parallel to $\vec{V}$, with the cross-sectional shape of the lifting arc. These conditions may be expected to exist for most practical lifting systems with relatively small maximum lift coefficient (Cone [7]).

Nonplanar lifting systems have components of induced velocity, due to the bound vortex, which act parallel to the free-stream velocity $\vec{V}$ (third term in equation (6.1)), thus producing an "induced lift." This is indicated in the accompanying sketch, after Cone [7] :

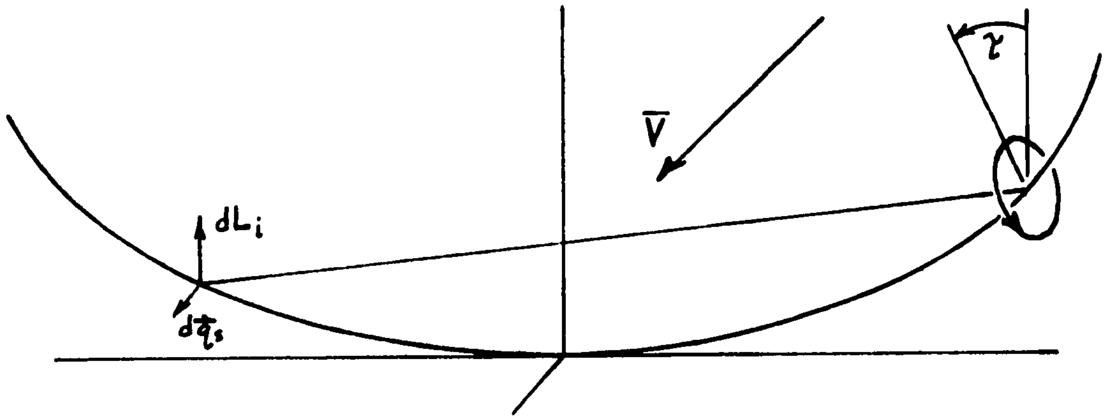

However, under the assumption of small induced velocities, $\vec{q}_s$ may be neglected in comparison with $\vec{V}$.

Except as specifically noted, the linearizing assumptions of small induced velocities in comparison with $\vec{V}$ and negligible wake deformations will be used in the derivations below.

Induced Velocity

Referring to Figure 34, consider the velocity induced at point P (y, z) of the bound-vortex arc (representing the channel wing) by the vortex filament emanating from point P$'$ (ζ, η) of the arc. The filament has strength

$$d\gamma = \frac{d\Gamma}{ds} ds \ ,$$

is parallel to the free-stream velocity (undistorted vortex sheet as discussed above), and extends downstream to infinity. For this case, the Biot-Savart Law reduces to

$$dq = \frac{d\gamma}{4\pi r} \ , \tag{6.2}$$

(Glauert [10]), where the induced velocity dq is normal to the plane containing $\vec{r}$ and the trailing filament, with direction as given by the right-hand rule for the circulation about the filament. But only the component of induced velocity normal to the bound-vortex arc is effective in changing the local section angle of attack and thus producing induced drag:

$$dq_n = \frac{d\gamma}{4\pi r} \cos(\tau - \theta) \quad . \tag{6.3}$$

The total effective induced velocity at P due to the entire vortex

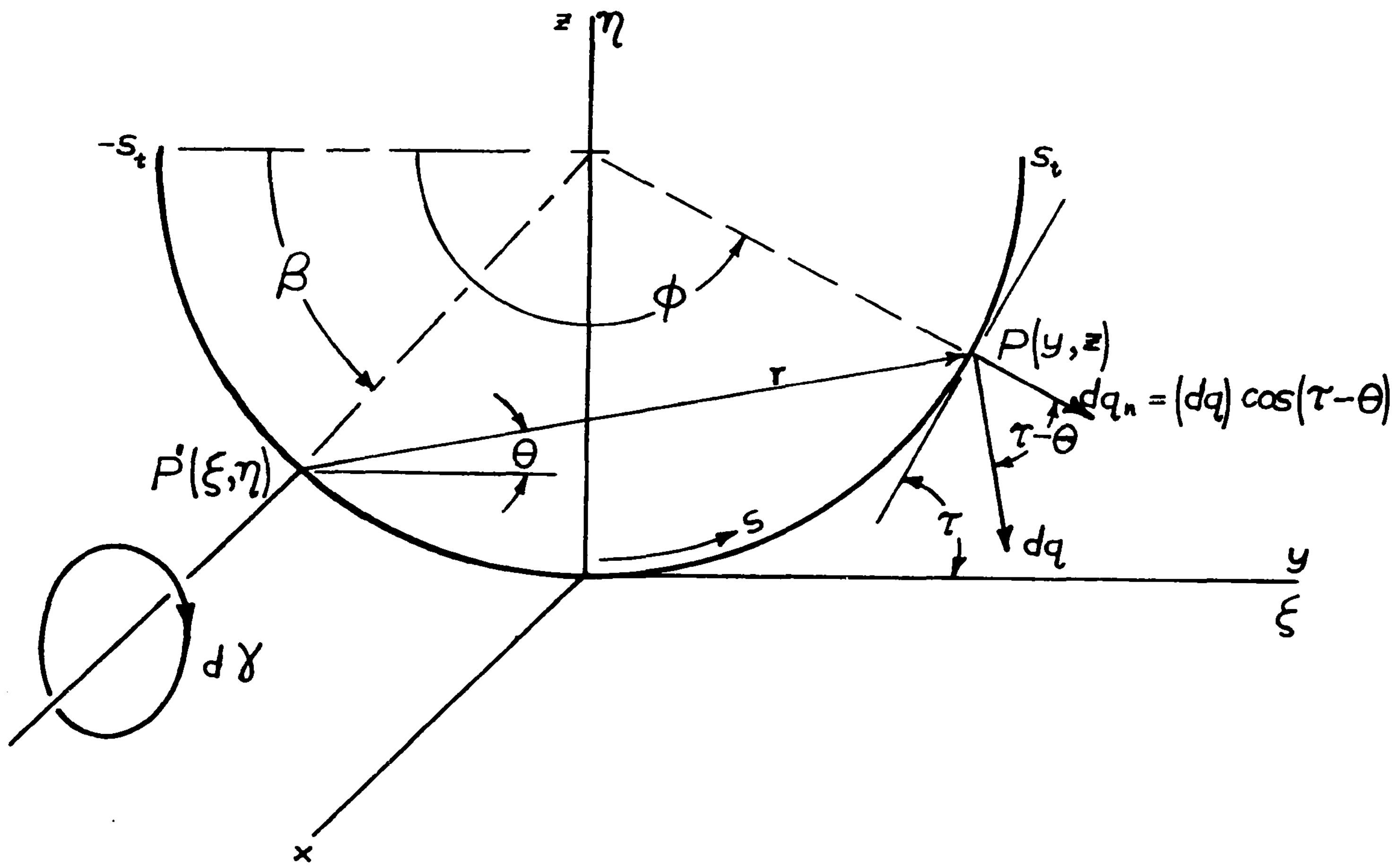

Figure 34. Velocity induced at point on channel wing lifting arc by a trailing vortex filament.

sheet is obtained by integrating along the lifting arc:

$$q_n(y, z) = \frac{1}{4\pi}\int_{-s_t}^{s_t} \frac{\cos(\tau - \theta)}{r}\left(\frac{d\Gamma}{ds}\right) ds \quad . \tag{6.4}$$

Local Effective Angle of Attack

Due to the finite span of the lifting arc, the local incidence at a wing station is reduced by the induced angle of attack. Therefore, the local airfoil section experiences the normal force corresponding to two-dimensional flow at the effective angle of attack,

$$\alpha_o = \alpha_a - \alpha_i \ , \tag{6.5}$$

where

$$\alpha_i = \tan^{-1}\left(q_n/V\right) \approx q_n/V \ , \tag{6.6}$$

see Figure 35. The approximation to α_i is consistent with the linearizing assumption made above (i.e., $q_n \ll V$). Note in Figure 35 that both α_o and α_i are measured from the relative wind, and that α_o and α_a are measured to the zero-lift line.

The absolute angle of attack α_a will be a function of ϕ for the channel wing. The local airfoil section angle of attack α_L is measured in the radial plane at that section. Referring to Figure 2, the velocity components in the radial plane are (assuming an untwisted wing)

$$V_x = V \cos\alpha \tag{6.7}$$

and

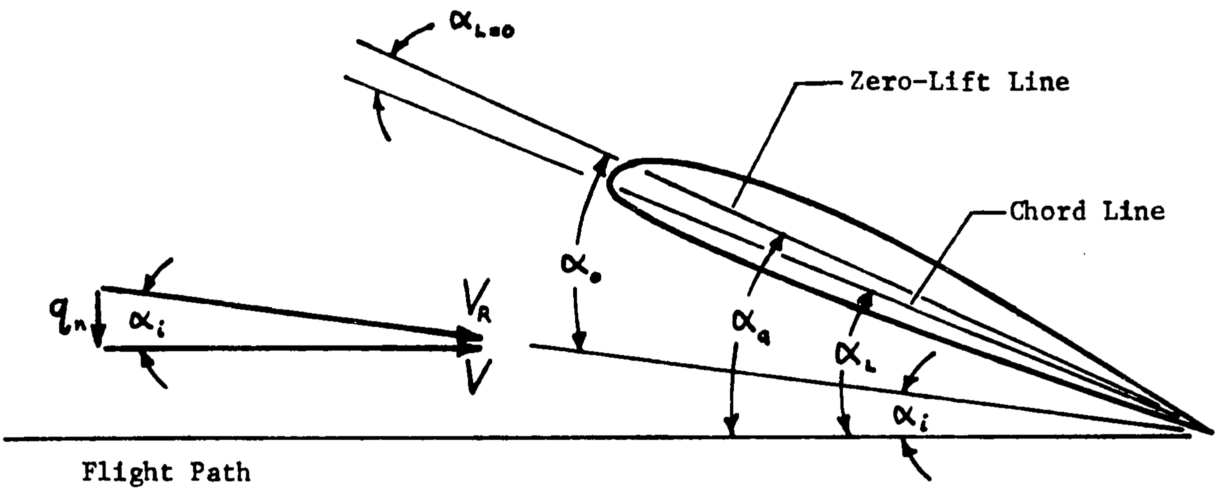

α_L = geometric angle of attack ≡ angle between flight path and chord line of section.

$\alpha_{L=0}$ = angle of zero-lift line ≡ geometric angle of attack for zero section lift.

α_a = absolute angle of attack ≡ angle between flight path and zero lift line.

α_i = induced angle of attack ≡ angle between relative wind V_R and flight path.

α_o = effective angle of attack ≡ angle between relative wind V_R and zero-lift line.

<u>Notes</u>: All angles are in the plane of the local airfoil section.

$\alpha_{L=0}$ is usually a negative number.

Figure 35. Angles associated with the local airfoil section.

$$V_r = V \sin\alpha_c \sin\phi \quad . \tag{6.8}$$

Then the tangent of the angle of the section chord line is

$$\tan\alpha_L = V_r/V_x = \frac{V\sin\alpha_c \sin\phi}{V\cos\alpha_c} ;$$

and thus

$$\tan\alpha_L = \tan\alpha_c \sin\phi$$

$$\alpha_L = \tan^{-1}(\tan\alpha_c \sin\phi) \quad . \tag{6.9}$$

If the airfoil section is cambered, the angle of zero lift must be considered:

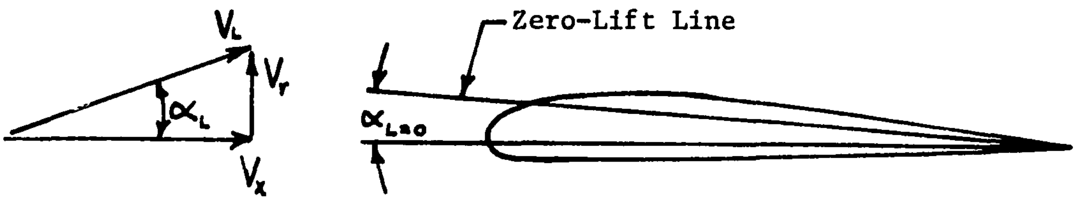

Then the local absolute angle of attack as measured from the section zero-lift line is

$$\alpha_a = \alpha_L - \alpha_{L=0}$$

$$\alpha_a = \tan^{-1}(\tan\alpha_c \sin\phi) - \alpha_{L=0} \tag{6.10}$$

($\alpha_{L=0}$ is given in airfoil data as a negative number), and the local effective angle of attack becomes

$$\alpha_o = \alpha_L - \alpha_{L=0} - q_n/V \quad . \tag{6.11}$$

Circulation

By the Kutta-Joukowski theorem, and with the linearization assumptions discussed above, the aerodynamic force, per unit arc length, normal to both the free-stream velocity and the local segment of the lifting arc is

$$\vec{F}_n{}' = \rho \vec{V} \times \Gamma \hat{s} \quad , \tag{6.12}$$

while the corresponding force parallel to $\vec{V}$ is

$$\vec{F}_p{}' = \rho \vec{q}_n \times \Gamma \hat{s} \quad . \tag{6.13}$$

The magnitude of the normal force intensity is

$$F_n' = \rho V \Gamma = c_l (\rho/2 \, V^2) c \, (1) \quad ,$$

so that the circulation is

$$\Gamma = 1/2 \, c_l c V \quad . \tag{6.14}$$

The local section lift coefficient is

$$c_l = a_o \alpha_o \quad , \tag{6.15}$$

where a_o is the section lift-curve slope,

$$a_o \equiv \frac{dc_l}{d\alpha_o} \quad .$$

Thus, with equation (6.11), equation (6.14) becomes

$$\Gamma = \frac{a_o c}{2} V \left(\alpha_L - \alpha_{L=0} - q_n/V \right) \quad . \tag{6.16}$$

Now, substituting equation (6.4) for q_n, we may write the local channel wing circulation as

$$\Gamma = \frac{a_o c}{2} V \left[\alpha_L - \alpha_{L=0} - \frac{1}{4\pi V} \int_{-s_t}^{s_t} \frac{\cos(\gamma - \theta)}{r} \left(\frac{d\Gamma}{ds} \right) ds \right] \quad . \tag{6.17}$$

Since $ds = R\,d\beta$, we write

$$\left(\frac{d\Gamma}{ds}\right) ds = \left(\frac{d\Gamma}{R\,d\beta}\right)\left(R\,d\beta\right) = \left(\frac{d\Gamma}{d\beta}\right) d\beta \,, \tag{6.18}$$

and

$$\Gamma = \frac{a_o c V}{2}\left[\alpha_L - \alpha_{L=0} - \frac{1}{4\pi V}\int_0^{\pi} \frac{\cos(\tau-\theta)}{r}\left(\frac{d\Gamma}{d\beta}\right) d\beta\right] \,. \tag{6.19}$$

The variables τ , θ , and r will be replaced by use of the relations

$$\cos(\tau-\theta) = \cos\tau\cos\theta + \sin\tau\sin\theta \tag{6.20}$$

and

$$r = \left[(z-\eta)^2 + (y-\xi)^2\right]^{1/2} \,, \tag{6.21}$$

and the coordinate relation (Cone [7]):

$$ds = \sqrt{1 + \left(dz/dy\right)^2}\; dy \,. \tag{6.22}$$

Referring to Figure 34, it is seen that

$$\cos\tau = \frac{dy}{ds} = \frac{1}{\sqrt{1 + \left(dz/dy\right)^2}} \tag{6.23}$$

$$\cos\theta = \frac{y-\xi}{r} = \frac{y-\xi}{\left[(z-\eta)^2 + (y-\xi)^2\right]^{1/2}} \tag{6.24}$$

$$\sin\theta = \frac{z-\eta}{r} = \frac{z-\eta}{\left[(z-\eta)^2 + (y-\xi)^2\right]^{1/2}} \tag{6.25}$$

$$\sin\tau = dz/ds = dz/dy \cdot dy/ds = \frac{dz/dy}{\sqrt{1 + \left(dz/dy\right)^2}} \,. \tag{6.26}$$

Then,

$$\cos(\Upsilon - \theta) = \frac{(y-\xi) + {}^{dz}\!/_{dy}\,(z-\eta)}{\sqrt{1 + \left({}^{dz}\!/_{dy}\right)^2}\,\left[(z-\eta)^2 + (y-\xi)^2\right]^{1/2}} , \qquad (6.27)$$

and equation (6.19) may be written as

$$\Gamma = \frac{a_0 c V}{2}\left[\alpha_L - \alpha_{L=0} - \frac{1}{4\pi V}\int_0^{\pi} \frac{(y-\xi) + {}^{dz}\!/_{dy}(z-\eta)}{\sqrt{1+\left({}^{dz}\!/_{dy}\right)^2}\left[(z-\eta)^2 + (y-\xi)^2\right]}\left(\frac{d\Gamma}{d\beta}\right)d\beta\right] . \qquad (6.28)$$

A further transformation will be useful, as suggested by Blick in unpublished notes. Again referring to Figure 34, we note that

$$z = R - R\sin\phi \qquad\qquad y = -R\cos\phi \qquad (6.29)$$

$$\eta = R - R\sin\beta \qquad\qquad \xi = -R\cos\beta , \qquad (6.30)$$

so $${}^{dz}\!/_{d\phi} = -R\cos\phi \qquad\qquad {}^{dy}\!/_{d\phi} = R\sin\phi , \qquad (6.31)$$

and thus $${}^{dz}\!/_{dy} = {}^{dz}\!/_{d\phi} \cdot {}^{d\phi}\!/_{dy} = -\frac{\cos\phi}{\sin\phi} . \qquad (6.32)$$

Substituting these expressions into equation (6.28), we have

$$\Gamma = \frac{a_0 c V}{2}\left[\alpha_L - \alpha_{L=0} - \frac{1}{4\pi V}\int_0^{\pi} \frac{R(\cos\beta - \cos\phi) - \frac{\cos\phi}{\sin\phi}R(\sin\beta - \sin\phi)}{\sqrt{1 + \frac{\cos^2\phi}{\sin^2\phi}}\left[R^2(\sin\beta - \sin\phi)^2 + R^2(\cos\beta - \cos\phi)^2\right]}\left(\frac{d\Gamma}{d\beta}\right)d\beta\right]$$

After some trigonometric manipulation, we arrive at

$$\Gamma(\phi) = \frac{a_o c V}{2}\left[\alpha_L - \alpha_{L=0} + \frac{1}{8\pi R V}\int_0^{\pi}\cot\left(\frac{\beta-\phi}{2}\right)\left(\frac{d\Gamma}{d\beta}\right)d\beta\right], \qquad (6.33)$$

where $\alpha_L = \tan^{-1}(\tan\alpha_c \sin\phi)$.

Within the assumptions discussed above, (6.33) is the basic equation for the local circulation about a channel wing represented by a lifting arc. Note that the chord c may be a function of ϕ if necessary. In the study reported herein, an approximate solution of equation (6.33) was obtained by using a collocation technique with an assumed infinite series expression for the circulation Γ . The solution is not valid in general near the wing tips, however.

Approximate Solution

The circulation distribution is assumed to be a Fourier sine series in ϕ , symmetrical about the wing midspan, and zero at the wing tips:

$$\Gamma(\phi) = VR\sum_{n=1}^{\infty} A_n \sin n\phi , \qquad n = 1, 3, 5, \ldots, \qquad (6.34)$$

where only the odd n's are retained due to the assumption of symmetry. With this expression, equation (6.33) becomes

$$\sum_{n=1}^{\infty} A_n \sin n\phi = \frac{a_o c}{2R}\left[\alpha_L - \alpha_{L=0} + \frac{1}{8\pi}\int_0^{\pi}\cot\left(\frac{\beta-\phi}{2}\right)\left(\sum_{n=1}^{\infty} n A_n \cos n\beta\right)d\beta\right], \qquad (6.35)$$

where n = 1, 3, 5 . . . . The integral is evaluated in Appendix B, where it is shown that

$$\sum_{n=1}^{\infty} \frac{nA_n}{8\pi}\int \cos n\beta \cot\left(\frac{\beta-\phi}{2}\right) d\beta$$

$$= \sum_{n=1}^{\infty} \frac{nA_n}{8\pi}\left[(\cos n\phi)K_n - (\sin n\phi)J_n\right] \qquad (6.36)$$

for n = 1, 3, 5, . . . ,

where $K_1 = 2 \log\left[\cot(\phi/2)\right] - 2\cos\phi$ (6.36a)

$K_n = K_{n-2} - \frac{2}{n}\cos n\phi - \frac{2}{n-2}\cos(n-2)\phi$, n=3, 5, . . . , (6.36b)

$J_1 = \pi + 2\sin\phi$ (6.36c)

$J_n = J_{n-2} + \frac{2}{n}\sin n\phi + \frac{2}{n-2}\sin(n-2)\phi$, n=3, 5 . . . . (6.36d)

With this result, equation (6.35) may be written as

$$\sum_{n=1}^{\infty} A_n\left\{\sin n\phi + \left(\frac{a_0 nc}{16\pi R}\right)\left[(\sin n\phi)J_n - (\cos n\phi)K_n\right]\right\}$$

$$= \left(\frac{a_0 c}{2R}\right)(\alpha_L - \alpha_{L=0}) , \qquad (6.37)$$

where n = 1, 3, 5, . . .

$\alpha_L = \tan^{-1}(\tan\alpha_c \sin\phi)$.

Equation (6.37) determines the coefficients A_n in the series

$\Gamma(\phi) = VR\sum_{n=1}^{\infty} A_n \sin n\phi$, n=1,3,5, . . .; (6.38)

however, since K_1 (equation (6.36a)) is infinite at $\phi = 0, \pi$, equation (6.37) is not in general valid at the wing tips. By proper selection of the collocation points for evaluation of equation (6.37), as described below, it was found possible to avoid difficulty with the wing tip singularity, and use equations (6.37) and (6.38) to estimate the lift and induced drag of channel wings. Also, if the problem is such that the chord distribution in the vicinity of the wing tips is at the discretion of the investigator, the tip region planform may be chosen such that the singularity in equation (6.37) is removed. This is demonstrated in a subsequent section of this chapter.

For the major part of the study reported herein, only channel wings with rectangular projected planforms (and thus square tips) were considered, since it is believed that this is the most likely form which might be encountered in practice. For this case, the chord c is constant, and equation (6.37) is invalid at the wing tips. However, this singularity did not destroy the value of the channel wing lifting arc theory for estimating the lift and induced drag for this case, since the collocation points were placed well away from the wing tips.

The divergence of K_1 at $\phi = 0, \pi$ leads to a more serious difficulty in the induced velocity. The latter is given by the negative of the right hand side of equation (6.36):

$$q_n/V = -\sum_{n=1}^{\infty} \frac{nA_n}{8\pi}\left[(\cos n\phi)K_n - (\sin n\phi)\,J_n\right] \quad , \tag{6.39}$$

as may be seen by comparing equations (6.16), (6.33), (6.35), and (6.36). It is seen in equation (6.39) that the induced velocity is infinite when K_1 is infinite; that is, at $\phi = 0, \pi$. As shown below, this mathematical singularity in the induced velocity expression is not carried over into the induced drag calculation. However, if one is interested in investigating the channel wing induced velocity distribution, the tip region must be avoided, or a rounded (in plan-form) tip assumed as discussed in a subsequent section of this chapter.

Collocation Method

Equation (6.37) determines the coefficients A_n in the infinite series (6.38), but since A_1, A_3, A_5, . . . decrease rapidly in magnitude, it is sufficient to retain only the first few coefficients. Glauert [10] , in his classical approximate solution for planar wings, which used an approach similar to the present channel wing solution, recommended retention of the first three or four coefficients. Retention of the first five coefficients was the principal choice for the present study, although the effect of the number of coefficients used was investigated, as described below. To determine m coefficients, m simultaneous equations are required, and these equations are obtained by evaluating equation (6.37) for m different values of ϕ along the channel wing lifting arc. The wing lift distribution is assumed to be symmetrical about the centerline; therefore, only points in the range $0° \leq \phi \leq 90°$ need be considered. Since equation (6.37) is not valid at the wing tip, $\phi = 0$ should not be chosen as one of the points to evaluate equation (6.37). These considerations led to evaluation of equation (6.37) at the points (when five coefficients are desired) ϕ = 18°, 36°, 54°, 72°, and 90°, thus yielding five equations for the five unknowns, A_1, A_3, A_5, A_7, and A_9. Evaluation of the coefficients of the simultaneous equations, and solution of the equations to find the A_n's, was performed by the digital computer program developed to mechanize the channel wing lifting-arc theory. The program is described in Chapter VII.

Channel Wing Lift

The channel wing circulation distribution for the symmetrical lift case is given by equation (6.38):

$$\Gamma(\phi) = VR\left[A_1 \sin\phi + A_3 \sin 3\phi + \ldots\right] , \tag{6.40}$$

where the A's are determined for the particular wing and angle of attack as described above. Then the normal force per unit span is

$$F_n' = \rho V \Gamma = \rho V^2 R\left[A_1 \sin\phi + A_3 \sin 3\phi + \ldots\right] . \tag{6.41}$$

The total channel wing lift is obtained by integrating the vertical component of F_n' along the wing:

$$L = \int_0^{\pi} (F_n' \sin\phi)(R\,d\phi)$$

$$L = \rho V^2 R^2 \int_0^{\pi} \left[A_1 \sin\phi + A_3 \sin 3\phi + \ldots \right] \sin\phi \, d\phi \quad . \tag{6.42}$$

But it is a well-known result from integral calculus that

$$\int_0^{\pi} \sin n\phi \sin\phi \, d\phi = \begin{cases} \pi/2 \ , & n = 1 \\ 0 \ , & n = 2, 3, 4, 5, \ldots ; \end{cases}$$

therefore,

$$L = \frac{\pi}{2} \rho V^2 R^2 A_1 \quad . \tag{6.43}$$

The dependence of the channel wing lift solely on the first coefficient A_1 parallels Glauert's [10] approximate solution for the planar wing.

In coefficient form based on the projected wing area $S = 2Rc$,

$$C_L = \frac{\pi}{2c} R A_1 \quad . \tag{6.44}$$

As in Chapter I, the aspect ratio of the channel wing is defined as

$$A\!\!R = \frac{(2R)^2}{S} = \frac{4R^2}{2Rc} = \frac{2R}{c} \ ,$$

so that the channel wing lift coefficient is

$$C_L = \pi/4 \, A\!\!R \, A_1 \quad . \tag{6.45}$$

The lift coefficient is not actually a linear function of aspect ratio, since A_1 is a function of $A\!\!R$.

Channel Wing Induced Drag

The magnitude of the force acting on the channel wing, due to the induced velocity, in the direction of the free-stream velocity is

$$F_p' = \rho q_n \Gamma \tag{6.46}$$

per unit arc length (see equation (6.13)). The circulation Γ is represented by equation (6.38), while the induced velocity q_n is given by equation (6.39). Thus equation (6.46) becomes

$$F_p' = \rho V^2 R \sum_{n=1}^{\infty} \frac{nA_n}{8\pi}\left[(\sin n\phi)\,J_n - (\cos n\phi)\,K_n\right] \cdot \sum_{m=1}^{\infty} A_m \sin m\phi \quad . \tag{6.47}$$

The total channel wing induced drag is obtained by integrating F_p' along the wing from tip to tip:

$$D_i = \int_0^{\pi} F_p'\,(R\,d\phi)$$

$$D_i = \frac{\rho V^2 R^2}{8\pi}\int_0^{\pi}\left\{\sum_{n=1}^{\infty} n A_n\left[(\sin n\phi)J_n - (\cos n\phi)K_n\right] \cdot \sum_{m=1}^{\infty} A_m \sin m\phi\right\} d\phi \ , \tag{6.48}$$

where n = 1, 3, 5, . . . , and m = 1, 3, 5, . . . , and K_n and J_n are given by equations (6.36a) through (6.36d). The integrand in equation (6.48) appears to have a singularity at $\phi = 0, \pi$ due to K_1 (see equation (6.36a)) being infinite at those points, as discussed above. However, it may be seen in equation (6.48) that K_1 is multiplied by $\sum_{m=1}^{\infty} A_m \sin m\phi$, yielding terms of the form

$$(\sin m\phi)\left[\log\left(\cot \phi/2\right)\right] \ ,$$

which is indeterminate at $\phi = 0, \pi$, since m is an integer.

Rewriting as

$$\frac{\log(\cot \phi/2)}{\csc m\phi} ,$$

and applying L'Hôpital's Rule, we write

$$\lim_{\phi \to 0,\pi} \frac{\log(\cot \phi/2)}{\csc m\phi} = \lim_{\phi \to 0,\pi} \frac{-\frac{1}{2}(\tan \phi/2)(\csc^2 \phi/2)}{-m(\cot m\phi)(\csc m\phi)}$$

$$= \lim_{\phi \to 0,\pi} \frac{\sin^2 m\phi}{2m \cos m\phi \cos \phi/2 \sin \phi/2}$$

$$= \lim_{\phi \to 0,\pi} \frac{\sin^2 m\phi}{m \cos m\phi \sin\phi} . \qquad (6.49)$$

Another application of L'Hôpital's Rule yields

$$\lim_{\phi \to 0,\pi} \frac{\log(\cot \phi/2)}{\csc m\phi} = \lim_{\phi \to 0,\pi} \frac{2m \sin m\phi \cos m\phi}{m[\cos m\phi \cos\phi - m \sin m\phi \sin\phi]}$$

$$= \lim_{\phi \to 0,\pi} \frac{\sin 2m\phi}{\cos m\phi \cos\phi + m\cos(m+1)\phi - m\cos m\phi \cos\phi}$$

$$= \lim_{\phi \to 0,\pi} \frac{\sin 2m\phi}{(1-m)(\cos m\phi \cos\phi) + m\cos(m+1)\phi}$$

$$= 0 \qquad . \qquad (6.50)$$

Thus the second term in equation (6.48) is zero in the limit as ϕ approaches zero or π, the integrand is not infinite at the wing tips, and the induced drag is finite.

The integral of equation (6.48) was evaluated in a subroutine of the aforementioned digital computer program for channel wings. The numerical quadrature used is a modified trapezoidal rule method. The particular value of the integral is, of course, a function of the wing parameters and the angle of attack, through the Fourier coefficients A_n.

If the integral in equation (6.48) is designated by I_D, then

$$D_i = \frac{\rho V^2 R^2}{8\pi} I_D \; ; \tag{6.51}$$

or

$$C_{D_i} = \frac{R I_D}{8\pi c} = \frac{AR}{16\pi} I_D \tag{6.52}$$

in coefficient form, based on $S_\ell = 2Rc$. Now, if the induced drag coefficient is defined as

$$C_{D_i} = \frac{C_L^2}{\pi e AR} \, , \tag{6.53}$$

where e is called the span efficiency factor, then

$$\frac{C_L^2}{\pi e AR} = \frac{AR}{16\pi} I_D$$

$$e = 16 \frac{C_L^2}{AR^2 I_D} \quad . \tag{6.54}$$

Substituting equation (6.45) for C_L, the channel wing span efficiency factor is

$$e = \frac{16}{AR^2 I_D} \left(\frac{\pi}{4} AR A_1\right)^2$$

$$e = \frac{\pi^2}{I_D} A_1^2 \quad . \tag{6.55}$$

Channel Wing Profile Drag

The profile drag coefficient of any wing may be represented as

$$C_{D_o} = \frac{1}{S_T}\int_{-S_t}^{S_t} c_d\, c\, ds \,, \qquad (6.56)$$

Abbott and von Doenhoff [18] , where c_d is the local (two-dimensional) section drag coefficient, and S_t is the wing curvilinear semispan (see Figure 34). Now c_d is obtained experimentally for infinite aspect ratio conditions; therefore, a strip-theory summation procedure is required for evaluation of equation (6.56). For the channel wing, the local strip is an element of arc length:

$$C_{D_o} = \frac{2}{S_T} \sum_j c_{d_j}\, c_j\, (R\Delta\phi)_j \,, \qquad 0^\circ \le \phi \le 90^\circ \,, \qquad (6.57)$$

where the symmetrical case has been assumed. Since a constant-chord channel wing is considered here,

$$C_{D_o} = \frac{2}{(\pi R c)}\,(Rc) \sum_j c_{d_j} (\Delta\phi)_j$$

$$C_{D_o} = \frac{2}{\pi} \sum_j c_{d_j} (\Delta\phi)_j \quad , \qquad 0^\circ \le \phi \le 90^\circ \quad . \qquad (6.58)$$

Note that $(\Delta\phi)_j$ here must be in radians.

Extensive data on the experimental two-dimensional characteristics of a large number of airfoil sections have been obtained by the NACA (e.g., Abbott, von Doenhoff, and Stivers [19]). Typically, section drag data are plotted as a function of section lift coefficient; thus section drag coefficient is a function of the local effective angle of attack, which is

$$\alpha_o = \alpha_L - \alpha_{L=0} - q_n/V \quad . \tag{6.11}$$

Recalling equations (6.9) and (6.39), we find that equation (6.11) becomes

$$\alpha_o = \tan^{-1}(\tan\alpha_c \sin\phi) - \alpha_{L=0}$$
$$+ \sum_{n=1}^{\infty} \frac{nA_n}{8\pi}\left[(\cos n\phi)K_n - (\sin n\phi)J_n\right] , \tag{6.59}$$

where K_n and J_n are given by equations (6.36a) through (6.36d). Assuming a linear lift-curve slope for normal angles of attack, the local section lift coefficient is

$$c_l = a_o\left\{\tan^{-1}(\tan\alpha_c \sin\phi) - \alpha_{L=0}\right.$$
$$\left. + \sum_{n=1}^{\infty} \frac{nA_n}{8\pi}\left[(\cos n\phi)K_n - (\sin n\phi)J_n\right]\right\} \quad . \tag{6.60}$$

Only the odd n's are retained, since the symmetrical case has been assumed. Equation (6.60) was evaluated by the channel wing digital computer program, Chapter VII, using the Fourier coefficients A_n determined by the program.

The channel wing lift and drag computer program, Chapter VII, accepts as input a table of airfoil section lift and drag coefficients for the particular wing being considered. Then values of local section c_l (calculated with equation (6.60)) are used to enter the airfoil section data table, the outputs being values of local section c_d for use in equation (6.58). As discussed above, K_1 becomes infinite at the wing tips; however, this presents no difficulty in evaluating equation (6.60), since C_{ℓ_j} and C_{d_j} are evaluated at the center of $(\Delta\phi)_j$.

Channel Wing Total Drag

The profile drag for any nonplanar wing must be based on the total wing area rather than projected wing area, since profile drag is composed of skin friction and pressure drag. This was done above in deriving the channel wing profile drag:

$$D_0 = q S_c C_{D_0} = q(\pi R c) C_{D_0} \quad . \tag{6.61}$$

However, it is convenient to base total channel wing lift and drag on projected wing area. For this purpose, the total channel wing drag is written as

$$C_D = \frac{D_0}{qS} + C_{D_i} = \frac{q(\pi R c)}{q(2Rc)} C_{D_0} + \frac{C_L^2}{\pi e A\!\!R}$$

$$C_D = \frac{\pi}{2} C_{D_0} + \frac{C_L^2}{\pi e A\!\!R} , \tag{6.62}$$

where C_{D_0} is given by equation (6.58) and e by equation (6.55), both of which are evaluated by the channel wing lift and drag computer program, Chapter VII.

Limitations of Lifting Line Theories

The basic idea of lifting line theory is that a stationary two-dimensional line vortex in a moving stream is the equivalent of a two-dimensional wing with circulation in otherwise uniform flow. This conclusion (Kuethe and Schetzer [2]) is based on the twin notions that (1) a unit length of a line vortex stationary with respect to the general flow experiences a force of magnitude $\rho V \Gamma$ in a direction perpendicular to both V and the line vortex, and (2) the lift force experienced by a unit span of a cylinder of any cross section is $\rho V \Gamma$, directed perpendicular to V and the cylinder axis (the Kutta-Joukowski theorem). The first-order effect of finite wing span is to reduce the local section incidence by an induced angle of attack. Therefore, the (two-dimensional) Kutta-Joukowski theorem may be used in the finite wing case by simply assuming that the force experienced by the local section is the same as would be felt by a section of an infinite wing set at an angle of attack equal to the geometric angle reduced by the induced angle. This assumption has been integral to finite-span lifting line analysis since the latter's foundation by Prandtl; however, the first-order effect of finite span has been derived formally by Ashley and Landahl [20] , who examined the matched inner and outer solutions associated with the process $\epsilon_A \rightarrow 0$ at fixed span (where ϵ_A is inversely proportional to aspect ratio), of the equation

$$(1 - M_\infty^2)\frac{\partial u}{\partial x} + \frac{\partial v}{\partial y} + \frac{\partial w}{\partial z} = 0 ,$$

assuming that $M_\infty = 0$ and the wing thickness, angle of attack, and camber are small.

This approach to the finite span problem, which was used in deriving the channel wing lifting arc theory, might appear to be inapplicable at low aspect ratios. On the contrary, however, it has been found to yield remarkably good results for wing lift and induced drag down to aspect ratio of unity. For example, the results of using finite-span lifting line theory to correlate experimental lift and drag data for wings of aspect ratio one through seven are presented in Figure 7-5 of Ashley and Landahl [20] , where the data are shown to collapse to a single lift curve and a single drag curve, within the experimental accuracy.

Although lifting line theory yields useful results for total lift and induced drag even for wings of low aspect ratio, Jordan [21] asserts that neither lifting line theory nor approximate (collocation methods) lifting surface theory can be considered reliable for studies of downwash distribution in the vicinity of the wing tip, for wings of any aspect ratio. Jordan's conclusion stems from his study of the circular planform (planar) wing, for which he obtained an exact solution for the pressure distribution and thus was able to accurately calculate the downwash distribution. It was found that the distribution changes sign, going to a large negative downwash (i.e., upwash) in the vicinity of the wing tip. Jordan states that, qualitatively, the same downwash distribution will be valid for other wing planforms, and that, consequently, elliptic span loading is invalid in the tip region. He also found that the use of approximate methods, such as lifting line analysis, to calculate the downwash distribution from the exact lift distribution (of the circular wing) leads to a divergence to infinite upwash at the wing tip. The conclusions of Jordan cast doubt on the validity of the calculated channel wing downwash distribution in the tip region, as obtained below in the section of this chapter on the rounded planform wing tip.

Convergence of the Approximate Solution

A formal proof of the convergence of the approximate solution for the channel wing lifting arc was deemed not possible, since the function to be represented by the infinite series is not known, but rather is the quantity sought. However, a practical indication of convergence of the solution was desired, especially in view of the divergence of K_1 (equation (6.36a)) at $\phi = 0, \pi$. Therefore, the convergence of the calculated circulation and induced velocity throughout a large sweep of the number of Fourier coefficients A_n was investigated.

For the convergence study, the channel wing computer program described in Chapter VII was modified to iterate on the number of coefficients A_n retained; that is on the number of (equally spaced) collocation points along the lifting arc ($0 < \phi \leq 90°$). Calculated values for circulation and induced velocity for a typical case are presented in Table 4. It may be seen that the lifting arc solution is stable and convergent through forty-five coefficients. This area of convergence represents a wide margin, since five coefficients provided sufficient accuracy for the studies reported herein. The number of A_n's used had little effect on the channel wing circulation distribution, as shown in Figure 36. An example of the variation of calculated channel wing lift and drag with the number of

TABLE 4

CALCULATED CHANNEL WING* CIRCULATION AND INDUCED VELOCITY AS A FUNCTION OF NUMBER OF FOURIER COEFFICIENTS RETAINED

Number of Fourier Coefficients Retained	Γ/Γ_0 At $\Phi = 45°$	$\Delta(\Gamma/\Gamma_0)$	q/V At $\phi = 45°$	$\Delta(q/V)$
3	0.8022		0.06656	
		0.0059		0.0069
5	0.8081		0.06725	
		0.0075		-0.0027
7	0.8156		0.06698	
		0.0011		0.0012
9	0.8167		0.06710	
		0.0022		-0.0009
11	0.8189		0.06701	
		0.0004		0.0004
13	0.8193		0.06705	
		0.0009		-0.0003
15	0.8202		0.06702	
		0.0002		0.0001
17	0.8204		0.06703	
		0.0005		-0.0002
19	0.8209		0.06701	
		0.0001		0.0001
21	0.8210		0.06702	
		0.0004		-0.0001
23	0.8214		0.06701	
		0.0000		0.0001
25	0.8214		0.06702	
		0.0002		-0.0001
27	0.8216		0.06701	
		0.0001		0.0000
29	0.8217		0.06701	
		0.0001		-0.0001
31	0.8218		0.06700	
		0.0001		0.0001
33	0.8219		0.06701	
		0.0001		-0.0001
35	0.8220		0.06700	
		0.0000		0.000
37	0.8220		0.06700	
		0.0001		0.000
39	0.8221		0.06700	
		0.0000		0.000
41	0.8221		0.06700	
		0.0001		0.000
43	0.8222		0.06700	
		0.0000		0.000
45	0.8222		0.06700	

* AR = 1.0 Model, NACA 4412, a_0 = 0.095/degree, $\alpha_c = 6°$

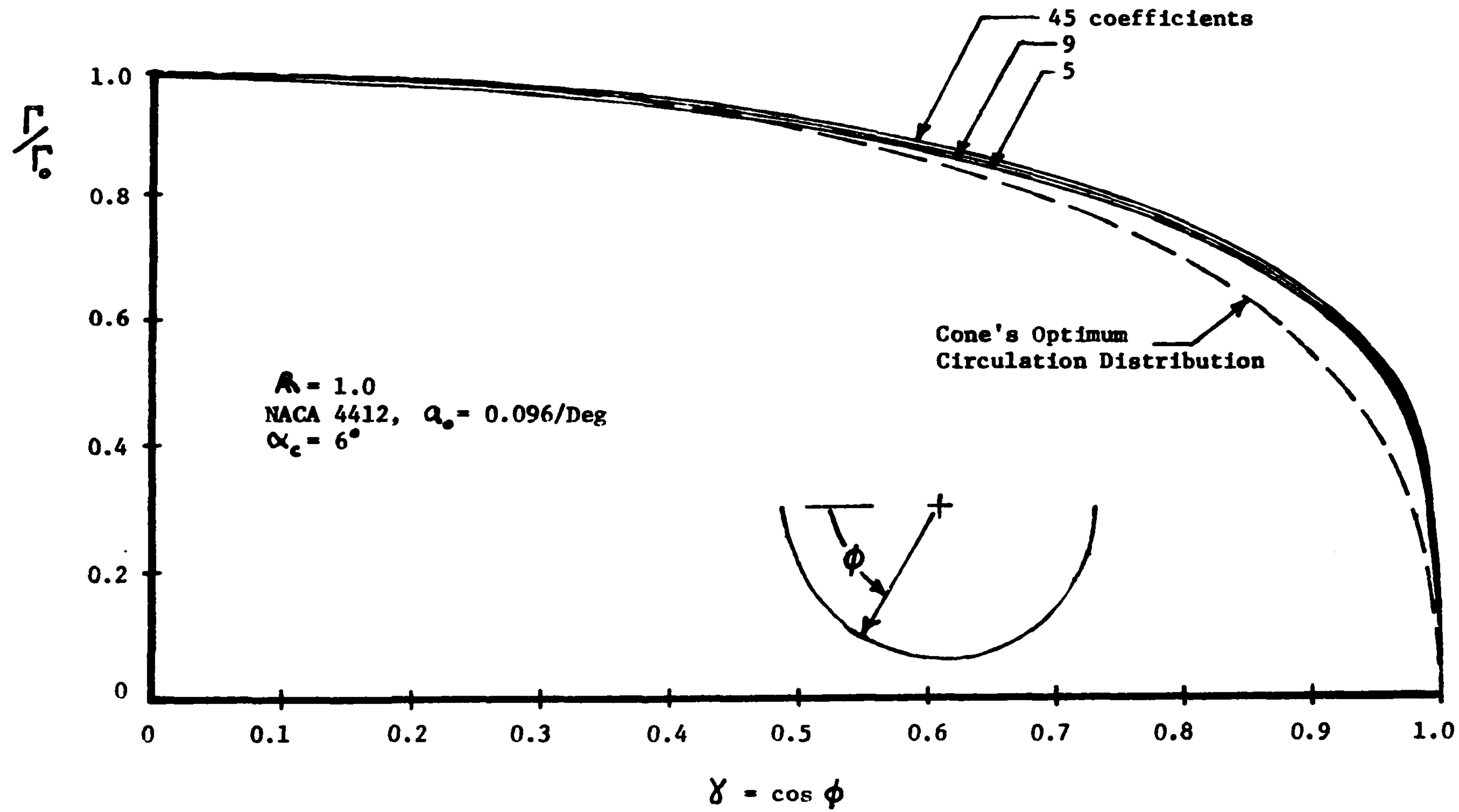

Figure 36. Effect of number of Fourier coefficients retained on channel wing circulation distribution.

coefficients retained is shown in Figures 37 and 38. Although the drag curves for only three through six coefficients are plotted in Figure 38, the drag curves through forty-five coefficients fall within the envelope shown.

Major William A. Edgington of the US Air Force Academy is presently engaged in a general study of lifting-line analysis of nonplanar wings. In a private communication with the author, Major Edgington discussed the results of his calculation of circulation distribution for several constant-chord nonplanar wings with elliptical spanwise curvature, including a semi-circular (channel) wing. Edgington found that if a collocation point is placed too close to the wing tip, the calculated circulation distribution exhibits excessive oscillation. For a collocation point at the wing tip, the solution is divergent, as was found in the study reported herein. Edgington found that the collocation point separation (from the wing tip) required to obtain a smooth circulation distribution varied with the eccentricity of the span curvature. For the case corresponding to the channel wing, the minimum angular separation allowable appears to be between 0.100 and 0.025 radians. The use of a maximum of forty-five Fourier coefficients, yielding a separation between the wing tip and the first collocation point of 0.035 radians, in the study described above was merely fortuitous, since the choice was made before the author became aware of Major Edgington's work.

The results discussed above indicate that the channel wing lifting arc solution given by equations (6.37) and (6.38) is

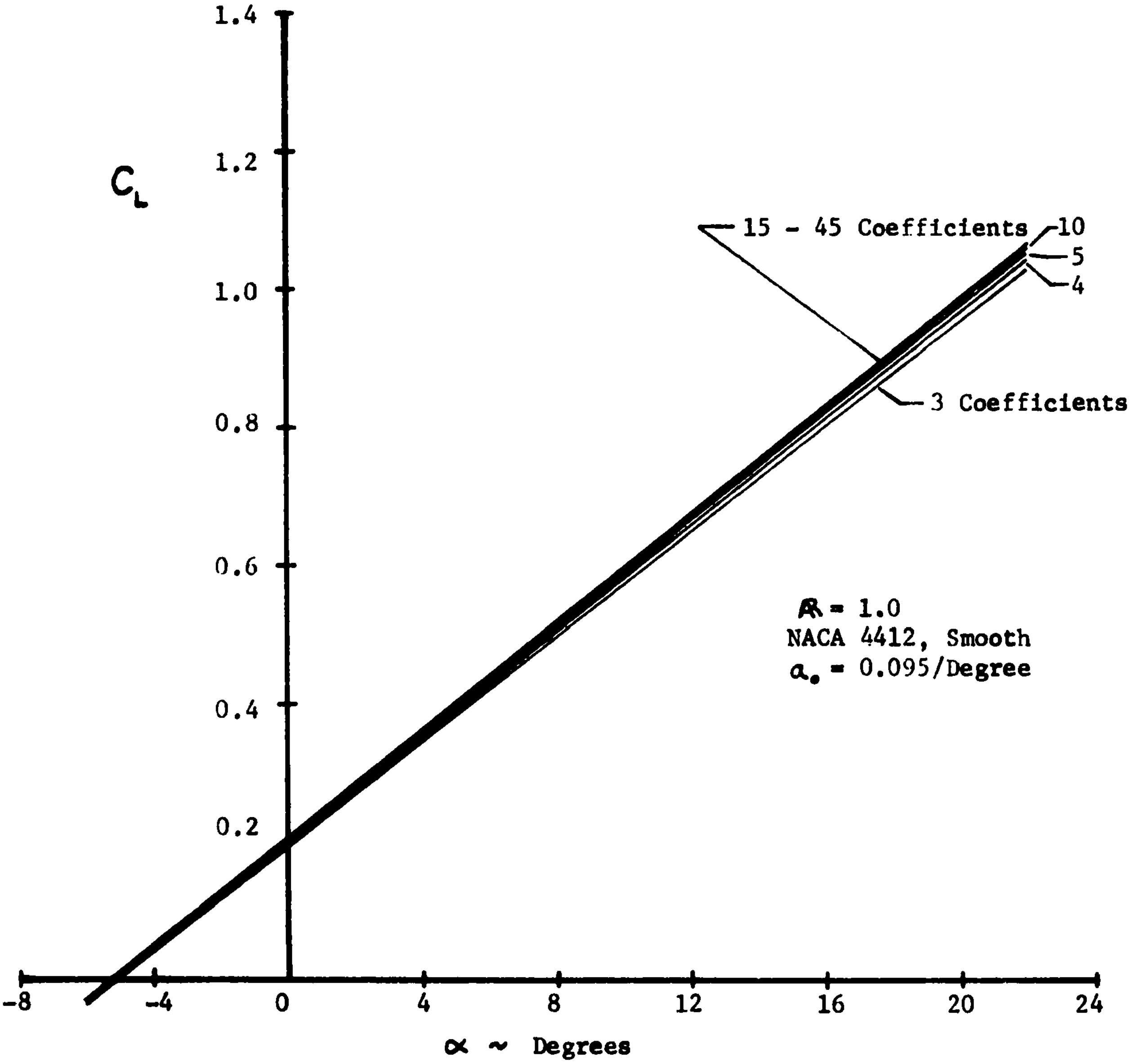

Figure 37. Effect of number of Fourier coefficients retained on predicted lift of a channel wing.

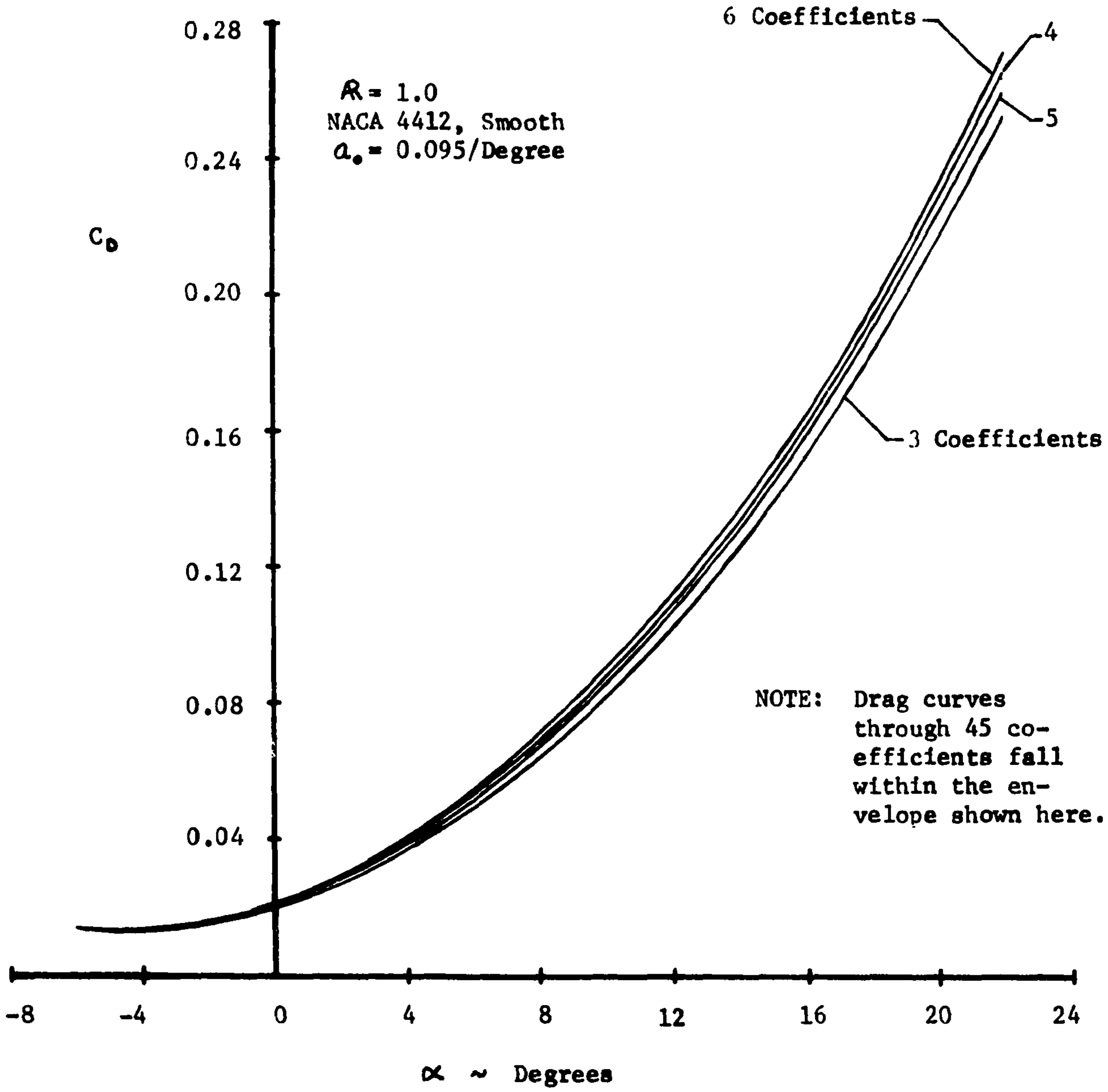

Figure 38. Effect of number of Fourier coefficients retained on predicted drag of a channel wing.

convergent at least through the range of forty-five Fourier coefficients. Ultimately, however, the solution would diverge as the number of coefficients is increased so as to cause the first collocation point to approach too close to the wing tip.

Rounded Planform Wing Tip

The majority of the channel wing study was devoted to constant chord channel wings because it was felt that this would be the planform selected in actual practice. However, the proper choice of a rounded wing tip was found to be useful for investigating the tip region, since the K_1 term (see equation (6.36a)) in equation (6.37) is infinite at $\phi = 0, \pi$ for the rectangular wing tip. Consider the chord distribution

$$c = c_0 \sin k\phi \ , \qquad (6.63)$$

where c_0 and k are constants. Substitution of this relation in equation (6.37) yields terms of the form

$$(\sin k\phi)\left[\log\left(\cot\frac{\phi}{2}\right)\right] \quad .$$

Now if k is an integer, this is exactly the same form as that which was shown above in the induced drag discussion to be finite even at $\phi = 0, \pi$. Therefore, the chord distribution given by equation (6.63) allows evaluation of equation (6.37) in the tip region. However, it is not practical to evaluate (6.37) exactly at $\phi = 0$, since in that case the equation is identically zero.

The constant k in equation (6.63) is determined from considerations of the size of the rounded tip region desired. At the junction of the tip and the constant chord portion of the channel wing, $c = c_0$, requiring that $\sin(k\phi) = 1$, or $k\phi = \pi/2$. Let the tip region curvilinear span be ΨR,

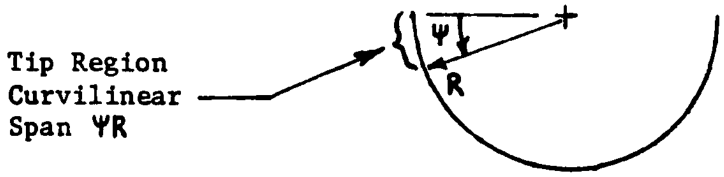

then at the junction of the tip region and the wing, $\phi = \Psi$, so that

$$k\phi = k\Psi = \pi/2$$

$$k = \frac{\pi}{2\Psi}, \qquad (6.64)$$

with the restriction that k must be an integer. It is likely that a channel wing will have constant chord over the great majority of its span. Therefore, Ψ will be small, requiring k to be large. For example, the channel wing wind tunnel models described in Chapter III were essentially rectangular in planform, the tips differing from this shape only by rounding of the edges to avoid sharp corners and edges. A value of $\Psi R = 0.2$ inches is representative of these models (this is not meant to imply that the wing tips were shaped to the distribution $c = c_0 \sin\phi$). The $\mathcal{R} = 1.0$ model had a 6 inch radius, so

$$\Psi = \frac{0.2}{6} = 0.0333 \text{ radians} = 1.9^\circ,$$

and

$$k = \frac{\pi}{2\Psi} = \frac{\pi}{2(.0333)} = 47.2 \quad .$$

Since k must be an integer, 47 would be used.

A brief study of the effect of the rounded tip on calculated induced velocity was conducted. The channel wing computer program described in Chapter VII was modified to use equation (6.63), and the induced velocity distributions for several values of tip region span, for a particular channel wing, are plotted in Figure 39. To obtain a smooth curve, it was found necessary to calculate the induced velocity at the same points along the span at which equation (6.37) was evaluated. A large number of coefficients were used to insure that tip region details of the induced velocity curve would be obtained. Figure 39 indicates the divergence of the calculated induced velocity at $\phi = 0$ for the rectangular tip case, and shows how q/V in the tip region is reduced as the tip span is increased. The tip region spans used in Figure 39 are small fractions of the total wing span. For example, the $\Psi = 3.8°$ case corresponds to a tip span to wing curvilinear semispan ratio of 0.042 for the $AR = 1.0$ wind tunnel model. A relatively small change in wing area is involved, and the performance is not appreciably effected, as can be seen in Table 5. In fact, even for the $\Psi = 11.3°$ case, the lift to drag ratio is reduced by less than one percent. For purposes of comparison, all coefficients in Table 5 are based on the (projected) area of the rectangular tip wing. Within the range tested, the rounded tip had no appreciable effect on the circulation.

Alternate Solution Attempted

In the course of the channel wing study reported herein, several assumed infinite series expressions for circulation other

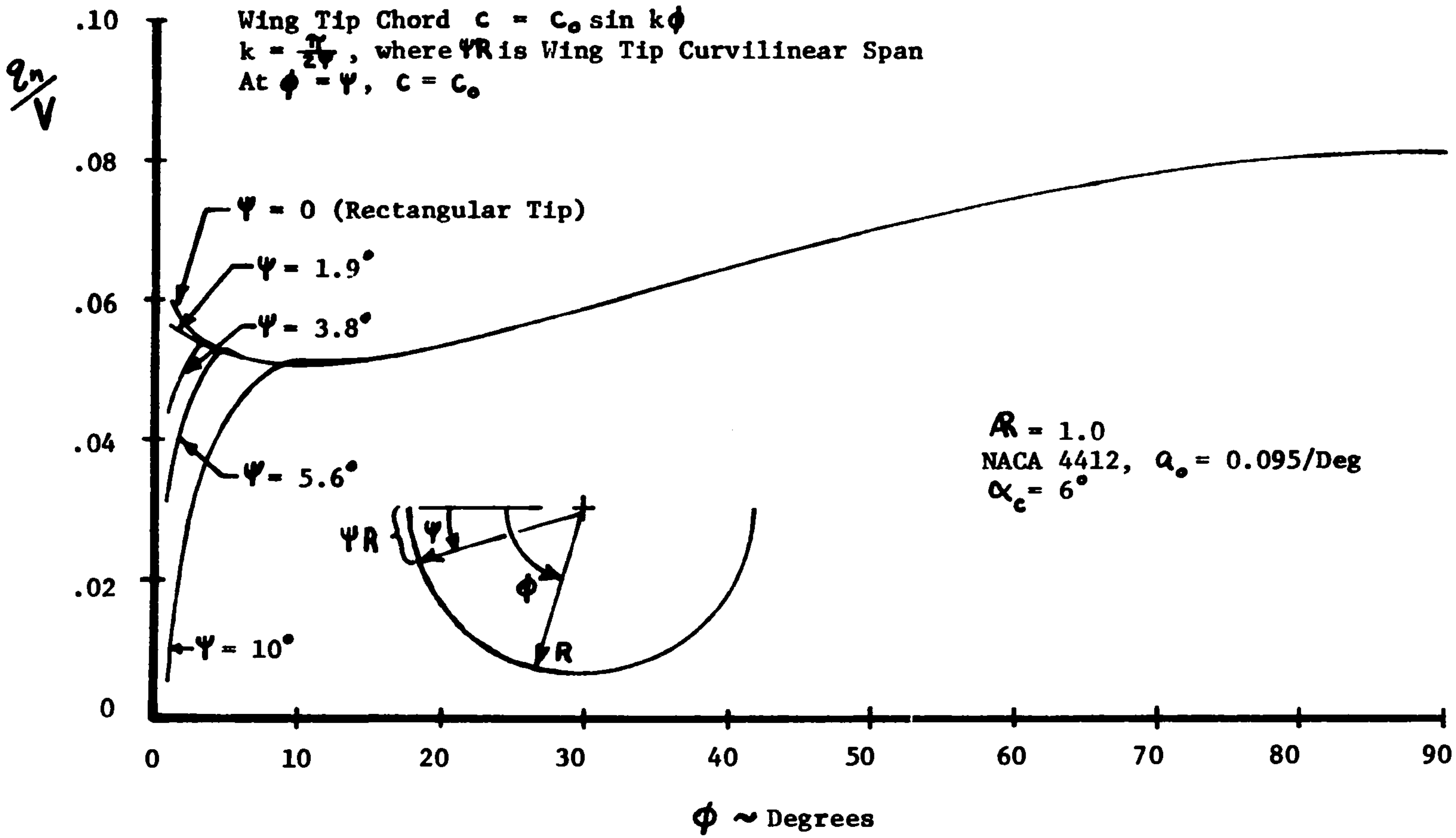

Figure 39. Effect of rounded tip on channel wing induced velocity distribution.

TABLE 5

EFFECT OF ROUNDED TIP ON CHANNEL WING* PERFORMANCE

ψ	Tip Span / Curv. Semispan Ratio	C_L	C_{D_i}	C_D	e (Span Efficiency Factor)
0°	0.0	0.4399	0.04156	0.05310	1.482
1.4°	0.016	0.4399	0.04156	0.05310	1.482
1.9°	0.021	0.4399	0.04156	0.05310	1.482
2.8°	0.031	0.4398	0.04155	0.05309	1.482
3.8°	0.042	0.4398	0.04155	0.05309	1.482
5.6°	0.062	0.4396	0.04155	0.05308	1.480
11.3°	0.126	0.4386	0.04188	0.05338	1.462

* $\mathcal{R}$ = 1.0 Model, NACA 4412, a_0 = 0.095/degrees, α_c = 6°; all coefficients are based on area of the rectangular tip wing.

than

$$\Gamma(\phi) = VR \sum_{n=1}^{\infty} A_n \sin(n\phi) \tag{6.34}$$

were investigated. In particular, the expression

$$\Gamma(\phi) = VR \sum_{n=1}^{\infty} A_n \sin^2(n\phi) \tag{6.65}$$

was carried through to a solution for the coefficients A_n in a manner similar to that used to obtain equation (6.37) above. The result was

$$\sum_{n=1}^{\infty} A_n \left\{ \sin^2 n\phi - \left(\frac{a_o c}{2R}\right)\left(\frac{n}{8\pi}\right)\left[(\cos 2n\phi)\, J_n \right.\right.$$

$$\left.\left. + (\sin 2n\phi) K_n \right]\right\} = \left(\frac{a_o c}{2R}\right)(\alpha - \alpha_{L=0}) \, , \tag{6.66}$$

where

$$J_1 = \pi + 4 \sin\phi \tag{6.66a}$$

$$J_n = J_{n-2} + \left(\frac{4}{2n-3}\right) \sin(2n-3)\phi + \left(\frac{4}{2n-1}\right) \sin(2n-1)\phi \, , \tag{6.66b}$$

$n = 3, 5, 7, \ldots$, and

$$K_1 = 2 \log(\cot \phi/2) - 4 \cos\phi \tag{6.66c}$$

$$K_n = K_{n-2} - \left(\frac{4}{2n-3}\right) \cos(2n-3)\phi - \left(\frac{4}{2n-1}\right) \cos(2n-1)\phi \, . \tag{6.68d}$$

$n = 3, 5, 7, \ldots .$

Although K_1 is infinite at $\phi = 0, \pi$ in this case also, the product $(\sin 2\phi)\, K_1$ in equation (6.68) is finite. This can be shown with L'Hôpital's Rule exactly as was done above in the discussion of induced drag. However, upon implementation in a computer program similar to that described in Chapter VII, the solution given by equations (6.67) and (6.68) was found to be unstable, yielding very poor accuracy if only three or four A_n's were retained, and completely meaningless results if more coefficients were used.

CHAPTER VII

CHANNEL WING DIGITAL COMPUTER PROGRAM

A digital computer program was developed by the author to implement the lifting arc theory for channel wings presented in Chapter VI. The source program was written in FORTRAN IV language, and compiled and executed on an IBM system 360 electronic digital computer. The program is described briefly in the following paragraphs, and a complete FORTRAN listing (including subroutines) is presented in Appendix C.

Program Description

The computer program first develops the simultaneous equations for the Fourier coefficients of the circulation distribution by evaluating equation (6.37) for as many ϕ values as the number of coefficients to be retained. Most of the computations reported here were done with five coefficients, and the FORTRAN listing given in Appendix C is set up for five coefficients. The effect of the number of coefficients retained in the circulation distribution is discussed in Chapter VI, page 114.

The simultaneous equations for the Fourier coefficients are solved by subroutine SIMQ, obtained from the IBM Scientific Subroutine Package. SIMQ uses a Gaussian elimination method and the "largest pivotal divisor" approach to obtain the solution of a set of simultaneous linear equations. The output of the subroutine is the set of coefficients A_n in the circulation distribution, equation (6.38).

The channel wing predicted lift is easily evaluated (see equation (6.45)) using the first Fourier coefficient, A_1. However, the induced drag, equation (6.48), requires the evaluation of a difficult integral. The double summation required to set up the induced drag integrand is performed by a function subroutine in the computer program. The summations are carried out only over the number of coefficients used in the circulation distribution, of course. Then the integral is evaluated by the subroutine QATR, another IBM Scientific Subroutine Package subroutine. The numerical quadrature used is a modified trapezoidal rule method. The numerical value of the induced drag integral is used in the computer program to calculate the induced drag coefficient and the span efficiency factor, equations (6.52) and (6.55), respectively.

The strip-theory method used to evaluate the channel wing profile drag was described in Chapter VI. The computer program evaluates equation (6.60) to obtain the local airfoil section lift coefficient. Then the local section drag coefficient is obtained from an input table of section lift and drag coefficients for the particular airfoil section and Reynolds number being considered. Interpolation in the data table is performed by the subroutines ATSG and ALI (again from the IBM Scientific Subroutine Package). The channel wing profile drag coefficient is estimated by summing the local section drag coefficients over the wing, equation (6.58).

The channel wing total drag is the sum of the induced drag and the profile drag, equation (6.62). The principal outputs of the channel wing computer program are the lift and drag coefficients calculated as functions of the wing geometry, airfoil section characteristics, and the wing centerline angle of attack, which the program steps through a range selected by the user. The program as listed in Appendix C is set up for a channel wing with rectangular planform (constant chord) and zero twist; however, it would be relatively simply to modify the program to allow variable chord and twist if so desired. Indeed, the author did modify the program for a linear (with ϕ) wing twist while investigating the correlation between the circulation distribution calculated with the lifting arc theory and Cone's [7] optimum circulation distribution. This is discussed in Chapter VIII.

Program Inputs and Outputs

The input data required for the channel wing computer program are listed and described in Table 6. Sample computer printouts of input and output data are presented in Appendix C with the program FORTRAN listing. The input data shown are for the $\mathcal{R} = 2.8$ wind tunnel model described in Chapter III. The input table of airfoil section data is not normally printed out. The section lift and drag data for the airfoils used for the wind tunnel models tested are presented in Appendix D.

TABLE 6

INPUTS REQUIRED FOR CHANNEL WING COMPUTER PROGRAM

FORTRAN Name	Input Format	Description	Units	Comments
CIDEN	10A4	Identification of Wing		
AERSEC	10A4	Identification of Airfoil		
IROW	I3	Number of points in airfoil section $C_\ell - C_d$ table.		50 points max.
CDERR	F10.0	Upper bound for interpolation error in $C_\ell - C_d$ table.		
CLMIN	F10.0	Minimum C_ℓ in $C_\ell - C_d$ table.		If exceeded, C_ℓ = CLMIN.
CLMAX	F10.0	Maximum C_ℓ in $C_\ell - C_d$ table.		If exceeded, C_ℓ = CLMAX.
TCL(I)	F10.0	Airfoil section C_ℓ for table data point (I).		*
TCD(I)	F10.0	Airfoil section C_d for table data point (I).		*
R	F10.0	Wing radius	Ft.	
C	F10.0	Wing chord	Ft.	
ASO	F10.0	Airfoil section lift-curve slope.	1/rad.	
ANZL	F10.0	Airfoil section angle for zero lift.	degrees	
ALPAS	F10.0	First wing (centerline) angle of attack point	degrees	
DALPA	F10.0	Wing (centerline) angle of attack increment.	degrees	
ALPAE	F10.0	Final wing (centerline) angle of attack point.	degrees	

*The airfoil section $C_\ell - C_d$ table data points are punched in pairs (C_ℓ, C_d), three data points to a card (6F10.0).

The calculated output data for one wing angle of attack (for the $AR = 2.8$ model) are also shown in Appendix C. These data include the coefficients of the circulation distribution, the span efficiency factor, the wing lift coefficient, and the profile, induced, and total wing drag coefficients. The program can be easily modified to print out other calculated values, such as the circulation distribution along the wing. In fact, this was done during the program development and checkout.

CHAPTER VIII

CORRELATION OF CHANNEL WING LIFTING ARC THEORY

Circulation Distribution and Span Efficiency Factor

Cone [7] predicted the circulation distributions required for minimum induced drag (maximum span efficiency factor) for many nonplanar wings (See Chapter II, page 21 above for a brief description of his method). Cone's optimum circulation distribution for a semi-circular arc wing (i.e., channel wing) is shown by the dashed line in Figure 40, where it is compared with the circulation distribution predicted by the author's lifting arc theory, for several aspect ratios. The latter distributions are displaced somewhat from Cone's optimum value, with the displacement increasing with aspect ratio (although apparently approaching a limiting value).

The channel wing span efficiency factors predicted by the lifting arc theory are slightly less than Cone's [7] predicted maximum value of 1.50. For the case shown in Figure 40, the lifting arc theory values for e are 1.466, 1.466, 1.450, and 1.441, for aspect ratio 1.0, 2.8, 6.0, and 12.0, respectively. If e = 1.50 is considered the nominal value, these lifting arc theory predictions for span efficiency factor are in error by only 2.3% to 3.9%. However, it is not clear that the correct (actual) value for an

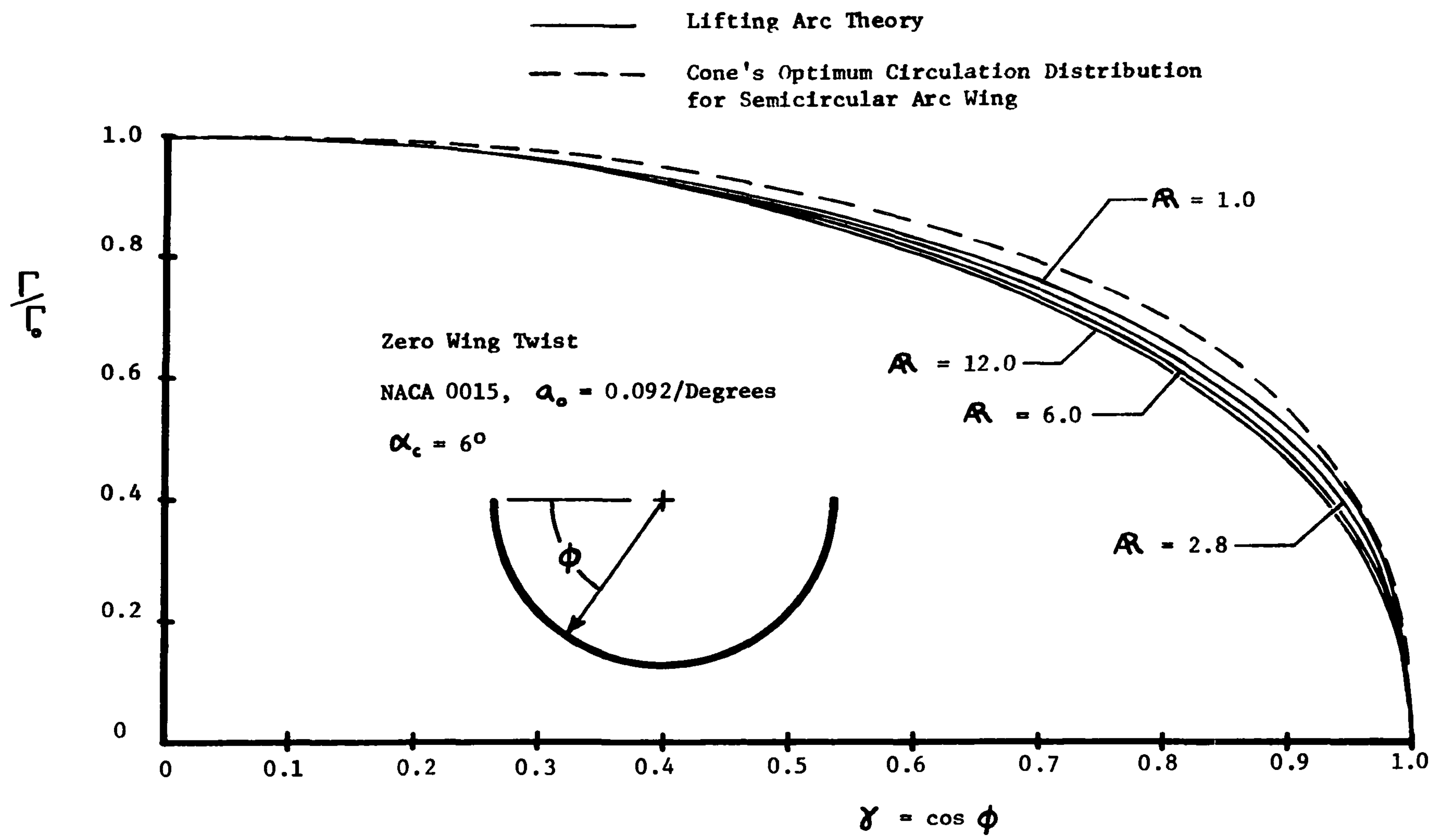

Figure 40. Effect of channel wing aspect ratio on circulation distribution.

untwisted channel wing is 1.5, since Cone's value is a theoretical maximum dependent on a certain optimum circulation distribution. Thus the lifting arc theory values for e may be more exact for an untwisted, constant chord channel wing than is e = 1.50.

The effect of geometric twist on the channel wing was investigated by modifying the digital computer program (Chapter VII) to allow for a linear (with ϕ) twist distribution along the wing span. Then the calculated circulation distribution was compared with Cone's [7] optimum distribution. Figures 41 and 42 indicate the effect of linear twist on the circulation distribution of channel wings of aspect ratio 1.0 and 6.0, respectively. α_t is the change in angle of attack at the wing tip due to the wing twist. The figures show that excessive twist causes the circulation distribution to "overshoot" Cone's optimum distribution, and this effect is stronger for the higher aspect ratio wing. It may be seen in Figure 41 that $\alpha_t = 0.8^\circ$ produces a circulation distribution very close to Cone's optimum for the $A\!R$ = 1.0 case. For the $A\!R$ = 6.0 case, $\alpha_t = 0.8^\circ$ gives the best agreement with Cone's distribution in the inboard region, while $\alpha_t = 1.0^\circ$ yields closer agreement in the outboard area. The correlation of circulation distributions shown in Figures 41 and 42 is probably as close as can be obtained with simple linear wing twist. A rather complicated twist distribution would be required to increase the correlation.

Although calculated circulation distributions are shown in Figures 41 and 42 which lie very close to Cone's [7] predicted

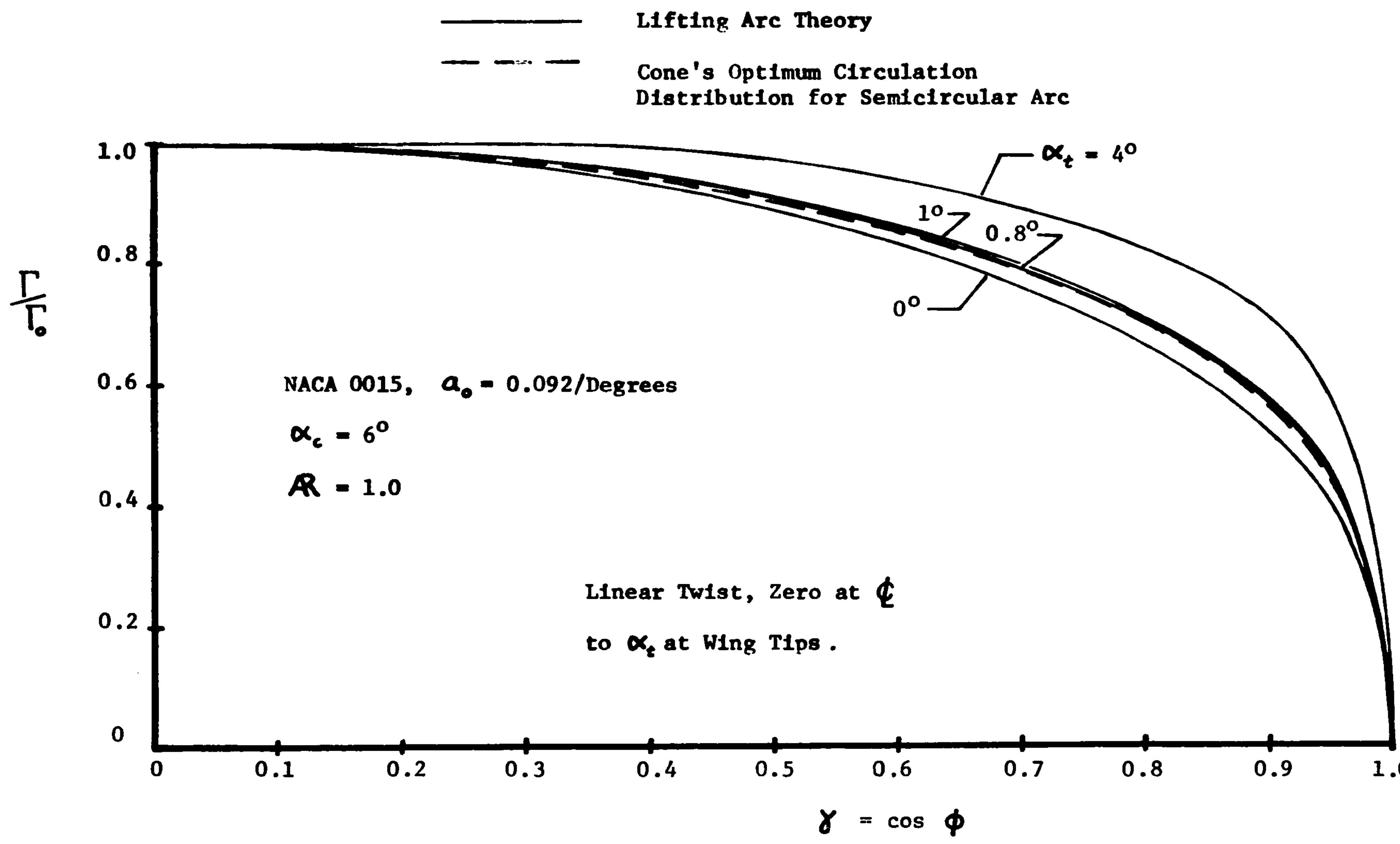

Figure 41. Effect of twist on AR = 1.0 channel wing circulation distribution.

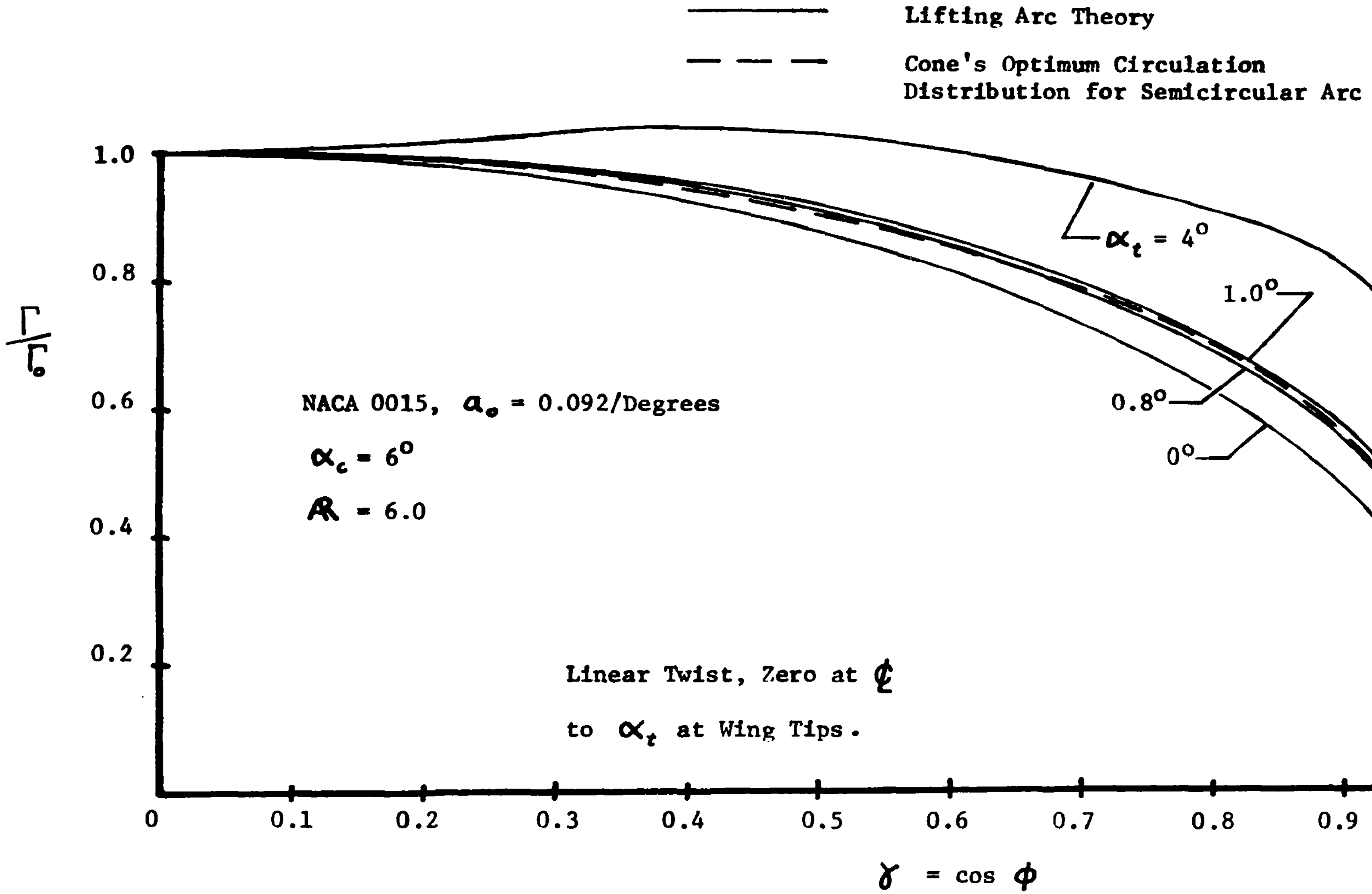

Figure 42. Effect of twist on AR = 6.0 channel wing circulation distribution.

optimum distribution, the calculated span efficiency factors do not quite reach Cone's predicted maximum, e = 1.50. As shown in Table 7 the span efficiency factor values predicted by the lifting arc theory for this case are slightly less than 1.50, but are maximum when the circulation distribution is closest to Cone's optimum distribution. However, the best linear twist yields only a 1.6% gain in span efficiency factor over the untwisted case, for AR = 6.0, and only 0.5% for AR = 1.0.

TABLE 7

CALCULATED CHANNEL WING* SPAN EFFICIENCY FACTOR AS A FUNCTION OF LINEAR WING TWIST

AR = 1.0		AR = 6.0	
Twist (Degrees)	e	Twist (Degrees)	e
0	1.466	0	1.450
0.8	1.473	0.8	1.472
1.0	1.473	1.0	1.473
4.0	1.443	4.0	1.382

*NACA 0015, a_0 = 0.092/Degree, $\alpha_c = 6°$.

An example of the effect of wing twist on calculated channel wing lift and drag is shown in Figures 43 and 44. As might be expected, lift increases with twist, at constant wing centerline angle of attack. However, this is at the expense of higher drag. The lift curve slope remains unchanged.

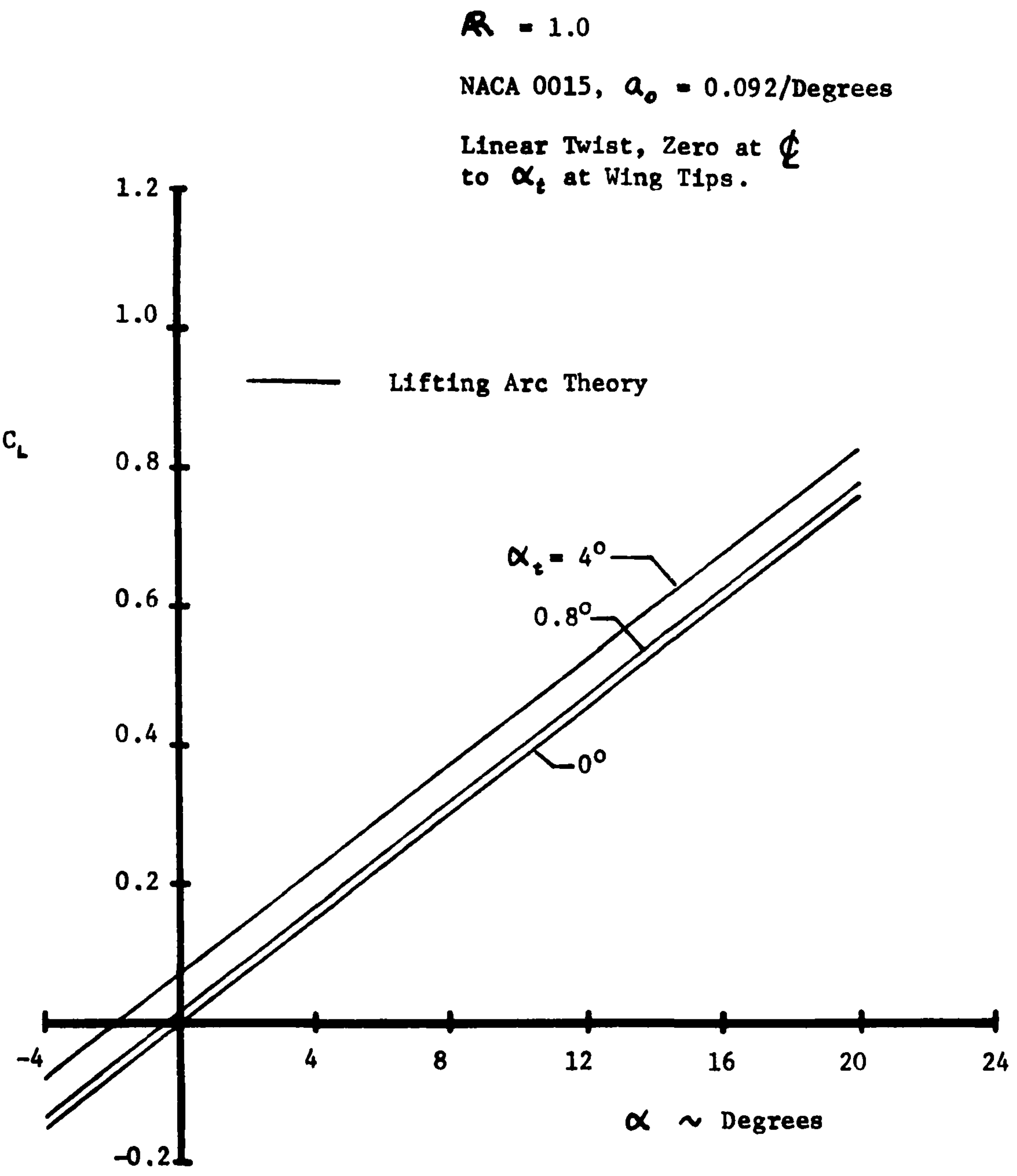

Figure 43. Effect of twist on calculated channel wing lift coefficient.

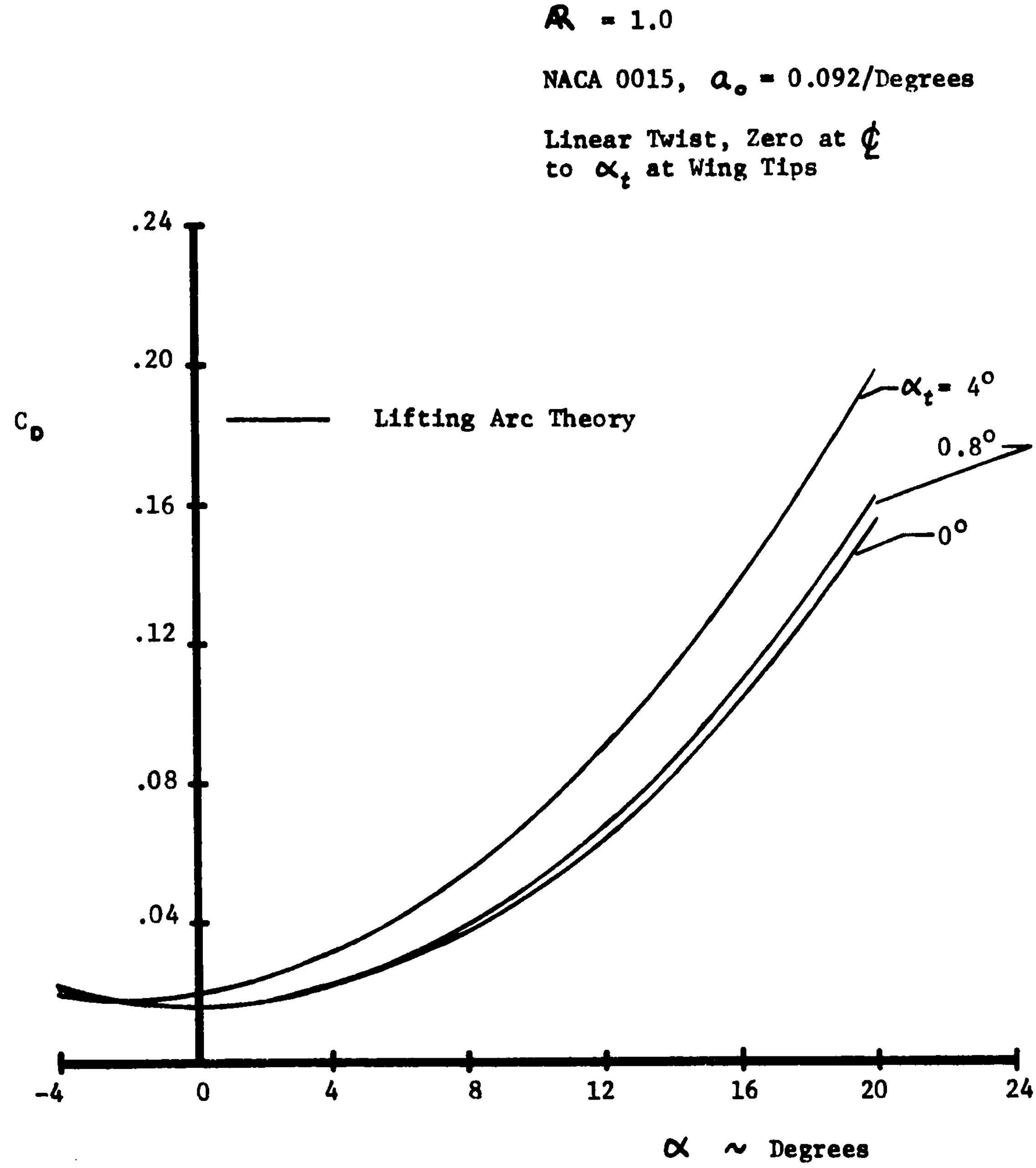

Figure 44. Effect of twist on calculated channel wing drag coefficient.

The effect of twist on channel wing performance is better illustrated by considering the lift to drag ratio, Figures 45 and 46. Note that the gain in L/D , over the untwisted case, for the best twist distribution investigated is very small, and L/D is reduced when the optimum twist is exceeded.

Lift and Drag Coefficients

Lift and drag coefficients calculated with the lifting arc theory are compared with the wind tunnel data (Chapter V) in Figures 47 through 50. For the $A\!R$ = 1.0 model (Figure 47) the calculated lift coefficient curve has almost the same slope as does the experimental curve. However, the theoretical curve is shifted to the right relative to the experimental curve -- 1.5° at $\alpha_c = 0°$. As discussed in Chapter V, the experimental data may have been shifted uniformly to the left by approximately one degree. If this actually is the case, then the correlation would be better than shown.

In Figure 48, the experimental $A\!R$ = 1.0 drag coefficient is compared with calculated data for both smooth and rough airfoil section data. The rough section data yields better correlation. The matching of experimental and theoretical drag coefficients around zero lift ($\alpha_c \approx -6°$) with the rough section data indicates that the wind tunnel model surface was more like NACA rough condition than NACA smooth condition. In both cases, the curvature of the calculated data agrees well with the wind tunnel data. This is to be expected, since the experimental and the theoretical span efficiency factor values are very close. Again, the correlation would be improved by a one degree shift of the experimental data.

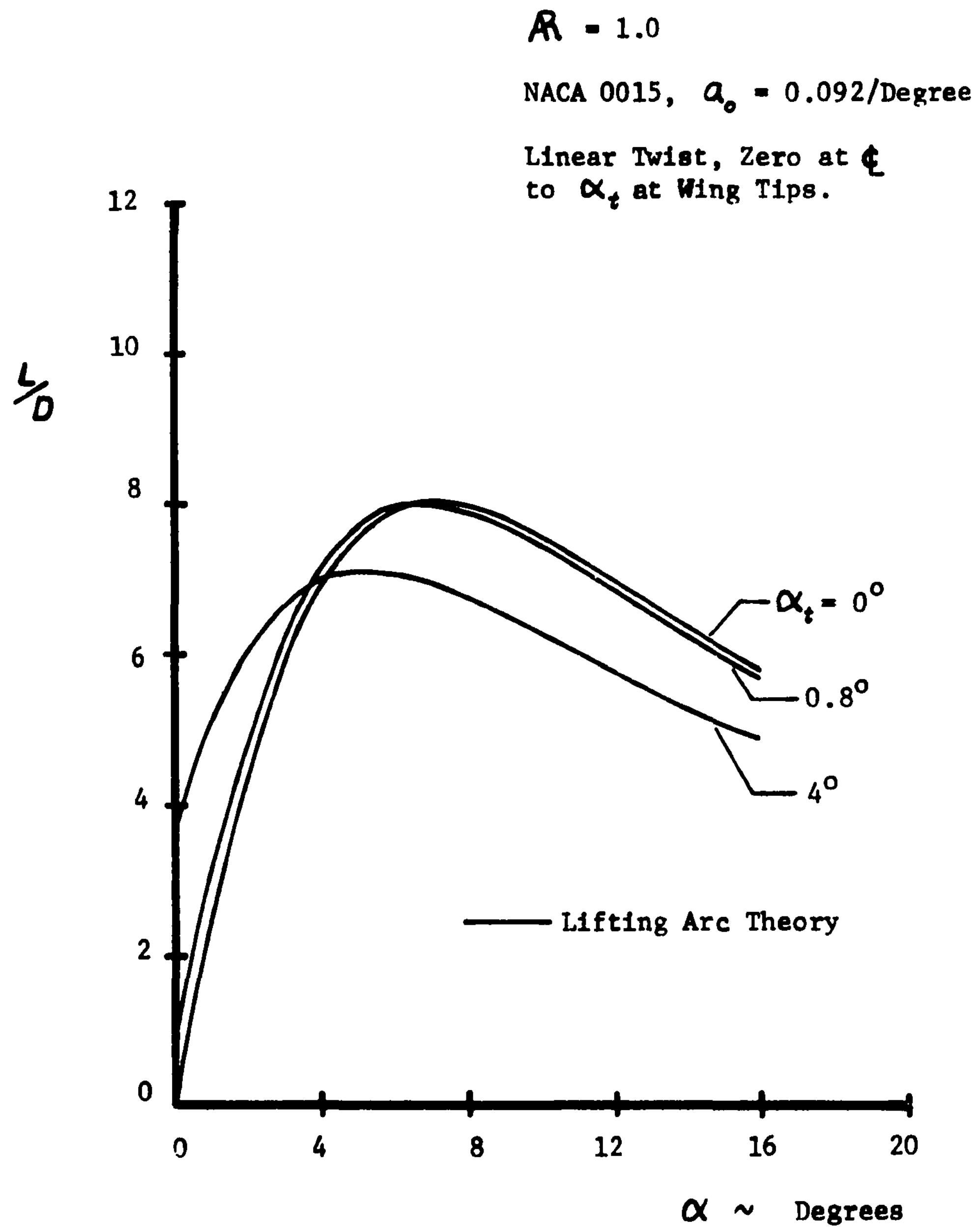

Figure 45. Effect of twist on calculated Æ = 1.0 channel wing lift-to-drag ratio.

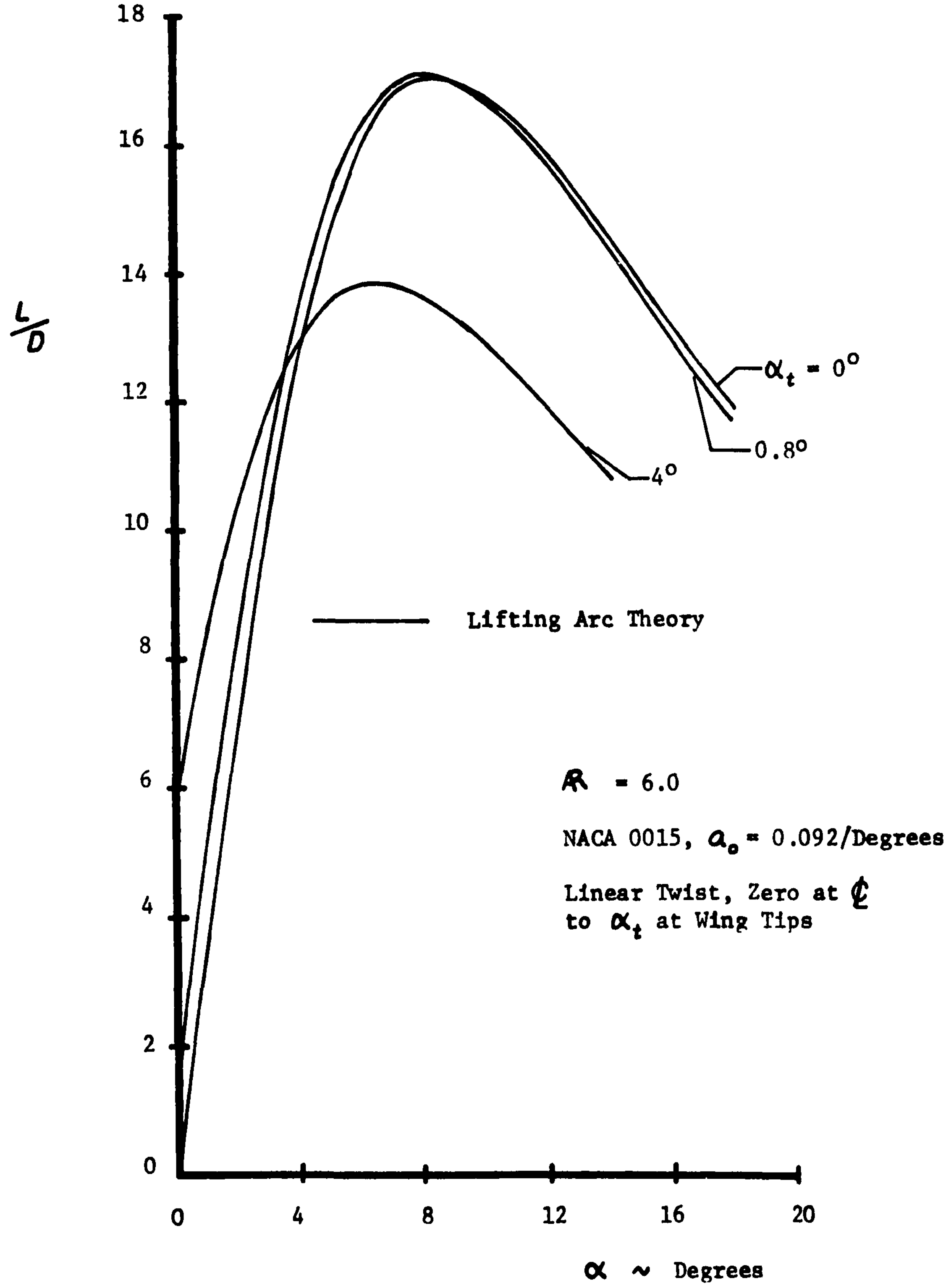

Figure 46. Effect of twist on calculated AR = 6.0 channel wing lift-to-drag ratio.

$Æ = 1.0$

NACA 4412

$Re_{eff} = 1.55 \times 10^6$

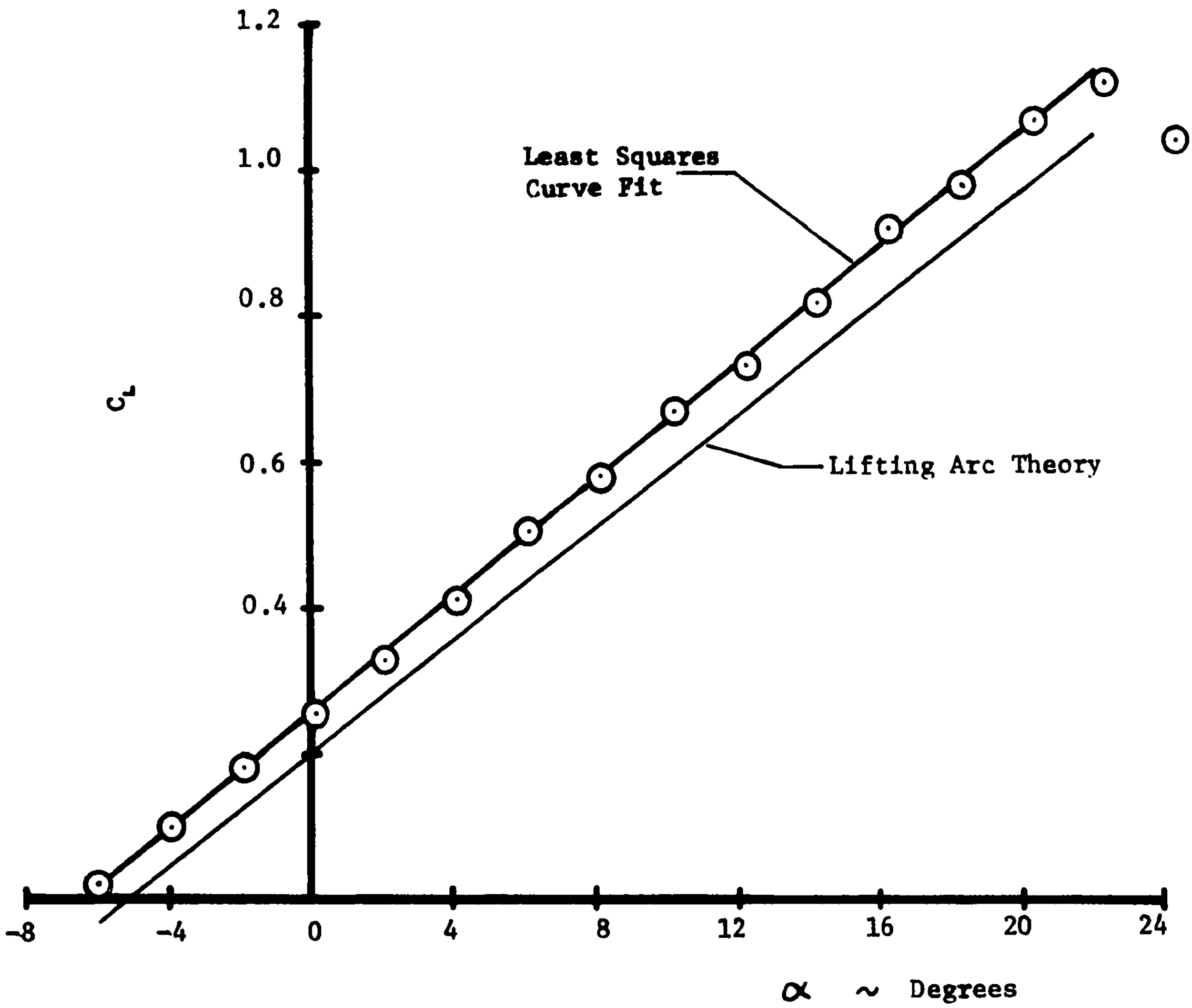

Figure 47. Comparison of theoretical and experimental lift coefficient for $Æ = 1.0$ channel wing.

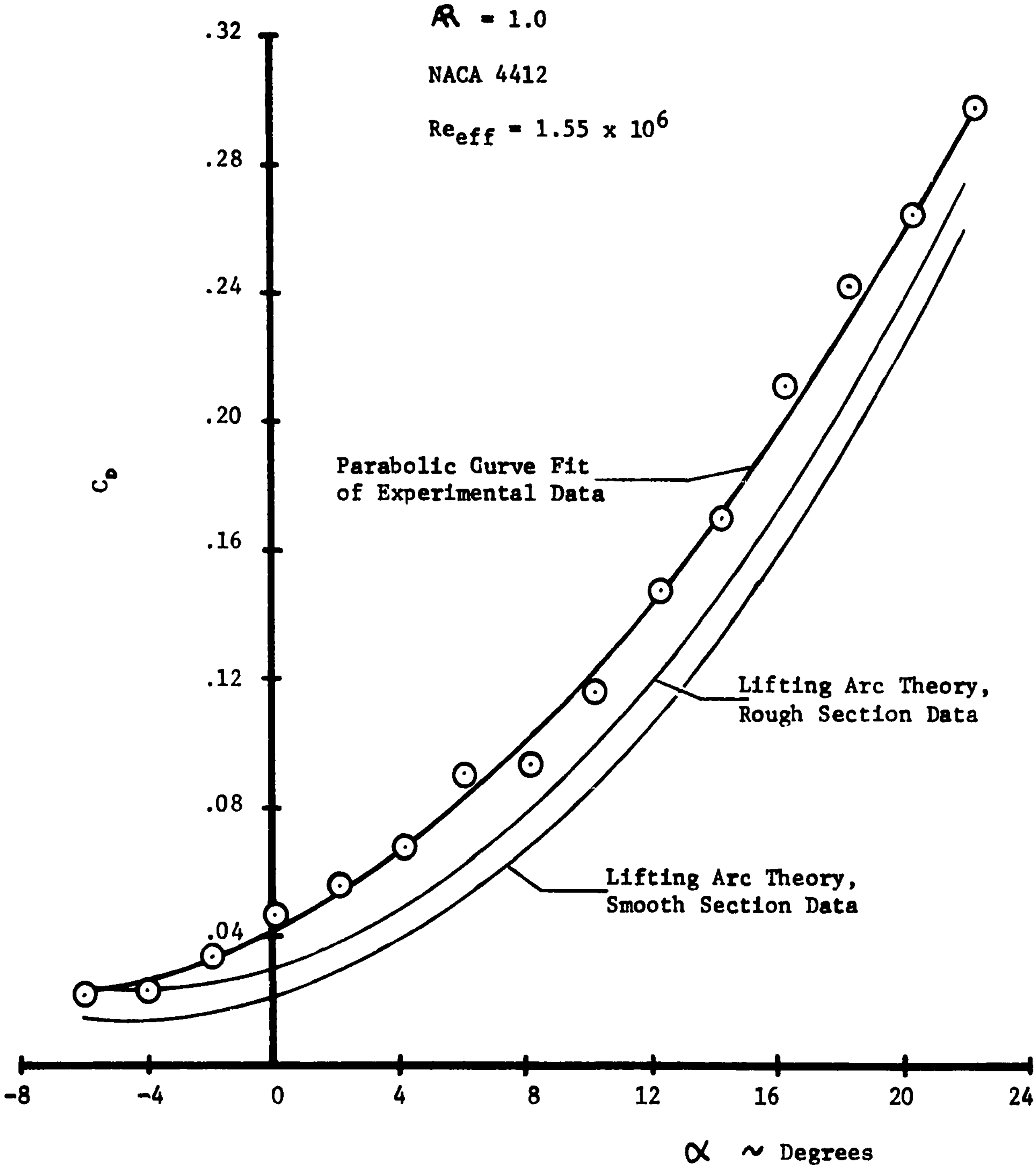

Figure 48. Comparison of theoretical and experimental drag coefficient for $A\!\!R$ = 1.0 channel wing.

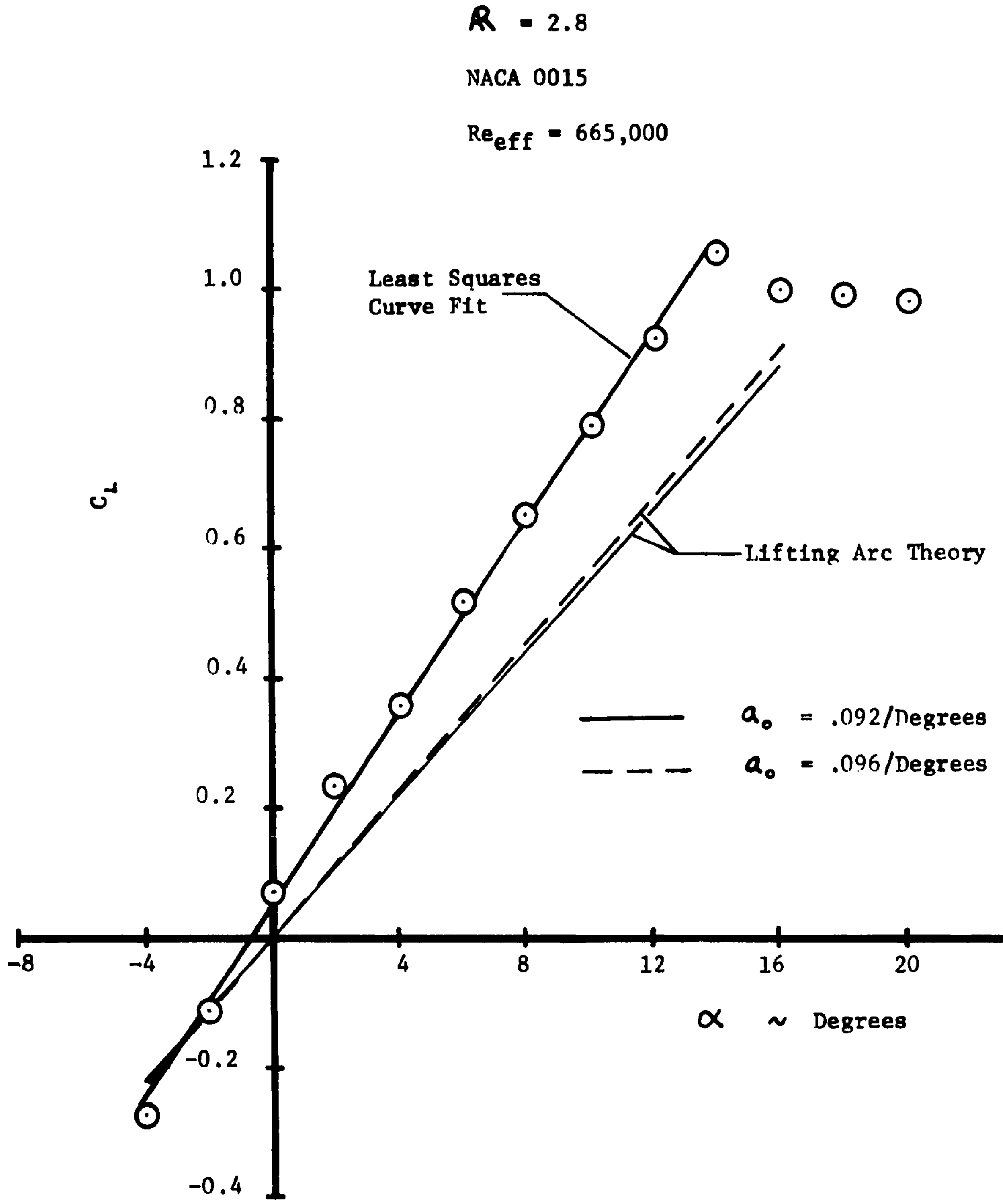

Figure 49. Comparison of theoretical and experimental lift coefficient for Æ = 2.8 channel wing.

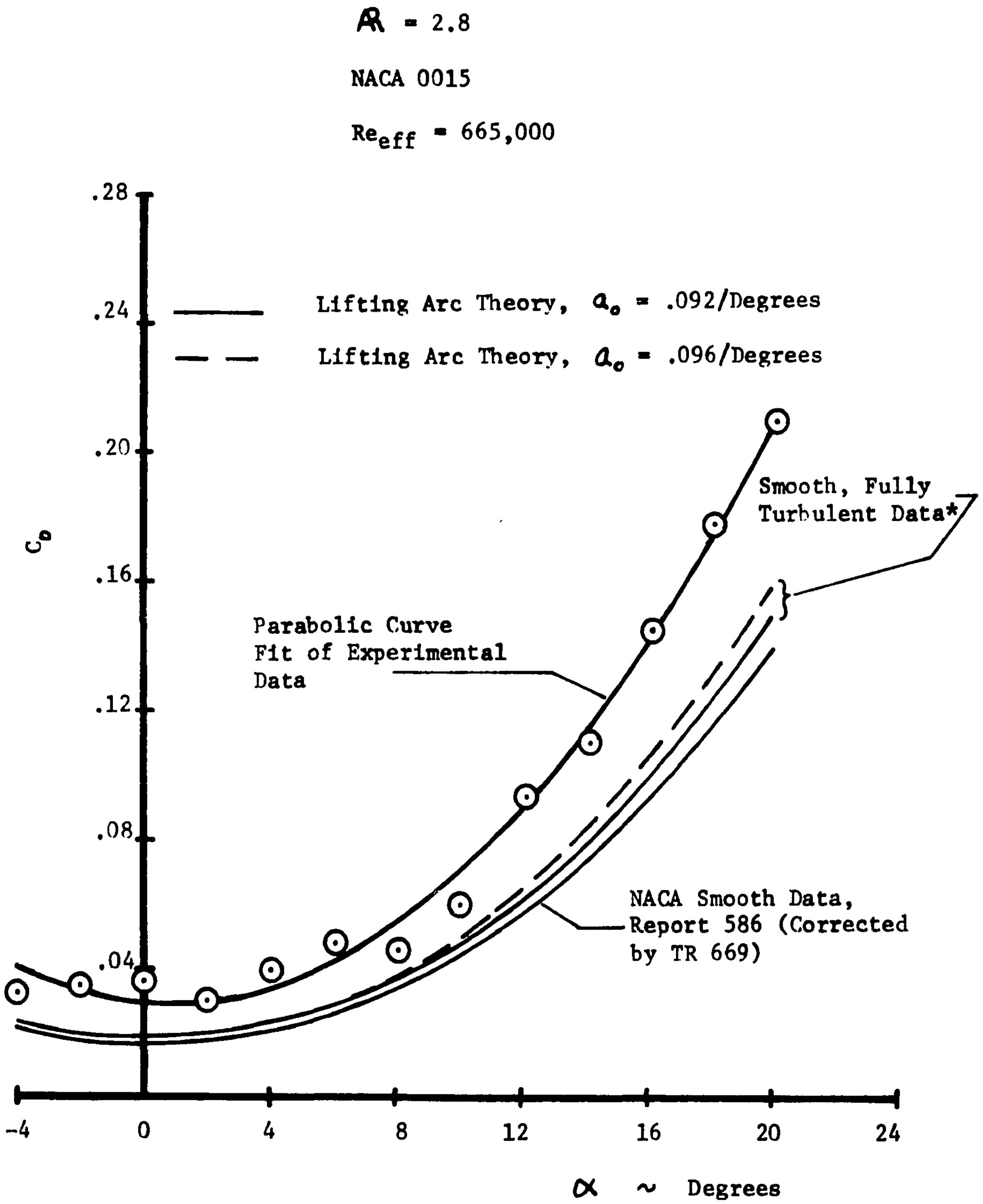

*Schwartzberg's Method, Appendix D.

Figure 50. Comparison of theoretical and experimental drag coefficient for AR = 2.8 channel wing.

Turning to the $\text{Æ} = 2.8$ case, it is seen in Figure 49 that the theoretical wing lift curve slope does not match the experimental slope as well as in the $\text{Æ} = 1.0$ case. Curves calculated for two values of the airfoil section lift curve slope are shown in Figure 49 to illustrate that the majority of the difference is not due to the section lift curve slope input to the computer program.

Calculated drag coefficient curves are compared with wind tunnel data for the $\text{Æ} = 2.8$ model in Figure 50. As discussed in Appendix D, section data for the NACA 0015, at low Reynolds number, which would be considered accurate by modern standards are not directly available. However, estimates for these data for NACA smooth (partial laminar flow) and smooth, fully turbulent flow are obtained in Appendix D, and were used to obtain the calculated curves in Figure 50. That these estimates were only partially successful is indicated by the failure to match the experimental drag coefficient around zero lift. However, this fault may be due to the lack of rough section data rather than the methods of Appendix D, since rough section data were required to match the drag coefficients at zero lift for the other wind tunnel model. The curvature of the calculated drag curves in Figure 50 corresponds well with the experimental curve.

Conclusions

The channel wing lifting arc theory developed herein predicts induced drag (span efficiency factors) which agree well with wind tunnel data and with Cone's [7] predicted value. The calculated lift curve slope is in good agreement with experiment at aspect ratio of 1.0, but is low by 24% at aspect ratio of 2.8.

CHAPTER IX

PERFORMANCE PREDICTIONS

Drag Polars

Drag polars for plane, channel, and ring wings are presented in Figures 51 through 54. The data for the channel wing were calculated with the digital computer program described in Chapter VII, while the ring wing data were obtained from Ribner's theory, Chapter I, with strip theory for the profile drag. The planar wing data shown are for a wing with elliptical lift distribution. In these figures, the channel and ring wings have rectangular (projected) planforms, and all coefficients are based on projected area.

Wings with symmetrical (NACA 0012) airfoil sections and $\mathcal{R} = 1$ are compared in Figure 51. As would be expected from consideration of wetted area, the plane wing has the lowest drag at very low C_L. But then its drag exceeds that of the channel wing at about $C_L = 0.2$, and that of the ring wing at approximately $C_L = 0.3$. The channel wing has less drag than the ring wing up to about $C_L = 0.4$. At higher C_L, the ring wing has the lowest predicted drag. These trends are due, of course, to the lower induced drag (as a consequence of higher span efficiency factors) of the nonplanar wings. As C_L increases, the induced drag becomes a larger portion of the total drag, until the higher profile drag of

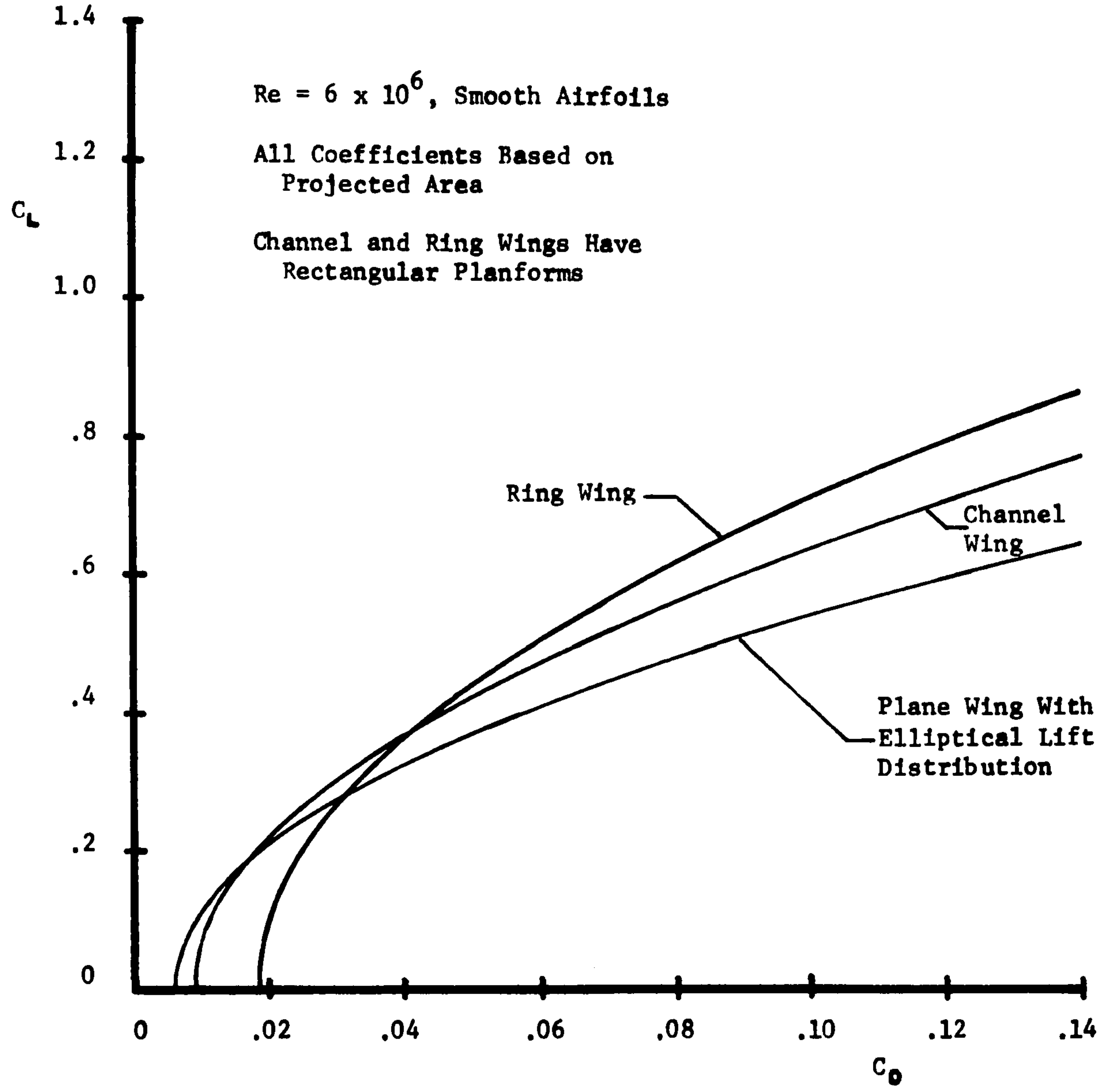

Figure 51. Drag polar for plane, channel, and ring wings of $\mathcal{R}$ = 1 and NACA 0012 section.

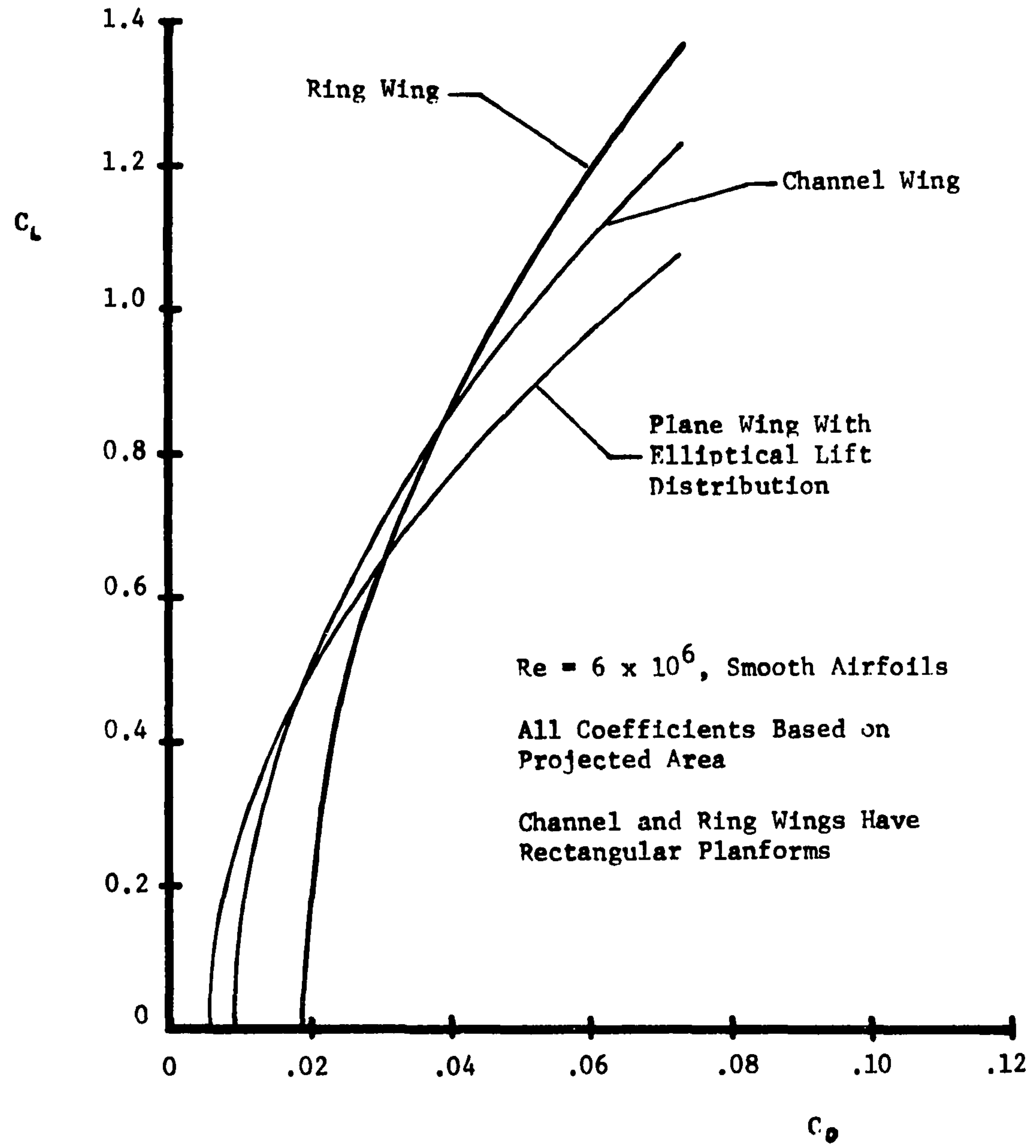

Figure 52. Drag polar for plane, channel, and ring wings of AR = 6 and NACA 0012 section.

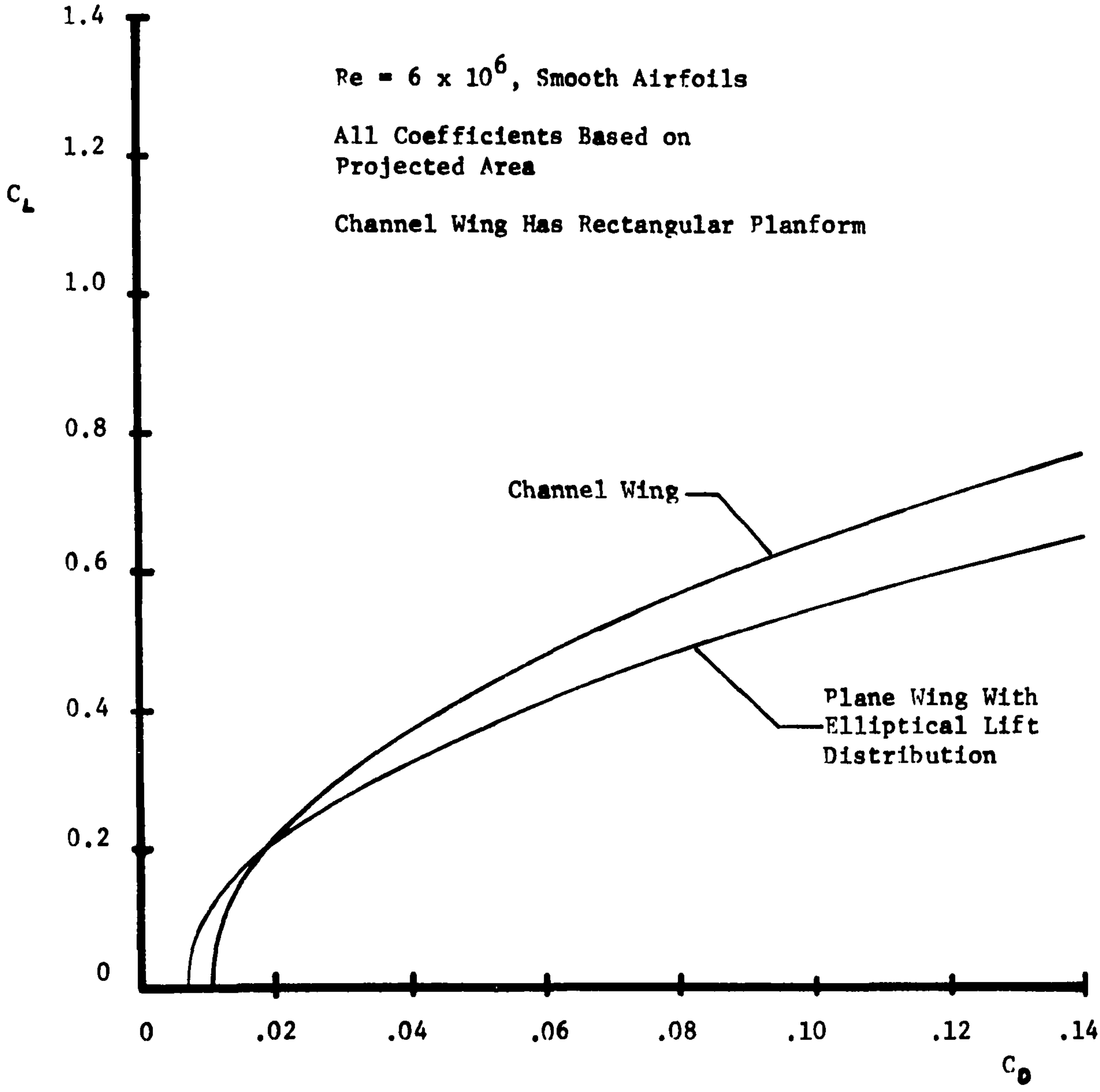

Figure 53. Drag polar for plane and channel wings of $\mathcal{R}$ = 1 and NACA 23012 section.

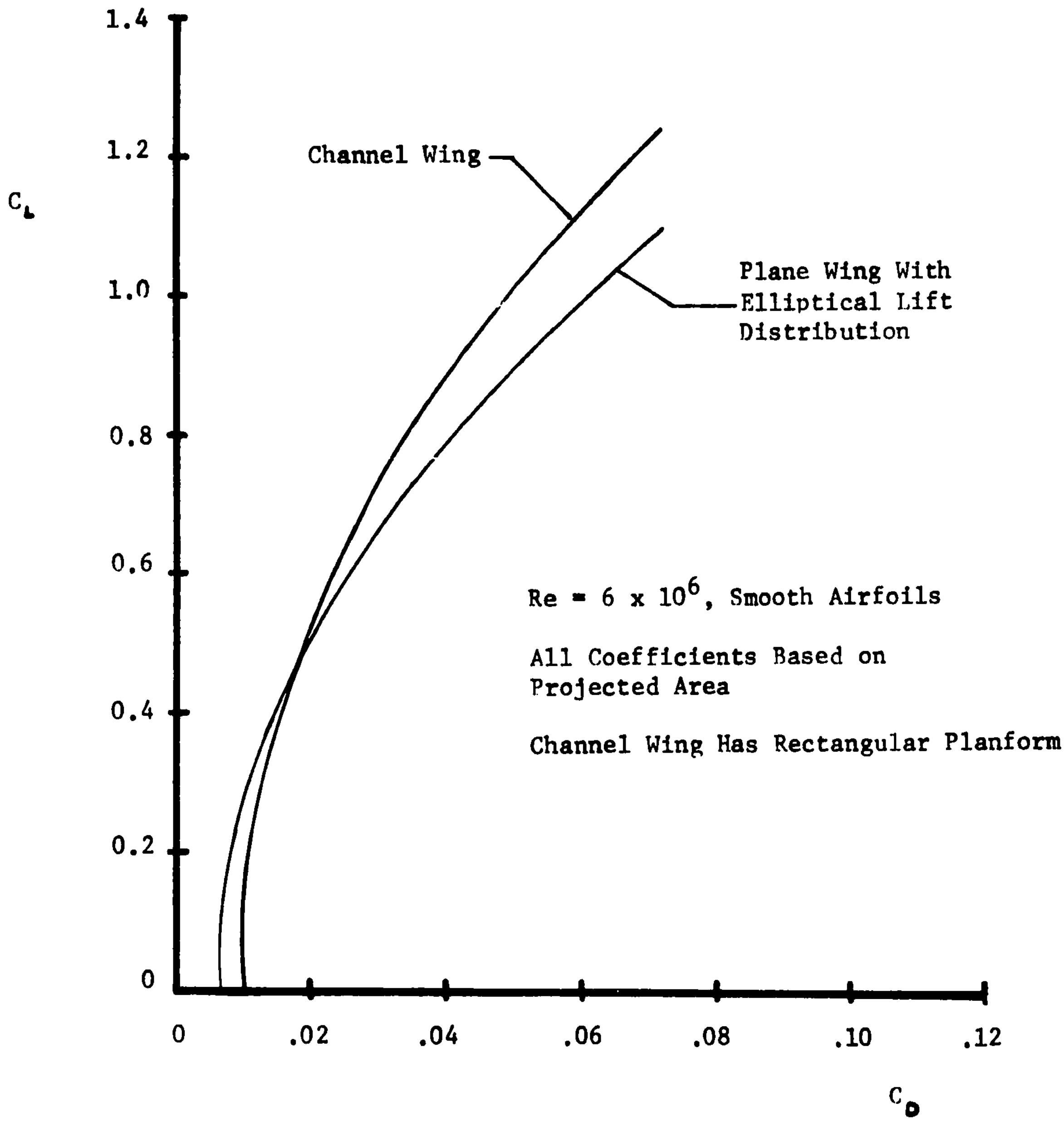

Figure 54. Drag polar for plane and channel wings of $\mathcal{R}$ = 6 and NACA 23012 section.

the nonplanar wing is more than offset by its lower induced drag.

Figure 52 repeats the cases of the previous figure, but with the aspect ratio increased to six. The crossovers observed for the $AR = 1$ cases occur in the same order, but at relatively higher lift coefficients. This is due to the fact that the induced drag becomes a smaller portion of the total drag as aspect ratio increases.

Drag polars for wings with NACA 23012 airfoil sections are presented in Figures 53 and 54. Ring wings were omitted for these cases because it was considered unlikely that a nonsymmetrical airfoil section would be used for a ring wing. The drag polars are little changed from the symmetrical cases, and the trends are the same.

Power Required for Level Flight

The power required for equilibrium level flight of an aircraft was derived in Appendix E, and suitable modifications for the increased weight and profile drag of aircraft with channel and ring wings were estimated. It was assumed that the aircraft propulsion and lift systems were not integrated (e.g., propeller(s) not mounted in the ring(s)). A generalized plot of power required for plane, channel, and ring wing aircraft is presented in Figure 55, where it is seen that both the channel wing and the ring wing aircraft require less power than the plane wing aircraft in the low speed range. This occurs because C_L must be large at low V, which means that induced drag becomes relatively more important, and the induced

Aircraft Type	Profile Drag Coefficient	Weight	Span	Projected Wing Area
Plane Wing	C_{D_0}	W	b	S
Channel Wing	1.228 C_{D_0}	1.057W	b	S
Ring Wing	1.858 C_{D_0}	1.214W	b	S

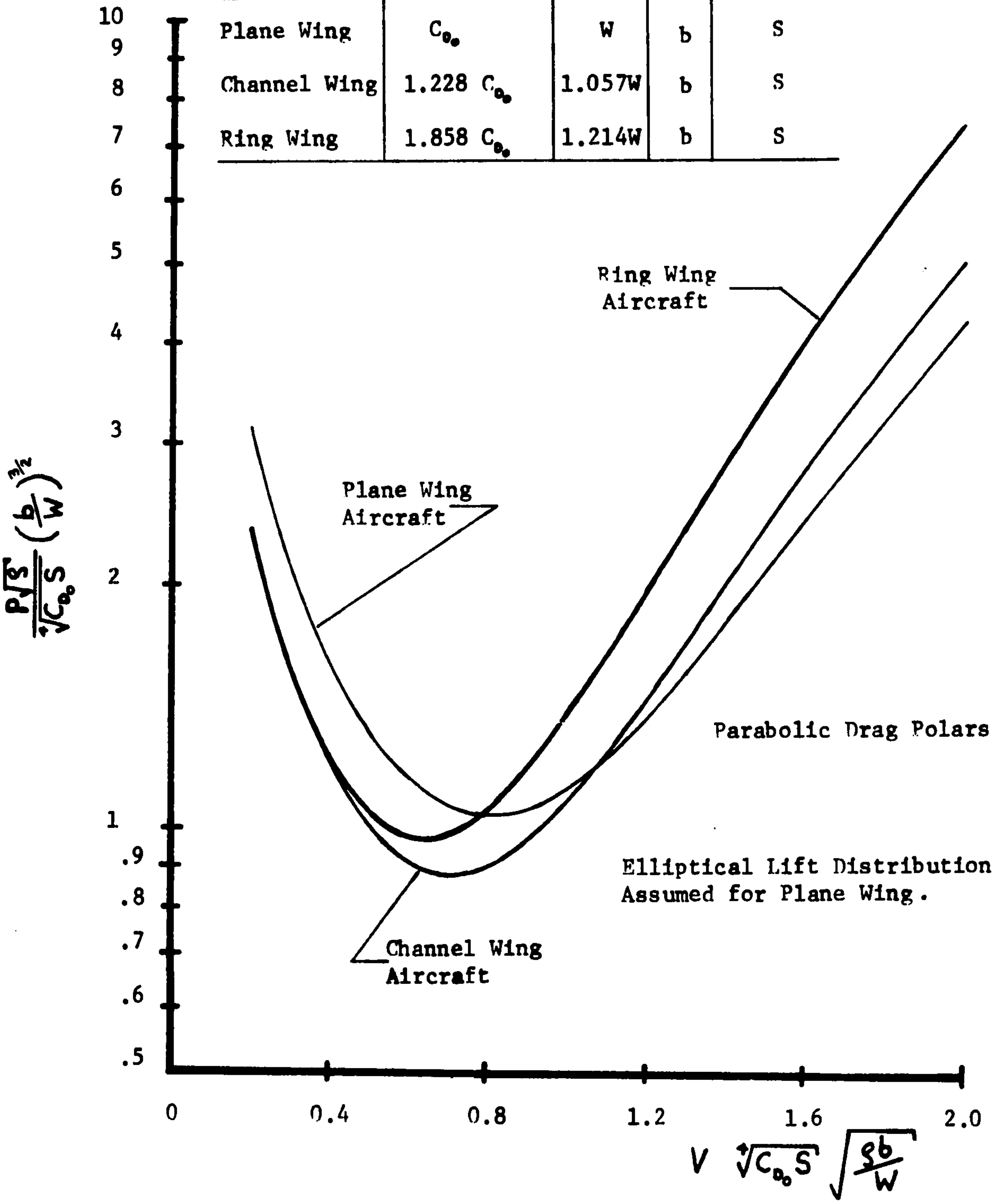

Figure 55. Generalized power required for level flight of plane, channel, and ring wing aircraft.

drag of the nonplanar wing aircraft is less than that of the plane wing aircraft. Figure 55 also shows that the channel wing aircraft retains its advantage over the plane wing aircraft to a higher speed than does the ring wing aircraft. This is due to the lower profile drag (which increases with V^2) of the channel wing as compared to the ring wing. The ring wing aircraft requires as much or more power for level flight at all velocities than does the channel wing aircraft.

The power required for a specific aircraft with plane, channel, or ring wings is plotted in Figure 56. In each case the aspect ratio is six, and the projected wing area is 182 $ft.^2$. The basic (i.e., that of the plane wing aircraft) weight and profile drag coefficient are 2700 pounds and 0.016. The weight and profile drag coefficient of the channel and ring wing aircraft were increased as described in Appendix E. The ring wing aircraft requires less power than the plane wing aircraft up to 65 knots, and the channel wing aircraft less power to 90 knots. If the aspect ratio is reduced to, say, three, the nonplanar wing aircraft retain their advantage over the plane wing aircraft to higher velocities, as shown in Figure 57. The ring wing aircraft requires less power up to 78 knots, the channel wing aircraft less power up to 110 knots. The result of further reduction of the aspect ratio to a value of one is shown in Figure 58. The channel wing aircraft requires less power than the plane wing aircraft up to 140 knots, the ring wing aircraft less power to 104 knots. This trend with aspect ratio is due to the greater importance of induced drag at low aspect ratio.

Aircraft Type	Profile Drag Coefficient	Weight	Span	Projected Wing Area
Plane Wing	C_{D_o}	W	b	S
Channel Wing	1.228 C_{D_o}	1.057W	b	S
Ring Wing	1.858 C_{D_o}	1.214W	b	S

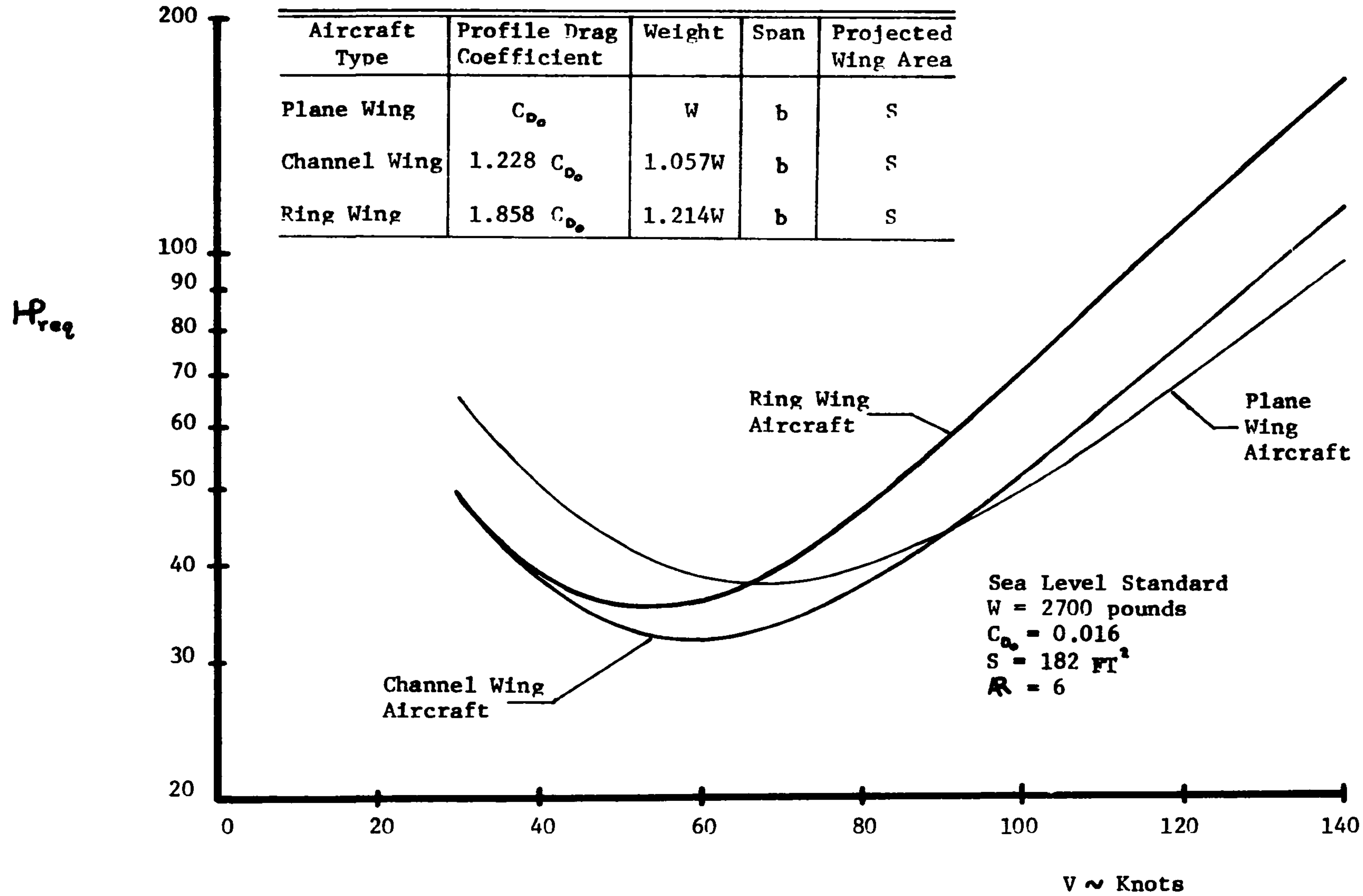

Figure 56. Power required for level flight of light aircraft of AR = 6.

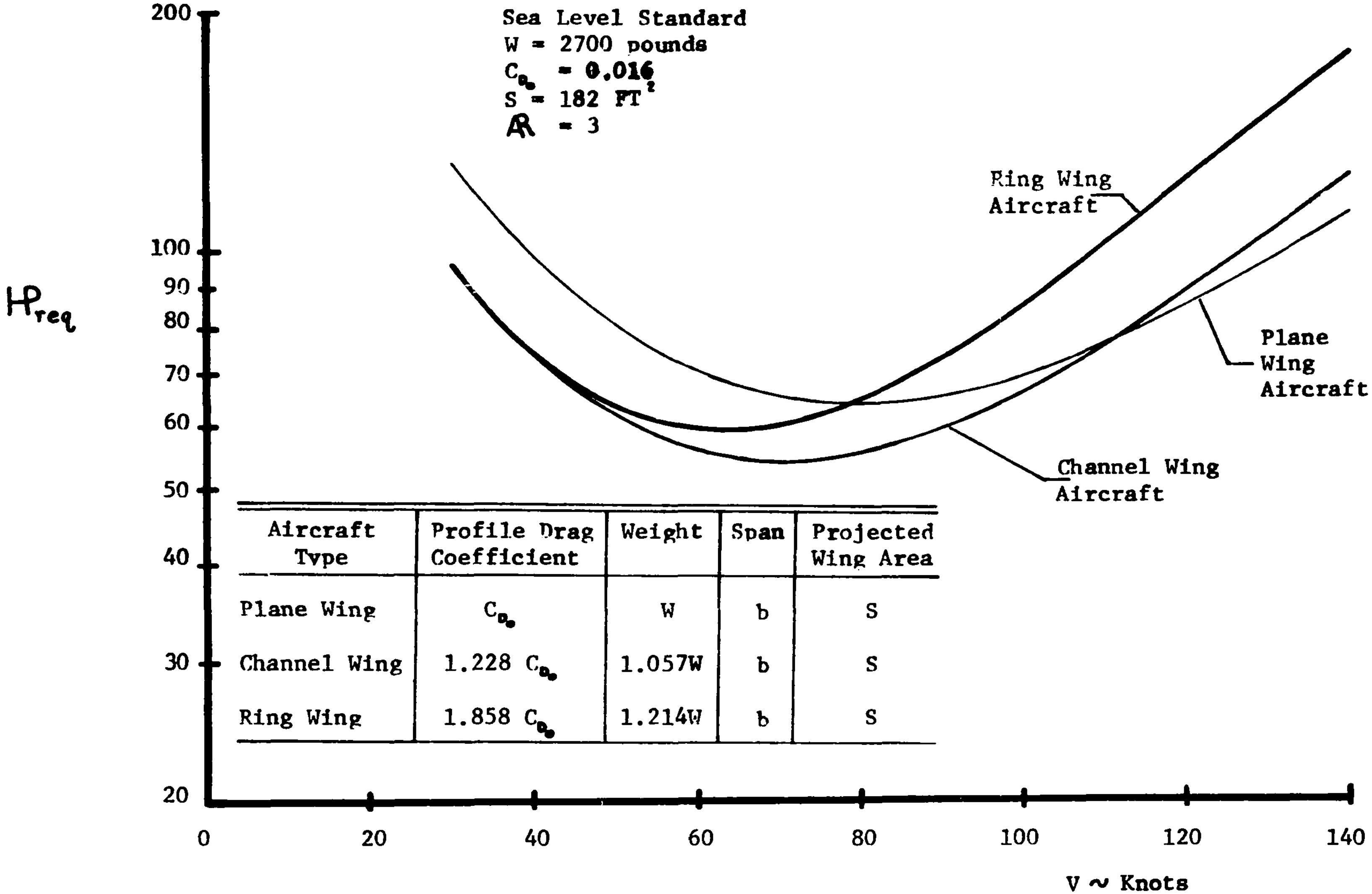

Aircraft Type	Profile Drag Coefficient	Weight	Span	Projected Wing Area
Plane Wing	C_{D_0}	W	b	S
Channel Wing	1.228 C_{D_0}	1.057W	b	S
Ring Wing	1.858 C_{D_0}	1.214W	b	S

Figure 57. Power required for level flight of light aircraft of Æ = 3.

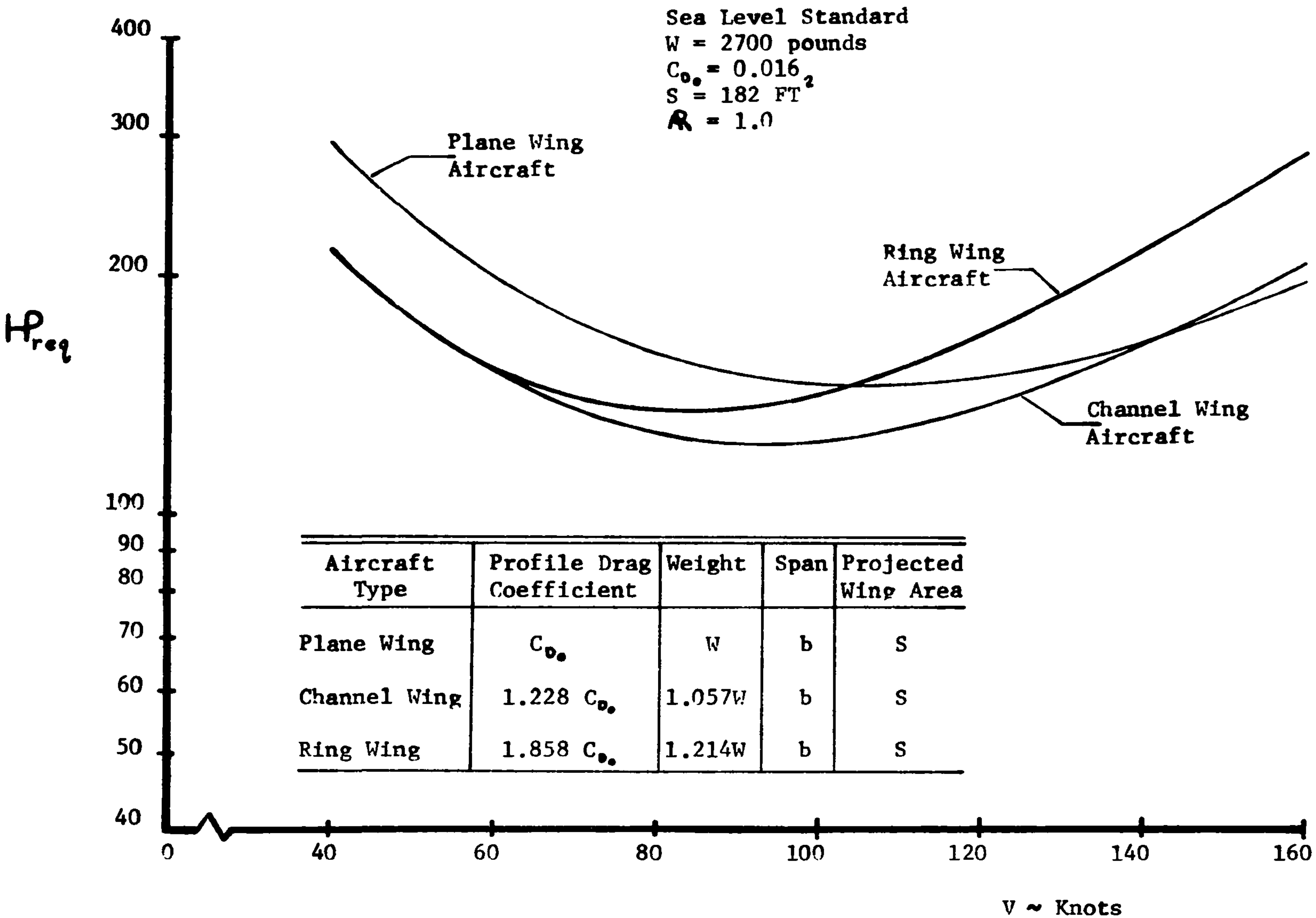

Aircraft Type	Profile Drag Coefficient	Weight	Span	Projected Wing Area
Plane Wing	C_{D_e}	W	b	S
Channel Wing	1.228 C_{D_e}	1.057W	b	S
Ring Wing	1.858 C_{D_e}	1.214W	b	S

Figure 58. Power required for level flight of light aircraft of R = 1.0.

The data of Figures 56, 57, and 58 show an advantage of the channel wing over the plane wing, for the same aspect ratio, in a significant portion of the low speed flight regime of a light aircraft. However, comparison of the figures indicates that the aircraft with the $\mathcal{R} = 6.0$ plane wing always requires less power than the aircraft with the channel wing of $\mathcal{R} = 3.0$, and similarly for the $\mathcal{R} = 3.0$ plane wing versus the $\mathcal{R} = 1.0$ channel wing. Thus the nonplanar wing will be advantageous only if the maximum span is fixed.

Maximum Range and Endurance

The Breguet formulas for aircraft maximum range and endurance are given by Perkins and Hage [22] as follows. For reciprocating engines, the maximum range in miles is

$$R_{max} = 375\left(C_L/C_D\right)_{max} \frac{\eta}{sfc} \log\left(W_0/W_1\right) , \qquad (9.1)$$

and the maximum endurance in hours is

$$E_{max} = 37.9\left(C_L^{3/2}/C_D\right)_{max} \frac{\eta}{(sfc)} \sqrt{\frac{\sigma S}{W_0}} \left[\left(W_0/W_1\right)^{1/2} - 1\right] . \qquad (9.2)$$

For aircraft powered by jet engines, the maximum range in miles is

$$R_{max} = \frac{2}{(sfc)'}\left(C_L^{1/2}/C_D\right)_{max} \sqrt{\frac{391\ W_0}{\sigma S}} \left[1 - \left(W_1/W_0\right)^{1/2}\right] , \qquad (9.3)$$

and the maximum endurance in hours is

$$E_{max} = \frac{1}{(sfc)'}\left(C_L/C_D\right)_{max} \log\left(W_0/W_1\right) . \qquad (9.4)$$

In these equations,

η = propulsive efficiency

sfc = specific fuel consumption in pounds per brake horse-power-hour

$(sfc)'$ = specific fuel consumption in pounds per hour per pound of thrust

W_o = initial weight

W_1 = final weight = $W_o - W_F$

$\sigma = \rho/\rho_o$.

For purposes of comparison of aircraft with planar and non-planar wings, one may consider η , sfc, $(sfc)'$, σ , and S to be the same for each aircraft. However, it would be unrealistic to assume that the structural weights of the nonplanar wing aircraft are equal to that of the planar wing aircraft, since more wing structure is required for the former. Therefore, W_o and W_1 must be increased for the channel wing and ring wing aircraft. The increase in aircraft flying weight due to the nonplanar wings was estimated in Appendix E:

$W' = 1.057W$ for the channel wing,

$W' = 1.214W$ for the ring wing,

where W is the gross weight of the planar wing aircraft. Then,

$$W_o = W'$$

$$W_1 = W' - W_F \quad ,$$

where W_F is the fuel weight (assumed constant).

Use of the Breguet formulas requires the evaluation of $\left(C_L/C_D\right)_{max}$, $\left(C_L^{1/2}/C_D\right)_{max}$, and $\left(C_L^{3/2}/C_D\right)_{max}$ for each type of aircraft. If a parabolic drag polar is assumed, Perkins and Hage [22] show that

$$C_{D_i} = C_{D_o} \tag{9.5}$$

and

$$C_L = \sqrt{\pi e \mathcal{R} C_{D_o}} \tag{9.6}$$

for $\left(C_L/C_D\right)_{max}$. These results were obtained by differentiating C_D/C_L with respect to C_L. A similar approach was used to obtain

$$C_{D_i} = 3\,C_{D_o} \tag{9.7}$$

$$C_L = \sqrt{3\pi e \mathcal{R} C_{D_o}} \tag{9.8}$$

for $\left(C_L^{3/2}/C_D\right)_{max}$ and

$$C_{D_i} = 1/3\ C_{D_o} \tag{9.9}$$

$$C_L = \sqrt{\pi/3\ e \mathcal{R} C_{D_o}} \tag{9.10}$$

for $\left(C_L^{1/2}/C_D\right)_{max}$. For the nonplanar wing aircraft, C_{D_o} is increased as described in Appendix E to account for the higher wing profile drag:

$C_{D_o}' = 1.228\ C_{D_o}$ for the channel wing,

$C_{D_o}' = 1.858\ C_{D_o}$ for the ring wing,

where C_{D_o} is the profile drag of the planar wing aircraft. Also, e values of 1.0, 1.5, and 2.0 must be used for the planar, channel and ring wing aircraft, respectively.

The Breguet range and endurance equations were evaluated for the light aircraft of Figures 56, 57, and 58, with the above modifications being used for the channel wing and ring wing cases. The results are plotted against aspect ratio in Figures 59, 60, 61 and 62. These figures show that the channel wing aircraft studied has greater range than the plane wing aircraft, when reciprocating engine powered, and longer endurance when powered with either jet or reciprocating engines. The advantage in range and jet-powered endurance is only about 4%, but the reciprocating-powered endurance increase is approximately 18%. The ring wing aircraft has 6% longer endurance than the plane wing aircraft, with reciprocating engine propulsion, but less endurance than the channel wing aircraft. Otherwise, the ring wing aircraft is inferior to the plane wing aircraft in range and endurance.

Although the data show an advantage in maximum range (reciprocating engine powered) and endurance for a channel wing light aircraft as compared to the plane wing aircraft of the same aspect ratio, it should be noted that a not unreasonable increase in aspect ratio of the plane wing aircraft will nullify the advantage of the channel wing aircraft. For example, an increase in aspect ratio from 4.5 to 6.0 for the plane wing aircraft yields more endurance than that of the channel wing aircraft of aspect ratio 4.5, for the reciprocating engine powered case. Therefore, as in the considerations above on power required for level flight, the plane wing aircraft would be preferred unless the maximum span is fixed.

Conclusions

Channel wings and ring wings have higher drag (at the same C_L) than does the plane wing at low lift coefficient, but lower

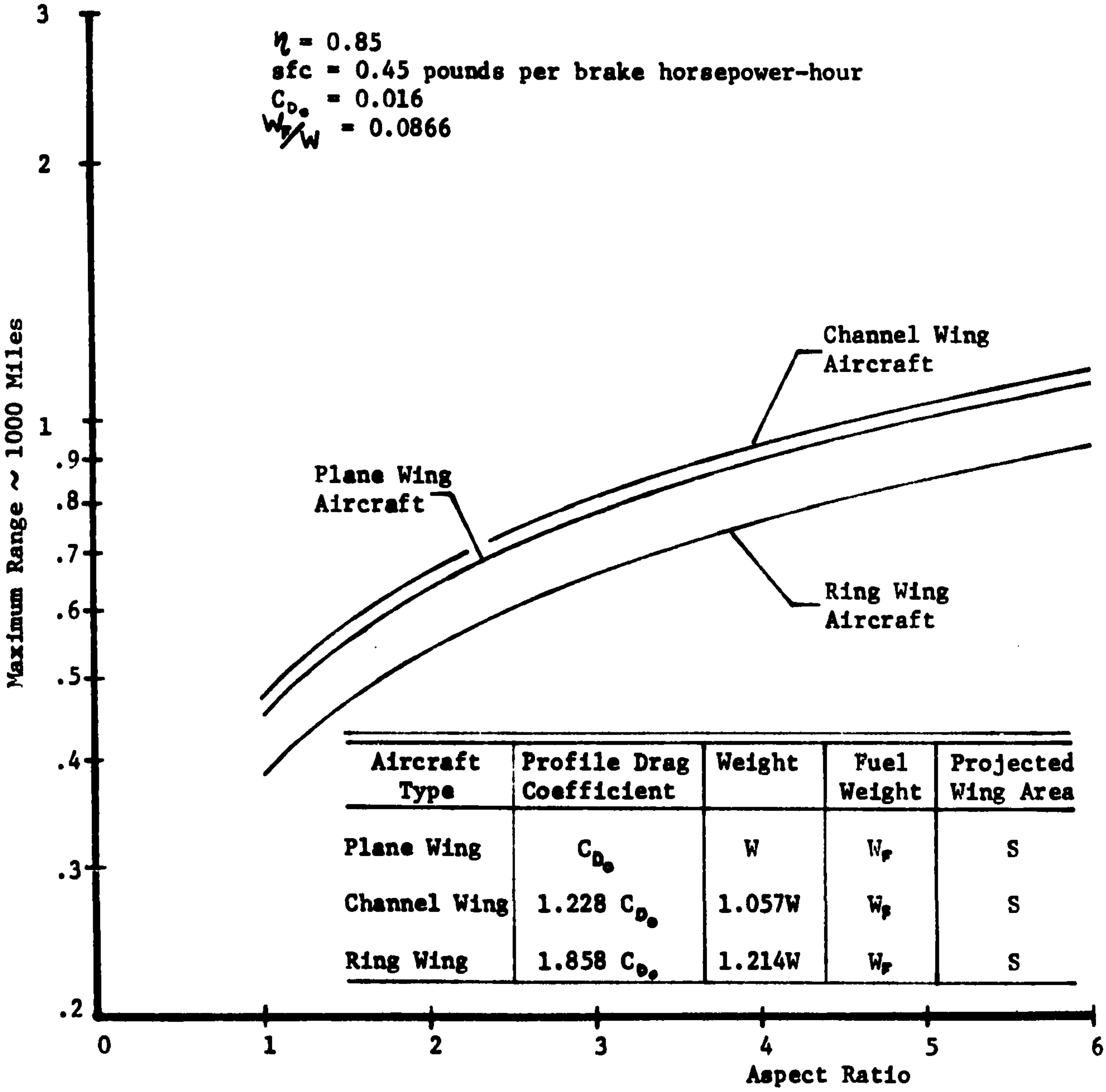

Aircraft Type	Profile Drag Coefficient	Weight	Fuel Weight	Projected Wing Area
Plane Wing	C_{D_e}	W	W_F	S
Channel Wing	1.228 C_{D_e}	1.057W	W_F	S
Ring Wing	1.858 C_{D_e}	1.214W	W_F	S

Figure 59. Maximum range of reciprocating engine powered light aircraft.

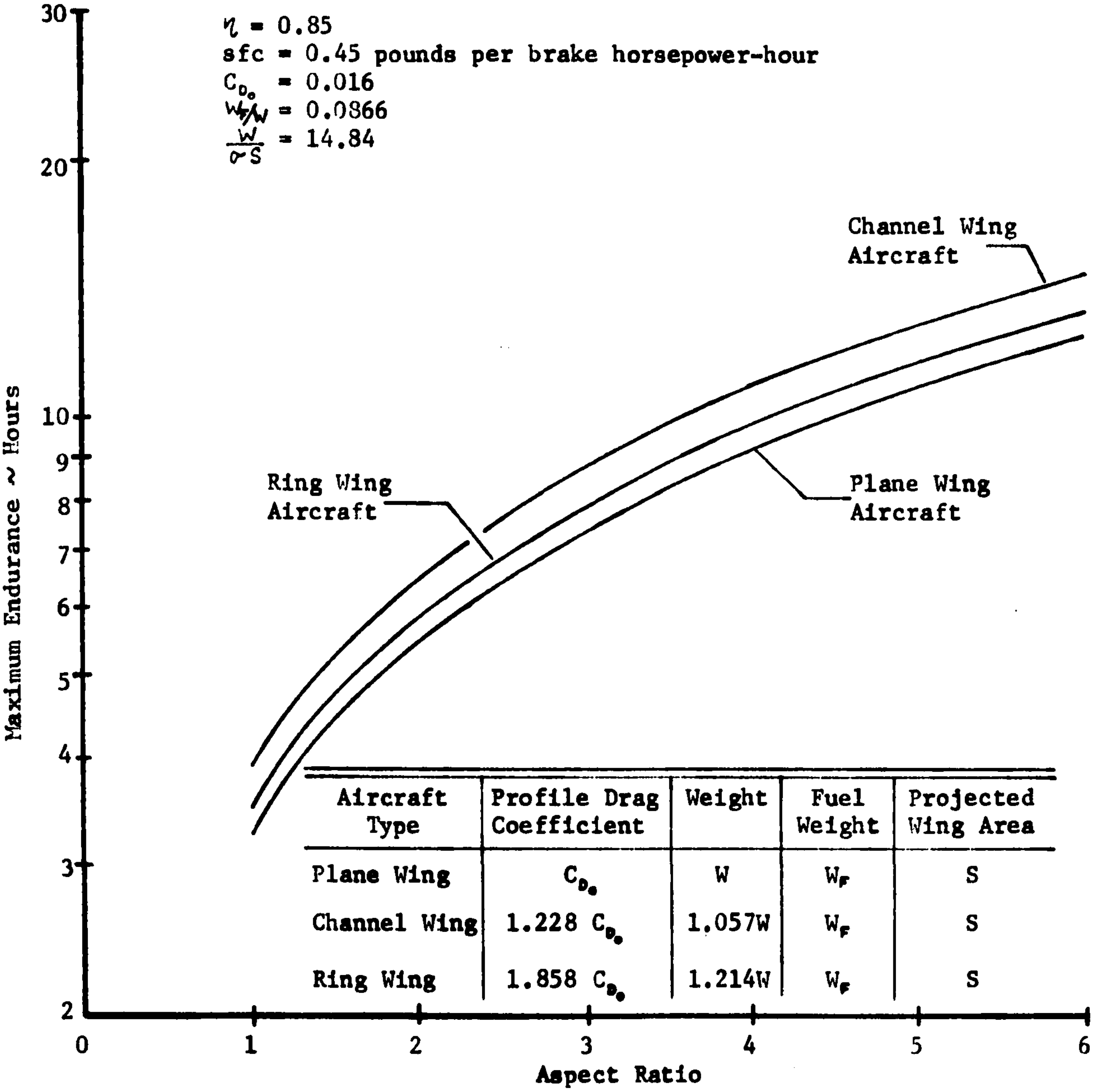

Aircraft Type	Profile Drag Coefficient	Weight	Fuel Weight	Projected Wing Area
Plane Wing	C_{D_o}	W	W_F	S
Channel Wing	1.228 C_{D_o}	1.057W	W_F	S
Ring Wing	1.858 C_{D_o}	1.214W	W_F	S

Figure 60. Maximum endurance of reciprocating engine powered light aircraft.

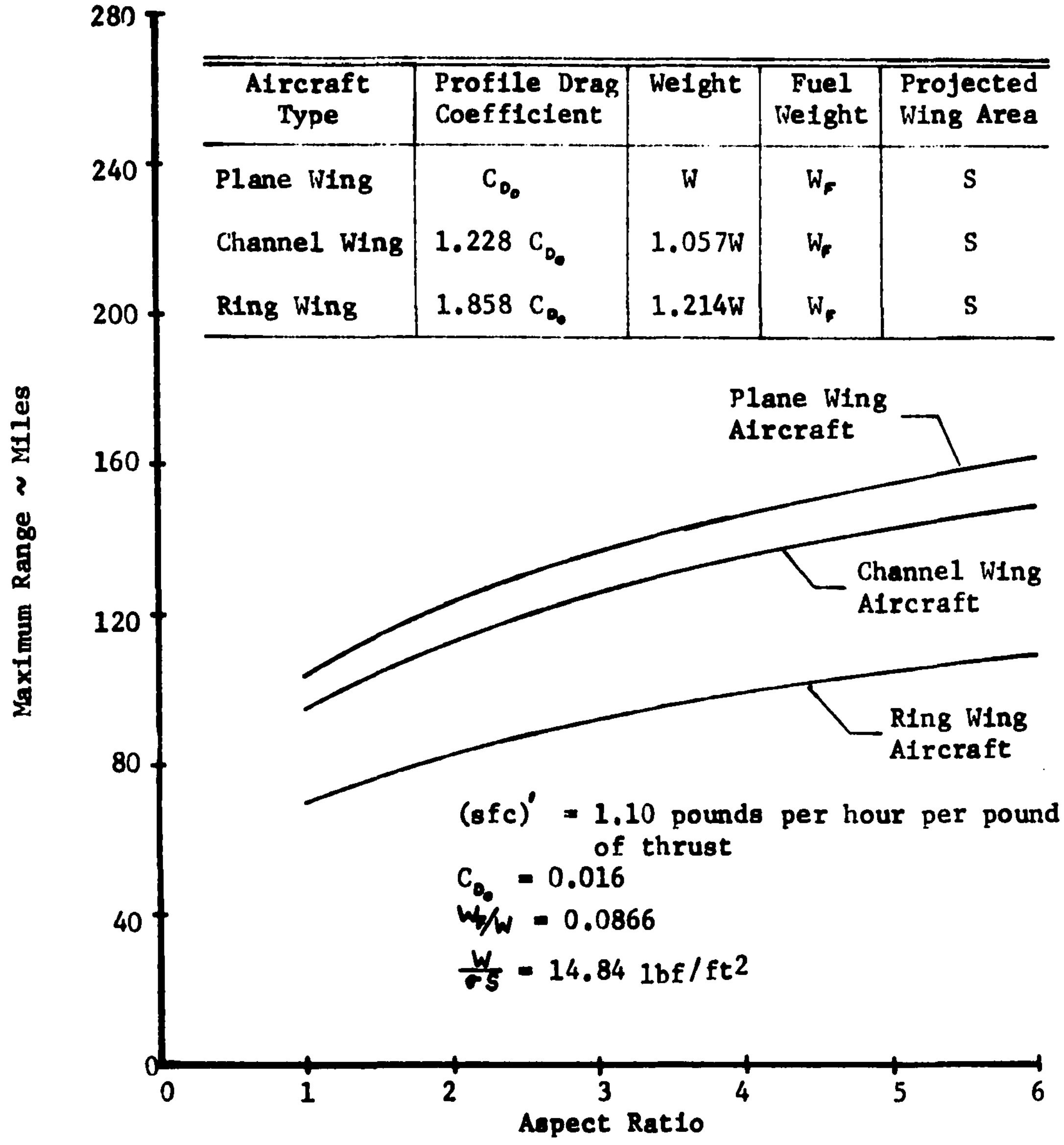

Aircraft Type	Profile Drag Coefficient	Weight	Fuel Weight	Projected Wing Area
Plane Wing	C_{D_0}	W	W_f	S
Channel Wing	1.228 C_{D_0}	1.057W	W_f	S
Ring Wing	1.858 C_{D_0}	1.214W	W_f	S

Figure 61 . Maximum range of jet engine powered light aircraft.

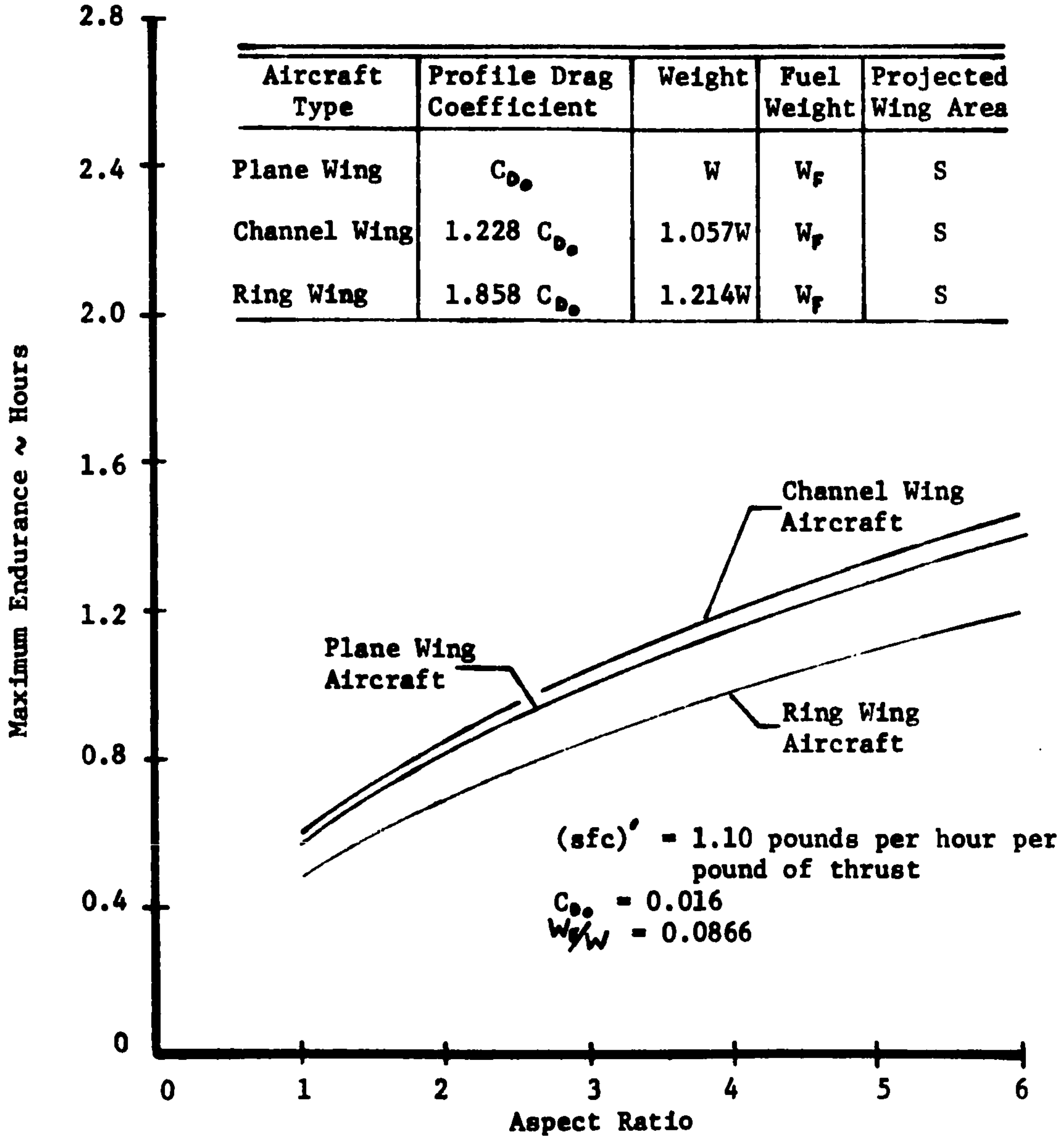

Aircraft Type	Profile Drag Coefficient	Weight	Fuel Weight	Projected Wing Area
Plane Wing	C_{D_0}	W	W_F	S
Channel Wing	1.228 C_{D_0}	1.057W	W_F	S
Ring Wing	1.858 C_{D_0}	1.214W	W_F	S

Figure 62. Maximum endurance of jet engine powered light aircraft.

drag (relatively) at high C_L. This is due to the higher profile drag but lower induced drag of the nonplanar wings. The ring wing exhibits this trend more strongly than does the channel wing, since the former has higher profile drag but lower induced drag than the latter.

Preliminary performance calculations for plane, channel and ring wing aircraft, with allowances for increased structural weight and profile drag of the nonplanar wings, showed certain advantages for aircraft with channel or ring wings. The calculations assumed that there were no power effects on wing aerodynamics (and therefore no engine or propeller mounted in the channel or ring wing). For the same aspect ratio, both the channel wing and the ring wing aircraft require less power for level flight than does the plane wing aircraft over a substantial portion of the low speed flight regime. This portion is larger for the channel wing aircraft than for the ring wing aircraft, and the relative magnitude of this segment of the flight regime increases with decreasing aspect ratio. With reciprocating engine propulsion, a channel wing light aircraft was predicted to demonstrate a significant increase in endurance as compared to a plane wing aircraft, with a lesser increase in range. Also, the jet-powered channel wing aircraft has slightly longer endurance than the plane wing aircraft. The reciprocating-powered ring wing light aircraft has greater endurance than the plane wing aircraft, but this advantage is accompanied by a decrease in range.

The calculated power required for the ring wing aircraft is always equal to or greater than that for the channel wing aircraft, and the ring wing aircraft has less range and endurance than does the channel wing aircraft. Therefore, the channel wing aircraft appears to be the more attractive of the two.

Although the performance calculations showed certain advantages of the nonplanar wings over the plane wing for fixed aspect ratio, it was also shown that a substantial increase in aspect ratio of the planar wing yielded better performance than going to the nonplanar wing at fixed aspect ratio. Therefore, the nonplanar wing will be advantageous only if the maximum span is fixed -- perhaps by operational requirements -- and if the design mission requires long endurance at low airspeed (high lift coefficient). If increased aspect ratio is allowed, the design rule should be (with apologies to Omar Khayyam): "Take the aspect ratio and let the efficiency factor go."

CONCLUSIONS

Ribner's [1] deflected streamtube theory for ring wings, and methods derived from his general conclusions, yield predictions for lift and induced drag which agree well with experimental data, and with other theoretical results. However, a similar deflected streamtube theory for channel wings, derived by the author, was not successful, as indicated by the channel wing wind tunnel model tests reported herein. The lift and drag data of these model tests apparently constitute the only experimental data available for isolated channel wings.

The channel wing lifting arc theory derived in Chapter VI provides good correlation of lift and induced drag data. The digital computer program developed to implement this theory allows rapid calculation of lift and drag coefficients of isolated channel wings as a function of wing geometry, airfoil section characteristics, and wing centerline angle of attack.

Experimental results for channel and ring wings indicate that these wings achieve span efficiency factors close to the theoretical maximums derived by Cone [7] .

Aircraft with channel or ring wings will require less power for level flight over a substantial portion of the low speed (high lift coefficient) flight regime than will a planar wing aircraft of the same aspect ratio. The width of this speed range increases as aspect ratio decreases. Power required for the ring wing aircraft is equal to or greater than that for the channel wing aircraft, at any flight speed. Power effects on wing aerodynamics were not considered.

The channel wing aircraft with reciprocating engine propulsion will have a significant increase in endurance as compared to a plane wing aircraft, and a lesser increase in range. The jet-powered channel wing aircraft has slightly longer endurance than does the plane wing aircraft. With reciprocating propulsion, the ring wing aircraft has more endurance but less range than the plane wing aircraft.

The channel wing is more attractive as a design alternative than is the ring wing, since the ring wing aircraft requires as much or more power and has less endurance and range.

The channel wing is an attractive design alternative to the planar wing if operational requirements restrict the wing span to a low value, and if the design mission requires long endurance at low airspeed. Such missions include battlefield surveillance, crop dusting, traffic control, and towing of aerial advertisement signs.

LIST OF REFERENCES

1. Ribner, H. S., "The Ring Airfoil in Nonaxial Flow," J. Aero. Sciences, Vol. 14, September, 1947, pp. 529-530.

2. Kuethe, A. M., and Schetzer, J. D., Foundations of Aerodynamics, J. Wiley and Sons, Inc., New York, 1950.

3. Fletcher, H. S., "Experimental Investigation of Lift, Drag, and Pitching Moment of Five Annular Airfoils," NACA Technical Note 4117, 1957.

4. Wood, K. D., Technical Aerodynamics, McGraw-Hill, New York, 1947.

5. Jacobs, E. N., and Rhode, R. V., "Airfoil Section Characteristics as Applied to the Prediction of Air Forces and Their Distribution on Wings," NACA Report 631, 1938.

6. Milla, J. H., "Experimental Determination of Aerodynamic Characteristics of a Model Airplane with Annular Airfoils," Master of Engineering Thesis, University of Oklahoma, Norman, Oklahoma, 1966. See also: Milla, J. H., and Blick, E. F., "Lift and Drag Characteristics of a Biannular Wing Airplane," J. Aircraft, November-December, 1966, pp. 586-587.

7. Cone, C. D., "The Theory of Induced Lift and Minimum Induced Drag of Nonplanar Lifting Systems," NASA Technical Report R-139, 1962.

8. Munk, M. M., "The Minimum Induced Drag of Aerofoils," NACA Report 121, 1921.

9. Reynolds, J. F., "Lifting-Surface Theory Applied to Isolated Ring Wings at Angle of Attack," NAVWEPS Report 8401, U.S. Naval Ordance Test Station, China Lake, California, 1963.

10. Glauert, H., The Elements of Aerofoil and Airscrew Theory, 2nd ed., Cambridge, 1948.

11. Crook, L., "Lift Forces on Single Scoop Airfoil and Straight Airfoil of Same Plan Form," Aerodynamical Report No. 557, Crook Aerodynamical Laboratory, Washington, D.C., September, 1943.

12. Chamberlain, J. F., "Changes in Lift and Drag When Channel Section Replaces Portion of Conventional Airfoil," Catholic University, Washington, D.C., February, 1952.

13. Hermes, M. E., "Aerodynamics of Custer Channel Wing," DAS Report No. 553, Devore Aviation Service Corp., August, 1969.

14. Dommasch, D. O., Sherby, S. S., and Connolly, T. F., Airplane Aerodynamics, Pitman Publishing Corp., New York, 1961.

15. Comp, L. A., "Laboratory Manual for Wind Tunnel Testing," University of Oklahoma, Norman, Oklahoma, June, 1964.

16. Pope, A., and Harper, J. J., Low-Speed Wind Tunnel Testing, J. Wiley and Sons, Inc., New York, 1966.

17. Hoerner, S. F., Fluid-Dynamic Drag, S. F. Hoerner, Brick Town, New Jersey, 1965.

18. Abbott, I. H., and Von Doenhoff, A. E., Theory of Wing Sections, Dover Publications, Inc., New York, 1959.

19. Abbott, I. H., Von Doenhoff, A. E., and Stivers, L. S., "Summary of Airfoil Data," NACA Report 824, 1945.

20. Ashley, H., and Landahl, M., Aerodynamics of Wings and Bodies, Addison-Wesley, Reading, Massachussetts, 1965.

21. Jordan, P. F., "Span Loading and Formation of Wake," in Aircraft Wake Turbulence and Its Detection, ed. by Olsen, J. H., Goldburg, A., and Rogers, M., Plenum Press, New York, 1971.

22. Perkins, C. D., and Hage, R. E., Airplane Performance, Stability and Control, J. Wiley and Sons, Inc., New York, 1949.

23. Loftin, L. K., and Smith, H. A., "Aerodynamic Characteristics of 15 NACA Airfoil Sections at Seven Reynolds Numbers," NACA Technical Note 1945, 1949.

24. Jacobs, E. N., and Sherman, A., "Airfoil Section Characteristics as Affected by Variations of the Reynolds Number," NACA Report 586, 1937.

25. Jacobs, E. N., and Abbott, I. H., "Airfoil Section Data Obtained in the NACA Variable Density Tunnel as Affected by Support Interference and Other Corrections," NACA Report 669, 1939.

26. Schwartzberg, M. A., "Airfoil Profile Drag Estimation," Unpublished Report, U.S. Army Air Mobility Research and Development Laboratory, 1971.

27. Corning, G., Supersonic & Subsonic Airplane Design, G. Corning, College Park, Maryland, 1964.

APPENDIX A

TABULATED WIND TUNNEL DATA REDUCTION AND CORRECTIONS

TABULATED WIND TUNNEL DATA REDUCTION

AND CORRECTIONS

The wind tunnel raw data, with the workup of data reduction and corrections, are tabulated in this appendix. As discussed in Chapter V, the test runs with transition strips installed on the models did not produce the desired results; therefore, the data from these runs is not presented.

The data reductions and corrections were carried out as described in Chapters IV and V. The density of manometer water, ρ_{H_2O} , was determined from standard tables as a function of balance room temperature. Air density and viscosity required to calculate Reynolds number were based on the average test section air temperature for a particular test run, while V for Reynolds number was obtained from the ΔP vs. V graph in Comp [15] , using average ΔP . Then the effective Reynolds number was calculated as the average Reynolds number for the four test runs for each model, multiplied by the wind tunnel turbulence factor.

The lift coefficients (for the $\mathcal{R} = 1.0$ model) obtained from the faired curves of Figure 26 are presented here also. Refer to Chapter V for a discussion of the use of these data.

WIND TUNNEL DATA REDUCTION

RUN 1 RUN TYPE I MODEL $\mathcal{R}$ = 2.8 TRANS. STRIP No

MODEL ATTITUDE Upright IMAGE SYSTEM No AMB. TEMP 91°F

CORR. BAR. PRESS. 28.96 in.Hg. ρ_{H_2O} = 62.0 lbm/ft³

$F_q = (.0920)\rho_{H_2O} = 5.70$ lbf/ft² per in.H_2O $S = 0.486$ ft²

$F_D = \frac{0.118}{S} = .2425 \frac{\text{lbf}}{\text{ft}^2\mu\text{in.}}$ $F_L = \frac{0.290}{S} = .596 \frac{\text{lbf}}{\text{ft}^2\mu\text{in.}}$

ρ = .00215 slugs/ft³ $\mu = 3.95\text{x}10^{-7} \frac{\text{lbf sec}}{\text{ft}^2}$ V = 219 ft/sec

Re = 496,000

SET α_M DEGREES	q $(F_q)\cdot(\Delta P)$ lbf/ft²	F_D' F_D/q 1/μin.	F_L' F_L/q 1/μin.	DRAG $\Delta\mu$in.	C_{D_u} $(F_D')\cdot(D)$	LIFT $\Delta\mu$in.	C_{L_u} $(F_L')\cdot(L)$
-4	51.5	.00471	.01158	41.5	.1955	-26.5	-.307
-2	51.5	.00471	.01158	40.5	.1908	-17.5	-.2025
0	51.5	.00471	.01158	39.5	.1860	- 7.5	-.0868
+2	51.5	.00471	.01158	38.5	.1813	+ 2.5	+.0289
4	51.4	.00472	.01161	38.5	.1820	+12.5	+.1452
6	51.4	.00472	.01161	38.5	.1820	+23.5	.273
8	50.8	.00478	.01173	38.5	.1840	34.5	.405
10	51.9	.00467	.01149	41.5	.1940	47.5	.546
12	51.4	.00472	.01161	44.5	.2100	57.5	.669
14	51.5	.00471	.01158	48.5	.2285	69.5	.805
16	51.5	.00471	.01158	55.5	.261	63.5	.735
18	51.6	.00470	.01155	62.5	.294	63.5	.734
20	51.5	.00471	.01158	67.5	.318	63.5	.735
22	51.5	.00471	.01158	82.5	.388	47.5	.550

WIND TUNNEL DATA REDUCTION

RUN 2 RUN TYPE II MODEL $\mathcal{R}$ = 2.8 TRANS. STRIP No

MODEL ATTITUDE Upright IMAGE SYSTEM Yes AMB. TEMP 91°F

CORR. BAR. PRESS. 28.96 in.Hg. ρ_{H_2O} = 62.0 lbm/ft^3

$F_q = (.0920)\rho_{H_2O} = 5.70\ lbf/ft^2$ per in. H_2O S = 0.486 ft^2

$F_D = \frac{0.118}{S} = .2425\ \frac{lbf}{ft^2 \mu in.}$ $F_L = \frac{0.290}{S} = .596\ \frac{lbf}{ft^2 \mu in.}$

$\rho = .002135\ slugs/ft^3$ $\mu = 3.95\text{x}10^{-7}\ \frac{lbf\ sec}{ft^2}$ V = 219 ft/sec

Re = 493,000

SET α_M DEGREES	q $(F_q)\cdot(\Delta P)$ lbf/ft^2	F_D' F_D/q $1/\mu in.$	F_L' F_L/q $1/\mu in.$	DRAG $\Delta\mu in.$	C_{D_U} $(F_D')\cdot(D)$	LIFT $\Delta\mu in.$	C_{L_U} $(F_L')\cdot(L)$
-4	50.5	.00480	.0118	70	.336	-24	-.283
-2	51.3	.00473	.01162	70	.331	-20	-.2325
0	51.6	.00469	.01154	70	.328	-15	-.1731
+2	51.6	.00469	.01154	71	.333	-11	-.1270
4	51.6	.00469	.01154	71	.333	- 4	-.0462
6	51.5	.00471	.01158	73	.344	- 1	-.01158
8	51.1	.00474	.01166	75	.358	+ 6	+.0700
10	51.3	.00473	.01162	78	.369	+13	+.1151
12	51.2	.00473	.01164	81	.383	+17	.1980
14	51.3	.00473	.01162	85	.402	+24	.279
16	51.3	.00473	.01162	90	.426	+30	.349
18	51.5	.00471	.01158	93	.438	+36	.417
20	51.3	.00473	.01162	98	.464	+40	.465
22	51.0	.00476	.01169	102	.485	+45	.526

WIND TUNNEL DATA REDUCTION

RUN 7 RUN TYPE III MODEL AR = 2.8 TRANS. STRIP No

MODEL ATTITUDE Inverted IMAGE SYSTEM No AMB. TEMP 95 °F

CORR. BAR. PRESS. 28.93 in.Hg. ρ_{H_2O} = 62.0 lbm/ft³

F_q = (.0920) ρ_{H_2O} = 5.70 lbf/ft² per in. H_2O S = 0.486 ft²

$F_D = \frac{0.118}{S} = .2425 \frac{\text{lbf}}{\text{ft}^2 \mu\text{in.}}$ $F_L = \frac{0.290}{S} = .596 \frac{\text{lbf}}{\text{ft}^2 \mu\text{in.}}$

ρ = .00212 slugs/ft³ $\mu = 3.95 \times 10^{-7} \frac{\text{lbf sec}}{\text{ft}^2}$ V = 220 ft/sec

Re = 492,000

SET α_M DEGREES	q $(F_q)\cdot(\Delta P)$ lbf/ft²	F_D' F_D/q 1/μin.	F_L' F_L/q 1/μin.	DRAG $\Delta\mu$in.	C_{D_U} $(F_D')\cdot(D)$	LIFT $\Delta\mu$in.	C_{L_U} $(F_L')\cdot(L)$
-4	51.0	.00475	.01169	36.5	.1733	-12	-.1402
-2	51.0	.00475	.01169	37.5	.1781	- 3	-.0351
0	51.0	.00475	.01169	38.5	.1829	+ 6	+.0701
+2	51.0	.00475	.01169	39.5	.1877	+15	+.1753
+4	51.3	.00472	.01162	41.5	.1960	22	.256
6	51.3	.00472	.01162	45.5	.215	30	.349
8	51.3	.00472	.01162	47.5	.2245	37	.430
10	51.3	.00472	.01162	50.5	.2385	42	.488
12	51.3	.00472	.01162	56.5	.267	50	.581
14	51.0	.00475	.01169	59.5	.283	56	.655
16	51.3	.00472	.01162	64.5	.3045	62	.721
18	51.0	.00475	.01169	67.5	.321	67	.784
20	50.7	.00478	.01177	72.5	.3465	70	.824
22	50.7	.00478	.01177	74.5	.356	74	.870

WIND TUNNEL DATA REDUCTION

RUN 8 RUN TYPE IV MODEL $\mathcal{R}$ = 2.8 TRANS. STRIP No

MODEL ATTITUDE Inverted IMAGE SYSTEM Yes AMB. TEMP 95°F

CORR. BAR. PRESS. 28.93 in.Hg. ρ_{H_2O} = 62.0 lbm/ft^3

F_q = (.0920) ρ_{H_2O} = 5.70 lbf/ft^2 per in. H_2O S = 0.486 ft^2

$F_D = \frac{0.118}{S} = .2425 \frac{\text{lbf}}{\text{ft}^2 \mu\text{in.}}$ $F_L = \frac{0.290}{S} = .596 \frac{\text{lbf}}{\text{ft}^2 \mu\text{in.}}$

ρ = .00211 slugs/ft^3 $\mu = 3.95\text{x}10^{-7} \frac{\text{lbf sec}}{\text{ft}^2}$ V = 220 ft/sec

Re = 490,000

SET α_M DEGREES	q $(F_q)\cdot(\Delta P)$ lbf/ft^2	F_D' F_D/q 1/μin.	F_L' F_L/q 1/μin.	DRAG $\Delta\mu$in.	C_{D_U} $(F_D')\cdot(D)$	LIFT $\Delta\mu$in.	C_{L_U} $(F_L')\cdot(L)$
-4	50.7	.00478	.01175	70	.335	- 5.5	-.0646
-2	50.7	.00478	.01175	70	.335	- 1.5	-.01763
0	51.0	.00475	.01169	70.5	.335	0	0
+2	51.0	.00475	.01169	72	.342	+ 5.5	+.0643
+4	51.0	.00475	.01169	72	.342	11.5	.1344
6	51.0	.00475	.01169	74	.3515	18.5	.2165
8	51.0	.00475	.01169	77	.366	25.5	.298
10	51.0	.00475	.01169	79	.375	31.5	.368
12	51.3	.00472	.01161	81	.3825	38.5	.448
14	51.3	.00472	.01161	85	.401	44.5	.517
16	51.0	.00475	.01169	87	.413	47.5	.555
18	51.3	.00472	.01161	92	.434	53.5	.621
20	51.0	.00475	.01169	93	.442	57.5	.672
22	51.0	.00475	.01169	98	.466	60.5	.707

WIND TUNNEL DATA REDUCTION

MODEL AR = 2.8 S = .486 ft^2 δ = .114 τ_2 = .10 Re_{Avg} = 493,000

$\delta(S/A_{TS})$ = .00269 (4) $\delta(S/A_{TS})(1+\tau_2)(57.3)$ = .170° (3) Re_{eff} = $(Re_{Avg})(TF)$ = 665,000

α_u	DRAG (1) I + III	C_{D_N} (1) − IV	$C_{D_{INV}}$ (1) − II	C_D $\frac{C_{D_N}+C_{D_{INV}}}{2}$	LIFT (2) I + III	C_{L_N} (2) − IV	$C_{L_{INV}}$ (2) − II	C_L $\frac{C_{L_N}+C_{L_{INV}}}{2}$	C_L^2	$\Delta\alpha$ (3) · C_L	ΔC_{D_i} (4) · C_L^2	$C_{D_{TS}}$	α $\alpha_u + \Delta\alpha$	C_{D_C} $C_D + \Delta C_{D_i} - C_{D_{TS}}$
-4°	.3688	.0338	.0328	.0333	-.4472	-.3826	-.1642	-.274	.0750	-.047°	.000202	.0013	-4.05°	.0322
-2	.3689	.0339	.0379	.0359	-.2376	-.2200	-.0051	-.1125	.0127	-.019	.000034	.0013	-2.02	.0346
0	.3689	.0339	.0409	.0374	-.0167	-.0167	+.1564	+.0698	.0049	+.012	.000013	.0013	+0.01	.0361
+2	.3690	.0270	.0360	.0315	+.2042	+.1399	+.3312	+.236	.0557	+.040	.000150	.0013	+2.04	.0304
4	.3780	.0360	.0450	.0405	+.4012	+.2668	.4474	.357	.1275	.061	.000343	.0013	4.06	.0395
6	.3970	.0455	.0530	.0492	.622	.4055	.6336	.519	.269	.088	.000725	.0014	6.09	.0485
8	.4085	.0425	.0505	.0465	.835	.537	.765	.651	.424	.111	.00114	.0015	8.11	.0461
10	.4325	.0575	.0635	.0605	1.034	.666	.919	.792	.627	.134	.00169	.0016	10.13	.0606
12	.4770	.0940	.0940	.0940	1.250	.802	1.052	.927	.860	.158	.00231	.0018	12.16	.0940
14	.5115	.1105	.1095	.1100	1.460	.943	1.181	1.061	1.127	.180	.00303	.0020	14.18	.1109
16	.5655	.1525	.1395	.1460	1.456	.901	1.107	1.004	1.008	.170	.00271	.0024	16.17	.1463
18	.6150	.1810	.1770	.1790	1.518	.897	1.101	.999	.998	.169	.00269	.0028	18.17	.1788
20	.6645	.2225	.2005	.2115	1.559	.887	1.094	.991	.982	.168	.00264	.0034	20.17	.2107
22°	.7440	.2780	.2590	.2685	1.420	.713	.894	.803	.645	.136°	.00174	.0040	22.14°	.266

WIND TUNNEL DATA REDUCTION

RUN 19 RUN TYPE I MODEL AR = 1.0 TRANS. STRIP No

MODEL ATTITUDE Upright IMAGE SYSTEM No AMB. TEMP 98°F

CORR. BAR. PRESS. 28.72 in.Hg. ρ_{H_2O} = 61.9 lbm/ft^3

F_q = (.0920)ρ_{H_2O} = 5.695 lbf/ft^2 per in. H_2O S = 1.0 ft^2

$F_D = \frac{0.118}{S} = 0.118 \frac{\text{lbf}}{\text{ft}^2\mu\text{in.}}$ $F_L = \frac{0.290}{S} = 0.290 \frac{\text{lbf}}{\text{ft}^2\mu\text{in.}}$

ρ = .00207 slugs/ft^3 $\mu = 4.02\times10^{-7} \frac{\text{lbf sec}}{\text{ft}^2}$ V = 223 ft/sec

Re = 1.15×10^6

SET α_M DEGREES	q $(F_q)\cdot(\Delta P)$ lbf/ft^2	F_D' F_D/q 1/μin.	F_L' F_L/q 1/μin.	DRAG $\Delta\mu$in.	C_{D_U} $(F_D')\cdot(D)$	LIFT $\Delta\mu$in.	C_{L_U} $(F_L')\cdot(L)$
-6	50.65	.002327	.005725	42	.0978	- 8	-.0458
-4	50.65	.002327	.005725	42	.0978	+ 5	+.0286
-2	50.65	.002327	.005725	42	.0978	17	.0974
0	50.65	.002327	.005725	46	.1071	31	.1775
+2	50.65	.002327	.005725	49	.1141	44	.252
+4	50.65	.002327	.005725	52	.1211	57	.3265
6	50.65	.002327	.005725	58	.1350	72	.4125
8	50.65	.002327	.005725	64	.1490	85	.487
10	50.65	.002327	.005725	73	.1700	100	.5725
12	51.25	.002303	.00566	83	.1912	112	.634
14	50.65	.002327	.005725	92	.214	125	.716
16	50.1	.002355	.00579	103	.2425	140	.811
18	51.25	.002303	.00566	117	.2695	153	.867
20	50.1	.002355	.00579	127	.299	164	.950
22	50.65	.002327	.005725	139	.3235	173	.991
24	51.25	.002303	.00566	141	.325	162	.917

WIND TUNNEL DATA REDUCTION

RUN 11 RUN TYPE II MODEL $\mathcal{R}$= 1.0 TRANS. STRIP No

MODEL ATTITUDE Upright IMAGE SYSTEM Yes AMB. TEMP 95°F

CORR. BAR. PRESS. 28.77 in.Hg. ρ_{H_2O} = 62.0 lbm/ft^3

F_q = (.0920)ρ_{H_2O} = 5.70 lbf/ft^2 per in. H_2O S = 1.0 ft^2

$F_D = \frac{0.118}{S} = 0.118 \frac{\text{lbf}}{\text{ft}^2\mu\text{in.}}$ $F_L = \frac{0.290}{S} = 0.290 \frac{\text{lbf}}{\text{ft}^2\mu\text{in.}}$

ρ = .002085 slugs/ft^3 $\mu = 4.00\times10^{-7} \frac{\text{lbf sec}}{\text{ft}^2}$ V = 221 ft/sec

Re = 1.15×10^6

SET α_M DEGREES	q $(F_q)\cdot(\Delta P)$ lbf/ft^2	F_D' F_D/q 1/μin.	F_L' F_L/q 1/μin.	DRAG $\Delta\mu$in.	C_{D_U} $(F_D')\cdot(D)$	LIFT $\Delta\mu$in.	C_{L_U} $(F_L')\cdot(L)$
-6	50.7	.002327	.00572	68	.1582	- 2	-.01145
-4	50.7	.002327	.00572	72	.1677	+ 7	+.04005
-2	50.7	.002327	.00572	72	.1677	+17	.0973
0	50.7	.002327	.00572	76	.1769	27	.1545
+2	50.7	.002327	.00572	82	.1909	36	.206
+4	50.7	.002327	.00572	87	.2025	44	.252
6	50.7	.002327	.00572	92	.214	50	.286
8	50.7	.002327	.00572	103	.240	50	.286
10	50.7	.002327	.00572	108	.2515	41	.235
12	50.7	.002327	.00572	110	.256	35	.2005
14	50.7	.002327	.00572	115	.268	38	.2175
16	50.7	.002327	.00572	117	.272	40	.229
18	50.7	.002327	.00572	124	.289	42	.2405
20	50.7	.002327	.00572	128	.298	47	.269
22	50.7	.002327	.00572	132	.307	50	.286
24	50.7	.002327	.00572	144	.335	53	.303

WIND TUNNEL DATA REDUCTION

RUN 18 RUN TYPE III MODEL $\mathcal{R}$= 1.0 TRANS. STRIP No

MODEL ATTITUDE Inverted IMAGE SYSTEM No AMB. TEMP 98°F

CORR. BAR. PRESS. 28.72 in.Hg. ρ_{H_2O} = 61.9 lbm/ft³

F_q = (.0920) ρ_{H_2O} = 5.695 lbf/ft² per in. H_2O S = 1.0 ft²

$F_D = \frac{0.118}{S} = 0.118 \frac{\text{lbf}}{\text{ft}^2 \mu\text{in.}}$ $F_L = \frac{0.290}{S} = 0.290 \frac{\text{lbf}}{\text{ft}^2 \mu\text{in.}}$

ρ = .00207 slugs/ft³ $\mu = 4.02\times10^{-7} \frac{\text{lbf sec}}{\text{ft}^2}$ V = 222 ft/sec

Re = 1.14×10^6

SET α_M DEGREES	q $(F_q)\cdot(\Delta P)$ lbf/ft²	F_D' F_D/q 1/μin.	F_L' F_L/q 1/μin.	DRAG $\Delta\mu$in.	C_{D_U} $(F_D')\cdot(D)$	LIFT $\Delta\mu$in.	C_{L_U} $(F_L')\cdot(L)$
-6	50.65	.002327	.005725	39	.0908	+17	+.0973
-4	50.1	.002355	.00579	42	.0989	29	.1679
-2	50.1	.002355	.00579	45	.1060	42	.243
0	50.1	.002355	.00579	50	.1178	52	.301
+2	50.65	.002327	.005725	56	.1304	61	.3495
4	50.65	.002327	.005725	64	.1490	70	.401
6	50.65	.002327	.005725	73	.1700	55	.315
8	50.1	.002355	.00579	77	.1813	55	.3185
10	50.1	.002355	.00579	82	.193	55	.3185
12	51.25	.002303	.00566	90	.207	60	.3395
14	50.65	.002327	.005725	94	.219	66	.378
16	50.65	.002327	.005725	101	.235	69	.395
18	50.65	.002327	.005725	107	.249	71	.407
20	49.55	.00238	.00585	107	.2545	73	.427
22	50.1	.002355	.00579	115	.271	78	.4515
24	50.65	.002327	.005725	127	.296	84	.481

WIND TUNNEL DATA REDUCTION

RUN 17 RUN TYPE IV MODEL $\mathcal{R}$ = 1.0 TRANS. STRIP No

MODEL ATTITUDE Inverted IMAGE SYSTEM Yes AMB. TEMP 98°F

CORR. BAR. PRESS. 28.72 in.Hg. ρ_{H_2O} = 61.9 lbm/ft³

$F_q = (.0920)\rho_{H_2O} = 5.695$ lbf/ft² per in. H_2O S = 1.0 ft²

$F_D = \dfrac{0.118}{S} = 0.118 \dfrac{\text{lbf}}{\text{ft}^2\mu\text{in.}}$ $F_L = \dfrac{0.290}{S} = 0.290 \dfrac{\text{lbf}}{\text{ft}^2\mu\text{in.}}$

ρ = .00209 slugs/ft³ $\mu = 3.99\times10^{-7} \dfrac{\text{lbf sec}}{\text{ft}^2}$ V = 221 ft/sec

Re = 1.16×10^{6}

SET α_M DEGREES	q $(F_q)\cdot(\Delta P)$ lbf/ft²	F_D' F_D/q 1/μin.	F_L' F_L/q 1/μin.	DRAG $\Delta\mu$in.	C_{D_U} $(F_D')\cdot(D)$	LIFT $\Delta\mu$in.	C_{L_U} $(F_L')\cdot(L)$
-6	50.65	.002327	.005725	75	.1748	+16	+.0916
-4	50.1	.002355	.00579	76	.1790	27	.1562
-2	50.65	.002327	.005725	74	.1723	37	.222
0	50.65	.002327	.005725	77	.1792	47	.269
+2	50.65	.002327	.005725	80	.1863	59	.338
4	50.65	.002327	.005725	87	.2025	67	.384
6	50.65	.002327	.005725	93	.2165	74	.424
8	50.65	.002327	.005725	101	.235	46	.2635
10	50.65	.002327	.005725	106	.247	48	.275
12	50.65	.002327	.005725	108	.2515	50	.286
14	50.65	.002327	.005725	114	.2655	53	.3035
16	50.65	.002327	.005725	116	.270	57	.3265
18	50.65	.002327	.005725	118	.275	60	.3435
20	50.65	.002327	.005725	125	.291	67	.384
22	50.65	.002327	.005725	129	.3005	71	.4065
24	50.65	.002327	.005725	139	.3235	76	.435

TABLE A-1

LIFT COEFFICIENTS OBTAINED BY FAIRING RUNS 11(TYPE II), 18(TYPE III), AND 17(TYPE IV) IN FIGURE 26*

α_u	C_{L_u}		
Degrees	II	III	IV
-6	-.011	.108	.095
-4	+.040	.168	.155
-2	.097	.225	.222
0	.150	.286	.268
+2	.205	.343	.324
+4	.255	.403	.384
6	.310	.463	.440
8	.363	.523	.498
10	.415	.581	.553
12	.470	.641	.612
14	.522	.701	.670
16	.576	.760	.727
18	.630	.820	.783
20	.682	.880	.841
22	.710	.920	.870
24	.620	.830	.788

*Model $\mathcal{R}$ = 1.0, no transition strip.

WIND TUNNEL DATA REDUCTION

MODEL $A\!\!R$ = 1.0 S = 1.0 ft^2 δ = .114 τ_2 = 0.23 Re_{Avg} = 1.15×10^6

$\delta(S/A_{TS})$ = .00554 ④ $\delta(S/A_{TS})(1+\tau_2)(57.3)$ = $.390^\circ$ ③ $Re_{eff} = (Re_{Avg})(TF)$ = 1.55×10^6

α_u	DRAG ① $I + III$	C_{D_N} ①$-IV$	$C_{D_{INV}}$ ①$-II$	C_D $\frac{C_{D_N}+C_{D_{INV}}}{2}$	LIFT ② $I + III$	C_{L_N} ②$-IV$	$C_{L_{INV}}$ ②$-II$	C_L $\frac{C_{L_N}+C_{L_{INV}}}{2}$	C_L^2	$\Delta\alpha$ ③$\cdot C_L$	ΔC_{D_i} ④$\cdot C_L^2$	$C_{D_{TS}}$	α $\alpha_u + \Delta\alpha$	C_{D_C} $C_D + \Delta C_{D_i} - C_{D_{TS}}$
-6°	.1186	.0138	.0304	.0221	.062	-.033	.073	.020	.0004	$.004^\circ$	.00000	Not Significant	-6.00°	.0221
-4	.1967	.0177	.0290	.0233	.197	+.042	.157	.100	.0100	.038	.00003		-3.96	.0233
-2	.2038	.0315	.0361	.0338	.322	.100	.225	.163	.0264	.070	.00018		-1.93	.0340
0	.2249	.0457	.0480	.0468	.464	.196	.314	.255	.0650	.104	.00040		+0.10	.0472
+2	.2445	.0582	.0536	.0559	.595	.271	.390	.331	.1092	.129	.00060		+2.13	.0565
+4	.2701	.0676	.0676	.0671	.730	.346	.475	.411	.1685	.160	.00093		4.16	.0680
6	.3050	.0885	.0910	.0898	.876	.436	.566	.506	.256	.145	.00077		6.15	.0906
8	.3303	.0953	.0903	.0928	1.010	.512	.647	.579	.335	.207	.00156		8.21	.0944
10	.3630	.1160	.1115	.1138	1.154	.601	.739	.670	.449	.248	.00224		10.25	.1160
12	.3982	.1467	.1422	.1445	1.275	.663	.805	.734	.539	.285	.00296		12.29	.1475
14	.4330	.1675	.1650	.1662	1.417	.747	.895	.821	.674	.325	.00384		14.33	.1700
16	.4775	.2075	.2055	.2060	1.571	.844	.995	.919	.845	.362	.00477		16.36	.2108
18	.5185	.2435	.2295	.2365	1.687	.904	1.057	.980	.960	.383	.00534		18.38	.2418
20	.5535	.2625	.2555	.2585	1.830	.989	1.148	1.069	1.142	.410	.00613		20.41	.2646
22	.5945	.2940	.2875	.2910	1.911	1.041	1.201	1.121	1.259	.428	.00667		22.43	.2977
24°	.621	.2975	.2860	.2915	1.747	0.959	1.127	1.043	1.088	$.401^\circ$	.00586		24.40°	.2974

APPENDIX B

EVALUATION OF THE INTEGRAL IN EQUATION (6.35)

EVALUATION OF THE INTEGRAL IN EQUATION (6-35)

The integral required in equation (6.35) is

$$I = \int_0^{\pi} \cos n\beta \cot\left(\frac{\beta - \phi}{2}\right) d\beta , \qquad n = 1, 3, 5, \ldots . \qquad \text{(b.1)}$$

Let $\beta - \phi = x$, then $d\beta = dx$, and the integral can be written as

$$I = \int_{-\phi}^{\pi-\phi} \cos n(x+\phi) \cot\left(\tfrac{x}{2}\right) dx \qquad \text{(b.2)}$$

$$= \int_{-\phi}^{\pi-\phi} \cos nx \cos n\phi \cot\left(\tfrac{x}{2}\right) dx - \int_{-\phi}^{\pi-\phi} \sin nx \sin n\phi \cot\left(\tfrac{x}{2}\right) dx$$

$$I = \cos n\phi \int_{-\phi}^{\pi-\phi} \cos nx \cot\left(\tfrac{x}{2}\right) dx - \sin n\phi \int_{-\phi}^{\pi-\phi} \sin nx \cot\left(\tfrac{x}{2}\right) dx . \qquad \text{(b.3)}$$

Define $$I \equiv I_1 - I_2 , \qquad \text{(b.4)}$$

where
$$I_1 = \cos n\phi \int_{-\phi}^{\pi-\phi} \cos nx \cot\left(\tfrac{x}{2}\right) dx \qquad \text{(b.4a)}$$

$$I_2 = \sin n\phi \int_{-\phi}^{\pi-\phi} \sin nx \cot\left(\tfrac{x}{2}\right) dx . \qquad \text{(b.4b)}$$

Consider I_2 first, and further define

$$I_2 \equiv (\sin n\phi)\, J_n , \qquad \text{(b.5)}$$

where

$$J_n = \int_{-\phi}^{\pi-\phi} \sin nx \cot\left(\frac{x}{2}\right) dx \quad . \tag{b.5a}$$

A recurrence relation for J_n (for $n \geq 3$) may be obtained by writing

$$J_n - J_{n-2} = \int_{-\phi}^{\pi-\phi} \sin nx \cot\left(\frac{x}{2}\right) dx - \int_{-\phi}^{\pi-\phi} \sin(n-2)x \cot\left(\frac{x}{2}\right) dx \quad . \tag{b.6}$$

Now substitute the trigonometric relation

$$\cot\left(\frac{x}{2}\right) = \frac{1+\cos x}{\sin x} : \tag{b.7}$$

$$J_n - J_{n-2} = \int_{-\phi}^{\pi-\phi} \sin nx \left(\frac{1+\cos x}{\sin x}\right) dx - \int_{-\phi}^{\pi-\phi} \sin(n-2)x \left(\frac{1+\cos x}{\sin x}\right) dx \quad . \tag{b.8}$$

The second and fourth terms of equation (b.8) can be expanded with the formulas for the sine of the difference and the sum of two angles, respectively:

$$J_n - J_{n-2} = \int_{-\phi}^{\pi-\phi} \frac{\sin nx}{\sin x} dx + \int_{-\phi}^{\pi-\phi} \frac{\sin(nx-x) + \cos nx \sin x}{\sin x} dx$$

$$- \int_{-\phi}^{\pi-\phi} \frac{\sin(nx-2x)}{\sin x} dx - \int_{-\phi}^{\pi-\phi} \frac{\sin(nx-2x+x) - \cos(nx-2x)\sin x}{\sin x} dx$$

$$J_n - J_{n-2} = \int_{-\phi}^{\pi-\phi} \frac{\sin nx}{\sin x} dx + \int_{-\phi}^{\pi-\phi} \cos nx \, dx - \int_{-\phi}^{\pi-\phi} \frac{\sin(nx-2x)}{\sin x} dx$$

$$+ \int_{-\phi}^{\pi-\phi} \cos(nx-2x) \, dx \quad . \tag{b.9}$$

Another application of the sine formula yields

$$J_n - J_{n-2} = \int_{-\phi}^{\pi-\phi} \frac{\sin nx}{\sin x}\, dx + \int_{-\phi}^{\pi-\phi} \cos nx\, dx$$

$$- \int_{-\phi}^{\pi-\phi} \frac{\sin nx \cos 2x - \cos nx \sin 2x}{\sin x}\, dx$$

$$+ \int_{-\phi}^{\pi-\phi} \cos(n-2)x\, dx ,$$

which becomes, with the aid of the trigonometric formulas for the cosine and sine of double angles,

$$J_n - J_{n-2} = \int_{-\phi}^{\pi-\phi} \frac{\sin nx}{\sin x}\, dx + \int_{-\phi}^{\pi-\phi} \cos nx\, dx + \int_{-\phi}^{\pi-\phi} \cos(n-2)x\, dx$$

$$- \int_{-\phi}^{\pi-\phi} \frac{\sin nx\,(1 - 2\sin^2 x)}{\sin x}\, dx + 2\int_{-\phi}^{\pi-\phi} \frac{\cos nx \sin x \cos x}{\sin x}\, dx$$

$$= \int_{-\phi}^{\pi-\phi} \cos nx\, dx + \int_{-\phi}^{\pi-\phi} \cos(n-2)x\, dx + 2\int_{-\phi}^{\pi-\phi} \sin nx \sin x\, dx$$

$$+ 2\int_{-\phi}^{\pi-\phi} \cos nx \cos x\, dx . \qquad \text{(b.10)}$$

The last two terms are recognized as the cosine of the difference of two angles, so

$$J_n - J_{n-2} = \int_{-\phi}^{\pi-\phi} \cos nx\, dx + \int_{-\phi}^{\pi-\phi} \cos(n-2)x\, dx$$

$$+ 2\int_{-\phi}^{\pi-\phi} \cos(nx - x)\, dx$$

$$J_n - J_{n-2} = \int_{-\phi}^{\pi-\phi} \cos nx \, dx + 2\int_{-\phi}^{\pi-\phi} \cos (n-1)x \, dx$$

$$+ \int_{-\phi}^{\pi-\phi} \cos (n-2) x \, dx \quad . \tag{b.11}$$

The simple integrals of equation (b.11) are easily evaluated, since $n = 3,5,7, \ldots$; thus

$$J_n - J_{n-2} = 2/n \sin n\phi + \frac{2}{n-2} \sin (n-2)\phi \quad . \tag{b.12}$$

Now consider J_n when $n = 1$:

$$J_1 = \int_{-\phi}^{\pi-\phi} \sin x \cot (x/2) \, dx = \int_{-\phi}^{\pi-\phi} \sin x \left(\frac{1 + \cos x}{\sin x} \right) dx$$

$$= \int_{-\phi}^{\pi-\phi} dx + \int_{-\phi}^{\pi-\phi} \cos x \, dx$$

$$J_1 = \pi + 2 \sin \phi \quad . \tag{b.13}$$

Therefore, the second integral in equation (b.3) is

$$I_2 = (\sin n\phi) \; J_n \quad , \tag{b.14}$$

where J_n is given by the recurrence relation

$$J_1 = \pi + 2 \sin\phi$$

$$J_n = J_{n-2} + 2/n \sin n\phi + \frac{2}{n-2} \sin (n-2)\phi \tag{b.12}$$

for n = 3, 5, 7, ...

Turning to I_1 , we define

$$I_1 \equiv (\cos n\phi) K_n \quad , \tag{b.15}$$

where

$$K_n = \int_{-\phi}^{\pi-\phi} \cos nx \cot(x/2)\, dx \quad . \tag{b.15a}$$

Again writing a recurrence relation for $n \geq 3$,

$$K_n - K_{n-2} = \int_{-\phi}^{\pi-\phi} \cos nx \cot(x/2) dx - \int_{-\phi}^{\pi-\phi} \cos(n-2)x \cot(x/2) dx \quad . \tag{b.16}$$

Substitution of equation (b.7) gives

$$K_n - K_{n-2} = \int_{-\phi}^{\pi-\phi} \cos nx \left(\frac{1+\cos x}{\sin x}\right) dx - \int_{-\phi}^{\pi-\phi} \cos(n-2)x \left(\frac{1+\cos x}{\sin x}\right) dx \; ; \tag{b.17}$$

the second and fourth terms are expanded by using the formula for the cosine of the difference and the sum of two angles, respectively:

$$K_n - K_{n-2} = \int_{-\phi}^{\pi-\phi} \frac{\cos nx}{\sin x} dx + \int_{-\phi}^{\pi-\phi} \frac{\cos(nx-x) - \sin nx \sin x}{\sin x} dx - \int_{-\phi}^{\pi-\phi} \frac{\cos(n-2)x}{\sin x} dx$$

$$- \int_{-\phi}^{\pi-\phi} \frac{\cos(nx-2x+x) + \sin(nx-2x)\sin x}{\sin x} dx$$

$$= \int_{-\phi}^{\pi-\phi} \frac{\cos nx}{\sin x} dx - \int_{-\phi}^{\pi-\phi} \sin nx\, dx - \int_{-\phi}^{\pi-\phi} \frac{\cos(n-2)x}{\sin x} dx$$

$$- \int_{-\phi}^{\pi-\phi} \sin(n-2)x\, dx$$

$$K_n - K_{n-2} = \int_{-\phi}^{\pi-\phi} \frac{\cos nx}{\sin x} dx - \int_{-\phi}^{\pi-\phi} \sin nx\, dx - \int_{-\phi}^{\pi-\phi} \sin(n-2)x\, dx$$

$$- \int_{-\phi}^{\pi-\phi} \frac{\cos nx \cos 2x + \sin nx \sin 2x}{\sin x} dx \tag{b.18}$$

Applying the trigonometric identities for cosine and sine of double angles,

$$K_n - K_{n-2} = \int_{-\phi}^{\pi-\phi} \frac{\cos nx}{\sin x}\, dx - \int_{-\phi}^{\pi-\phi} \sin nx\, dx - \int_{-\phi}^{\pi-\phi} \sin(n-2)x\, dx$$

$$- \int_{-\phi}^{\pi-\phi} \frac{\cos nx\,(1-2\sin^2 x)}{\sin x}\, dx \quad - 2\int_{-\phi}^{\pi-\phi} \frac{\sin nx \sin x \cos x}{\sin x}\, dx$$

$$K_n - K_{n-2} = -\int_{-\phi}^{\pi-\phi} \sin nx\, dx - \int_{-\phi}^{\pi-\phi} \sin(n-2)x\, dx + 2\int_{-\phi}^{\pi-\phi} \cos nx \sin x\, dx$$

$$-2\int_{-\phi}^{\pi-\phi} \sin nx \cos x\, dx \quad . \tag{b.19}$$

The arguments of the last two terms of equation (b.19) are recognized as the sine of (n x-x):

$$K_n - K_{n-2} = -\int_{-\phi}^{\pi-\phi} \sin nx\, dx \; - 2\int_{-\phi}^{\pi-\phi} \sin(n-1)x\, dx \; - \int_{-\phi}^{\pi-\phi} \sin(n-2)x\, dx \quad . \tag{b.20}$$

Now the integrals of the recurrence relation can be evaluated:

$$K_n - K_{n-2} = -2/n \cos n\phi \; - \; \frac{2}{n-2} \cos(n-2)\phi \tag{b.21}$$

since n = 3,5,7, . . .

K_n for n =1 must be evaluated:

$$K_1 = \int_{-\phi}^{\pi-\phi} \cos x \cot\left(\tfrac{x}{2}\right) dx \quad = \int_{-\phi}^{\pi-\phi} \frac{\cos x \cos(x/2)}{\sin(x/2)}\, dx$$

$$= \int_{-\phi}^{\pi-\phi} \frac{\cos(x - x/2) - \sin x \sin(x/2)}{\sin(x/2)}\, dx$$

$$K_1 = \int_{-\phi}^{\pi-\phi} \cot\left(\frac{x}{2}\right) dx - \int_{-\phi}^{\pi-\phi} \sin x \, dx \tag{b.22}$$

$$K_1 \equiv K_{11} - K_{12} \quad . \tag{b.22a}$$

The second integral K_{12} is easily evaluated, yielding

$$K_{12} = 2 \cos\phi \quad ; \tag{b.23}$$

however, the evaluation of K_{11} requires special care, since cot ($x/2$) becomes infinite at x = 0. First, let $y = x/2$, then $dx = 2\,dy$, and

$$K_{11} = 2\int_{-\phi/2}^{\frac{\pi-\phi}{2}} \cot(y)\,dy \quad . \tag{b.24}$$

In order to avoid the singularity at $y = 0$, it will be shown that this integral may be replaced by

$$K_{11} = 2\int_{+\phi/2}^{\frac{\pi-\phi}{2}} \cot(y)\,dy \quad .$$

The integration interval is divided into three segments:

$$K_{11} = 2\int_{-\phi/2}^{0} \cot(y)\,dy + 2\int_{0}^{\phi/2} \cot(y)\,dy + 2\int_{\phi/2}^{\frac{\pi-\phi}{2}} \cot(y)\,dy$$

$$= 2\int_{-\phi/2}^{0} \cot(y)\,dy - 2\int_{\phi/2}^{0} \cot(y)\,dy + 2\int_{\phi/2}^{\frac{\pi-\phi}{2}} \cot(y)\,dy$$

$$K_{11} = 2\Big[\log \sin y\Big]_{-\phi/2}^{0} - 2\Big[\log \sin y\Big]_{\phi/2}^{0} + 2\int_{\phi/2}^{\frac{\pi-\phi}{2}} \cot(y)\,dy$$

$$= 2\log\left[\frac{\sin(0)}{\sin(-\phi/2)}\right] - 2\log\left[\frac{\sin(0)}{\sin(\phi/2)}\right] + 2\int_{\phi/2}^{\frac{\pi-\phi}{2}} \cot(y)\,dy$$

$$K_{11} = 2\log(0) - 2\log(0) + 2\int_{\phi/2}^{\frac{\pi-\phi}{2}} \cot(y)\,dy$$

$$K_{11} = 2\int_{\phi/2}^{\frac{\pi-\phi}{2}} \cot(y)\,dy \; . \qquad \text{(b.25)}$$

This result can be deduced also from consideration of the graph of cot (y). Evaluation of eq. (b.25) is straightforward:

$$K_{11} = 2\Big[\log \sin y\Big]_{\phi/2}^{\frac{\pi-\phi}{2}} = 2\log\left[\frac{\sin(\pi/2 - \phi/2)}{\sin(\phi/2)}\right]$$

$$= 2\log\left[\frac{\sin\frac{\pi}{2}\cos\frac{\phi}{2} - \cos\frac{\pi}{2}\sin\frac{\phi}{2}}{\sin\frac{\phi}{2}}\right]$$

$$= 2\log\left[\frac{\cos\frac{\phi}{2}}{\sin\frac{\phi}{2}}\right]$$

$$K_{11} = 2\log\left(\cot\frac{\phi}{2}\right) \; . \qquad \text{(b.26)}$$

It is interesting to note that a straightforward application of the Cauchy Principal Value method,

$$\int_a^b f(x)\,dx = \lim_{\epsilon \to 0} \left[\int_a^{A-\epsilon} f(x)\,dx + \int_{A+\epsilon}^b f(x)\,dx \right] \tag{b.27}$$

for $f(x) = \infty$ at $x = A$, to K_{11} in the form shown in equation (b.22) yields

$$K_{11} = 2 \log\left(- \cot \phi/2 \right) ,$$

which cannot be evaluated.

Thus we have

$$K_1 = K_{11} - K_{12} = 2 \log(\cot \phi/2) - 2 \cos\phi , \tag{b.28}$$

and

$$I_1 = (\cos n\phi) K_n , \tag{b.29}$$

where K_n is given by the recurrence relation

$$K_1 = 2 \log(\cot \phi/2) - 2 \cos\phi \tag{b.28}$$

$$K_n = K_{n-2} - 2/n \cos n\phi - \frac{2}{n-2} \cos(n-2)\phi , \tag{b.21}$$

for $n = 3, 5, 7, \ldots$

The integral required, equation (b.1), is

$$\int_0^{\pi} \cos n\beta \cot\left(\frac{\beta-\phi}{2}\right) d\beta = (\cos n\phi) K_n - (\sin n\phi) J_n \,, \qquad \text{(b.30)}$$

$n = 1,3,5, \ldots$, where

$$K_1 = 2 \log(\cot \phi/2) - 2\cos\phi \qquad \text{(b.30a)}$$

$$K_n = K_{n-2} - 2/n \cos n\phi - \frac{2}{n-2}\cos(n-2)\phi \,, \qquad \text{(b.30b)}$$

$n = 3,5,7, \ldots$, and

$$J_1 = \pi + 2\sin\phi \qquad \text{(b.30c)}$$

$$J_n = J_{n-2} + 2/n \sin n\phi + \frac{2}{n-2}\sin(n-2)\phi \,, \qquad \text{(B.30d)}$$

$n = 3,5,7, \ldots$

APPENDIX C

FORTRAN LISTING OF CHANNEL WING COMPUTER PROGRAM, WITH SAMPLE INPUT AND OUTPUT

FORTRAN LISTING OF CHANNEL WING COMPUTER

PROGRAM, WITH SAMPLE INPUT AND OUTPUT

The FORTRAN listing of the digital computer program described in Chapter VII is presented in this appendix, along with sample computer printout of input and output data. This program, written in FORTRAN IV, utilizes the lifting arc theory developed in Chapter VI to calculate the lift and drag coefficients of a channel wing as a function of wing geometry, airfoil section characteristics, and wing angle of attack. Several IBM Scientific Subroutine Package subroutines are utilized; these are included in the FORTRAN listing.

```
C    *** LIFT AND DRAG COEFFICIENTS OF A CHANNEL WING ***
C
      DIMENSION RHV(5), TJ(9),TK(9), ACOF(9), ADI(5,5), ASI(25),
     1 AUX(200), A(9), CIDEN(10), AERSEC(10), TCL(50), TCD(50), WORK(50)
     2, ARG(50), VAL(50)
      EQUIVALENCE(ADI(1,1), ASI(1))
      EXTERNAL FCT
      COMMON A
C              INPUT DATA
    5 READ(5,10,END = 99) CIDEN, AERSEC, IROW, CLMIN, CLMAX, CDERR
   10 FORMAT(10A4,/10A4,/2X, I3, 5X, 3F10.0)
C              AIRFOIL SECTION CL VS. CD TABLE LIMITED TO 50 POINTS
      READ(5,11)(TCL(I), TCD(I), I = 1,IROW)
   11 FORMAT(6F10.0)
      READ(5,12) R, C, ASO, ANZL
   12 FORMAT(4F10.0)
      READ(5,13) ALPAS, DALPA, ALPAE
   13 FORMAT(3F10.0)
C              PRINT CHANNEL WING INPUT DATA
      WRITE(6,20)
   20 FORMAT(1H1, 30X, 23HCHANNEL WING INPUT DATA)
      WRITE(6,21) CIDEN, AERSEC
   21 FORMAT(1H0, 6HWING: , 10A4// 18H AIRFOIL SECTION: , 10A4)
      WRITE(6,22) R, C, ASO, ANZL
   22 FORMAT(/  20H WING RADIUS, FT. = , 1PE16.6,// 19 H WING CHORD, FT.
     1= , 1PE16.6, // 48H AIRFOIL SECTION LIFT-CURVE SLOPE, PER RADIAN =
     2 , 1PE16.6,// 48H AIRFOIL SECTION ANGLE FOR ZERO LIFT, DEGREES = ,
     31PE16.6,//)
C     * CALCULATION OF COEFFICIENTS OF SIMULTANEOUS EQUATIONS
                       FOR FOURIER COEFFICIENTS *
      PIF = 3.141593
      ANZL = ANZL * 0.0174533
      CS1 = ASO * C/(2.0 * R)
```

```
      ALPAC = ALPAS
   94 IF(ALPAC - ALPAE) 92, 92, 5
   92 WRITE(6,23) ALPAC
   23 FORMAT(1H1, 43HWING CENTERLINE ANGLE OF ATTACK, DEGREES = ,
     1  F10.2)
      ALPAC = ALPAC * 0.0174533
      PHI = 0.0
      DO 62 I = 1,5
      M = 0
      PHI = PHI + (18.0 * 0.0174533)
      ALPAL = ATAN(SIN(ALPAC) * SIN(PHI)/COS(ALPAC))
      RHV(I) = CS1 *(ALPAL - ANZL)
      DO 60 N = 1,9,2
      M = M + 1
      RELN = N
      RNPHI = RELN * PHI
      IF(N-1) 64, 64, 66
   64 TJ(1) = PIF + 2.0 * SIN(PHI)
      COTF = COS(PHI/2.0)/SIN(PHI/2.0)
      TK(1) = 2.0 * ALOG(COTF) - 2.0 * COS(PHI)
      GO TO 68
   66 RELN2 = N - 2
      RN2PHI = RELN2 * PHI
      TJ(N) = TJ(N-2) + (2.0/RELN)*SIN(RNPHI) + (2.0/RELN2)*SIN(RN2PHI)
      TK(N) = TK(N-2) - (2.0/RELN)*COS(RNPHI) - (2.0/RELN2)*COS(RN2PHI)
   68 T1 - SIN(RNPHI)
      T2 = CS1 * RELN/(8.0 * PIF)*(SIN(RNPHI)*TJ(N) - COS(RNPHI)*TK(N))
      ACOF(N) = T1 + T2
   60 ADI(I,M) = ACOF(N)
   62 CONTINUE
C        * SOLUTION OF THE SIMULTANEOUS EQUATIONS FOR FOURIER COEFFICIENTS
           OF CIRCULATION DISTRIBUTION *
```

```
      WRITE(6,28)
   28 FORMAT(//1HO,20X,49HFOURIER COEFFICIENTS FOR CIRCULATION DISTRIBUT
     1ION, / )
      CALL SIMQ(ASI, RHV, 5, KS)
      IF(KS - 1) 70, 72, 70
   72 WRITE(6,19)
   19 FORMAT(1HO, 18HMATRIX IS SINGULAR)
      WRITE(6,15)
   15 FORMAT(1HO, 18HGO ON TO NEXT CASE)
      GO TO 5
   70 IX = -1
      DO 74 I = 1, 5
      IX = IX + 2
      A(IX) = RHV(I)
   74 WRITE(6,32) IX, A(IX)
   32 FORMAT(1H , 30X, 1HA, I1, 3H = , 1PE20.7)
C              * EVALUATION OF INDUCED DRAG INTEGRAL *
      XL = 0.0
      XU = PIF
      EPS = 5.0E-4
      NDIM = 101
      CALL QATR(XL, XU, EPS, NDIM, FCT, DINT, ITGER, AUX)
      WRITE(6,37)
   37 FORMAT(//1HO, 20X, 24HINDUCED DRAG INTEGRATION )
      WRITE(6,38) DINT, ITGER
   38 FORMAT(  1HO, 30X, 18HINTEGRAL OF FCT = , 1PE16.6,//
     1  30X, 25H ERROR PARAMETER ITGER = , I1)
C              * SPAN EFFICIENCY FACTOR *
      E = (PIF**2)*(A(1)**2)/DINT
      WRITE(6,40) E
```

```
 40   FORMAT(1HO,30X, 38HCHANNEL WING SPAN EFFICIENCY FACTOR = ,
     1 1PE12.5, //)
C          * CALCULATE CHANNEL WING PROFILE DRAG COEFFICIENT *
      PHI = 0.0
      CDSUM = 0.0
      DPHI = 4.50 * 0.0174533
      DO 76 J = 1, 20
      IF(J - 1) 78, 78, 80
   78 PHI = PHI + DPHI/2.0
      GO TO 82
   80 PHI = PHI + DPHI
   82 CLT1 = ATAN(SIN(ALPAC) * SIN(PHI)/COS(ALPAC))
C              INDUCED ANGLE OF ATTACK
      CLT3 = 0.0
      DO 84 N = 1, 9, 2
      RELN = N
      RNPHI = RELN * PHI
      IF(N -1) 86, 86, 88
   86 COTF = COS(PHI/2.0)/SIN(PHI/2.0)
      TK(1) = 2.0 * ALOG(COTF) - 2.0 * COS(PHI)
      TJ(1) = PIF + 2.0 * SIN(PHI)
      GO TO 90
   88 RELN2 = N - 2
      RN2PHI = RELN2 * PHI
      TK(N) = TK(N-2) - (2.0/RELN) * COS(RNPHI) - (2./RELN2)*COS(RN2PHI)
      TJ(N) = TJ(N-2) + (2.0/RELN) * SIN(RNPHI) + (2./RELN2)*SIN(RN2PHI)
   90 CLT3 = CLT3 + (RELN * A(N)/(8.0 * PIF))*(COS(RNPHI)* TK(N) - SIN(
     1RNPHI) * TJ(N))
   84 CONTINUE
C              SECTION LIFT COEFFICIENT
      CLSEC = ASO * (CLT1 - ANZL + CLT3)
C              CHECK SECTION CL TO BE IN DATA RANGE
      IF(CLMIN - CLSEC) 81, 81, 83
```

```
   83 CLSEC = CLMIN
      GO TO 89
   81 IF(CLSEC - CLMAX) 85, 85, 87
   87 CLSEC = CLMAX
   89 PHIPD = PHI * 57.29578
      WRITE(6,47) PHIPD, CLSEC
   47 FORMAT (  49H *** SECTION CL EXCEEDS RANGE OF CL VS. CD TABLE, 7X,
     1   5HPHI =, F9.4, 10X, 13HSET SEC. CL =, 1PE13.5)
C        ORDER SECTION CL VS. CD TABLE FOR INTERPOLATION ROUTINE
   85 CALL ATSG(CLSEC, TCL, TCD, WORK, IROW, 1, ARG, VAL, IROW)
C        INTERPOLATE SECTION CD VALUE AT SECTION CL
      CALL ALI(CLSEC, ARG, VAL, CDSEC, IROW, CDERR, IER)
C        SUM SECTION CD OVER WINGSPAN
   76 CDSUM = CDSUM + CDSEC * DPHI
      CDO = (2.0/PIF) * CDSUM
C           * LIFT AND DRAG COEFFICIENTS *
      ASPRO = 2.0 * R/C
      CL = (PIF/4.0) * ASPRO * A(1)
      CDI = (CL**2)/(E * PIF * ASPRO)
      CD = (PIF/2.0) * CDO + CDI
      ALPAC = ALPAC * 57.29578
      WRITE(6,42)
   42 FORMAT(  1HO,  20X,39HCHANNEL WING LIFT AND DRAG COEFFICIENTS //)
      WRITE(6,44) CDO,CDI,CL,CD
   44 FORMAT(33H WING PROFILE DRAG COEFFICIENT = , 1PE16.6 /// 33H WING
     1INDUCED DRAG COEFFICIENT = , 1PE16.6/// 25H WING LIFT COEFFICIENT
     2 = , 1PE16.6///25H WING DRAG COEFFICIENT = , 1PE16.6)
C             INCREMENT WING ANGLE OF ATTACK
      ALPAC = ALPAC + DALPA
      GO TO 94
   99 STOP
      END
```

```
C         SUBROUTINE SIMQ
C
C         PURPOSE
C            OBTAIN SOLUTION OF A SET OF SIMULTANEOUS LINEAR
C            EQUATIONS, AX = B
C
C         USAGE
C            CALL SIMQ(A,B,N,KS)
C
C         DESCRIPTION OF PARAMETERS
C            A-MATRIX OF COEFFICIENTS STORED COLUMNWISE.  THESE ARE
C              DESTROYED IN THE COMPUTATION.  THE SIZE OF MATRIX A IS
C              N BY N.
C            B-VECTOR OF ORIGINAL CONSTANTS (LENGTH N).  THESE ARE
C              REPLACED BY FINAL SOLUTION VALUES, VECTOR X.
C            N-NUMBER OF EQUATIONS AND VARIABLES. N MUST BE .GT. ONE.
C            KS-OUTPUT DIGIT
C               0 FOR A NORMAL SOLUTION
C               1 FOR A SINGULAR SET OF EQUATIONS
C         REMARKS
C            MATRIX A MUST BE GENERAL. IF MATRIX A IS SINGULAR, SOLUTION
C            VALUES ARE MEANINGLESS.
C         METHOD
C            METHOD OF SOLUTION IS BY ELIMINATION USING LARGEST PIVOTAL
C            DIVISOR. EACH STAGE OF ELIMINATION CONSISTS OF INTERCHANGING
C            ROWS WHEN NECESSARY TO AVOID DIVISION BY ZERO OR SMALL
C            ELEMENTS.
C            THE FORWARD SOLUTION TO OBTAIN VARIABLE N IS DONE IN N
C            STAGES. THE BACK SOLUTION FOR THE OTHER VARIABLES IS
C            CALCULATED BY SUCCESSIVE SUBSTITUTIONS. FINAL SOLUTION
C            VALUES ARE DEVELOPED IN VECTOR B, WITH VARIABLE 1 IN B(1),
C            VARIABLE 2 IN B(2),........, VARIABLE N IN B(N).
C            IF NO PIVOT CAN BE FOUND EXCEEDING A TOLERANCE OF 0.0,
```

```
C                THE MATRIX IS CONSIDERED SINGULAR AND KS IS SET TO 1. THIS
C                TOLERANCE CAN BE MODIFIED BY REPLACING THE FIRST STATEMENT.
C
      SUBROUTINE SIMQ(A,B,N,KS)
      DIMENSION A(1),B(1)
C
C     FORWARD SOLUTION
C
      TOL=0.0
      KS=0
      JJ=-N
      DO 65 J=1,N
      JY=J+1
      JJ=JJ+N+1
      BIGA=0
      IT=JJ-J
      DO 30 I=J,N
C
C     SEARCH FOR MAXIMUM COEFFICIENT IN COLUMN
C
      IJ=IT+I
      IF(ABS(BIGA)-ABS(A(IJ)))20,30,30
   20 BIGA=A(IJ)
      IMAX=I
   30 CONTINUE
C
C     TEST FOR PIVOT LESS THAN TOLERANCE(SINGULAR MATRIX)
      IF(ABS(BIGA)-TOL)35,35,40
   35 KS=1
      RETURN
C
C     INTERCHANGE ROWS IF NECESSARY
```

```
C
   40 I1=J+N*(J-2)
      IT=IMAX-J
      DO 50 K=J,N
      I1-I1+N
      I2=I1+IT
      SAVE=A(I1)
      A(I1)=A(I2)
      A(I2)=SAVE
C
C     DIVIDE EQUATION BY LEADING COEFFICIENT
C
   50 A(I1)=A(I1)/BIGA
      SAVE=B(IMAX)
      B(IMAX)=B(J)
      B(J)=SAVE/BIGA
C
CC    ELIMINATE NEXT VARIABLE
C
      IF(J-N)55,70,55
   55 IQS=N*(J-1)
      DO 65 IX=JY,N
      IXJ=IQS+IX
      IT=J-IX
      DO 60 JX=JY,N
      IXJX=N*(JX-1)+IX
      JJX=IXJX+IT
   60 A(IXJX)=A(IXJX)-(A(IXJ)*A(JJX))
   65 B(IX)=B(IX)-(B(J)*A(IXJ))
C
C     BACK SOLUTION
C
   70 NY=N-1
```

```
      IT=N*N
      DO 80 J=1,NY
      IA=IT-J
      IB=N-J
      IC=N
      DO 80 K=1,J
      B(IB)=B(IB)-A(IA)*B(IC)
      IA=IA-N
   80 IC=IC-1
      RETURN
      END
```

```
C        FUNCTION SUBROUTINE FCT(X)
C             THIS SUBROUTINE PERFORMS THE DOUBLE SUMMATION REQUIRED TO
C             SET UP THE INDUCED DRAG INTEGRAND.
C
      FUNCTION FCT(X)
      DIMENSION A(9), TJ(9), TK(9)
      COMMON A
      PIF = 3.141593
      IF(X .LE. 0.0) GO TO 30
      IF(X .GE. PIF) GO TO 30
      COTF = COS(X/2.0)/SIN(X/2.0)
      FCT = 0.0
      DO 20 N = 1,9,2
      RELN = N
      RNX = RELN * X
      IF(N-1) 12,12,14
   12 TJ(1) = PIF + 2.0 * SIN(X)
      TK(1) = 2.0 * ALOG(COTF) - 2.0 * COS(X)
      GO TO 16
   14 RELN2 = N - 2
      RN2X = RELN2 * X
      TJ(N) = TJ(N-2) + (2.0/RELN) * SIN(RNX) + (2.0/RELN2) * SIN(RN2X)
      TK(N) = TK(N-2) - (2.0/RELN) * COS(RNX) - (2.0/RELN2) * COS(RN2X)
   16 T1 = RELN * A(N) * (TJ(N) * SIN(RNX) - TK(N) * COS(RNX))
      DO 20 M = 1,9,2
      RELM = M
      RMX = RELM * X
      T2 = A(M) * SIN(RMX)
      SBT = T1 * T2
   20 FCT = FCT + SBT
      RETURN
   30 FCT = 0.0
      RETURN
      END
```

```
C
C     ..................................................................
C
C        SUBROUTINE QATR
C
C        PURPOSE
C           TO COMPUTE AN APPROXIMATION FOR INTEGRAL (FCT(X), SUMMED
C           OVER X FROM XL TO XU).
C
C        USAGE
C           CALL QATR (XL,XU,EPS,NDIM,FCT,Y,IER,AUX)
C           PARAMETER FCT REQUIRES AN EXTERNAL STATEMENT.
C
C        DESCRIPTION OF PARAMETERS
C           XL     - THE LOWER BOUND OF THE INTERVAL.
C           XU     - THE UPPER BOUND OF THE INTERVAL.
C           EPS    - THE UPPER BOUND OF THE ABSOLUTE ERROR.
C           NDIM   - THE DIMENSION OF THE AUXILIARY STORAGE ARRAY AUX.
C                    NDIM-1 IS THE MAXIMAL NUMBER OF BISECTIONS OF
C                    THE INTERVAL (XL,XU).
C           FCT    - THE NAME OF THE EXTERNAL FUNCTION SUBPROGRAM USED.
C           Y      - THE RESULTING APPROXIMATION FOR THE INTEGRAL VALUE.
C           IER    - A RESULTING ERROR PARAMETER.
C           AUX    - AN AUXILIARY STORAGE ARRAY WITH DIMENSION NDIM.
C
C        REMARKS
C           ERROR PARAMETER IER IS CODED IN THE FOLLOWING FORM
C           IER#0  - IT WAS POSSIBLE TO REACH THE REQUIRED ACCURACY.
C                    NO ERROR.
C           IER#1  - IT IS IMPOSSIBLE TO REACH THE REQUIRED ACCURACY
C                    BECAUSE OF ROUNDING ERRORS.
C           IER#2  - IT WAS IMPOSSIBLE TO CHECK ACCURACY BECAUSE NDIM
C                    IS LESS THAN 5, OR THE REQUIRED ACCURACY COULD NOT
```

```
C                BE REACHED WITHIN NDIM-1 STEPS. NDIM SHOULD BE
C                INCREASED.
C
C        SUBROUTINES AND FUNCTION SUBPROGRAMS REQUIRED
C           THE EXTERNAL FUNCTION SUBPROGRAM FCT(X) MUST BE CODED BY
C           THE USER.  ITS ARGUMENT X SHOULD NOT BE DESTROYED.
C
C        METHOD
C           EVALUATION OF Y IS DONE BY MEANS OF TRAPEZOIDAL RULE IN
C           CONNECTION WITH ROMBERGS PRINCIPLE. ON RETURN Y CONTAINS
C           THE BEST POSSIBLE APPROXIMATION OF THE INTEGRAL VALUE AND
C           VECTOR AUX THE UPWARD DIAGONAL OF ROMBERG SCHEME.
C           COMPONENTS AUX(I) (I#1,2,...,IEND, WITH IEND LESS THAN OR
C           EQUAL TO NDIM) BECOME APPROXIMATIONS TO INTEGRAL VALUE WITH
C           DECREASING ACCURACY BY MULTIPLICATION WITH (XU-XL).
C        FOR REFERENCE, SEE
C        (1) FILIPPI, DAS VERFAHREN VON ROMBERG-STIEFEL-BAUER ALS
C            SPEZIALFALL DES ALLGEMEINEN PRINZIPS VON RICHARDSON,
C            MATHEMATIK-TECHNIK-WIRTSCHAFT, VOL. 11, ISS.2 (1964),
C            PP.49-54.
C        (2) BAUER, ALGORITHM 60, CACM, VOL.4, ISS.6 (1961), PP.255.
C
C     ..................................................................
C
      SUBROUTINE QATR(XL,XU,EPS,NDIM,FCT,Y,IER,AUX)
C
C
      DIMENSION AUX(1)
C
C     PREPARATIONS OF ROMBERG-LOOP
      AUX(1)=.5*(FCT(XL)+FCT(XU))
      H=XU-XL
      IF(NDIM-1)8,8,1
```

```
    1 IF(H)2,10,2
C
C     NDIM IS GREATER THAN 1 AND H IS NOT EQUAL TO 0.
    2 HH=H
      E=EPS/ABS(H)
      DELT2=0.
      P=1.
      JJ=1
      DO 7 I=2,NDIM
      Y=AUX(1)
      DELT1=DELT2
      HD=HH
      HH=.5*HH
      P=.5*P
      X=XL+HH
      SM=0.
      DO 3 J=1,JJ
      SM=SM+FCT(X)
    3 X=X+HD
      AUX(I)=.5*AUX(I-1)+P*SM
C     A NEW APPROXIMATION OF INTEGRAL VALUE IS COMPUTED BY MEANS OF
C     TRAPEZOIDAL RULE.
C
C     START OF ROMBERGS EXTRAPOLATION METHOD.
      Q=1.
      JI=I-1
      DO 4 J=1,JI
      II=I-J
      Q=Q+Q
      Q=Q+Q
    4 AUX(II)=AUX(II+1)+(AUX(II+1)-AUX(II))/(Q-1.)
C     END OF ROMBERG-STEP
C
```

```
      DELT2=ABS(Y-AUX(1))                                               QATR 100
      IF(I-5)7,5,5                                                      QATR 101
    5 IF(DELT2-E)10,10,6                                                QATR 102
    6 IF(DELT2-DELT1)7,11,11                                            QATR 103
    7 JJ=JJ+JJ                                                          QATR 104
    8 IER=2                                                             QATR 105
    9 Y=H*AUX(1)                                                        QATR 106
      RETURN                                                            QATR 107
   10 IER=0                                                             QATR 108
      GO TO 9                                                           QATR 109
   11 IER=1                                                             QATR 110
      Y=H*Y                                                             QATR 111
      RETURN                                                            QATR 112
      END                                                               QATR 113
```

```
C
C     ..................................................................
C
C        SUBROUTINE ATSG
C
C        PURPOSE
C           NDIM POINTS OF A GIVEN GENERAL TABLE ARE SELECTED AND
C           ORDERED SUCH THAT ABS(ARG(I)-X).GE.ABS(ARG(J)-X) IF I.GT.J.
C
C        USAGE
C           CALL ATSG (X,Z,F,WORK,IROW,ICOL,ARG,VAL,NDIM)
C
C        DESCRIPTION OF PARAMETERS
C           X      - THE SEARCH ARGUMENT.
C           Z      - THE VECTOR OF ARGUMENT VALUES (DIMENSION IROW).
C           F      - IN CASE ICOL#1, F IS THE VECTOR OF FUNCTION VALUES
C                    (DIMENSION IROW).
C                    IN CASE ICOL#2, F IS AN IROW BY 2 MATRIX, THE FIRST
C                    COLUMN SPECIFIES THE VECTOR OF FUNCTION VALUES AND
C                    THE SECOND THE VECTOR OF DERIVATIVES.
C           WORK   - A WORKING STORAGE (DIMENSION IROW).
C           IROW   - THE DIMENSION OF VECTORS Z AND WORK AND OF EACH
C                    COLUMN IN MATRIX F.
C           ICOL   - THE NUMBER OF COLUMNS IN F (I.E. 1 OR 2).
C           ARG    - THE RESULTING VECTOR OF SELECTED AND ORDERED
C                    ARGUMENT VALUES (DIMENSION NDIM).
C           VAL    - THE RESULTING VECTOR OF SELECTED FUNCTION VALUES
C                    (DIMENSION NDIM) IN CASE ICOL#1. IN CASE ICOL#2
C                    VAL IS THE VECTOR OF FUNCTION AND DERIVATIVE VALUES
C                    (DIMENSION 2*NDIM) WHICH ARE STORED IN PAIRS (I.E.
C                    EACH FUNCTION VALUE IS FOLLOWED BY ITS DERIVATIVE
C                    VALUE).
C           NDIM   - THE NUMBER OF POINTS WHICH MUST BE SELECTED OUT OF
```

```
C                THE GIVEN TABLE (Z,F).
C
C        REMARKS
C           NO ACTION IN CASE IROW LESS THAN 1.
C           IF INPUT VALUE NDIM IS GREATER THAN IROW, THE PROGRAM
C           SELECTS ONLY A MAXIMUM TABLE OF IROW POINTS. THEREFORE THE
C           USER OUGHT TO CHECK CORRESPONDENCE BETWEEN TABLE (ARG,VAL)
C           AND ITS DIMENSION BY COMPARISON OF NDIM AND IROW, IN ORDER
C           TO GET CORRECT RESULTS IN FURTHER WORK WITH TABLE (ARG,VAL).
C           THIS TEST MAY BE DONE BEFORE OR AFTER CALLING
C           SUBROUTINE ATSG.
C           SUBROUTINE ATSG ESPECIALLY CAN BE USED FOR GENERATING THE
C           TABLE (ARG,VAL) NEEDED IN SUBROUTINES ALI, AHI, AND ACFT.
C
C        SUBROUTINES AND FUNCTION SUBPROGRAMS REQUIRED
C           NONE
C
C        METHOD
C           SELECTION IS DONE BY GENERATING THE VECTOR WORK WITH
C           COMPONENTS WORK(I)#ABS(Z(I)-X) AND AT EACH OF THE NDIM STEPS
C           (OR IROW STEPS IF NDIM IS GREATER THAN IROW)
C           SEARCHING FOR THE SUBSCRIPT OF THE SMALLEST COMPONENT, WHICH
C           IS AFTERWARDS REPLACED BY A NUMBER GREATER THAN
C           MAX(WORK(I)).
C
C     ..................................................................
C
      SUBROUTINE ATSG(X,Z,F,WORK,IROW,ICOL,ARG,VAL,NDIM)
C
C
      DIMENSION Z(1),F(1),WORK(1),ARG(1),VAL(1)
      IF (IROW)11,11,1
```

```
    1 N=NDIM                                                           ATSG 066
C     IF N IS GREATER THAN IROW, N IS SET EQUAL TO IROW.               ATSG 067
      IF(N-IROW)3,3,2                                                  ATSG 068
    2 N=IROW                                                           ATSG 069
C                                                                      ATSG 070
C     GENERATION OF VECTOR WORK AND COMPUTATION OF ITS GREATEST ELEMENT. ATSG 071
    3 B=0.                                                             ATSG 072
      DO 5 I=1,IROW                                                    ATSG 073
      DELTA=ABS(Z(I)-X)                                                ATSG 074
      IF (DELTA-B)5,5,4                                                ATSG 075
    4 B=DELTA                                                          ATSG 076
    5 WORK(I)=DELTA                                                    ATSG 077
C                                                                      ATSG 078
C     GENERATION OF TABLE (ARG,VAL)                                    ATSG 079
      B=B+1.                                                           ATSG 080
      DO 10 J=1,N                                                      ATSG 081
      DELTA=B                                                          ATSG 082
      DO 7 I=1,IROW                                                    ATSG 083
      IF(WORK(I)-DELTA)6,7,7                                           ATSG 084
    6 II=I                                                             ATSG 085
      DELTA=WORK(I)                                                    ATSG 086
    7 CONTINUE                                                         ATSG 087
      ARG(J)=Z(II)                                                     ATSG 088
      IF(ICOL-1)8,9,8                                                  ATSG 089
    8 VAL(2*J-1)=F(II)                                                 ATSG 090
      III=II+IROW                                                      ATSG 091
      VAL(2*J)=F(III)                                                  ATSG 092
      GO TO 10                                                         ATSG 093
    9 VAL(J)=F(II)                                                     ATSG 094
   10 WORK(II)=B                                                       ATSG 095
   11 RETURN                                                           ATSG 096
      END                                                              ATSG 097
```

```
C
C     ..................................................................
C
C        SUBROUTINE ALI
C
C        PURPOSE
C           TO INTERPOLATE FUNCTION VALUE Y FOR A GIVEN ARGUMENT VALUE
C           X USING A GIVEN TABLE (ARG,VAL) OF ARGUMENT AND FUNCTION
C           VALUES.
C
C        USAGE
C           CALL ALI (X,ARG,VAL,Y,NDIM,EPS,IER)
C
C        DESCRIPTION OF PARAMETERS
C           X      - THE ARGUMENT VALUE SPECIFIED BY INPUT.
C           ARG    - THE INPUT VECTOR (DIMENSION NDIM) OF ARGUMENT
C                    VALUES OF THE TABLE (NOT DESTROYED).
C           VAL    - THE INPUT VECTOR (DIMENSION NDIM) OF FUNCTION
C                    VALUES OF THE TABLE (DESTROYED).
C           Y        THE RESULTING INTERPOLATED FUNCTION VALUE.
C           NDIM   - AN INPUT VALUE WHICH SPECIFIES THE NUMBER OF
C                    POINTS IN TABLE (ARG,VAL).
C           EPS    - AN INPUT CONSTANT WHICH IS USED AS UPPER BOUND
C                    FOR THE ABSOLUTE ERROR.
C           IER    - A RESULTING ERROR PARAMETER.
C
C        REMARKS
C           (1) TABLE (ARG,VAL) SHOULD REPRESENT A SINGLE-VALUED
C               FUNCTION AND SHOULD BE STORED IN SUCH A WAY, THAT THE
C               DISTANCES ABS(ARG(I)-X) INCREASE WITH INCREASING
C               SUBSCRIPT I. TO GENERATE THIS ORDER IN TABLE (ARG,VAL),
C               SUBROUTINES ATSG, ATSM OR ATSE COULD BE USED IN A
C               PREVIOUS STAGE.
```

```
C          (2) NO ACTION BESIDES ERROR MESSAGE IN CASE NDIM LESS      ALI  034
C              THAN 1.                                                ALI  035
C          (3) INTERPOLATION IS TERMINATED EITHER IF THE DIFFERENCE   ALI  036
C              BETWEEN TWO SUCCESSIVE INTERPOLATED VALUES IS          ALI  037
C              ABSOLUTELY LESS THAN TOLERANCE EPS, OR IF THE ABSOLUTE ALI  038
C              VALUE OF THIS DIFFERENCE STOPS DIMINISHING, OR AFTER   ALI  039
C              (NDIM-1) STEPS. FURTHER IT IS TERMINATED IF THE        ALI  040
C              PROCEDURE DISCOVERS TWO ARGUMENT VALUES IN VECTOR ARG  ALI  041
C              WHICH ARE IDENTICAL. DEPENDENT ON THESE FOUR CASES,    ALI  042
C              ERROR PARAMETER IER IS CODED IN THE FOLLOWING FORM     ALI  043
C               IER#0 - IT WAS POSSIBLE TO REACH THE REQUIRED         ALI  044
C                       ACCURACY (NO ERROR).                          ALI  045
C               IER#1 - IT WAS IMPOSSIBLE TO REACH THE REQUIRED       ALI  046
C                       ACCURACY BECAUSE OF ROUNDING ERRORS.          ALI  047
C               IER#2 - IT WAS IMPOSSIBLE TO CHECK ACCURACY BECAUSE   ALI  048
C                       NDIM IS LESS THAN 3, OR THE REQUIRED ACCURACY ALI  049
C                       COULD NOT BE REACHED BY MEANS OF THE GIVEN    ALI  050
C                       TABLE. NDIM SHOULD BE INCREASED.              ALI  051
C               IER#3 - THE PROCEDURE DISCOVERED TWO ARGUMENT VALUES  ALI  052
C                       IN VECTOR ARG WHICH ARE IDENTICAL.            ALI  053
C                                                                     ALI  054
C        SUBROUTINES AND FUNCTION SUBPROGRAMS REQUIRED                ALI  055
C           NONE                                                      ALI  056
C                                                                     ALI  057
C        METHOD                                                       ALI  058
C           INTERPOLATION IS DONE BY MEANS OF AITKENS SCHEME OF       ALI  059
C           LAGRANGE INTERPOLATION. ON RETURN Y CONTAINS AN INTERPOLATED ALI  060
C           FUNCTION VALUE AT POINT X, WHICH IS IN THE SENSE OF REMARK ALI  061
C           (3) OPTIMAL WITH RESPECT TO GIVEN TABLE. FOR REFERENCE, SEE ALI  062
C           F.B.HILDEBRAND, INTRODUCTION TO NUMERICAL ANALYSIS        ALI  063
C           MCGRAW-HILL, NEW YORK/TORONTO/LONDON, 1956, PP.49-50.     ALI  064
C                                                                     ALI  065
```

```
C     ...............................................................
C
      SUBROUTINE ALI(X,ARG,VAL,Y,NDIM,EPS,IER)
C
C
      DIMENSION ARG(1),VAL(1)
      IER=2
      DELT2=0.
      IF(NDIM-1)9,7,1
C
C     START OF AITKEN-LOOP
    1 DO 6 J=2,NDIM
      DELT1=DELT2
      IEND=J-1
      DO 2 I=1,IEND
      H=ARG(I)-ARG(J)
      IF(H)2,13,2
    2 VAL(J)=(VAL(I)*(X-ARG(J))-VAL(J)*(X-ARG(I)))/H
      DELT2=ABS(VAL(J)-VAL(IEND))
      IF(J-2)6,6,3
    3 IF(DELT2-EPS)10,10,4
    4 IF(J-5)6,5,5
    5 IF(DELT2-DELT1)6,11,11
    6 CONTINUE
C     END OF AITKEN-LOOP
C
    7 J=NDIM
    8 Y=VAL(J)
    9 RETURN
C
C     THERE IS SUFFICIENT ACCURACY WITHIN NDIM-1 ITERATION STEPS
   10 IER=0
      GOTO 8
```

```
C
C     TEST VALUE DELT2 STARTS OSCILLATING
   11 IER=1
   12 J=IEND
      GOTO 8
C
C     THERE ARE TWO IDENTICAL ARGUMENT VALUES IN VECTOR ARG
   13 IER=3
      GOTO 12
      END
```

Sample Input and Output Data Printout

The input data required for the computer program are listed and described in Table 6. A sample computer printout of input data is presented on the following page. The data shown are for the $\mathcal{R}$ = 2.8 wind tunnel model described in Chapter III. See Appendix D for airfoil section data for this model. Following the input data is a sample printout for one wing angle of attack.

CHANNEL WING INPUT DATA

WING: MODEL ASPECT RATIO = 2.8

AIRFOIL SECTION: NACA 0015, RE = 8.7E5, SMOOTH

WING RADIUS, FT. = 5.833000E-01

WING CHORD, FT. = 4.166999E-01

AIRFOIL SECTION LIFT-CURVE SLOPE, PER RADIAN = 5.271999E 00

AIRFOIL SECTION ANGLE FOR ZERO LIFT, DEGREES = 0.0

OUTPUT DATA

WING CENTERLINE ANGLE OF ATTACK, DEGREES = 8.00

FOURIER COEFFICIENTS FOR CIRCULATION DISTRIBUTION

A1 = 1.9793904E-01
A3 = 7.2712824E-03
A5 = 3.2314486E-03
A7 = 1.4179884E-03
A9 = 3.7647272E-04

INDUCED DRAG INTEGRATION

INTEGRAL OF FCT = 2.651325E-01

ERROR PARAMETER ITGER = 0

CHANNEL WING SPAN EFFICIENCY FACTOR = 1.45848E 00

CHANNEL WING LIFT AND DRAG COEFFICIENTS

WING PROFILE DRAG COEFFICIENT = 1.228187E-02

WING INDUCED DRAG COEFFICIENT = 1.476696E-02

WING LIFT COEFFICIENT = 4.352306E-01

WING DRAG COEFFICIENT = 3.405927E-02

APPENDIX D

SECTION DATA FOR NACA 4412 AND 0015 AIRFOILS

SECTION DATA FOR NACA 4412 AND 0015 AIRFOILS

The channel wing digital computer program described in Chapter VII requires as input a table of lift and drag coefficients for the particular airfoil section and Reynolds number being considered. The wind tunnel models of the tests reported herein used the NACA 4412 and the NACA 0015 airfoil sections. Therefore, for correlation purposes, data for these sections at relatively low Reynolds numbers were required.

NACA 4412

The wind tunnel tests of the $AR = 1.0$ channel wing model were conducted at an effective Reynolds number of 1.55×10^6. Section drag coefficient data as a function of lift coefficient at $Re = 1.5 \times 10^6$ were obtained from Loftin and Smith [23] . This reference presents section data for several NACA airfoils, over a wide range of Reynolds numbers. The data were obtained from tests conducted in the Langley two-dimensional low-turbulence tunnel, and include data for both smooth airfoils and those with NACA standard roughness.

NACA 0015

Smooth Section Data

The effective Reynolds number for the wind tunnel tests of the $AR = 2.8$ model was 665,000. Despite an extensive literature search, the author was unable to find section data for the 0015 at such a low Reynolds number which would be considered accurate by modern standards. Therefore, the best data available is apparently that of NACA Report 586, Jacobs and Sherman [24] , when modified as directed by NACA Report 669, Jacobs and Abbott [25] . The data of Report 586 were obtained from tests of three-dimensional, aspect ratio 6.0 model wings in an NACA variable density tunnel in 1932 and "corrected . . . for infinite-aspect-ratio characteristics." Subsequently, in Report 669, the NACA recommended further corrections. More recently, the NACA recommended that Report 586 and Report 669 be considered superseded by NACA Report 824, Abbott, von Doenhoff, and Stivers [19] , which presents section data obtained under actual two-dimensional conditions. Unfortunately, the 0015 section was not included in the tests of Report 824.

NACA Report 669, Jacobs and Abbott [25] , recommends the following corrections to the drag curves of NACA Report 586, Jacobs and Sherman [24] :

$$Re_{eff} = 2.64 \; Re_{test} \tag{d.1}$$

$$\alpha_o = \alpha_o' + 0.39 C_L \qquad \text{in degrees} \tag{d.2}$$

$$c_d = C_D + 0.0016 C_L^2 - 1/3(t-6)(0.0002), \tag{d.3}$$

where Re_{test} , α_o' , C_L , and C_D are read from the Report 586 drag plots, and t is the maximum airfoil section thickness in percent chord. The angle for zero lift and the section lift curve slope do not require correction, and so may be obtained from Table I of Report 586, but as a function of Re_{eff} rather than Re_{test} . The Re_{test} curve of the NACA 0015 data of Report 586 which yields Re_{eff} closest to 665,000 is Re_{test} = 331,000. Thus

$$Re_{eff} = 2.64(331,000) = 874,000 ,$$

and Table I of Report 586 gives

$$\alpha_{L=0} = 0^{\circ}$$

$$a_o = 0.092 \text{ per degree} .$$

Then the "corrected" section coefficients for the NACA 0015 are given by

$$\alpha_o = \alpha_o' + 0.39C_L \qquad \text{in degrees} \qquad (d.4)$$

$$c_l = a_o \alpha_o = 0.092\,\alpha_o \qquad (d.5)$$

$$c_d = C_D + 0.0016C_L^2 - 1/3(15-6)(0.0002)$$

$$c_d = C_D + 0.0016C_L^2 - 0.0006 \quad . \qquad (d.6)$$

Using equations (d.4), (d.5), and (d.6), and data read from the C_L and C_D curves of NACA Report 586, c_l and c_d for NACA 0015 at Re = 874,000 were obtained, Table D-1. However, when plotted, Figure D-1, the calculated data showed a slight scatter due to error in reading the Report 586 curves. Therefore, a faired curve

TABLE D-1

NACA 0015 AIRFOIL SECTION DATA AT Re_{eff} = 874,000, FROM NACA REPORT 586, CORRECTED BY NACA REPORT 669

Report 586			Corrected by Report 669		
α_o'	C_L	C_D	α_o	c_l	c_d
0°	0.000	.0110	0.00°	0.000	.0105
2°	0.200	.0115	2.08°	0.191	.0110
4°	0.400	.0120	4.16°	0.383	.0115
6°	0.590	.0145	6.23°	0.573	.0145
8°	0.780	.0190	8.30°	0.764	.0194
9°	0.840	.0215	9.33°	0.858	.0220
10°	0.900	.0235	10.35°	0.952	.0242
11°	0.970	.0275	11.38°	1.047	.0284

was drawn through the plotted points, and values from this curve were used as input to the channel wing computer program. These final data for the 0015 airfoil at Re = 874,000 are presented in Table D-2.

Fully Turbulent Boundary Layer Section Data

The airfoil section data of NACA Report 586, Jacobs and Sherman [24] , are only for smooth sections with, consequently, extensive but undetermined amounts of laminar boundary layer flow. That is, no rough or fully turbulent section data are available for the NACA 0015 at or near the test Reynolds number of 665,000. However, a semi-empirical method developed by Schwartzberg [26] allows the estimation of the profile drag coefficient of smooth, symmetrical

TABLE D-2

NACA 0015 AIRFOIL SECTION DATA AT Re_{eff} = 874,000, FROM FAIRED CURVE THROUGH DATA OF TABLE D-1

c_ℓ	c_d
0.00	0.0105
0.10	0.0107
0.20	0.0110
0.30	0.0114
0.40	0.0122
0.50	0.0133
0.60	0.0149
0.70	0.0170
0.80	0.0195
0.90	0.0227
1.00	0.0267
1.10	0.0317

aifoils with fully turbulent boundary layer at any Reynolds number. Briefly, the method forms the airfoil section profile drag as the sum of friction drag and pressure drag. The former is assumed to be that of a smooth flat plate in turbulent flow at the desired Reynolds number, and the latter is obtained from NACA section data as the difference between total drag and friction drag. The actual procedure is complicated, and Schwartzberg [26] provides graphs to facilitate the calculations. In the present case of the NACA 0015 at Re = 665,000, the result is

$$c_d = 0.01196 + 1.86\ (\alpha)^{2.7}\quad , \tag{d.7}$$

where α is in radians. With the assumption of a linear lift curve slope of the same value as given by NACA Report 586 for the 0015 at Re_{eff} = 874,000, a_0 = 0.092 per degree, c_ℓ versus c_d data for smooth, turbulent flow were estimated. These data are given in Table D-3, and plotted in Figure D-1.

TABLE D-3

NACA 0015 AIRFOIL SECTION DATA FOR FULLY TURBULENT BOUNDARY LAYER, AT Re_{eff} = 665,000, BY SCHWARTZBERG'S METHOD

C_l	C_d
0.00	0.0110
0.10	0.0120
0.20	0.0122
0.30	0.0128
0.40	0.0137
0.50	0.0152
0.60	0.0172
0.70	0.0200
0.80	0.0234
0.90	0.0278
1.00	0.0329
1.10	0.0391

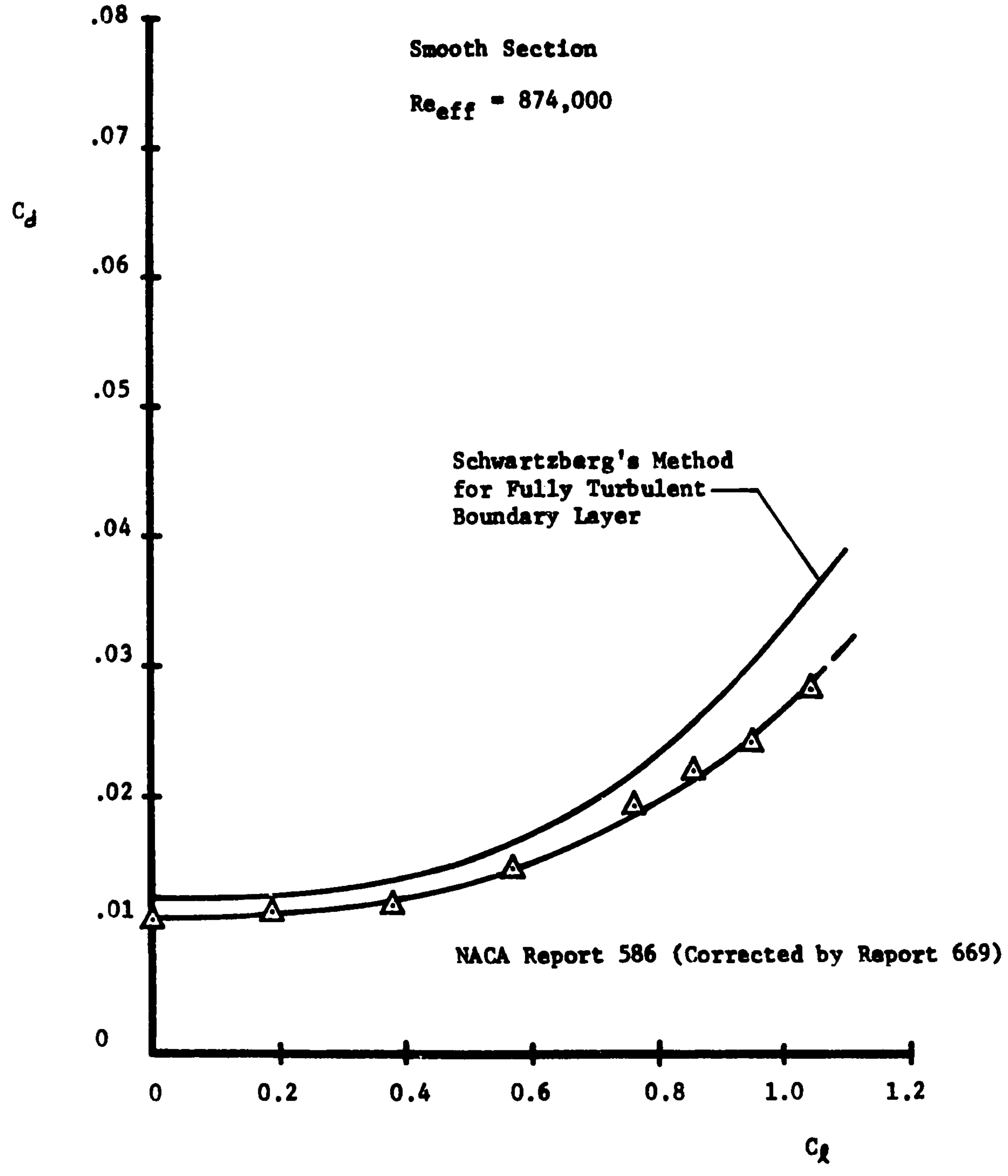

Figure D-1. NACA 0015 airfoil section data.

APPENDIX E

POWER REQUIRED FOR LEVEL FLIGHT

POWER REQUIRED FOR LEVEL FLIGHT

Thrust Required

For equilibrium level flight at constant altitude and speed,

$$T = D = C_D q S \,, \tag{e.1}$$

if it is assumed that the thrust vector is aligned with the direction of flight. Assuming a parabolic drag polar, we write

$$D = \left(C_{D_0} + \frac{C_L^2}{\pi e A\!\!R}\right) q S \quad . \tag{e.2}$$

Now

$$L = W,$$

so

$$C_L = W/qS \quad ,$$

and thus the thrust required is

$$T = \left[C_{D_0} + \left(\frac{1}{\pi e A\!\!R}\right)\left(\frac{W^2}{q^2 S^2}\right)\right] q S \quad . \tag{e.3}$$

But the aspect ratio is defined as

$$A\!\!R \equiv b^2/S \quad ,$$

so $$T = C_{D_0} q S + \frac{1}{\pi e q}\left(\frac{W}{b}\right)^2$$

or $$T = \left(\rho/2 \; C_{D_0} S\right) V^2 + \frac{2}{\pi e \rho}\left(\frac{W}{b}\right)^2 1/V^2 \quad . \tag{e.4}$$

Nondimensional Thrust Required

The first term in equation (e.4) is called the parasite thrust required, and the second term is called the effective induced thrust required (Perkins and Hage [22]). The former increases with V^2 and the latter decreases with V^2 . The two terms are equal at one speed only, and it can be shown that this is the speed for minimum thrust required (minimum drag). Write equation (e.4) as

$$T = AV^2 + B/V^2 ,$$

where

$$A \equiv \left(\rho/2 \; C_{D_0} \; S \right)$$

$$B \equiv \frac{2}{\pi e \rho} \left(W/b \right)^2 ;$$

then

$$\frac{dT}{dV} = 2AV - 2B/V^3 . \qquad \text{(e.5)}$$

Setting dT/dV equal to zero and solving for $V_{(T)_{min}}$:

$$V_{(T)_{min}} = \sqrt[4]{B/A} = \sqrt[4]{\frac{2}{\pi e \rho} \left(\frac{W}{b}\right)^2 \frac{2}{\rho C_{D_0} S}}$$

$$V_{(T)_{min}} = \frac{1.061}{\sqrt[4]{e C_{D_0} S}} \sqrt{\frac{W}{\rho b}} . \qquad \text{(e.6)}$$

But we have assumed equilibrium level flight above, with T = D, so

$$V_{(L/D)_{max}} = V_{(D)_{min}} = V_{(T)_{min}}$$

$$V_{(L/D)_{max}} = \frac{1.061}{\sqrt[4]{e C_{D_0} S}} \sqrt{\frac{W}{\rho b}} . \qquad \text{(e.7)}$$

Thrust at the speed for $(L/D)_{max}$ is found by substitution into equation (e.4):

$$T_{(L/D)_{max}} = A\,V^2_{(L/D)_{max}} + \frac{B}{V^2_{(L/D)_{max}}}$$

$$= A\sqrt{B/A} + B\sqrt{A/B} = \sqrt{AB} + \sqrt{AB} \,,$$

confirming that the two terms of equation (e.4) are equal at minimum thrust. Then

$$T_{(L/D)_{max}} = 2\sqrt{AB} = 2\left[\left(\rho/2\, C_{D_0} S\right)\left(\frac{2}{\pi e \rho}\right)\left(W/b\right)^2\right]^{1/2}$$

$$T_{(L/D)_{max}} = 1.127\left(W/b\right)\sqrt{\frac{C_{D_0} S}{e}} \,. \qquad \text{(e.8)}$$

The thrust required at any flight velocity can be nondimensionalized with $T_{(L/D)_{max}}$

$$T/T_{(L/D)_{max}} = \frac{A}{2\sqrt{AB}}\,V^2 + \frac{B}{2\sqrt{AB}}\,\frac{1}{V^2}$$

$$= 1/2\left[\sqrt{A/B}\;V^2 + \sqrt{B/A}\;\frac{1}{V^2}\right] \,. \qquad \text{(e.9)}$$

Since $V^2_{(L/D)_{max}} = V^2_{(T)_{min}} = \sqrt{B/A}$, the nondimensional thrust required for level flight is

$$\frac{T}{T_{(L/D)_{max}}} = \frac{1}{2}\left[\left(\frac{V}{V_{(L/D)_{max}}}\right)^2 + \frac{1}{\left(\frac{V}{V_{(L/D)_{max}}}\right)^2}\right] , \qquad \text{(e.10)}$$

where $V_{(L/D)_{max}}$ and $T_{(L/D)_{max}}$ are given by equations (e.7) and (e.8), respectively.

Nondimensional Power Required

The power required for equilibrium level flight is obtained from the relation P = TV:

$$\frac{P}{P_{(L/D)_{max}}} = \frac{T}{T_{(L/D)_{max}}} \frac{V}{V_{(L/D)_{max}}} . \qquad \text{(e.11)}$$

Substituting equation (e.10), we find that

$$\frac{P}{P_{(L/D)_{max}}} = \frac{1}{2}\left[\left(\frac{V}{V_{(L/D)_{max}}}\right)^3 + \frac{1}{\frac{V}{V_{(L/D)_{max}}}}\right] . \qquad \text{(e.12)}$$

The power required at the speed for $(L/D)_{max}$ is obtained from equations (e.8) and (e.7):

$$P_{(L/D)_{max}} = T_{(L/D)_{max}} V_{(L/D)_{max}}$$

$$= (1.127)\left(\frac{W}{b}\right)\sqrt{\frac{C_{D_0} S}{e}} \frac{1.061}{\sqrt[4]{e\, C_{D_0} S}} \sqrt{\frac{W}{\rho b}}$$

$$P_{(L/D)_{max}} = \frac{1.195}{\sqrt{e\,C_{D_0} S}} \sqrt{\frac{C_{D_0} S}{e\,\rho}} \left(W/b\right)^{3/2} . \qquad \text{(e.13)}$$

This power equation has units of ft - lb/sec.

It should be noted that the above development is for low Mach numbers only, since the drag polar will not be parabolic as the critical Mach number is approached.

Generalized Power Required

In order to compare power required for aircraft with plane, channel, and ring wings on a generalized plot, $P/P_{(L/D)_{max}}$ is formed with equation (e.13):

$$P/P_{(L/D)_{max}} = \frac{P}{1.195} \frac{\sqrt{e^{3/2}\,\rho}}{\sqrt[4]{C_{D_0} S}} \left(b/W\right)^{3/2}$$

$$\frac{P\sqrt{\rho}}{\sqrt[4]{C_{D_0} S}}\left(b/W\right)^{3/2} = \left(\frac{1.195}{e^{3/4}}\right) P/P_{(L/D)_{max}} . \qquad \text{(e.14)}$$

Also, using equation (e.7), we nondimensionalize the velocity:

$$V/V_{(L/D)_{max}} = \frac{V}{1.061} \sqrt[4]{e\,C_{D_0} S} \sqrt{\frac{\rho b}{W}} . \qquad \text{(e.15)}$$

Substituting (e.12) and (e.15) into (e.14), we find that

$$\frac{P\sqrt{\rho}}{\sqrt[4]{C_{D_0} S}}\left(b/W\right)^{3/2} = \frac{1.195}{2\,e^{3/4}}\left[\left(\frac{e^{1/4}}{1.061}\right)^3\left(V \sqrt[4]{C_{D_0} S}\sqrt{\frac{\rho b}{W}}\right)^3 + \frac{1.061/e^{1/4}}{V\sqrt[4]{C_{D_0} S}\sqrt{\frac{\rho b}{W}}}\right]$$

$$\frac{P\sqrt{\rho}}{\sqrt[4]{C_{D_0} S}}\left(\frac{b}{W}\right)^{3/2} = 0.597\left[0.836\left(V\,\sqrt[4]{C_{D_0} S}\,\sqrt{\frac{\rho b}{W}}\right)^3 + \frac{1.061/e}{V\,\sqrt[4]{C_{D_0} S}\,\sqrt{\rho b/W}}\right] . \quad \text{(e.16)}$$

Thus $\frac{P\sqrt{\rho}}{\sqrt[4]{C_{D_0} S}}\left(b/W\right)^{3/2}$ can be plotted versus $V\,\sqrt[4]{C_{D_0} S}\,\sqrt{\frac{\rho b}{W}}$ to obtain a generalized plot of power required for level flight.

Modifications for Channel and Ring Wings

The power required for level flight for any aircraft was developed above as a function of aircraft weight. In order to compare aircraft with plane, channel and ring wings, an estimate of the relative weights is required. Simply increasing the weight W of the nonplanar wing aircraft by the ratio of wing total area to projected area would put the channel and ring wing aircraft at a very large and unfair disadvantage, since wing weight is only a fraction of aircraft structural weight, and an even smaller fraction of flying weight. Some examples of the ratio of wing weight to take-off weight from Corning [27] are:

TABLE E-1

WING WEIGHT AS A FUNCTION OF AIRCRAFT TAKE-OFF WEIGHT

Aircraft Type	Take-Off Weight	Wing Structural Weight / Take-Off Weight
Light private	2,000 lbs.	0.10
Light private	3,000 lbs.	0.09
DC-3 size transport	30,000 lbs.	0.12
DC-6 size transport	100,000 lbs.	0.09

It is seen that wing structural weight is typically about 10% of take-off weight. Then the weight increase for the nonplanar wings may be estimated as the wing area ratio applied to 10% of the aircraft weight. For the channel wing aircraft the modified weight is

$$W' = 0.9\,W + \left(\frac{\pi Rc}{2\,Rc}\right)(0.1\,W) = 1.057\,W\;, \tag{e.17}$$

and for the ring wing aircraft,

$$W' = 0.9\,W + \left(\frac{2\pi Rc}{2Rc}\right)(0.1\,W) = 1.214\,W\;, \tag{e.18}$$

where W is the take-off weight of the plane wing aircraft.

Other modifications to the results of the previous sections are necessary. It is convenient to retain S as projected area, but then the profile drag coefficient must be increased for the channel wing and ring wing aircraft. However, since the aircraft profile drag coefficient C_{D_e} is composed of fuselage, tail, etc., drag as well as wing form drag, the C_{D_e} should not be increased by the ratio of total channel (or ring) wing area to projected channel (or ring) wing area. Hoerner [17] gives the following examples of the ratio of wing profile drag to aircraft total parasite drag (induced drag excluded from total):

TABLE E-2

WING PROFILE DRAG AS A FRACTION OF TOTAL AIRCRAFT PARASITE DRAG

Aircraft Type	Wing Profile Drag / Total Aircraft Parasite Drag
Me-262	0.33
Me-109G	0.41
Ju-88	0.44

A ratio of 0.40 is chosen as a representative value for the work here. Then the C_{D_o} increase due to the nonplanar wings is estimated as the wing area ratio applied to 40% of the planar wing aircraft profile drag. For the channel wing aircraft the profile drag coefficient becomes

$$C'_{D_o} = 0.60\,C_{D_o} + \left(\frac{\pi R_c}{2 R_c}\right)(0.40)\,C_{D_o} = 1.228\,C_{D_o} \quad , \qquad (e.19)$$

and for the ring wing aircraft,

$$C'_{D_o} = 0.60\,C_{D_o} + \left(\frac{2\pi R_c}{2 R_c}\right)(0.40)\,C_{D_o} = 1.858\,C_{D_o} \quad , \qquad (e.20)$$

where C_{D_o} is the profile drag coefficient of the plane wing aircraft. With these changes, the wing span b becomes 2R for the channel wing and ring wing aircraft. W' and C'_{D_o} are used in the power required equations in lieu of W and C_{D_o} , respectively.

Finally, of course, the correct span efficiency factor e for each type of wing must be used. For the channel and ring wings, e was shown in previous chapters to be 1.5 and 2.0, respectively. To provide conservative comparisons, the maximum theoretical value for e for planar wings, 1.0, will be used.